

Combined Author Index

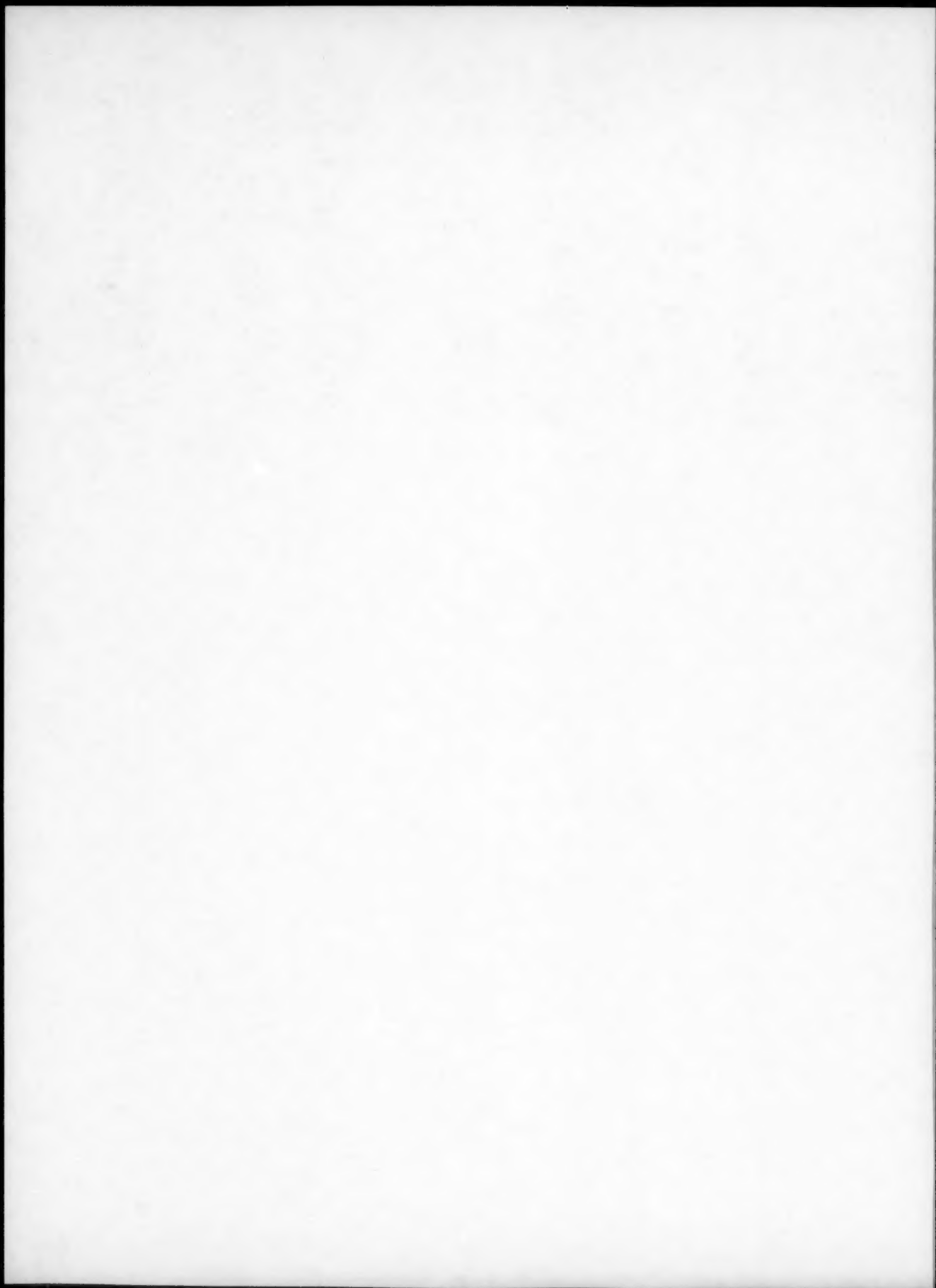
- Abbaschian, R. 4049-4059A
 Abe, T. 1585-1594A
 Abraham, D.P. 2151-2159A
 Abuluwefa, H. 993-997B
 Acoff, V.L. 2692-2703A
 Aermoudt, E. 2347-2358A
 Aganwal, A. 2985-2993A
 Agren, J. 1073-1080A
 Ahn, C.C. 2934-2946A
 Ahn, S. 3881-3891A
 Ajersch, F. 993-997B
 Akselsen, O.M. 3630-3638A
 Albarran, J.L. 3601-3611A
 Albers, M. 3569-3575A
 Ali, A. 1141-1147A
 Alonso, M. 801-807B
 Alpas, A.T. 3135-3148A
 Altunoglu, A.K. 2495-2503A
 Allynova, M. 1837-1844A
 Alvarez, L.F. 1799-1805A
 Ananthasivan, K. 1919-1924A
 Anderson, K.R. 1217-1227A
 Andrews, S. 2023-2034A
 Ankem, S. 2366-2373A
 Anthonyamy, S. 1919-1924A
 Antia, D.P. 1127-1132A
 Anton, D.L. 3007-3018A
 Araki, H. 1807-1814A
 Ardell, A.J. 2888-2896A
 Arjuna Rao, A. 791-800A
 Arnborg, L. 2305-2313A
 Arsenault, R.J. 995-1001A
 Arvanitidis, I. 409-416B
 Arya, V.K. 3279-3291A
 Asaro, R.J. 81-99A
 Asundi, M.K. 757-761A
 Atrens, A. 2686-2691A
 Avery, S. 773-779B
 Avramovic-Cingara, G. 3478-3490A
 Ayensu, A. 901-907A
 Ayer, R. 2510-2517A
 Aziz, M.J. 671-686A
 725-730A
 Babu, S.S. 763-774A
 Badrinarayanan, K. 3781-3792A
 Baek, E.-R. 3335-3340A
 3881-3891A
 Bahr, D.F. 3793-3800A
 Baik, W.-H. 3120-3125A
 Baker, T.N. 4039-4047A
 Balasubramanian, R. 2985-2993A
 3993-4002A
 4003-4010A
 Balch, D.K. 3700-3717A
 Balzer, M. 3066-3073A
 Banerjee, D. 2593-2604A
 Banerjee, R. 2047-2050A
 Barbante, G.G. 3187-3191A
 Barker, J. 923-928A
 Barrett, C.A. 3279-3291A
 Bartholomew, M.F. 127-134A
 Bartlett, R.W. 2086-2093A
 Bate, P.S. 3250-3258A
 3747-3748A
 Bay, F. 81-99B
 Beckermann, C. 2754-2764A
 2765-2783A
 2784-2795A
 81-99B
 Bellet, M. 3576-3590A
 Bender, W. 2470-2478A
 Bennett, C.G. 3530-3541A
 Berns, H. 1845-1859A
 Bewlay, B.P. 3801-3808A
 Bhaduri, A. 3718-3726A
 Bhanu Sankara Rao, K. 255-267A
 851-861A
 Bhargava, S. 2985-2993A
 Bhattacharyya, A. 2359-2365A
 Bhattacharyya, P.K. 139-141B
 Biermann, H. 1003-1014A
 Bilger, P. 1823-1835A
 Biswas, S. 5-17A
 71-79A
 Bitler, W.R. 146-148B
 Blackwell, P.L. 3747-3748A
 Blakely, J. 2057-2061A
 Blakey, B.C. 555-566B
 Blue, C.A. 4011-4018A
 Blue, R.A. 4011-4018A
 Boettinger, W.J. 657-669A
 Boisson, M. 2904-2910A
 Boivin, J.-A. 322-325B
 Bonnet, C. 371-379A
 Bordia, R. 839-849A
 Borgenstam, A. 1499-1510A
 Bouchard, D. 101-113B
 Bourke, M.A.M. 2820-2836A
 Bracconi, P. 371-379A
 Braithwaite, N.St.J. 2495-2503A
 Bray, D.W. 3362-3370A
 3371-3380A
 163-175B
 Brimacombe, J.K. 4095-4111A
 4113-4120A
 271-276B
 Bronson, A. 1217-1227A
 Broyles, S.E. 269-279A
 Buchheit, T.E. 297-304B
 Bul, R.T. 1015-1023B
 371-379A
 Buisson, L. 2383-2385A
 Byrne, J.G. 1431-1440A
 Cahni, J.W. 4121-4132A
 Cantor, B. 979-986B
 Cardinale, A.M. 1431-1440A
 Carter, W.C. 3259-3266A
 Caruana, G. 231-239B
 Castello-Branco, M.A.S.C. 4205-4210A
 Catalina, A.V. 2916-2922A
 Cerri, E. 3871-3879A
 791-800A
 Chakraborty, M. 4213-4216A
 Chakravorty, D. 3466-3472A
 Chan, J.W. 2518-2531A
 Chan, K.S. 2540-2556A
 3007-3018A
 1919-1924A
 Chandramouli, V. 2708-2721A
 Chang, S. 3182-3189A
 Chang, Y. 2005-2012A
 Chao, C.-G. 809-818A
 Chao, C.G. 3809-3816A
 Chao, J. 297-304B
 Charette, A. 503-505A
 Chatterjee, S.K. 2053-2057A
 Chattopadhyay, K. 503-505A
 Chattopadhyay, S.K. 785-790A
 Chaturvedi, M.C. 1676-1682A
 Chen, G. 2429-2435A
 Chen, H. 745-756B
 Chen, J.H. 1909-1917A
 Chen, J.K. 1676-1682A
 Chen, L.H. 1683-1686A
 Chen, M.C. 1683-1686A
 Chen, R. 3662-3668A
 Chen, S. 29-40A
 3391-3398A
 2722-2726A
 1379-1394A
 2994-3006A
 2923-2933A
 567-576B
 4113-4120A
 4095-4111A
 4031-4038A
 393-398B
 610-616B
 81-99B
 Chenot, J.-L. 687-694A
 Chernov, A.A. 765-772B
 Chihara, T. 3817-3825A
 Chiu, H. 315-318B
 Cho, S.S. 1273-1281A
 Choi, B.G. 923-928A
 Choi, C.S. 2532-2539A
 Chokshi, A.H. 3335-3340A
 Choo, S.-H. 3881-3891A
 1687-1692A
 Chopra, H.D. 2005-2012A
 Chou, M.-C. 3747-3748A
 Choubey, R. 2057-2061A
 Chrysanthou, A. 555-566B
 Chu, Y.C. 4011-4018A
 Chuang, T.H. 4011-4018A
 Chun, B.S. 2904-2910A
 Chung, T.-W. 322-325B
 Clapp, P.C. 371-379A
 Claveau, A. 839-849A
 Clavel, M. 1499-1510A
 Cockcroft, S.L. 101-113B
 2820-2836A
 371-379A
 2495-2503A
 3362-3370A
 3371-3380A
 163-175B
 4095-4111A
 4113-4120A
 271-276B
 1217-1227A
 269-279A
 297-304B
 1015-1023B
 371-379A
 2383-2385A
 1431-1440A
 4121-4132A
 979-986B
 1431-1440A
 3259-3266A
 231-239B
 4205-4210A
 2916-2922A
 3871-3879A
 791-800A
 4213-4216A
 3466-3472A
 2518-2531A
 2540-2556A
 3007-3018A
 1919-1924A
 2708-2721A
 3182-3189A
 2005-2012A
 809-818A
 3809-3816A
 297-304B
 503-505A
 2053-2057A
 503-505A
 785-790A
 1676-1682A
 2429-2435A
 745-756B
 1909-1917A
 1676-1682A
 1683-1686A
 1683-1686A
 3662-3668A
 29-40A
 3391-3398A
 2722-2726A
 1379-1394A
 2994-3006A
 2923-2933A
 567-576B
 4113-4120A
 4095-4111A
 4031-4038A
 393-398B
 610-616B
 81-99B
 687-694A
 765-772B
 3817-3825A
 315-318B
 1273-1281A
 923-928A
 2532-2539A
 3335-3340A
 3881-3891A
 1687-1692A
 2005-2012A
 Chou, Y.T. 3473-3477A
 Choubey, R. 431-440A
 Chrysanthou, A. 827-838B
 Chu, Y.C. 165-182A
 Chuang, T.H. 2617-2627A
 2653-2662A
 315-318B
 29-34B
 1476-1488A
 322-325B
 3043-3058A
 119-127B
 129-137B
 1554-1568A
 2314-2327A
 687-694A
 2436-2444A
 1991-1997A
 1999-2004A
 889-894B
 717-730B
 59-69A
 2221-2228A
 801-808A
 3649-3661A
 891-900A
 1837-1844A
 2305-2313A
 1283-1292A
 707-717A
 81-99A
 1229-1240A
 1618-1629A
 4213-4216A
 3669-3674A
 763-774A
 2540-2556A
 3007-3018A
 4095-4111A
 4113-4120A
 3357-3361A
 3019-3029A
 583-593A
 2881-2887A
 2504-2509A
 3773-3780A
 1095-1110A
 794-800B
 951-960A
 43-50B
 2105-2114A
 81-99B
 794-800B
 979-986B
 879-890A
 577-584B
 585-594B
 1333-1346A
 686-689B
 695-705A
 839-845B
 3259-3266A
 305-314B
 467-469A
 1642-1654A
 3903-3912A
 71-79B
 5-17B
 241-253B
 3126-3134A
 3126-3134A
 363-374B
 577-584B
 585-594B
 2314-2327A
 3214-3225A
 1073-1080A
 2978-2984A
 3963-3970A
 1403-1405A
 3318-3329A
 1823-1835A
 183-191A
 193-203A
 2820-2836A
 481-489B
 Colvin, D.J. 1554-1568A
 Combeau, H. 2314-2327A
 Coriell, S.R. 687-694A
 Cortie, M.B. 2436-2444A
 Courtney, T.H. 1991-1997A
 1999-2004A
 889-894B
 717-730B
 Cox, A. 59-69A
 Cramb, A.W. 2221-2228A
 Cserhati, C. 801-808A
 Cul, Y.Y. 3649-3661A
 Current, P.A. 891-900A
 Czerwinski, F. 1837-1844A
 Dahn, G.S. 2305-2313A
 1283-1292A
 707-717A
 81-99A
 1229-1240A
 1618-1629A
 4213-4216A
 3669-3674A
 763-774A
 2540-2556A
 3007-3018A
 4095-4111A
 4113-4120A
 3357-3361A
 3019-3029A
 583-593A
 2881-2887A
 2504-2509A
 3773-3780A
 1095-1110A
 794-800B
 951-960A
 43-50B
 2105-2114A
 81-99B
 794-800B
 979-986B
 879-890A
 577-584B
 585-594B
 1333-1346A
 686-689B
 695-705A
 839-845B
 3259-3266A
 305-314B
 467-469A
 1642-1654A
 3903-3912A
 71-79B
 5-17B
 241-253B
 3126-3134A
 3126-3134A
 363-374B
 577-584B
 585-594B
 2314-2327A
 3214-3225A
 1073-1080A
 2978-2984A
 3963-3970A
 1403-1405A
 3318-3329A
 1823-1835A
 183-191A
 193-203A
 2820-2836A
 481-489B
 Durrant, G. 3812-3820A
 Dutrizac, J.E. 4121-4132A
 Dwarakadasa, E.S. 567-576B
 1283-1292A
 Earthman, J.C. 863-872A
 Eckert, J. 2934-2946A
 Eggeler, G. 879-890A
 Eissa, M.M. 1693-1699A
 Ekstrand, M.E. 1676-1682A
 El-Bealy, M. 689-693B
 999-1014B
 2374-2382A
 4210-4213A
 747-756A
 775-783A
 1489-1498A
 3809-3816A
 2727-2739A
 3181-3186A
 2916-2922A
 3871-3879A
 19-27B
 Evans, J.W. 2100-2104A
 Ewsuk, K.G. 2122-2129A
 4193-4204A
 2100-2104A
 2122-2129A
 1533-1543A
 747-756A
 2140-2150A
 911-920B
 3381-3390A
 3043-3058A
 2045-2046A
 255-261B
 1773-1778A
 379-384B
 979-986B
 923-928A
 1267-1271A
 2397-2418A
 3700-3717A
 819-821A
 595-609A
 863-868B
 3226-3240A
 3381-3390A
 829-837A
 1845-1859A
 1229-1240A
 1293-1302A
 2047-2050A
 794-800B
 889-894B
 407-414A
 999-1014B
 1889-1898A
 3030-3042A
 3827-3839A
 2869-2880A
 775-783A
 41-48A
 717-730B
 469-471A
 846-851B
 183-191A
 193-203A
 929-935B
 4145-4151A
 3841-3851A
 2934-2946A
 1047-1053A
 1630-1641A
 363-369A
 1925-1931A
 3621-3629A
 3491-3502A
 4121-4132A
 695-705A
 2727-2739A
 2178-2186A
 1823-1835A
 3391-3398A
 29-40A
 Fail, I. 2160-2177A
 Fang, H.-S. 1533-1543A
 Farag, M. 747-756A
 Farber, L. 2140-2150A
 Farouk, B. 911-920B
 Faulkner, R.G. 3381-3390A
 Feaugas, X. 3043-3058A
 Fedotov, V.G. 2045-2046A
 Fellner, P. 255-261B
 Feng, C. 1773-1778A
 Fernández Navarro, J.M. 379-384B
 Ferro, R. 979-986B
 Fields, R.J. 923-928A
 Fine, M.E. 1267-1271A
 2397-2418A
 Fitzgerald, T.J. 3700-3717A
 Flanagan, W.F. 819-821A
 Flemings, M.C. 595-609A
 863-868B
 3226-3240A
 3381-3390A
 829-837A
 1845-1859A
 1229-1240A
 1293-1302A
 2047-2050A
 794-800B
 889-894B
 407-414A
 999-1014B
 1889-1898A
 3030-3042A
 3827-3839A
 2869-2880A
 775-783A
 41-48A
 717-730B
 469-471A
 846-851B
 183-191A
 193-203A
 929-935B
 4145-4151A
 3841-3851A
 2934-2946A
 1047-1053A
 1630-1641A
 363-369A
 1925-1931A
 3621-3629A
 3491-3502A
 4121-4132A
 695-705A
 2727-2739A
 2178-2186A
 1823-1835A
 3391-3398A
 29-40A
 Frisk, K. 3812-3820A
 Fröba, M. 4121-4132A
 Froes, F.H. 567-576B
 Fruehan, R.J. 1283-1292A
 Fujii, Y. 863-872A
 Fukagawa, H. 2934-2946A
 Fukami-Ushiro, K.L. 183-191A
 193-203A
 Fukatsu, N. 929-935B
 Fukui, Y. 4145-4151A
 Fukuoka, C. 3841-3851A
 Fultz, B. 2934-2946A
 Funkenbusch, P.D. 1047-1053A
 Furuhara, T. 1630-1641A
 Gale, W.F. 363-369A
 1925-1931A
 3621-3629A
 3491-3502A
 4121-4132A
 695-705A
 2727-2739A
 2178-2186A
 1823-1835A
 3391-3398A
 29-40A
 Gall, K. 3812-3820A
 Gallmeault, M. 4121-4132A
 Gandin, Ch.-A. 695-705A
 2727-2739A
 2178-2186A
 1823-1835A
 3391-3398A
 29-40A
 Gangli, P. 3812-3820A
 Gantois, M. 4121-4132A
 Gao, M. 695-705A
 2727-2739A
 2178-2186A
 1823-1835A
 3391-3398A
 29-40A

Gao, Z.	2293-2298A	Han, K.N.	355-361B	Iswaran, C.V.	3524-3529A	Kim, J.	2574-2582A
García de Andrés, C.	1799-1805A	Hänninen, H.	1815-1821A		3957-3962A	Kim, N.J.	1241-1250A
García, C.I.	951-960A		2796-2808A	Itoh, G.	3081-3088A		3881-3891A
Garg, A.	3170-3180A	Hansen, G.	569-581A	Iwase, M.	375-378B	Kim, S.	1889-1898A
Garrett, R.K., Jr.	737-745A	Hansen, P.N.	4085-4093A		385-392B	Kim, S.B.	493-496A
Gassior, W.	2419-2428A	Hanumanth, G.S.	663-671B		595-603B	Kim, Y.G.	493-496A
Gaskell, D.R.	139-141B	Hao, S.M.	2429-2435A	Izaki, M.	483-486A	King, J.E.	353-361A
	693-694B	Harlow, D.G.	3391-3398A	Jackman, J.A.	431-440A		363-369A
Gatica, J.E.	3669-3674A	Hashimoto, S.	317-326A	Jackson, M.R.	3801-3808A		3019-3029A
Gauthier, J.	1785-1798A	Hatta, T.	967-972B	Jacob, K.T.	647-651B	Kirkaldy, J.S.	101-113B
Gavriljuk, V.G.	1815-1821A	Hawbolt, E.B.	1544-1553A		1919-1924A		1606-1617A
Genin, J.-M.R.	2160-2177A		3399-3409A	Jacobus, K.	3066-3073A	Kishore, R.	757-761A
Gerberich, W.W.	3793-3800A		3410-3423A	Jakobsson, A.	318-322B		3340-3343A
German, R.M.	441-450A		4095-4111A	Järvisträt, N.	501-508B	Kivlahti, J.K.	59-69A
	901-909B		4113-4120A	Jeng, S.-C.	2722-2726A		2229-2238A
Ghosh, A.	3993-4002A	He, Z.	731-736A	Jeniski, R.A., Jr.	19-27A	Klaar, H.-J.	2285-2292A
	4003-4010A	Hegazy, M.M.	1693-1699A	Jha, A.	827-838B	Klam, H.-J.	879-890A
Ghosh, A.K.	1889-1898A	Hei, Z.	1347-1352A	Jiang, H.G.	71-79B	Kleff, J.	1845-1859A
	3030-3042A	Heilmair, M.	3861-3870A	Jiang, J.-Q.	3250-3258A	Kleppe, O.J.	417-422B
	3827-3839A	Helbert, A.L.	3043-3058A	Jiang, L.	2796-2808A	Kloc, L.	3871-3879A
Ghosh, A.K.	909-921A	Hellawell, A.	229-232A	Jiang, X.-G.	863-872A	Klug, R.C.	1963-1978A
Giannuzzi, L.A.	146-148B		569-581A	Jiao, Y.	1025-1029B	Ko, S.K.	315-318B
Gibeling, J.C.	1217-1227A	Hemptenmacher, J.	1403-1405A	Jiménez, J.A.	1799-1805A	Kobayashi, S.	945-949A
Giumelli, A.	3399-3409A	Henager, C.H., Jr.	839-849A		1861-1867A	Kobayashi, T.	652-657B
Gjennes, L.	2338-2346A	Henein, H.	1045-1056B	Jo, B.L.	490-493A		1979-1989A
Glass, S.J.	2122-2129A	Heo, N.H.	1015-1020A	Johari, G.P.	2461-2469A		2013-2021A
Glatzel, U.	1229-1240A	Heo, N.H.	3059-3065A	John, R.	3074-3080A		3925-3935A
Gleeson, B.	3761-3772A	Heuzey, M.-C.	808-826B	Johnson, J.L.	441-450A	Kocaceli, D.	1015-1023B
Glikson, M.E.	557-567A	Hilbert, M.	480-483A		901-909B	Koczak, M.	2130-2139A
Gnanamorthy, J.B.	1313-1325A		1499-1510A	Johnson, W.C.	1460-1475A	Koczak, M.J.	2140-2150A
	2881-2887A	Hilpert, K.	2673-2677A	Johnson, W.L.	2934-2946A	Kodentsov, A.A.	59-69A
Goetz, R.L.	1709-1720A		3569-3575A	Jonas, J.J.	155-164A		2229-2238A
	3903-3912A		3576-3590A		232-235A	Kohtoku, Y.	3307-3317A
Goldstein, J.I.	3192-3202A	Hines, A.L.	29-34B		1303-1312A	Kornopoulos, K.	381-390A
Goller, G.	3727-3738A	Hirai, T.	4210-4213A		1869-1876A	Konno, T.J.	4210-4213A
Gomankov, V.I.	2045-2046A	Hirth, J.P.	1489-1498A		1877-1887A	Koo, Y.	3149-3161A
González, J.	281-290A	Hiskey, J.B.	393-398B		2178-2186A	Kool, B.J.	1055-1061A
	291-304A		610-616B		2347-2358A		1063-1071A
González-Carrasco, J.L.	3259-3266A	Hives, J.	255-261B		3346-3348A	Koseki, T.	3226-3240A
	3809-3816A	Ho, N.-J.	2479-2494A	Jones, R.H.	3963-3970A	Koster, J.N.	686-689B
González-Donoel, G.	1861-1867A	Ho, S.	3241-3249A	Jong, S.-H.	389-849A	Koty, D.P.	3727-3738A
	2837-2842A	Honda, K.	2843-2851A	Jong, S.-H.	1951-1962A	Koursaris, A.	287-296B
	3809-3816A	Hong, J.W.	1273-1281A	Jong-Leng, L.	633-646B	Koyama, T.	945-949A
Gooding, R.J.	1203-1216A	Hong, L.B.	2934-2946A	Jonsen, P.	2196-2208A	Krauss, G.	1554-1568A
Gopinathan, V.	3718-3726A	Hong, S.H.	493-496A	Jung, W.	51-55B		1569-1584A
Gotman, I.	2071-2079A	Hopkins, J.A.	477-480A	Justice, I.	486-490A		1845-1859A
	2130-2139A	Hort, W.	1460-1475A	Kadioglu, Y.	3491-3502A	Kroupa, A.	1963-1978A
	2140-2150A	Hoshino, H.	375-378B	Kagawa, Y.	2843-2851A	Kruger, J.	1149-1165A
	195-201B		585-603B	Kainuma, R.	2167-2195A	Kuang, Z.	1031-1044B
Gou, H.	3853-3860A	Hovland, R.	195-193B		2445-2453A	Kuehmann, C.J.	177-183B
Goulet, R.U.	3126-3134A	Howe, J.M.	1618-1629A		4153-4162A	Kumar, S.G.	937-943A
Govier, D.	459-465A		3362-3370A	Kakehi, K.	317-326A	Kuramoto, S.	1121-1126A
Gray, G.T., III	2994-3006A	Howell, P.R.	3371-3380A	Kaliappan, I.	1919-1924A	Kuranaga, T.	3081-3088A
	3739-3746A	Hsiao, Y.-H.	146-148B	Kamara, A.B.	2888-2896A	Kurita, N.	35-41B
Gray, N.B.	221-230B	Hsieh, Y.M.	891-900A	Kang, C.G.	277-285B	Kurita, N.	929-935B
	633-646B	Hsu, F.-Y.	245-253A	Kang, C.Y.	4019-4029A	Kurz, W.	625-634A
Grebe, H.A.	1749-1759A	Hsu, K.C.	2285-2292A	Kang, S.-J.L.	3120-3125A	Kuwata, M.	57-64B
Greenberg, R.R.	3682-3687A	Hu, C.	399-408B	Kannan, K.	2947-2957A	Kwon, Y.-G.	2557-2564A
Greer, A.L.	549-555A	Hu, C.	4039-4047A	Kanno, M.	3081-3088A	Kwon, D.	1241-1250A
Griffiths, J.R.	115-118B	Hu, X.	1837-1844A	Kao, W.H.	1363-1370A		3893-3901A
Gronq, Ø.	3630-3638A	Hu, Z.	1025-1029B	Kapala, J.	2673-2677A	Kwon, H.	3843-3851A
Gross, T.S.	3853-3860A	Hu, Z.Q.	71-79B	Kar, R.N.	351-354B	Lahiri, A.K.	695-697B
Groz, J.R.	1217-1227A		2221-2228A	Karjalainen, L.P.	4031-4038A		757-764B
Gruzeski, J.E.	929-936A	Huang, J.C.	2479-2494A	Karlhuber, S.	921-927B	Lakshmikantha, M.G.	961-972A
Gu, N.	719-724A		2923-2933A	Karlsson, L.	2196-2208A	Lance, J.J.	3841-3851A
	3108-3111A		3095-3107A	Karma, A.	635-656A	Landry, K.	3181-3186A
Guan, H.	1327-1331A	Huang, W.	480-483A	Karwan-Baczewska, J.	2978-2984A	Langberg, D.E.	773-779B
Guan, Y.	3621-3629A		3591-3600A	Kashyap, B.P.	2274-2284A		780-787B
Guan, Y.C.	355-361B	Huang, X.	617-632B	Kath, D.	2673-2677A	Langdon, T.G.	873-878A
Gülpen, J.H.	59-69A	Huhtala, T.	785-790A		3569-3575A		901-907A
Gundel, D.B.	2035-2043A	Hunt, J.D.	2196-2208A	Kaufman, M.J.	819-821A		2532-2539A
Guo, Q.	417-422B	Hwang, K.S.	611-623A		3524-3529A	Larson, E.M.	3871-3879A
Guo, S.Q.	2843-2851A		203-211B		3542-3557A	Last, H.R.	775-783A
Gupta, D.	695-697B		245-253A		3957-3962A	Lavens, E.J.	737-745A
	757-764B	Hwang, N.M.	2809-2819A	Kaukler, W.F.	801-808A		2115-2121A
Guthrie, R.I.L.	993-997B	Iaccoca, R.G.	145-153A	Kauppinen, V.	2796-2808A	Lee, B.J.	81-99A
Gutiérrez-Solana, F.	281-290A	Ibáñez, J.	3809-3816A	Kawakami, N.	3925-3935A	Lee, D.N.	955-966B
	291-304A	Iguchi, M.	35-41B	Kayser, W.A.	1700-1708A	Lee, H.-C.	1015-1020A
	2071-2079A		765-772B	Ke, W.	1327-1331A	Lee, H.C.	3149-3161A
Gutmanas, E.Y.	2130-2139A	Ilegbusi, O.J.	35-41B	Kestens, L.	155-164A	Lee, H.M.	3466-3472A
	2140-2150A	Ioku, S.	1668-1675A		2178-2186A	Lee, J.-H.	1749-1759A
	493-496A	Irie, K.	929-935B		2347-2358A	Lee, J.H.	3343-3346A
Haeberle, R.M.	241-253B	Irons, G.A.	195-201B	Khani, M.K.	1333-1346A	Lee, J.K.	1449-1459A
Hajra, J.P.	255-267A		663-671B	Khatak, H.S.	1313-1325A	Lee, J.K.	1273-1281A
Halford, G.R.	851-861A	Ishida, A.	3753-3759A	Kilici, A.A.	2297-2304A	Lee, K.N.	3279-3291A
	3279-3291A	Ishida, K.	2187-2195A	Kikuchi, A.	469-471A	Lee, K.R.	423-431B
Hall, M.G.	1517-1532A		2445-2453A	Kim, C.	1889-1898A	Lee, L.B.	3343-3346A
Hamano, R.	471-476A		4153-4162A	Kim, C.K.	3203-3213A	Lee, M.S.	213-219B
Hamilton, C.H.	2947-2957A	Ishida, Y.	3925-3935A	Kim, C.M.	3343-3346A	Lee, S.	1241-1250A
Hampel, F.G.	433-443B	Ishii, H.	2653-2662A	Kim, D.-Y.	51-55B		3149-3161A
Hampikian, J.M.	491-500B	Ishikuro, M.	4210-4213A	Kim, H.-J.	2557-2564A		3335-3340A
		Isono, N.	725-730A				

Lei, T.C.	3881-3891A	Mathews, C.K.	1919-1924A	Nagamori, M.	322-325B	Park, J.	2151-2159A
Lesuer, D.R.	3893-3901A	Mathews, S.A.	2858-2860A	Nagarathnam, K.	381-390A	Park, J.S.	498-498A
	391-400A	Matlock, C.A.	698-701B	Nagata, K.	658-662B		2328-2337A
	111-118A	Matlock, D.K.	1251-1266A	Nagumo, M.	489-471A		2740-2753A
	343-352A		1963-1978A		2574-2582A	Park, L.J.	493-496A
Leucht, R.	1403-1405A	Matson, D.M.	863-868B	Nagy, A.	987-992B	Park, S.-H.	1241-1250A
Levilliant, C.	81-99B	Matsuda, A.	1363-1370A	Nakagawa, Y.G.	3841-3851A	Park, S.W.	51-55B
Lewandowski, J.J.	3292-3306A	Matsuyama, Y.	3925-3935A	Nakai, H.	929-935B	Park, Y.J.	2809-2819A
	3937-3947A	Maurice, D.	1991-1997A	Nakanishi, N.	719-724A	Paro, J.	2786-2808A
			1999-2004A	Nakano, H.	4153-4162A	Pascheto, W.	2481-2469A
Leyens, C.	1700-1708A	Maziasz, P.J.	1655-1667A	Nakatsuka, T.	1807-1814A	Pascual, L.	379-384B
Li, B.J.	809-818A	Mazumdar, D.	704-708B	Nam, S.W.	490-493A	Patwardhan, A.K.	3513-3523A
Li, C.	2293-2296A	McCay, M.H.	477-480A		1273-1281A	Paul, R.L.	3682-3687A
Li, C.M.	1533-1543A	McCay, T.D.	477-480A	Namjoshi, S.	1761-1771A	Pedersen, A.S.	4085-4093A
Li, C.X.	1533-1543A	McClung, R.C.	2540-2556A	Nana, S.	2436-2444A	Pehike, R.D.	745-756B
Li, D.	2221-2228A	McDavid, R.M.	672-685B	Naohara, T.	2454-2480A		852-882B
Li, G.	509-525B	McDavid, S.M.	2151-2159A	Narayana, K.L.	3424-3430A	Pel, Y.T.	391-400A
Li, J.B.	3662-3668A	McFadden, G.B.	687-694A	Nastac, L.	351-354B	Pelton, A.D.	808-826B
Li, Q.C.	2221-2228A	McGuire, S.M.	1267-1271A		4061-4074A	Pefla, M.	271-276B
Li, S.	135-143A	McKelvey, A.L.	2704-2707A		4075-4083A	Peng, G.-J.	2923-2933A
Li, Y.	467-469A		3781-3782A	Neale, K.W.	232-235A	Peng, H.	3108-3111A
Li, Y.Z.	3473-3477A	McMahon, M.E.	2252-2262A	Nemat-Nasser, S.	1739-1748A	Peng, Z.	41-48A
Liang, J.	2293-2296A	McNelly, T.R.	2252-2262A	Nes, E.	4133-4144A	Perezpezo, J.H.	509-524A
Lichter, B.D.	819-821A	McNulty, J.C.	1899-1907A	Nethercott, R.B.	3530-3541A		533-547A
Liebligh, M.	3259-3266A	McQueen, H.J.	3478-3490A	Nicholas, T.	2239-2251A		1618-1629A
Lin, H.K.	157-162B	Meadowcroft, T.R.	3399-3409A	Nicolau, P.D.	1709-1720A	Perkins, C.A.	1251-1266A
Lin, R.Y.	527-532B	Menai, M.	81-99B		3112-3119A	Perovic, D.D.	3478-3490A
	1379-1394A	Mendelsohn, D.A.	3853-3860A		3675-3681A		4019-4029A
Lindahl, K.A.	2958-2965A	Mendiratta, M.G.	2583-2592A	Nicolini, G.	747-756A	Peter, S.	297-304B
Lindholm, M.	2897-2903A		3903-3912A	Niinomi, M.	3925-3935A	Peters, M.	1700-1708A
Lindroos, V.K.	4171-4181A	Meng, L.	3089-3094A	Nilles, P.E.	541-553B	Pickard, S.M.	909-921E
	4183-4191A	Menon, E.S.K.	1642-1654A	Nilmani, M.	773-779B	Pickles, C.A.	363-374B
Lindstrom, R.M.	3682-3687A	Meyer, W.W.	325-327B		780-787B	Pigrova, G.D.	498-502A
Lipsitt, H.A.	3801-3808A	Meyers, M.A.		Nilsson, J.-O.	327-341A	Pillai, U.T.S.	995-1001A
Liu, C.T.	3473-3477A	Michaud, V.J.	3700-3717A		2196-2208A		1283-1292A
Liu, G.	213-219A	Miki, T.	937-941B	Nioui, C.-S.	1773-1778A	Pilling, J.	229-232A
Liu, Q.	1025-1029B	Mikula, A.	921-927B	Nishida, Y.	4163-4169A	Pirttaho, L.	2057-2061A
Liu, S.	1327-1331A	Miltzer, M.	1544-1553A	Nix, W.D.	1033-1041A	Pirwitz, F.	2285-2292A
Liu, W.	2293-2296A		3399-3409A		1229-1240A	Pollock, T.M.	1081-1094A
Liu, W.-P.	1951-1962A	Miller, M.K.	763-774A	Noebe, R.D.	2628-2641A	Ponce, J.	2023-2034A
	3558-3568A	Minamino, Y.	1807-1814A		3170-3180A	Potocnik, V.	297-304B
Liu, X.J.	2429-2435A	Miodownik, A.P.	3718-3726A		3542-3557A	Potter, D.I.	491-500B
Liu, Z.	407-414A	Miracle, D.B.	2035-2043A	Nohmi, S.	1021-1031A		981-993A
Liu, Z.B.	895-900B		2583-2592A	Nomura, K.	3753-3759A	Poza, P.	486-490A
Liu, Z.T.	2904-2910A	Mishra, R.S.	305-316A	Norring, K.	327-341A	Pradhan, S.K.	4213-4216A
Lorca, J.	486-490A	Mitra, S.	3913-3923A	North, T.H.	4019-4029A	Prasad, B.K.	3513-3523A
Lloyd, D.J.	4113-4120A	Mittermeier, E.J.	1055-1061A	Nourbakhsh, S.	451-458A	Prasad, S.	465-474B
Loehman, R.E.	2100-2104A		1063-1071A	O'Handley, R.C.	3203-3213A	Prasad, Y.V.R.K.	119-126A
	2122-2129A		3445-3465A	Oda, Y.	3307-3317A		235-236A
Lombard, C.M.	3112-3119A	Miyamoto, S.	929-935B	Oh, C.-S.	955-966B		2593-2604A
Longton, R.J.	567-576B	Miyamoto, Y.	1807-1814A	Ohashi, T.	929-935B	Prikryl, M.	1149-1165A
López, F.A.	379-384B	Miyazaki, S.	3753-3759A	Ohmori, M.	401-405A	Prisbrey, K.A.	2086-2093A
	801-807B	Miyazaki, T.	945-949A	Ohta, H.	263-270B	Privett, H.M., III	3682-3687A
López, H.F.	3601-3611A	Mo, A.	2314-2327A	Ohtani, H.	943-953B	Qian, B.	4031-4038A
López-Deigado, A.	379-384B	Mogilvesky, P. DLR	2071-2079A	Ohtani, H.	2445-2453A	Qian, F.	911-920B
Lou, B.Y.	3095-3107A	Mohamed, F.A.	863-872A	Ohyu, K.	2574-2582A	Qiao, L.	3949-3956A
Lu, J.	2565-2573A	Mohan, S.	1057-1060B	Oishi, T.	839-845B		3949-3956A
Lu, S.-Z.	611-623A	Montemayor-Aldrete, J.	3330-3335A	Okabe, T.H.	839-845B	Qiao, Z.	973-978B
Lu, S.-Z.	569-581A		232-235A	Okazaki, M.	1021-1031A	Quesnel, D.J.	1047-1053A
Lu, W.-K.	195-201B	Montheillet, F.	3346-3348A	Olevsky, F.	2071-2079A	Raabe, D.	49-57A
Lui, T.S.	1683-1686A		163-175B	Olsen, A.	604-609B	Rado, C.	3181-3186A
Lum, J.W.	863-868B	Morgan, G.J.	652-657B	Olsen, S.E.	5-17B	Raghavan, V.	1127-1132A
Luo, Z.P.	1779-1784A	Morita, K.	846-851B	Olson, D.L.	2958-2965A	Raghuathan, R.	3601-3611A
Lynch, S.P.	3530-3541A		937-941B	Omi, T.	483-486A	Raghuathan, V.S.	1175-1186A
Lytle, M.T.	3503-3512A	Morita, Z.-I.	35-41B	Omori, M.	4210-4213A		2966-2977A
Ma, Y.	873-878A		765-772B	Ono, H.	846-851B	Ramachandra, C.	1167-1173A
Macció, D.	979-986B	Morris, J.W., Jr.	1187-1201A	Ono, K.	839-845B	Ramakrishnan, P.	3718-3726A
Machmeier, P.M.	2510-2517A		3466-3472A	Orel, S.V.	1925-1931A	Ramanujan, R.V.	1655-1667A
Mackenbrock, A.	869-879B	Mortensen, A.	3700-3717A	Ørsund, R.	4133-4144A	Ramos, C.	271-276B
Mahajan, Y.R.	305-316A		2419-2428A	Osman, T.M.	3937-3947A	Ranganath, S.	237-240A
Majumdar, B.	2053-2057A	Moser, Z.	829-837A	Qiyang, J.H.	391-400A	Ranganathan, S.	2966-2977A
Majumdar, B.S.	2035-2043A	Moss, S.J.	2881-2887A	Övecoglu, M.L.	1033-1041A	Rao, G.M.	1057-1060B
Maki, T.	1630-1641A	Mudali, U.K.	1003-1014A	Overfelt, R.A.	698-701B	Rao, J.G.	2366-2373A
Malakondiah, G.	2239-2251A	Mughrabi, H.	3410-3423A	Ozbayraktar, S.	287-296B	Rao, P.R.V.	1919-1924A
Malik, M.K.	2274-2284A	Mukunthan, K.	929-936A	Pagounis, E.	4171-4181A	Rappaz, M.	695-705A
Mannan, S.L.	119-126A	Mulazimoglu, M.H.	475-480B		4183-4191A		2314-2327A
Mannoy, R.R.	135-143A	Munir, Z.A.	2080-2085A	Pal, B.C.	1283-1292A		3214-3225A
Mao, X.	3817-3825A		4049-4059A	Pal, M.	4213-4216A	Rath, B.B.	1511-1516A
Marder, A.R.	481-489B	Munitz, A.	3330-3335A	Palit, S.K.	465-474B	Ratke, L.	2470-2478A
	3192-3202A	Muñoz-Andrade, D.	3761-3772A	Palle, N.	707-717A	Ratke, S.K.	788-793B
Margolin, H.	451-458A	Muralidharan, K.	2593-2604A	Palmiere, E.J.	951-960A	Ravi, M.	1283-1292A
Mari, D.	183-191A	Muralidhar, G.K.	1057-1060B	Panchanadikar, V.V.	351-354B	Ravichandran, K.S.	2383-2385A
	2820-2836A	Murphy, W.H.	1081-1094A	Pandey, A.B.	305-316A		2583-2592A
Marquis, F.	557-567A	Murray, L.E.	1773-1778A	Pandey, B.D.	465-474B	Rawers, J.	3126-3134A
Marsh, S.P.	4133-4144A	Murray, B.T.	687-694A	Pandey, R.	1544-1553A	Reddy, R.G.	1121-1126A
Martinsen, K.	3330-3335A	Murray, M.T.	115-118B	Pangborn, R.N.	3841-3851A	Reed-Hill, R.E.	3524-3529A
Martinez, E.	486-490A	Murty, B.S.	791-800A	Papangelakis, V.G.	555-566B		3957-3962A
Martinez, J.L.	3601-3611A	Musulin, I.	3530-3541A	Paradies, C.J.	2305-2313A	Ren, G.	2911-2915A
Masamura, K.	385-392B	Mutharasan, R.	911-920B	Paransky, E.	2130-2139A	Reppich, B.	3861-3870A
Mataya, M.C.	1251-1266A	Nabarro, F.R.N.	513-530A	Paray, F.	929-936A	Reuter, M.A.	1031-1044B
Matera, S.	3773-3780A			Park, D.S.	490-493A	Reynolds, W.T., Jr.	1676-1682A
				Park, H.-D.	3120-3125A	Rhee, W.H.	451-458A

Richards, N.L.	785-790A	Semeels, A.	3357-3361A	Sui, H.X.	1779-1784A	Trivedi, R.	509-824A
Richards, W.J.	3682-3687A	Seyhan, I.	2470-2478A	Sui, Z.T.	71-79B		625-634A
Rifkin, J.A.	1476-1488A	Sha, H.	305-314B	Suito, H.	57-64B		2727-2739A
Rigney, J.D.	3292-3306A	Shah, R.	1353-1362A		263-270B	Tsai, P.C.	399-408B
Rios, P.R.	1132-1134A	Shang, J.K.	205-211A		423-431B	Tsai, T.C.	2617-2627A
Ritchie, R.O.	3781-3792A		213-219A	Sukla, L.B.	943-953B	Tsubakino, H.	1668-1675A
Roberts, J.A.	2820-2836A	Shankar, P.	221-228A	Sukonnk, I.M.	351-354B	Tsukihashi, F.	967-972B
	3739-3746A	Shao, Y.	1175-1186A	Sumin, V.V.	2051-2053A	Tumbull, D.	725-730A
Robino, C.V.	65-69B	Sharfivker, V.S.	1476-1488A	Sumiyama, K.	2045-2046A	Ueda, H.	35-41B
Rodriguez, P.	1313-1325A	Sharp, W.	788-793B	Sun, H.	4210-4213A		765-772B
	2881-2887A	Shekhar, R.	923-928A	Sun, X.	852-862B	Uhrenius, B.	2869-2880A
Rohatgi, P.K.	277-285B	Shen, Y.-L.	19-27B	Sundaraman, D.	355-361B	Ullakko, K.	1815-1821A
Rokhlin, S.I.	165-182A	Sherby, O.D.	3700-3717A		1175-1186A	Ulvesson, J.H.	3630-3638A
Rolseth, S.	177-183B		111-118A	Sundman, B.	2966-2977A	Urao, R.	401-405A
	185-193B	Sherif El-Eskandarany, M.	2837-2842A	Suni, J.P.	2897-2903A	Uttomark, M.J.	533-547A
	739-744B	Shi, N.	3267-3278A	Suresh, S.	1045-1056B	Uwakweh, O.N.C.	2904-2910A
Rönkä, K.J.	2229-2238A	Shiau, M.Y.	3739-3746A	Suryanarayana, C.	3700-3717A	Vaidya, R.U.	459-465A
Root, J.H.	993-997B	Shifflet, G.J.	203-211B		41-48A	Valentini, R.	3773-3780A
Roy, N.	415-429A		1595-1605A	Suzuki, K.	1033-1041A	Valiente, A.	291-304A
Roy, T.	1167-1173A	Shigematsu, T.	3431-3444A	Suzuki, M.	4210-4213A	Van Aken, D.C.	2565-2573A
Roy, T.K.	3993-4002A	Shih, H.-C.	719-724A	Svensson, I.	3307-3317A	Van Houtte, P.	2347-2358A
	4003-4010A	Shim, J.-H.	2479-2494A	Svensson, I.L.	81-99B	Van Loo, F.J.J.	59-69A
Royal, T.E.	1761-1771A	Shimizu, K.	955-966B		2209-2220A		2229-2238A
Roytburd, A.L.	1687-1692A	Shirayanagi, I.	719-724A	Swamy, K.M.	2047-2050A	Van Loon, P.J.J.	2229-2238A
Ruano, O.A.	1861-1867A	Shtessel, V.E.	4163-4169A	Sweet, E.D.	351-354B	Van Zyl, B.P.	1203-1216A
Rubin, J.B.	2297-2304A	Sichen, D.	2852-2858A	Swinbourne, D.R.	3530-3541A	Vandermeer, R.A.	1511-1516A
Russell, K.C.	1441-1448A		318-322B	Symons, D.M.	3187-3191A	Varghese, V.	647-651B
Ruuskanen, P.R.	2297-2304A	Sikka, V.K.	409-416B	Syn, C.K.	101-110A	Varin, R.A.	5-17A
Ryum, N.	2916-2922A	Silkhai, N.	4011-4018A	Szpunar, J.A.	111-118A		71-79A
Saccone, A.	979-986B	Singh, A.K.	3669-3674A	Tacke, K.-H.	3649-3661A	Varma, S.K.	2023-2034A
Sadoway, D.R.	839-845B	Singh, J.	1167-1173A	Tada, S.	869-879B	Varona, J.M.	281-290A
Sagar, P.K.	2593-2604A	Singh, M.	3135-3148A	Tadaki, T.	1585-1594A		291-304A
Sahay, S.S.	2383-2385A	Sinha, T.K.	3669-3674A	Tagami, M.	719-724A	Vatne, H.E.	4133-4144A
Sahin, O.	451-458A	Skitzki, B.	3727-3738A	Takada, K.	1668-1675A	Vecchio, K.S.	1739-1748A
Sáinz, E.	379-384B	Skybakmoen, E.	3340-3343A	Takagishi, S.	4210-4213A	Venkateswara Rao, K.T.	3781-3792A
	801-807B	Smeltzer, W.W.	3431-3444A	Takahashi, T.	1630-1641A		
Sakai, Y.	4163-4169A	Smith, B.J.	739-744B		2187-2195A	Venugopal, S.	119-126A
Sakaki, T.	317-326A	Smith, P.M.	3649-3661A	Takagi, S.	1047-1053A	Venugopalan, H.	43-50B
Salas, D.	2023-2034A	Smouk, S.Yu.	3192-3202A	Takagishi, T.	1585-1594A	Venugopalan, R.	731-738B
Salvens, G.	3126-3134A	Soboyejo, W.O.	725-730A	Takei, A.	3753-3759A	Verhoeven, J.D.	496-498A
Samarasekera, I.V.	4095-4111A	Sohn, H.Y.	3074-3080A	Taleff, E.M.	111-118A		2328-2337A
	4113-4120A	Solheim, A.	1815-1821A	Talvite, M.	343-352A		2740-2753A
Samuel, A.M.	415-429A	Solima, A.	2263-2273A	Tamura, M.	4171-4181A	Verlinden, B.	3357-3361A
	1785-1798A	Solis, M.	213-219B	Tanabe, J.	1871-1891A	Verma, R.	1889-1898A
Samuel, F.H.	415-429A	Solnordal, C.B.	739-744B	Tanaka, M.	385-392B	Vetrano, J.S.	2947-2957A
	1785-1798A	Somers, M.A.J.	3773-3780A	Tang, S.	658-662B	Vijay, P.L.	731-738B
Sanders, T.H., Jr.	19-27A		2023-2034A	Tankala, K.	2678-2685A	Vijaya, H.S.	1057-1060B
Sano, N.	852-857B	Sommer, F.	221-230B	Tarasenko, A.V.	827-838B	Vinokur, A.	2852-2858A
	846-851B	Song, H.	1055-1061A	Tawara, E.	43-50B	Vinokur, B.B.	2852-2858A
	937-941B		1063-1071A	Tekin, A.	1815-1821A	Vinsand, T.	604-609B
Saqib, M.	491-500B	Song, S.	921-927B	Terakado, K.	967-972B	Visvesvaran, P.	973-980A
Sarkisian, A.	635-656A	Song, S.G.	51-55B	Tewari, S.N.	3727-3738A	Viswanathan, U.K.	757-761A
Sarma, B.	717-730B		1095-1110A		401-405A	Vitek, J.M.	763-774A
Sarral-Mamoory, R.	577-584B		1111-1119A		1095-1110A	Vivès, C.	445-455B
	585-594B		3381-3390A	Thadhandi, N.N.	1111-1119A		457-464B
Sathiyamoorthy, D.	731-738B		3669-3674A		1353-1362A	Voorhees, P.W.	937-943A
Sato, F.	929-935B	Sopousek, J.	3739-3746A		3669-3674A		2470-2478A
Sato, M.	3753-3759A	Serlie, M.	701-704B	Thakur, A.	3727-3738A	Voskamp, A.P.	3445-3465A
Saunders, F.I.	2605-2616A	Sosnin, V.V.	177-183B		1749-1759A	Vrestal, J.	701-704B
Sauthoff, G.	1395-1400A	Spanos, G.	2045-2046A		1761-1771A	Wadsworth, J.	343-352A
	2642-2652A	Spencer, C.W.	1517-1532A	Thanaboonsombut, B.	1739-1748A	Wagner, C.N.J.	2888-2896A
Savva, G.C.	1606-1617A	Spigarello, S.	1676-1682A		2274-2284A	Wagoner, R.H.	2605-2616A
Schaefer, M.	1293-1302A	Spooner, S.	3871-3879A		19-27A		3971-3981A
Schiffers, H.	255-267A	Stackpole, M.M.	2934-2946A	Thévoz, Ph.	695-705A	Waide, P.A.	775-783A
Schmidt, P.	81-99B	Steele, J.H.	839-849A	Thomas, B.G.	509-525B	Waku, Y.	3307-3317A
Schoenung, J.M.	2115-2121A	Steele, J.K.	3431-3444A		617-632B	Wallace, T.C., Sr.	141-146B
Schulze, T.P.	583-593A	Stefanescu, D.M.	433-443B		672-685B		433-443B
Schuster, H.	255-267A		981-993A	Thompson, A.W.	689-693B	Walls, D.P.	1899-1907A
	851-861A		2708-2721A	Thompson, R.G.	101-110A	Wan, C.C.	1363-1370A
Schwartz, D.S.	2263-2273A		4061-4074A		2692-2703A	Wang, C.-C.	3162-3169A
Schwenker, S.W.	4193-4204A		4075-4083A	Thompson, S.W.	1251-1266A	Wang, C.Y.	2754-2764A
Schwerdtfeger, K.	231-239B		4205-4210A		1554-1568A		2765-2783A
	305-314B		255-261B	Thonstad, J.	1569-1584A		2784-2795A
Schwitzgebel, G.	2419-2428A	Steube, R.S.	739-744B		177-183B	Wang, G.-X.	2285-2292A
Seetharaman, S.	318-322B	Stiller, K.	569-581A		185-193B	Wang, G.Z.	1909-1917A
	409-416B	Steen, L.	327-341A		255-261B	Wang, H.Z.	2385-2389A
	2105-2114A	Store, T.	739-744B	Tian, D.W.	4031-4038A	Wang, J.-J.	1533-1543A
	2978-2984A	Strahan, A.	3187-3191A	Tiedje, N.	4085-4093A	Wang, L.	1347-1352A
Seetharaman, V.	1933-1950A	Strehler, M.	1003-1014A	Tjong, S.C.	2385-2389A	Wang, L.L.	141-146B
	2051-2053A	Stubbergh, J.R.	604-609B		2663-2672A		433-443B
Sehiloglu, H.	3066-3073A		895-900B	Tjotta, S.	501-508B	Wang, M.	819-821A
	3491-3502A	Su, Q.	2858-2860A	Toda, H.	2013-2021A	Wang, R.	3108-3111A
Sekhar, J.A.	961-972A	Subbanna, G.N.	1057-1060B	Tornsett, A.	297-304B	Wang, S.	3318-3329A
Semiatin, S.L.	1709-1720A	Subrahmanyam, J.	237-240A	Tornslia, A.P.	2100-2104A	Wang, W.	3971-3981A
	1933-1950A	Subramanian, P.R.	1642-1654A		2122-2129A	Wang, X.-J.	3971-3981A
	2051-2053A	Subramanian, S.V.	1149-1165A	Tøndel, P.A.	2305-2313A	Wang, Z.F.	2686-2691A
	3112-3119A	Subramanian, V.	961-972A	Torchane, L.	1823-1835A	Wang, Z.G.	3662-3668A
	3675-3681A	Sudhakar, V.	704-708B	Toriama, O.	3925-3935A	Wang, Z.M.	1595-1605A
Sen, R.	503-505A	Sudhölter, S.	1031-1044B	Torres-Villaseñor, G.	3330-3335A	Warren, J.A.	657-669A
Senkov, O.N.	1303-1312A	Suh, D.	3149-3161A	Torvund, T.	3630-3638A	Warrier, S.G.	527-532B
	1869-1876A		3893-3901A	Totemeier, T.C.	353-361A		1379-1394A
	1877-1887A				363-369A		2035-2043A
	3963-3970A			Trefny, J.U.	2958-2965A	Watanabe, H.	1630-1641A

Watanabe, Y.	4145-4151A	Wolff, I.M.	1395-1400A	Yamamoto, A.	1668-1675A	Zurek, A.K.	1400-1403A
Watwe, A.S.	493-496A		2642-2652A	Yamamoto, T.	385-392B	Zeng, X.	2115-2121A
Weatherly, G.C.	1149-1165A		3688-3699A	Yamane, T.	1807-1814A	Zhang, D.L.	3983-3991A
Weaver, M.L.	1606-1617A	Won, C.W.	315-318B	Yamano-Uchi, N.	385-392B	Zhang, H.	891-900A
Webster, G.A.	3542-3557A	Wong, J.	775-783A	Yang, H.R.	3343-3346A	Zhang, J.	2094-2099A
Wei, B.	829-837A	Wu, D.	2293-2296A	Yang, J.-M.	1363-1370A		2293-2296A
Wei, R.P.	2293-2296A	Wu, L.-T.	3639-3648A	Yang, L.	2094-2099A	Zhang, L.	794-800B
	29-40A	Wu, S.K.	527-532B	Yang, S.T.	863-872A	Zhang, P.	2105-2114A
Wei, S.	3391-3398A		1379-1394A	Yang, Y.	1025-1029B		2978-2984A
Weinem, D.	973-978B	Wu, S.Q.	2385-2389A	Yang, Z.-G.	1533-1543A	Zhang, S.Q.	1779-1784A
Wells, M.E.	1700-1708A	Wu, W.	3639-3648A	Ye, F.	2263-2273A	Zhang, Z.	205-211A
Weng, G.J.	698-701B	Wu, X.	157-162B	Yegneswaran, A.H.	3513-3523A		221-228A
	317-326A	Wu, Y.	2115-2121A	Yeh, J.-W.	1951-1962A		2911-2915A
	2359-2365A	Wuttig, M.	1687-1692A		3558-3568A		3983-3991A
Wert, J.A.	127-134A		2858-2860A	Yin, F.	719-724A	Zheng, L.	3089-3094A
	269-279A	Xiao, H.	185-193B	Yitlalo, M.	49-57A	Zheng, X.L.	1533-1543A
	3503-3512A	Xing, X.	973-978B	Yokoyama, K.	2574-2582A	Zheng, Y.K.	2045-2046A
Wessén, M.	2209-2220A	Xu, C.	2094-2099A	Yoc, C.H.	3466-3472A	Zhigalina, O.M.	1047-1053A
Westwood, A.R.C.	337-350B	Xu, D.M.	2221-2228A	Yoon, D.-Y.	3120-3125A	Zhou, Y.	2094-2099A
	1413-1426A	Xu, H.B.	3662-3668A	Yoon, D.Y.	2809-2819A	Zhu, D.	819-821A
Wheeler, R.	2047-2050A	Xu, L.Y.	2429-2435A	Yoon, Y.C.	1273-1281A	Zhu, M.	2663-2672A
Whittenberger, J.D.	2628-2641A	Xu, P.	1187-1201A	Yu, D.P.	2911-2915A	Zhu, S.M.	1327-1331A
	3170-3180A	Xu, R.	2221-2228A	Yu, S.Y.	2653-2662A	Zhu, Z.	1899-1907A
Wiezorek, J.M.K.	2047-2050A	Xu, X.	1347-1352A	Yu, Z.	1347-1352A	Zok, F.W.	459-465A
Wilson, A.	2196-2208A	Xue, H.	475-480B	Zaki, M.	1043-1046A		
Windisch, C.F., Jr.	839-849A	Xue, X.M.	71-79B	Zakulski, W.	2419-2428A		
Wiskel, J.B.	119-127B	Yamada, H.	1021-1031A	Zaluska, A.	929-936A		
	129-137B	Yamada, S.	1979-1989A	Zbiral, J.	1371-1377A		



Combined Subject Index

- Abrasion resistant coatings, Mechanical properties**
Correlation of microstructure and fracture toughness in high-chromium white iron hardfacing alloys. 3881-3891A
- Abrasive wear**
The wear behavior between hardfacing materials. 3639-3648A
Influence of reinforcement volume fraction and size on the microstructure and abrasion wear resistance of hot isostatic pressed white iron matrix composites. 4171-4181A
Influence of matrix structure on the abrasion wear resistance and toughness of a hot isostatic pressed white iron matrix composites. 4183-4191A
- Abrasive wear, Coating effects**
Wear-resistant coatings produced by shock-wave compaction of powders. 2297-2304A
- Abrasives**
Friability and crushing strength of micrometer-size diamond abrasives used in microgrinding of optical glass. 1047-1053A
- Accuracy**
Solid-state contributions to densification during liquid-phase sintering. 901-909B
Studies of interface deformations in single- and multi-layered liquid baths due to an impinging gas jet. 911-920B
A thermodynamic evaluation of the Ti-Mo-C system. 955-966B
Plastic zone and pileup around large indentations. 3793-3800A
Measurement of friction under sheet forming conditions. 3971-3981A
High-temperature oxidation of Ti₃Al-based titanium aluminides in oxygen. 3993-4002A
Macrotransport-solidification kinetics modeling of equiaxed dendritic growth. II. Computation problems and validation on Inconel 718 superalloy casting. 4075-4083A
Modeling particle fracture during the extrusion of aluminum/alumina composites. 4113-4120A
- Acid leaching**
Zinc reduction of MoO₃ in a self propagating high temperature synthesis process. 315-318B
- Acoustic emission testing**
Creep deformation and damage in a continuous fiber-reinforced Ti-6Al-4V composite. 4193-4204A
- Activated sintering**
Synthesis of RuAl by reactive powder processing. 3688-3699A
- Activation**
Internal friction in hydrogen-charged CrNi and CrNiMn austenitic stainless steels. 1815-1821A
- Activation energy**
Preparation of fine copper powders from organic media by reaction with hydrogen under pressure. II. The kinetics of particle nucleation, growth, and dispersion. 585-594B
Viscosity of superalloy 718 by the oscillating vessel technique. 698-701B
Recrystallization in oxide-dispersion strengthened mechanically alloyed sheet steel. 1963-1978A
Deformation behavior of an Al-3.37 wt.% Li alloy. 2274-2284A
- Activity (chemical)**
Chemical potentials of components of the system CaO-P₂O₅-Fe₂O₃ at 1673K. 595-603B
Thermodynamics of sulfur in the BaO-MnO-SiO₂ flux system. 652-657B
Use of solid-electrolyte galvanic cells to determine the activity of CaO in the CaO-ZrO₂ system and the standard Gibbs free energies of formation of CaZrO₃ from CaO and ZrO₂. 658-662B
- Adsorption, Temperature effects**
Applicability of Butler's equation in interpreting the thermodynamic behavior of surfaces and adsorption in Fe-S-O melts. 241-253B
- Aerospace**
Materials and society—impacts and responsibilities. 337-350B
Identification of precipitate phases in a mechanically alloyed rapidly solidified Al-Fe-Ce alloy. 1033-1041A
- Aging (artificial)**
Carbide diagrams and precipitation of alloying elements during aging of low-alloy steels. 498-502A
Characterization of the formation of α_1 plates from the β_3 phase in a Cu-Zn-Au alloy. 719-724A
Mechanical properties and 95°C aging characteristics of zircon reinforced Zn-4Al-3Cu alloy. 809-818A
Microstructural stability on aging of an α - β titanium alloy: Ti-6Al-1.6Zr-3.3Mo-0.30Si. 1167-1173A
Heterogeneous nucleation of δ on dislocations in a dilute aluminum-lithium alloy. 1595-1605A
Dense CoAl-based alloys with improved ductility: solid-state synthesis and microstructure control. 2140-2150A
- Mössbauer spectroscopy study of the aging and tempering of high nitrogen quenched Fe-N alloys: kinetics of formation of Fe₁₆N₂ nitride by interstitial ordering in martensite. 2160-2177A
Effects of low-temperature aging on the microstructure and soft magnetic properties of rapidly quenched Fe-Si-B alloys. 2454-2460A
Precipitation behaviors in Al-Cu-Mg and 2024 aluminum alloys. 2479-2494A
Atmospheric stress corrosion cracking of a superplastic 7475 aluminum alloy. 2617-2627A
Influence of thermal aging on the intergranular corrosion resistance of types 304LN and 316LN stainless steels. 2881-2887A
Low quench sensitivity of superplastic 8090 Al-Li thin sheets. 2923-2933A
On the effect of stress on nucleation and growth of precipitates in an Al-Cu-Mg-Ag alloy. 3431-3444A
The plastic anisotropy of an Al-Li-Cu-Zr alloy extrusion in unidirectional deformation. 3503-3512A
Effect of aging on shape memory behavior of Ti-51.3 at.% Ni thin films. 3753-3759A
- Aging (natural), Alloying effects**
Effect of magnesium on the aging behavior of Al-Zn-Mg-Cu/Al₂O₃ metal matrix composites. 2005-2012A
- Air, Environment**
Hydrogen-induced cleavage fracture of Fe₃Al-based intermetallics. 3949-3956A
- Aircraft components, Materials selection**
Tension characteristics of notched specimens for Al-Li-Cu-Zr alloys sheets with various cerium contents. 3089-3094A
- Alkali metals, Impurities**
Effects of alkali-metal impurities on fracture toughness of 2090 Al-Li-Cu extrusions. 3530-3541A
- Alkalies, Environment**
Stress corrosion cracking of pressure vessel steels in high-temperature caustic aluminate solutions. 1327-1331A
- Alloy powders, Phase transformations**
Thermally assisted and mechanically driven solid-state reactions for formation of amorphous Al₁₃Ta₆₇ alloy powders. 3267-3278A
- Alloy powders, Phases (state of matter)**
Kinetics of phase evolution of Zn-Fe intermetallics. 2904-2916A
Incipient chemical instabilities of nanophase Fe-Cu alloys prepared by mechanical alloying. 2934-2946A
- Alloying**
The production of nickel-zinc alloys by powder injection. 780-787B
- Aluminothemic reactions, Temperature effects**
Modeling of sequential reactions during microprecipitation synthesis. 961-972A
- Aluminum, Alloying additive**
Retardation of intermetallic phase formation in experimental superferitic stainless steels. 2436-2444A
- Aluminum, Alloying elements**
Solubility of carbon in CaO-Al₂O₃ melts. 57-64B
- Aluminum, Binary systems**
Critical evaluation and optimization of the thermodynamic properties of liquid tin solutions. 808-826B
Inverse melting in binary systems: morphology and microscopy of catatctic alloys. 979-986B
Mechanistic processes influencing shock chemistry in powder mixtures of the Ti-Si, Ti-Al, and Ti-B systems. 1761-1771A
- Aluminum, Bonding**
Microstructural development in NiAl/Ni-Si-B/Ni transient liquid phase bonds. 1925-1931A
- Aluminum, Casting**
Thermomechanics of the cooling stage in casting processes: three-dimensional finite element analysis and experimental validation. 81-99B
Heat-flow-based analysis of surface crack formation during the start-up of the direct chill casting process. I. Development of the inverse heat-transfer model. 119-127B
Influence of chromium and impurities on the grain refining behavior of aluminum. 791-800A
- Aluminum, Composite materials**
Subcritical crack growth at bimaterial interfaces. I. Flexural peel technique. 205-211A
Subcritical crack growth at bimaterial interfaces. III. Shear-enhanced fatigue crack growth resistance at polymer/metal interface. 221-228A
Reinforcement stresses during deformation of sphere- and particulate-reinforced aluminum-matrix composites. 486-490A
The Bauschinger effect in a SiC/Al composite. 995-1001A
A one-phase model of the mixing of Al-SiC composite melt. 1015-1023B

- Theoretical analysis of the particle gradient distribution in centrifugal field during solidification. 1025-1029B
- Microstructure and properties of $Al_2O_3-Al(Si)$ and $Al_2O_3-Al(Si)-Si$ composites formed by in situ reaction of aluminum with aluminosilicate ceramics. 2122-2129A
- The effect of volume percent and morphology of phases on the damping behavior of epoxy-aluminum composites. 2366-2373A
- Ni_3Al intermetallic particles as wear-resistant reinforcement for Al-base composites processed by powder metallurgy. 3259-3266A
- Thermal expansion of metals reinforced with ceramic particles and microcellular foams. 3700-3717A
- Flow and fracture of bimaterial systems based on aluminum alloys. 3937-3947A
- Infiltration of fibrous preform by molten aluminum in a centrifugal force field. 4163-4169A
- Aluminum, Crystal growth**
- Crystallization of amorphous phase in sputter-deposited Ti-Al thin films. 2047-2050A
- Determination of the solidification curves of commercial aluminum alloys. 2722-2726A
- Aluminum, Diffusion**
- Anomalous diffusion of iron in liquid aluminum measured by the pulsed laser technique. 725-730A
- Aluminum, Dopants**
- Improved oxidation resistance of group VB refractory metals by Al^+ ion implantation. 491-500B
- Aluminum, Electrical properties**
- Physical modeling studies of electrolyte flow due to gas evolution and some aspects of bubble behavior in advanced Hall cells. III. Predicting the performance of advanced Hall cells. 19-27B
- Aluminum, Extraction**
- Studies on the corrosion and the behavior of inert anodes in aluminum electrolysis. 185-193B
- Electrical conductivity of molten cryolite based mixtures obtained with a tube type cell made of pyrolytic boron nitride. 255-261B
- Liquidus temperatures for primary crystallization of cryolite in molten salt systems of interest for aluminum electrolysis. 739-744B
- The transported entropy of Na^+ in solid state cryolite. 788-793B
- Reference electrode of simple galvanic cells for developing sodium sensors for use in molten aluminum. 794-800B
- Aluminum, Forming**
- Reply: Dynamic materials model. Basis and principles. 235-236A
- Aluminum, Mechanical properties**
- Communication: Mechanical deformation of dendrites by fluid flow. 229-232A
- Temperature dependence of the rate sensitivity and its effect on the activation energy for high-temperature flow. 3346-3348A
- Plastic zones and fatigue-crack closure under plane-strain double slip. 3491-3502A
- Aluminum, Oxidation**
- Reoxidation of aluminum in Fe-Al-M (M=C, Mn, and Ti) melts with $CaO-Al_2O_3-FeO$ (3 mass%) slags. 423-431B
- Aluminum, Physical properties**
- Variation of contact angles with temperature and time in the $Al-Al_2O_3$ system. 51-55B
- Aluminum, Quaternary systems**
- An isothermal section at 550°C in the Al-rich corner of the Al-Fe-Mn-Si system. 3357-3361A
- Aluminum, Rolling**
- Quantitative characterization of the surface topography of rolled sheets by laser scanning microscopy and Fourier transformation. 2338-2346A
- Modeling recrystallization kinetics, grain sizes, and textures during multipass hot rolling. 4133-4144A
- Aluminum, Ternary systems**
- Evolution of microstructures in the nickel modified titanium tri-aluminides near the L_{12} phase field. 5-17A
- Mechanical behavior of the in situ composite alloys in the Al-Ni-Ti system near the L_{12} phase field. 71-79A
- Mechanical properties of Ru-Ni-Al alloys. 1395-1400A
- Experimental study of the phase equilibria in the Fe-Mn-Al system. 2429-2435A
- Thermodynamic activities and phase boundaries for the alloys of the Ni_3Al-Ni_3Ti pseudobinary section in the Ni-Al-Ti system. 2673-2677A
- Thermodynamic activities and partial enthalpies of mixing in the solid solution of Fe in Ni_3Al . 3569-3575A
- Martensitic transformations in NiMnAl β phase alloys. 4153-4162A
- Aluminum base alloys**
- The improved microstructures and properties of 7075 alloys produced by a water-cooling centrifugal casting method. 1951-1962A
- Aluminum base alloys, Alloy development**
- Formation of aluminum-silicon alloys from feldspars—determination of silicon, light, and heavy elements in silumin by scanning electron microscopy. 604-609B
- Aluminum base alloys, Casting**
- Scaling of intragranular dendritic microstructure in ingot solidification. 101-113B
- Heat-flow-based analysis of surface crack formation during the start-up of the direct chill casting process. II. Experimental study of an AA5182 rolling ingot. 129-137B
- Porosity formation in Al-9 wt.% Si-3 wt.% Cu alloy systems: metallographic observations. 415-429A
- Effects of forced electromagnetic vibrations during the solidification of aluminum alloys. I. Solidification in the presence of crossed alternating electric fields and stationary magnetic fields. 445-455B
- Effects of forced electromagnetic vibrations during the solidification of aluminum alloys. II. Solidification in the presence of colinear variable and stationary magnetic fields. 457-464B
- The improved microstructures and properties of 7075 alloys produced by a water-cooling centrifugal casting method. 1951-1962A
- Effect of grain refinement on the fluidity of two commercial Al-Si foundry alloys. 2305-2313A
- A model for macrosegregation and its application to Al-Cu castings. 2708-2721A
- Modeling of ingot distortions during direct chill casting of aluminum alloys. 3214-3225A
- The squeeze casting of hypoeutectic binary Al-Cu. 4121-4132A
- Aluminum base alloys, Composite materials**
- Probing the initial stage of synthesis of Al_2O_3/Al composites by directed oxidation of Al-Mg alloys. 43-50B
- Subcritical crack growth at bimaterial interfaces. II. Microstructural effects on fracture resistance of metal/ceramic interfaces. 213-219A
- Transient thermal analysis of solidification in a centrifugal casting for composite materials containing particle segregation. 277-285B
- Effect of a solid solution on the steady-state creep behavior of an aluminum matrix composite. 305-316A
- Stacking faults in SiC particles and their effect on the fracture behavior of a 15 vol.% SiC/6061-Al matrix composite. 459-465A
- Effect of manganese dispersoid on the fatigue crack propagation of Al-Zn-Mg alloys. 490-493A
- The x-ray diffraction study of deformation in the composite matrix of Al-Mg-Zn and SiC. 503-505A
- Solidification of binary hypoeutectic alloy matrix composite castings. 595-609A
- Solidification of particle-reinforced metal-matrix composites. Effect of magnesium on the aging behavior of Al-Zn-Mg-Cu/ Al_2O_3 metal matrix composites. 663-671B
- 2005-2012A
- The control of grain size and distribution of particles in a (6061 alloy)/(Al_2O_3)_p composite by solutionizing treatment. 2023-2034A
- On the role of magnesium and silicon in the formation of alumina from aluminum alloys by means of DIMOX processing. 2094-2099A
- Wear behavior of aluminum-based metal matrix composites reinforced with a preform of aluminosilicate fiber. 2385-2389A
- Corrosive wear of SiC whisker- and particulate-reinforced 6061 aluminum alloy composites. 2653-2662A
- Tensile ductility and fracture of superplastic aluminum-SiC composites under thermal cycling conditions. 2837-2842A
- Failure characteristics of 6061/ Al_2O_3 /15_p and 2014/ Al_2O_3 /15_p composites as a function of loading rate. 3095-3107A
- High-temperature wear and deformation processes in metal matrix composites. 3135-3148A
- Thermal residual stresses in functionally graded and layered 6061 Al/SiC materials. 3241-3249A
- Structure of phases in the $\delta-Al_2O_3$ fiber studied by convergent beam electron diffraction. 3318-3329A
- Microstructural changes in a mechanically alloyed Al-6.2Zn-2.5Mg-1.7Cu alloy (7010) with and without particulate SiC reinforcement. 3718-3726A
- Reinforcement shape effects on the fracture behavior and ductility of particulate-reinforced 6061-Al matrix composites. 3739-3746A
- Microstructure and fracture of SiC-particulate-reinforced cast A356 aluminum alloy composites. 3893-3901A
- Flow and fracture of bimaterial systems based on aluminum alloys. 3937-3947A
- Mathematical modeling of the extrusion of 6061/ Al_2O_3 /20p composite. 4095-4111A
- Modeling particle fracture during the extrusion of aluminum/alumina composites. 4113-4120A
- Analysis of thermal residual stress in a thick-walled ring of Duralcan-base Al-SiC functionally graded material. 4145-4151A
- Aluminum base alloys, Corrosion**
- Atmospheric stress corrosion cracking of a superplastic 7475 aluminum alloy. 2617-2627A
- Aluminum base alloys, Crystal growth**
- Modeling of microsegregation in macrosegregation computations. 2314-2327A
- Determination of the solidification curves of commercial aluminum alloys. 2722-2726A
- Equiaxed dendritic solidification with convection. I. Multiscale/multiphase modeling. 2754-2764A
- Equiaxed dendritic solidification with convection. II. Numerical simulations for an Al-4 wt.% Cu alloy. 2765-2783A

- Equiaxed dendritic solidification with convection. III. Comparisons with $\text{NH}_4\text{Cl-H}_2\text{O}$ experiments. 2784-2795A
- Effects of alloy modification and thermomechanical processing on recrystallization of Al-Mg-Mn alloys. 2947-2957A
- Aluminum base alloys, Diffusion**
- Analysis on the amplitude of serrated flow associated with the Portevin-LeChatelier effect of substitutional fcc alloys. 1683-1686A
- Aluminum base alloys, Forming**
- Reply: Dynamic materials model. Basis and principles. 235-236A
- Aluminum base alloys, Heat treatment**
- A process model for on-line quenching of aluminum extrusions. 501-508B
- Low quench sensitivity of superplastic 8090 Al-Li thin sheets. 2923-2933A
- Aluminum base alloys, Mechanical properties**
- Enhanced ductility in coarse-grained Al-Mg alloys. 343-352A
- Mechanical behavior and properties of mechanically alloyed aluminum alloys. 737-745A
- A study of the influence of mischmetal additions to Al-7Si-0.3Mg (LM 25/356) alloy. 1283-1292A
- Effect of strontium modification on near-threshold fatigue crack growth in an Al-Si-Cu die cast alloy. 1293-1302A
- On microsuperplasticity in AA7475 domes. 1400-1403A
- Increased ductility in high velocity electromagnetic ring expansion. 1837-1844A
- Characterization of superplastic deformation behavior of a fine grain 5083 Al alloy sheet. 1889-1898A
- Growth behavior of microstructurally short cracks in the 6061 aluminum alloy with and without 22 vol.% SiC whiskers. 2013-2021A
- Deformation behavior of an Al-3.37 wt.% Li alloy. 2274-2284A
- Control of superplastic deformation rate during uniaxial tensile tests. 3030-3042A
- Intergranular fracture in some precipitation-hardened aluminum alloys at low temperatures. 3081-3088A
- Tension characteristics of notched specimens for Al-Li-Cu-Zr alloys sheets with various cerium contents. 3089-3094A
- Simulation of the hot-tension test under cavitating conditions. Hot deformation mechanisms of a solution-treated Al-Li-Cu-Mg-Zr alloy. 3112-3119A
- The plastic anisotropy of an Al-Li-Cu-Zr alloy extrusion in unidirectional deformation. 3478-3490A
- Effects of alkali-metal impurities on fracture toughness of 2090 Al-Li-Cu extrusions. 3503-3512A
- The cracking mechanism of silicon particles in an A357 aluminum alloy. 3530-3541A
- Microstructural evolution and superplastic deformation behavior of fine grain 5083Al. 3558-3568A
- Evidence of fracture surface interference for cracks loaded in shear detected by phase-shifted speckle interferometry. 3827-3839A
- An evaluation of the creep properties of two Al-Si alloys produced by rapid solidification processing. 3853-3860A
- Elevated temperature deformation behavior of a dispersion-strengthened Al-Fe, V, Si alloy. 3871-3879A
- The quench sensitivity of cast Al-7 wt.% Si-0.4 wt.% Mg alloy. 3913-3923A
- 3983-3991A
- Aluminum base alloys, Metal working**
- An investigation by interactive electron backscatter pattern analysis of processing and superplasticity in an aluminum-magnesium alloy. 2252-2262A
- Aluminum base alloys, Microstructure**
- The effect of iron and manganese on the recrystallization behavior of hot-rolled and solution-heat-treated aluminum alloy 6013. 19-27A
- Crystallization of amorphous alloys. 549-555A
- Numerical modeling of cellular/dendritic array growth: spacing and structure predictions. 611-623A
- Heterogeneous nucleation of δ on dislocations in a dilute aluminum-lithium alloy. 1595-1605A
- Aluminum base alloys, Phase transformations**
- Banded solidification microstructures. 625-634A
- Computer simulation of ledge migration under elastic interaction. 1489-1498A
- Phase transformations in condensed systems revisited: industrial applications. 2397-2418A
- The relationship between microstructural and plastic instability in Al-4.0 wt.% Cu alloy. 2916-2922A
- Alloy phase analysis from measurements of bulk magnetic properties. 2958-2965A
- An isothermal section at 550°C in the Al-rich corner of the Al-Fe-Mn-Si system. 3357-3361A
- Aluminum base alloys, Phases (state of matter)**
- Mechanical alloying of Nb-Al powders. 41-48A
- Nucleation controlled solidification kinetics. 533-547A
- Real time x-ray transmission microscopy of solidifying Al-In alloys. 801-808A
- Electron microscope study of Al-Fe-Si intermetallics in 6201 aluminum alloy. 929-936A
- Identification of precipitate phases in a mechanically alloyed rapidly solidified Al-Fe-Ce alloy. 1033-1041A
- A high resolution transmission electron microscopy study of interfaces between the γ , B2, and α_2 phases in a Ti-Al-Mo alloy. 1618-1629A
- Microstructural aspects of the dissolution and melting of Al_2Cu phase in Al-Si alloys during solution heat treatment. 1785-1798A
- High-resolution electron microscopy analysis of structural defects in a (2/1, 5/3)-type approximant of a decagonal quasicrystal of an Al-Pd-Mn alloy. 2911-2915A
- Aluminum base alloys, Rolling**
- Modeling recrystallization kinetics, grain sizes, and textures during multipass hot rolling. 4133-4144A
- Aluminum base alloys, Structural hardening**
- Precipitation behaviors in Al-Cu-Mg and 2024 aluminum alloys. On the effect of stress on nucleation and growth of precipitates in an Al-Cu-Mg-Ag alloy. 2479-2494A
- 3431-3444A
- Aluminum base alloys, Surface properties**
- Measurement of friction under sheet forming conditions. 3971-3981A
- Aluminum compounds**
- Martensitic transformations in NiMnAl β phase alloys. 4153-4162A
- Aluminum compounds, Alloying elements**
- Notch fracture in γ -titanium aluminides. 3903-3912A
- Aluminum compounds, Coating**
- The deposition of aluminide and silicide castings on γ -TiAl using the halide-activated pack cementation method. 3761-3772A
- Aluminum compounds, Coatings**
- Isothermal fatigue of an aluminide-coated single-crystal superalloy. I. 353-361A
- Isothermal fatigue of an aluminide-coated single-crystal superalloy. II. Effects of brittle precracking. 363-369A
- Aluminum compounds, Composite materials**
- Investigation of the reaction zone between TiAl and molybdenum. 2285-2292A
- Ni_3Al intermetallic particles as wear-resistant reinforcement for Al-base composites processed by powder metallurgy. 3259-3266A
- Aluminum compounds, Joining**
- Transient liquid-phase bonding in the NiAl/Cu/Ni system—a microstructural investigation. 3621-3629A
- Aluminum compounds, Mechanical properties**
- Non-Schmid effects on the behavior of polycrystals, with applications to Ni_3Al . 81-99A
- Effect of creep strain on microstructural stability and creep resistance of a TiAl/Ti₃Al lamellar alloy. 127-134A
- Rafting in superalloys. 513-530A
- High-temperature deformation properties of NiAl single crystals. 1229-1240A
- Influence of temperature transients on the hot workability of a two-phase gamma titanium aluminide alloy. 1933-1950A
- High-temperature low-cycle fatigue of a gamma titanium aluminide alloy Ti-46Al-2Nb-2Cr. 2239-2251A
- High-temperature deformation processing of Ti-24Al-20Nb. 2593-2604A
- Elevated temperature compressive properties of zirconium-modified NiAl. 2628-2641A
- Effect of thermomechanical treatments on the room-temperature mechanical behavior of iron aluminide Fe_3Al . 2985-2993A
- Elevated temperature compressive properties of N-doped NiAl. 3170-3180A
- High-temperature deformation and failure of an orthorhombic titanium aluminide sheet material. 3675-3681A
- Shear ligament phenomena in Fe_3Al intermetallics and micro-mechanics of shear ligament toughening. 3817-3825A
- Hydrogen-induced cleavage fracture of Fe_3Al -based intermetallics. 3949-3956A
- Aluminum compounds, Oxidation**
- High-temperature oxidation of Ti₃Al-based titanium aluminides in oxygen. 3993-4002A
- Effect of nitrogen on the oxidation behavior of Ti₃Al-based intermetallic alloys. 4003-4010A
- Aluminum compounds, Phase transformations**
- Molecular dynamics simulation of martensitic transformations in NiAl. 1476-1488A
- Effect of alloying elements on martensitic transformation in the binary NiAl(β) phase alloys. 2445-2453A
- Aluminum compounds, Powder technology**
- Mechanistic processes influencing shock chemistry in powder mixtures of the Ti-Si, Ti-Al, and Ti-B systems. 1761-1771A
- Pressure-assisted reactive synthesis of titanium aluminides from dense 50Al-50Ti elemental powder blends. 2130-2139A
- Dense CoAl-based alloys with improved ductility: solid-state synthesis and microstructure control. 2140-2150A
- Synthesis of RuAl by reactive powder processing. 3688-3699A
- Aluminum compounds, Reactions (chemical)**
- Thermodynamics of calcium and oxygen in molten titanium and titanium-aluminum alloy. 967-972B

- Aluminum compounds, Structural hardening**
Manifestations of dynamic strain aging in soft-oriented NiAl single crystals. 3542-3557A
- Aluminum compounds, Thermal properties**
Thermodynamic activities and partial enthalpies of mixing in the solid solution of Fe in Ni₃Al. 3569-3575A
- Aluminum killed steels, Crystal growth**
Austenite grain growth kinetics in Al-killed plain carbon steels. 3399-3409A
- Aluminum killed steels, Metal working**
Analysis and prevention of vertical cracking phenomena during deep drawing of hot-rolled SG295 steel strips. 1241-1250A
- Aluminum killed steels, Welding**
Forming of tailor-welded blanks. 2605-2616A
- Aluminum oxide, Composite materials**
Probing the initial stage of synthesis of Al₂O₃/Al composites by directed oxidation of Al-Mg alloys. 43-50B
Subcritical crack growth at bimaterial interfaces. II. Microstructural effects on fracture resistance of metal/ceramic interfaces. 213-219A
Transient thermal analysis of solidification in a centrifugal casting for composite materials containing particle segregation. 277-285B
Effect of a solid solution on the steady-state creep behavior of an aluminum matrix composite. 305-316A
Microstructure of Al₂O₃ fiber-reinforced superalloy (Inconel 718) composites. 451-458A
Solidification of binary hypoeutectic alloy matrix composite castings. 595-609A
Bridge toughening enhancement in double-notched MoSi₂/Nb model composites. 909-921A
Creep deformation of dispersion-strengthened copper. 1217-1227A
Effect of magnesium on the aging behavior of Al-Zn-Mg-Cu/Al₂O₃ metal matrix composites. 2005-2012A
The control of grain size and distribution of particles in a (6061 alloy)_m/(Al₂O₃)_p composite by solutionizing treatment. 2023-2034A
On the role of magnesium and silicon in the formation of alumina from aluminum alloys by means of DIMOX processing. 2094-2099A
Formation of structural intermetallics by reactive metal penetration of titanium and nickel oxides and aluminates. 2100-2104A
Failure characteristics of 6061/Al₂O₃/15_p and 2014/Al₂O₃/15_p composites as a function of loading rate. 3095-3107A
High-temperature wear and deformation processes in metal matrix composites. 3135-3148A
Structure of phases in the δ-Al₂O₃ fiber studied by convergent beam electron diffraction. 3318-3329A
A model for coupled growth of reaction layers in reactive brazing of ZrO₂-toughened Al₂O₃. 3630-3638A
Reinforcement shape effects on the fracture behavior and ductility of particulate-reinforced 6061-Al matrix composites. 3739-3746A
Mathematical modeling of the extrusion of 6061/Al₂O₃/20p composite. 4095-4111A
Modeling particle fracture during the extrusion of aluminum/alumina composites. 4113-4120A
Infiltration of fibrous preform by molten aluminum in a centrifugal force field. 4163-4169A
- Aluminum oxide, Physical properties**
Variation of contact angles with temperature and time in the Al-Al₂O₃ system. 51-55B
- Aluminum oxide, Reactions (chemical)**
Activities in CaO-SiO₂-Al₂O₃ slags and deoxidation equilibria of silicon and aluminum. 943-953B
- Amorphization, Alloying effects**
Mechanical alloying of Nb-Al powders. 41-48A
- Amorphous structure**
Crystallization of amorphous phase in sputter-deposited Ti-Al alloy thin films. 2047-2050A
- Amorphous structure, Heating effects**
Effects of low-temperature aging on the microstructure and soft magnetic properties of rapidly quenched Fe-Si-B alloys. 2454-2460A
- Amorphous structure, Temperature effects**
Crystallization of amorphous alloys. 549-555A
- Amplitude**
Multiple matrix cracking in a fiber-reinforced titanium matrix composite under high-cycle fatigue. 1899-1907A
- Anisotropy**
Effect of phase composition and hydrogen level on the deformation behavior of titanium-hydrogen alloys. 1869-1876A
- Anisotropy, Heating effects**
The plastic anisotropy of an Al-Li-Cu-Zr alloy extrusion in unidirectional deformation. 3503-3512A
- Annealing**
Effect of primary grain size on the secondary recrystallization of mechanically alloyed oxide dispersion strengthened nickel-based superalloy. 493-496A
- Transition between internal and external nitridation of Ni-Ti alloys. 1806-1817A
Influence of long term annealing on tensile properties and fracture of near-α titanium alloy Ti-6Al-2.75Sn-4Zr-0.4Mo-0.45Si. 1700-1708A
An analysis of static recrystallization during continuous, rapid heat treatment. 2051-2053A
The role of coincident site lattice boundaries during selective growth in interstitial-free steels. 2178-2186A
Orientation selective recrystallization of nonoriented electrical steels. 2347-2358A
- Anode sludge, Oxidation**
Influence of gold content on copper oxidation from silver-gold-copper alloys. 3187-3191A
- Anodes**
An extended two-dimensional mathematical model of vertical ring furnaces. 297-304B
Fundamental studies of copper anode passivation during electrorefining. II. Surface morphology. 610-616B
- Anodes, Corrosion**
Studies on the corrosion and the behavior of inert anodes in aluminum electrolysis. 185-193B
- Antimony, Impurities**
Behavior of antimony (III) during copper electrowinning in chloride solutions. 157-162B
- Armor, Mechanical properties**
Ballistic impact behavior of multilayered armor plates processed by hardfacing. 3335-3340A
- Atmospheric corrosion, Heating effects**
Atmospheric stress corrosion cracking of a superplastic 7475 aluminum alloy. 2617-2627A
- Atomic properties**
Atomistic Mechanisms of Nucleation and Growth in Solids.
- Atomic structure**
A high resolution transmission electron microscopy study of interfaces between the γ, B2, and α₂ phases in a Ti-Al-Mo alloy. 1618-1629A
- Atomic structure, Alloying effects**
Thermodynamics and long-range order of nitrogen in γ-Fe₄N_{1-x}. 1055-1061A
Precipitation in lead-calcium alloys containing tin. 1668-1675A
- Atomic structure, Composition effects**
An evaluation of the Fe-N phase diagram considering long-range order of nitrogen atoms in γ-Fe₄N_{1-x} and ε-Fe₂N_{1-x}. 1063-1071A
- Atomic structure, Radiation effects**
Sputter-induced pits on {100} nickel surfaces. 981-993A
Theory of nucleation with cluster loss and injection: application to plastic deformation and irradiation. 1441-1448A
- Atomic structure, Stress effects**
Stacking faults in SiC particles and their effect on the fracture behavior of a 15 vol.% SiC/6061-Al matrix composite. 459-465A
A study on coherency strain and precipitate morphology via a discrete atom method. 1449-1459A
Molecular dynamics simulation of martensitic transformations in NiAl. 1476-1488A
- Atomizing**
Characterization and mechanical properties of ultrahigh boron steels produced by powder metallurgy. 1861-1867A
Microstructural development of a gas-atomized and hot-pressed super-α₂ alloy. 2221-2228A
- Austempering**
Neutron diffraction study of austempered ductile iron. 923-928A
Effect of bainite transformation and retained austenite on mechanical properties of austempered spheroidal graphite cast steel. 1585-1594A
Effect of holding time in the (α+γ) temperature range on toughness of specially austempered ductile iron. 1979-1989A
- Austenite**
NiTi and NiTi-TiC composites. II. Compressive mechanical properties. 183-191A
Microstructure and tensile behavior of nitrogen-alloyed, dual-phase stainless steels. 1845-1859A
Microstructure and phase identification in type 304 stainless steel-zirconium alloys. 2151-2159A
- Austenite, Alloying effects**
The influence of niobium supersaturation in austenite on the static recrystallization behavior of low carbon microalloyed steels. 951-960A
A study on morphology and plate mean dimensions in Fe-Ni and Fe-Ni-Cr alloys. 973-980A
- Austenite, Cooling effects**
The role of grain corners in nucleation. 480-483A
Austenite decomposition during continuous cooling of an HSLA-80 plate steel. 1554-1568A

- Copper precipitation during continuous cooling and isothermal aging of A710 type steels. 1569-1584A
- Austenite, Crystal growth**
Austenite grain growth kinetics in Al-killed plain carbon steels. 3399-3409A
- Austenite, Deformation effects**
Experimental investigation of the transformation texture in hot-rolled ferritic stainless steel using single orientation determination. 49-57A
Precipitation behavior in a medium carbon, Ti-V-N microalloyed steel. 1149-1165A
- Austenite, Heating effects**
Pearlite in ultrahigh carbon steels: heat treatments and mechanical properties. 111-118A
Neutron diffraction study of austempered ductile iron. 923-928A
Effect of bainite transformation and retained austenite on mechanical properties of austempered spheroidal graphite cast steel. 1585-1594A
- Austenite, Phases (state of matter)**
Ferrite nucleation and growth during continuous cooling. 1544-1553A
- Austenite, Temperature effects**
Phase stability and atom probe field ion microscopy of type 308 CRE stainless steel weld metal. 763-774A
The driving force for martensitic transformations in low alloy steels. 1127-1132A
The formation mechanism(s), morphology, and crystallography of ferrite sideplates. 1517-1532A
- Austenitic stainless steels**
Gibbs energies of formation of chromium carbides. 1919-1924A
- Austenitic stainless steels, Casting**
Effect of superheat on the solidification structures of AISI 310S austenitic stainless steel. 287-296B
- Austenitic stainless steels, Cladding**
Ballistic impact behavior of multilayered armor plates processed by hardfacing. 3335-3340A
- Austenitic stainless steels, Coating**
Microstructural analysis and oxidation behavior of laser-processed Fe-Cr-Al-Y alloy coatings. 381-390A
- Austenitic stainless steels, Corrosion**
Studies on the influence of metallurgical variables on the stress corrosion behavior of AISI 304 stainless steel in sodium chloride solution using the fracture mechanics approach. 1313-1325A
Influence of thermal aging on the intergranular corrosion resistance of types 304LN and 316LN stainless steels. 2881-2887A
- Austenitic stainless steels, Machining**
Active wear and failure mechanisms of titanium nitride-coated high speed steel and titanium nitride-coated cemented carbide tools when machining powder metallurgically made stainless steels. 2796-2808A
- Austenitic stainless steels, Mechanical properties**
Temperature and strain-rate effects on low-cycle fatigue behavior of alloy 800H. 255-267A
Effect of multiaxial stresses on creep damage of 316 stainless steel weldments. 891-900A
Prediction of fatigue crack formation in 304 stainless steel. 1267-1271A
Internal friction in hydrogen-charged CrNi and CrNiMn austenitic stainless steels. 1815-1821A
Temperature dependence of the rate sensitivity and its effect on the activation energy for high-temperature flow. 3346-3348A
Fracture characteristics, microstructure, and tissue reaction of Ti-5Al-2.5Fe for orthopedic surgery. 3925-3935A
- Austenitic stainless steels, Metal working**
Optimization of cold and warm workability in 304 stainless steel using instability maps. 119-126A
Flow stress and microstructural evolution during hot working of alloy 22Cr-13Ni-5Mn-0.3N austenitic stainless steel. 1251-1266A
- Austenitic stainless steels, Microstructure**
Electron microscopic study of Cr₂N formation in thermally aged 316LN austenitic stainless steels. 1175-1186A
- Austenitic stainless steels, Phase transformations**
Hydride formation and decomposition in electrolytically charged metastable austenitic stainless steels. 29-40A
- Austenitic stainless steels, Phases (state of matter)**
Phase stability and atom probe field ion microscopy of type 308 CRE stainless steel weld metal. 763-774A
- Austenitic stainless steels, Welding**
Dilution in single pass arc welds. 481-489B
- Austenitic stainless steels phases (state of matter)**
Microstructure and phase identification in type 304 stainless steel-zirconium alloys. 2151-2159A
- Austenitizing**
Pearlite in ultrahigh carbon steels: heat treatments and mechanical properties. 111-118A
- Effect of holding time in the (α - γ) temperature range on toughness of specially austempered ductile iron. 1979-1989A
- Autoclaves**
A study of solid-aqueous equilibria by the speciation approach in the hydronium alunite-sulfuric acid-water system at high temperatures. 555-566B
- Automobiles**
Materials and society—impacts and responsibilities. 337-350B
- Automotive components**
Materials and society—impacts and responsibilities. 337-350B
- Automotive components, Forming**
Forming of tailor-welded blanks. 2605-2616A
- Automotive components, Materials substitution**
Microstructural evolution and superplastic deformation behavior of fine grain 5083Al. 3827-3839A
- Axial stress**
Effect of multiaxial stresses on creep damage of 316 stainless steel weldments. 891-900A
Effect of uniaxial stress on coarsening of precipitate clusters. 1460-1475A
The influence of stress triaxiality on the damage mechanisms in an equiaxed α/β Ti-6Al-4V alloy. 3043-3058A
- Backscattering**
The formation mechanism(s), morphology, and crystallography of ferrite sideplates. 1517-1532A
- Bacterial leaching**
Bioleaching of lateritic nickel ore by ultrasound. 351-354B
- Bainite**
The effects of microstructure, strength level, and crack propagation mode on stress corrosion cracking behavior of 4135 steel. 281-290A
Formation of bainite in ferrous and nonferrous alloys through sympathetic nucleation and ledge-wise growth mechanism. 1533-1543A
- Bainite, Cooling effects**
Bainite in the light of rapid continuous cooling information. 1499-1510A
Austenite decomposition during continuous cooling of an HSLA-80 plate steel. 1554-1568A
- Bainite, Heating effects**
Characterization of the formation of α_1 plates from the β_2 phase in a Cu-Zn-Au alloy. 719-724A
Bainitic microstructures formed by split isothermal transformation in an Fe-C-Si-Mn-Mo steel. 1141-1147A
Effect of bainite transformation and retained austenite on mechanical properties of austempered spheroidal graphite cast steel. 1585-1594A
- Baking**
An extended two-dimensional mathematical model of vertical ring furnaces. 297-304B
- Ball bearings, Microstructure**
Crystallographic preferred orientation induced by cyclic rolling contact loading. 3445-3465A
- Ball milling**
Tensile properties of mechanically alloyed/milled ODS-Ni-based alloys. 1371-1377A
Kinetics of phase evolution of Zn-Fe intermetallics. 2904-2910A
- Ballistic impact tests**
Ballistic impact behavior of multilayered armor plates processed by hardfacing. 3335-3340A
- Banded structure**
Microstructure and tensile behavior of nitrogen-alloyed, dual-phase stainless steels. 1845-1859A
- Banded structure, Temperature effects**
Banded solidification microstructures. 625-634A
- Barium, Quaternary systems**
Thermodynamic properties of complex oxides in the Sm-Ba-Cu-O system. 973-978B
- Bauschinger effect**
Bauschinger effect in Haynes 230 alloy: influence of strain rate and temperature. 1739-1748A
- Bearing steels, Mechanical properties**
High-temperature wear and deformation processes in metal matrix composites. 3135-3148A
- Bearing steels, Microstructure**
Crystallographic preferred orientation induced by cyclic rolling contact loading. 3445-3465A
- Bend strength, Microstructural effects**
Communication: Mechanical deformation of dendrites by fluid flow. 229-232A
Temperature dependent deformation of polydomain phases in an In-22.5 at.% Ti shape memory alloy. 1687-1692A
Microstructure and mechanical behavior of Cr-Cr₂Hf in situ intermetallic composites. 2583-2592A

- Fracture characteristics, microstructure, and tissue reaction of Ti-5Al-2.5Fe for orthopedic surgery. 3925-3935A
- Bend tests**
Failure characteristics of 6061/Al₂O₃/15p and 2014/Al₂O₃/15p composites as a function of loading rate. 3095-3107A
- Bend tests, Development**
Measurement of friction under sheet forming conditions. 3971-3981A
- Beryllium, Powder technology**
Physical chemistry of the powder metallurgy of beryllium: chemical characterization of the powder in relation to its granularity. 371-379A
- Bimetals, Mechanical properties**
Flow and fracture of bimaterial systems based on aluminum alloys. 3937-3947A
- Binary systems, Crystal growth**
Effects of shear flow and anisotropic kinetics on the morphological stability of a binary alloy. 687-694A
Modeling of microsegregation in macrosegregation computations. 2314-2327A
- Binary systems, Phases (state of matter)**
Standard enthalpies of formation of dysprosium alloys, Dy+Me (Me=Ni, Ru, Rh, Pd, Ir, and Pt), by high-temperature direct synthesis calorimetry. 417-422B
Critical evaluation and optimization of the thermodynamic properties of liquid tin solutions. 808-826B
Generalized enthalpy method for multicomponent phase change. 869-879B
Inverse melting in binary systems: morphology and microscopy of catatectic alloys. 979-986B
Control of iron nitride layers growth kinetics in the binary Fe-N system. 1823-1835A
Thermodynamic studies and the phase diagram of the Li-Mg system. 2419-2428A
A thermodynamic evaluation of the nickel-silicon system. 2897-2903A
Thermochemistry of the Ni-Hf system—intermetallic phases. 3576-3590A
Thermodynamic assessment of the Nb-N system. 3591-3600A
- Binary systems, Powder technology**
Mechanistic processes influencing shock chemistry in powder mixtures of the Ti-Si, Ti-Al, and Ti-B systems. 1761-1771A
- Binary systems, Reactions (chemical)**
Thermal decomposition of silicon carbides: discussion of "the effect of an electric field on self sustaining combustion synthesis, I and II", and author's reply. 322-325B
- Biocompatibility**
Fracture characteristics, microstructure, and tissue reaction of Ti-5Al-2.5Fe for orthopedic surgery. 3925-3935A
- Biomedical materials**
Fracture characteristics, microstructure, and tissue reaction of Ti-5Al-2.5Fe for orthopedic surgery. 3925-3935A
- Blast furnace chemistry**
Reaction equilibria in the production of manganese ferroalloys. 5-17B
Reoxidation of aluminum in Fe-Al-M (M=C, Mn, and Ti) melts with CaO-Al₂O₃-FeO (3 mass%) slags. 423-431B
- Blast furnace slags**
Reaction equilibria in the production of manganese ferroalloys. 5-17B
Water model experiment on the liquid flow behavior in a bottom blown bath with top layer. 35-41B
The use of blast furnace slag and derived materials in the vitrification of electric arc furnace dust. 379-384B
A study of the thermal decomposition of BaCO₃. 409-416B
Reoxidation of aluminum in Fe-Al-M (M=C, Mn, and Ti) melts with CaO-Al₂O₃-FeO (3 mass%) slags. 423-431B
- Blast furnace slags, Reactions (chemical)**
Preparation of glass-forming materials from granulated blast furnace slag. 801-807B
- Blowing**
The separation of the solids from the carrier gas during submerged powder injection. 773-779B
- Bonding**
Microstructure of bonding zones in laser-clad nickel-alloy-based composite coatings reinforced with various ceramic powders. 391-400A
Microstructural development in NiAl/Ni-Si-B/Ni transient liquid phase bonds. 1925-1931A
- Bonding strength**
Microstructure of Al₂O₃ fiber-reinforced superalloy (Inconel 718) composites. 451-458A
Interface effects on the micromechanical response of a transversely loaded single fiber SCS-6/Ti-6Al-4V composite. 2035-2043A
- Borides, Composite materials**
Extending the compositional limit of combustion-synthesized B₄C-TiB₂ composites by field activation. 475-480B
- Bottom blown converters**
Water model experiment on the liquid flow behavior in a bottom blown bath with top layer. 35-41B
Model study of bubble and liquid-flow characteristics in a bottom blown bath under reduced pressure. 765-772B
- Brasses, Composite materials**
Nanoscale brass/steel multilayer composites produced by cold rolling. 2383-2385A
- Brasses, Phase transformations**
Influence of training time and temperature on shape memory effect in Cu-Zn-Al alloys. 3108-3111A
- Brasses, Surface properties**
Measurement of friction under sheet forming conditions. 3971-3981A
- Breeder reactors, Materials selection**
Influence of thermal aging on the intergranular corrosion resistance of types 304LN and 316LN stainless steels. 2881-2887A
- Brinell hardness, Composition effects**
A study of the influence of mischmetal additions to Al-7Si-0.3Mg (LM 25/356) alloy. 1283-1292A
- Brittle fracture**
Simulation of the hot-tension test under cavitating conditions. 3112-3119A
- Brittle fracture, Heating effects**
Influence of long term annealing on tensile properties and fracture of near- α titanium alloy Ti-6Al-2.75Sn-4Zr-0.4Mo-0.45Si. 1700-1708A
- Brittle fracture, Welding effects**
Microstructures relevant to brittle fracture initiation at the heat-affected zone of weldment of a low carbon steel. 2574-2582A
- Brittleness**
Flow and fracture of bimaterial systems based on aluminum alloys. 3937-3947A
- Brittleness, Microstructural effects**
Bridge toughening enhancement in double-notched MoSi₂/Nb model composites. 909-921A
- Bronzes, Crystal growth**
Modeling of primary and secondary dendrites in a Cu-6 wt.% tin alloy. 4085-4093A
- Bronzes, Mechanical properties**
Characterization of the wear response of a modified zinc-based alloy vis-à-vis a conventional zinc-based alloy and a bearing bronze at a high sliding speed. 3513-3523A
- Bubbles**
Model study of bubble and liquid-flow characteristics in a bottom blown bath under reduced pressure. 765-772B
Van der Waals approximation for potassium bubbles in tungsten. 987-992B
- Bubbling**
The separation of the solids from the carrier gas during submerged powder injection. 773-779B
- Bulk modulus, Alloying effects**
Elastic moduli of titanium-hydrogen alloys in the temperature range 20°C to 1100°C. 3963-3970A
- Cadmium base alloys, Phase transformations**
Characterization of a massive transformation by microstructural analysis. 1511-1516A
- Calcium, Binary systems**
Critical evaluation and optimization of the thermodynamic properties of liquid tin solutions. 808-826B
- Calcium, Chemical analysis**
Formation of aluminum-silicon alloys from feldspars—determination of silicon, light, and heavy elements in silumin by scanning electron microscopy. 604-609B
- Calorimetry**
Standard enthalpies of formation of dysprosium alloys, Dy+Me (Me=Ni, Ru, Rh, Pd, Ir, and Pt), by high-temperature direct synthesis calorimetry. 417-422B
Thermodynamic investigations of the ternary Au-Sn-Zn system. 921-927B
Thermodynamic properties of complex oxides in the Sm-Ba-Cu-O system. 973-978B
Thermally assisted and mechanically driven solid-state reactions for formation of amorphous Al₃₃Ta₆₇ alloy powders. 3267-3278A
Martensitic transformations in NiMnAl β phase alloys. 4153-4162A
- Carbide tools, Mechanical properties**
Active wear and failure mechanisms of titanium nitride-coated high speed steel and titanium nitride-coated cemented carbide tools when machining powder metallurgically made stainless steels. 2796-2808A
- Carbides**
Effect of carbide precipitation on the creep behavior of alloy 800HT in the temperature range 700-900°C. 747-756A

- Splitting phenomena occurring in the martensitic transformation of Cr13 and CrMoV14 stainless steels in the absence of carbide precipitation. 1799-1805A
- A comparison of fracture behavior of low alloy steel with different sizes of carbide particles. 1909-1917A
- Carbides, Composite materials**
Extending the compositional limit of combustion-synthesized B_4C-TiB_2 composites by field activation. 475-480B
- Carbides, Crystal growth**
Abnormal growth of faceted (WC) grains in a (Co) liquid matrix. M_2C precipitates in isothermal tempering of high Co-Ni secondary hardening steel. 2809-2819A
- Carbides, High temperature effects**
Carbide diagrams and precipitation of alloying elements during aging of low-alloy steels. 3466-3472A
- Carbon, Alloying elements**
Structural characterization of martensitic iron-carbon alloy films electrodeposited from an iron(II) sulfate solution. Influence of titanium and carbon contents on the hydrogen trapping of microalloyed steels. 483-486A
- Carbon, Binary systems**
Thermal decomposition of silicon carbides: discussion of "the effect of an electric field on self sustaining combustion synthesis, I and II", and author's reply. Generalized enthalpy method for multicomponent phase change. 3773-3780A
- Carbon, Composite materials**
Permeability of microporous carbon preforms. Wear and friction behavior of metal impregnated microporous carbon composites. 322-325B
- Carbon, Diffusion**
Modeling of ferrite growth in nodular cast iron. Annealing and aging of interstitial C in α -Fe, as measured by internal friction. 869-879B
- Carbon, End uses**
Permeability of microporous carbon preforms. 3669-3674A
- Carbon, Impurities**
Physical chemistry of the powder metallurgy of beryllium: chemical characterization of the powder in relation to its granularity. 3727-3738A
- Carbon, Quaternary systems**
An experimental study and thermodynamic calculations of phase equilibria in the Fe-Mo-C-N system. 2209-2220A
- Carbon, Reactions (chemical)**
Reduction of FeO in smelting slags by solid carbon: experimental results. 2461-2469A
- Carbon, Solubility**
Solubility of carbon in $CaO-Al_2O_3$ melts. 3669-3674A
- Carbon, Ternary systems**
 $M_{23}C_6$ carbide equilibria in the Fe-Cr-C system. A thermodynamic evaluation of the Ti-Mo-C system. 371-379A
- Carbon dioxide, Reactions (chemical)**
Modeling and experimental study of gaseous oxidation of liquid iron alloys. 2869-2880A
- Carbon manganese steels, Irradiation**
A model describing neutron irradiation-induced segregation to grain boundaries in dilute alloys. 717-730B
- Carbon manganese steels, Mechanical properties**
A comparison of fracture behavior of low alloy steel with different sizes of carbide particles. 57-64B
- Carbon monoxide, Reactions (chemical)**
Modeling and experimental study of gaseous oxidation of liquid iron alloys. 701-704B
- Carbon steels, Casting**
Intermixing model of continuous casting during a grade transition. 955-966B
- Carbon steels, Corrosion**
Influence of microalloying on the corrosion resistance of steel in saturated calcium hydroxide. 852-862B
- Carbon steels, Phases (state of matter)**
Ferrite nucleation and growth during continuous cooling. 3381-3390A
- Carbonitrides**
Nonuniform distribution of carbonitride particles and its effect on prior austenite grain size in the simulated coarse-grained heat-affected zone of thermomechanical control-processed steels. 1909-1917A
- Carbonitriding**
Surface morphology and compound layer pores of plasma nitrocarburized low carbon steel. Simultaneous plasma treatment for carburizing and carbonitriding using hollow cathode discharge. 852-862B
- Theoretical treatment of nitriding and nitrocarburizing of iron. Corrosion fatigue in nitrocarburized quenched and tempered steels. 1073-1080A
- Carbothermic reactions**
A kinetic study of the reaction of zinc oxide with iron powder. Phase equilibria in the metal-sulfur-oxygen system and selective reduction of metal oxides and sulfides. I. The carbothermic reduction and calcination of complex mineral sulfides. Phase equilibria in the metal-sulfur-oxygen system and selective reduction of metal oxides and sulfides. I. The carbothermic reduction and calcination of complex mineral sulfides. 363-374B
- Carburizing**
Simultaneous plasma treatment for carburizing and carbonitriding using hollow cathode discharge. High cycle fatigue behavior of gas-carburized medium carbon Cr-Mo steel. 827-838B
- Case depth**
High cycle fatigue behavior of gas-carburized medium carbon Cr-Mo steel. 827-838B
- Cast iron, Melting**
Modeling and experimental study of gaseous oxidation of liquid iron alloys. 401-405A
- Cast iron, Microstructure**
Transitions between type A flake, type D flake, and coral graphite eutectic structures in cast irons. 2557-2564A
- Castability**
Effect of grain refinement on the fluidity of two commercial Al-Si foundry alloys. 2557-2564A
- Casting**
Solidification of particle-reinforced metal-matrix composites. Prediction of dendrite arm spacing for low alloy steel casting processes. 852-862B
- Casting alloys, Casting**
Effect of grain refinement on the fluidity of two commercial Al-Si foundry alloys. 2740-2753A
- Casting defects**
A model for macrosegregation and its application to Al-Cu castings. 2305-2313A
- Casting defects, Cooling effects**
Porosity formation in Al-9 wt.% Si-3 wt.% Cu alloy systems: metallographic observations. Macrotransport-solidification kinetics modeling of equiaxed dendritic growth. II. Computation problems and validation on Inconel 718 superalloy casting. 683-671B
- Casting defects, Temperature effects**
Heat-flow-based analysis of surface crack formation during the start-up of the direct chill casting process. II. Experimental study of an AA5182 rolling ingot. Modeling of ingot distortions during direct chill casting of aluminum alloys. 689-693B
- Castings, Crystal growth**
A model for macrosegregation and its application to Al-Cu castings. 2305-2313A
- Castings, Heat treatment**
Effect of bainite transformation and retained austenite on mechanical properties of austempered spheroidal graphite cast steel. 2708-2721A
- Castings, Mechanical properties**
Mechanical properties and 95°C aging characteristics of zircon reinforced Zn-4Al-3Cu alloy. Effect of strontium modification on near-threshold fatigue crack growth in an Al-Si-Cu die cast alloy. 1585-1594A
- Castings, Microstructure**
Porosity formation in Al-9 wt.% Si-3 wt.% Cu alloy systems: metallographic observations. Effects of forced electromagnetic vibrations during the solidification of aluminum alloys. II. Solidification in the presence of co-linear variable and stationary magnetic fields. Some consequences of thermosolutal convection: the grain structure of castings. Solidification of binary hypoeutectic alloy matrix composite castings. Prediction of grain structures in various solidification processes. Influence of chromium and impurities on the grain refining behavior of aluminum. Macrosegregation during dendritic arrayed growth of hypoeutectic Pb-Sn alloys: influence of primary arm spacing and mushy zone length. Phase transformations in condensed systems revisited: industrial applications. 809-818A
- Castings, Structural hardening**
Effect of magnesium on the aging behavior of Al-Zn-Mg-Cu/ Al_2O_3 metal matrix composites. 1293-1302A

- Cavitation**
The measurement of hydrogen activities in molten copper using an oxide protonic conductor. 929-935B
Characterization of superplastic deformation behavior of a fine grain 5083 Al alloy sheet. 1889-1898A
Deformation behavior of an Al-3.37 wt.% Li alloy. 2274-2284A
Simulation of the hot-tension test under cavitating conditions. 3112-3119A
- Cavitation, Deformation effects**
High-temperature deformation and failure of an orthorhombic titanium aluminide sheet material. 3675-3681A
- Cemented carbides, Coatings**
Wear-resistant coatings produced by shock-wave compaction of powders. 2297-2304A
- Cemented carbides, Powder technology**
Abnormal growth of faceted (WC) grains in a (Co) liquid matrix. 2809-2819A
- Cementite, Heating effects**
Pearlite in ultrahigh carbon steels: heat treatments and mechanical properties. 111-118A
- Centrifugal casting**
Transient thermal analysis of solidification in a centrifugal casting for composite materials containing particle segregation. 277-285B
Theoretical analysis of the particle gradient distribution in centrifugal field during solidification. 1025-1029B
The improved microstructures and properties of 7075 alloys produced by a water-cooling centrifugal casting method. 1951-1962A
- Centrifugal castings, Structural hardening**
Theoretical analysis of the particle gradient distribution in centrifugal field during solidification. 1025-1029B
- Centrifugal force**
Theoretical analysis of the particle gradient distribution in centrifugal field during solidification. 1025-1029B
Infiltration of fibrous preform by molten aluminum in a centrifugal force field. 4163-4169A
- Ceramic coatings**
Investigation of the temperature field developed by a spinning beam in laser processing. 4039-4047A
- Ceramics, Composite materials**
Microstructure of bonding zones in laser-clad nickel-alloy-based composite coatings reinforced with various ceramic powders. 391-400A
Reinforcement stresses during deformation of sphere- and particulate-reinforced aluminum-matrix composites. 486-490A
- Cerium, Alloying additive**
Tension characteristics of notched specimens for Al-Li-Cu-Zr alloys sheets with various cerium contents. 3089-3094A
- Cerium, Binary systems**
Critical evaluation and optimization of the thermodynamic properties of liquid tin solutions. 808-826B
Inverse melting in binary systems: morphology and microscopy of catatctic alloys. 979-986B
- Cerium, Dopants**
The growth and structure of thin oxide films on cerium ion-implanted nickel. 3649-3661A
- Chalcocite, Reduction (chemical)**
Kinetics of the flash converting of MK (chalcocite) concentrate. 163-175B
- Chalcopyrite, Reactions (chemical)**
Kinetics of sulfation of chalcopyrite with steam and oxygen in the presence of ferric oxide. 465-474B
- Charging**
Hydride formation and decomposition in electrolytically charged metastable austenitic stainless steels. 29-40A
- Chemical composition**
Formation of aluminum-silicon alloys from feldspars—determination of silicon, light, and heavy elements in silumin by scanning electron microscopy. 604-609B
Intermixing model of continuous casting during a grade transition. 617-632B
On the role of magnesium and silicon in the formation of alumina from aluminum alloys by means of DIMOX processing. 2094-2099A
Structural stability of super duplex stainless weld metals and its dependence on tungsten and copper. 2196-2208A
- Chemical equilibrium**
Reaction equilibria in the production of manganese ferroalloys. 5-17B
Representation of mixed reactive gases on free energy (Ellingham-Richardson) diagrams. 65-69B
- Chemical equilibrium, Alloying effects**
Identification of precipitate phases in a mechanically alloyed rapidly solidified Al-Fe-Ce alloy. 1033-1041A
- Chemical equilibrium, Cooling effects**
Vacuum evaporation of KCl-NaCl salts. II. Vaporization-rate model and experimental results. 433-443B
- Chemical potential**
Thermodynamic properties of oxygen in yttrium-oxygen solid solutions. 839-845B
- Chemical potential, Composition effects**
Thermodynamic activities and partial enthalpies of mixing in the solid solution of Fe in Ni₃Al. 3569-3575A
- Chemical processing equipment, Corrosion**
Initiation of stress corrosion cracking for pipeline steels in a carbonate-bicarbonate solution. 2686-2691A
- Chromium, Alloying elements**
A study on morphology and plate mean dimensions in Fe-Ni and Fe-Ni-Cr alloys. 973-980A
The effects on fracture toughness of ductile-phase composition and morphology in Nb-Cr-Ti and Nb-Si in situ composites. 3007-3018A
- Chromium, Binary systems**
Critical evaluation and optimization of the thermodynamic properties of liquid tin solutions. 808-826B
- Chromium, Diffusion**
Analysis of mean square penetration depth in grain boundary diffusion. 3473-3477A
- Chromium, Impurities**
Influence of chromium and impurities on the grain refining behavior of aluminum. 791-800A
- Chromium, Ternary systems**
M₂₃C₆ carbide equilibria in the Fe-Cr-C system. 701-704B
Internal sulfide precipitation in low Cr-Fe alloys. 3192-3202A
Solidification of undercooled Fe-Cr-Ni alloys. II. Microstructural evolution. 3226-3240A
- Chromium base alloys, Composite materials**
The fracture toughness of niobium-based, in situ composites. 2518-2531A
- Chromium base alloys, Corrosion**
Internal sulfide precipitation in low Cr-Fe alloys. 3192-3202A
- Chromium base alloys, Mechanical properties**
Microstructure and mechanical behavior of Cr-Cr₂Hf in situ intermetallic composites. 2583-2592A
- Chromium carbide**
Correlation of microstructure and fracture toughness in high-chromium white iron hardfacing alloys. 3881-3891A
- Chromium carbide, Physical properties**
Gibbs energies of formation of chromium carbides. 1919-1924A
- Chromium molybdenum steels, Cladding**
Solidification of an alloy 625 weld overlay. 3612-3620A
The wear behavior between hardfacing materials. 3639-3648A
- Chromium molybdenum steels, Corrosion**
The effects of microstructure, strength level, and crack propagation mode on stress corrosion cracking behavior of 4135 steel. 281-290A
A strain-based fracture model for stress corrosion cracking of low-alloy steels. 291-304A
- Chromium molybdenum steels, Heat treatment**
Simultaneous plasma treatment for carburizing and carbonitriding using hollow cathode discharge. 401-405A
Corrosion fatigue in nitrocarburized quenched and tempered steels. 1333-1346A
- Chromium molybdenum steels, Irradiation**
A model describing neutron irradiation-induced segregation to grain boundaries in dilute alloys. 3381-3390A
- Chromium molybdenum steels, Mechanical properties**
High cycle fatigue behavior of gas-carburized medium carbon Cr-Mo steel. 2557-2564A
Analysis of the stress-strain curves of a modified 9Cr-1Mo steel by the Voce equation. 3340-3343A
Effect of alloying additions on fracture behavior of molybdenum-containing secondary hardening steels. 3343-3346A
- Chromium molybdenum steels, Welding**
Effect of postweld treatment on the fatigue crack growth rate of electron-beam-welded AISI 4130 steel. 3162-3169A
- Chromium molybdenum vanadium steels, Phases (state of matter)**
Carbide diagrams and precipitation of alloying elements during aging of low-alloy steels. 498-502A
- Chromium steels, Mechanical properties**
High-temperature wear and deformation processes in metal matrix composites. 3135-3148A
- Chromium steels, Microstructure**
Crystallographic preferred orientation induced by cyclic rolling contact loading. 3445-3465A
- Circulation**
Studies of interface deformations in single- and multi-layered liquid baths due to an impinging gas jet. 911-920B
A one-phase model of the mixing of Al-SiC composite melt. 1015-1023B

Clad metals, Mechanical properties

- Ballistic impact behavior of multilayered armor plates processed by hardfacing. 3335-3340A

Cladding

- Microstructure of bonding zones in laser-clad nickel-alloy-based composite coatings reinforced with various ceramic powders. 391-400A

Cleavage

- Microstructure and tensile behavior of nitrogen-alloyed, dual-phase stainless steels. 1845-1859A
- The influence of stress triaxiality on the damage mechanisms in an equiaxed α/β Ti-6Al-4V alloy. 3043-3058A
- Loading rate and test temperature effects on fracture of in situ niobium silicide-niobium composites. 3292-3306A

Cleavage, Microstructural effects

- A comparison of fracture behavior of low alloy steel with different sizes of carbide particles. 1909-1917A

Cleavage, Welding effects

- Cleavage initiation in the intercritically reheated coarse-grained heat affected zone. II. Failure criteria and statistical effects. 3019-3029A

Coatings, Mechanical properties

- Structural characterization of martensitic iron-carbon alloy films electrodeposited from an iron(II) sulfate solution. 483-486A

Cobalt, Binary systems

- Critical evaluation and optimization of the thermodynamic properties of liquid tin solutions. 808-826B

Cobalt, Composite materials

- Abnormal growth of faceted (WC) grains in a (Co) liquid matrix. 2809-2819A

Cobalt, Extraction

- A study of solid-aqueous equilibria by the speciation approach in the hydronium alunite-sulfuric acid-water system at high temperatures. 555-566B
- Phase equilibria in the metal-sulfur-oxygen system and selective reduction of metal oxides and sulfides. I. The carbothermic reduction and calcination of complex mineral sulfides. 827-838B

Cobalt base alloys, Claddings

- The wear behavior between hardfacing materials. 3639-3648A

Cobalt base alloys, Crystal growth

- Microstructure of Cu-Co alloys solidified at various supercoolings. 4049-4059A

Cobalt base alloys, Magnetic properties

- Development of a magnetoelastic resonant sensor using iron-rich, nonzero magnetostrictive amorphous alloys. 3203-3213A

Cobalt base alloys, Phase transformations

- High-resolution transmission electron microscopy investigation of the face-centered cubic/hexagonal close-packed martensite transformation in Co-31.8 wt.% Ni alloy. I. Plate interfaces and growth ledges. 3362-3370A
- High-resolution transmission electron microscopy investigation of the face-centered cubic/hexagonal close-packed martensite transformation in Co-31.8 wt.% Ni alloy. II. Plate intersections, extended defects, and nucleation mechanisms. 3371-3380A

Cobalt compounds, Powder technology

- Dense CoAl-based alloys with improved ductility: solid-state synthesis and microstructure control. 2140-2150A

Coercive force

- Development of a magnetoelastic resonant sensor using iron-rich, nonzero magnetostrictive amorphous alloys. 3203-3213A

Coercive force, Heating effects

- Effects of low-temperature aging on the microstructure and soft magnetic properties of rapidly quenched Fe-Si-B alloys. 2454-2460A

Cold rolling

- The role of coincident site lattice boundaries during selective growth in interstitial-free steels. 2178-2186A
- Orientation selective recrystallization of nonoriented electrical steels. 2347-2358A
- Nanoscale brass/steel multilayer composites produced by cold rolling. 2383-2385A

Cold rolling, Quality control

- Quantitative characterization of the surface topography of rolled sheets by laser scanning microscopy and Fourier transformation. 2338-2346A

Cold working

- Optimization of cold and warm workability in 304 stainless steel using instability maps. 119-126A

Columnar structure, Temperature effects

- Some consequences of thermosolutal convection: the grain structure of castings. 569-581A

Combustion

- Communication: On the in situ formation of TiC and Ti₃C reinforcements in combustion-assisted synthesis of titanium matrix composites. 237-240A

- Thermal decomposition of silicon carbides: discussion of "the effect of an electric field on self sustaining combustion synthesis, I and II", and author's reply. 322-325B

- Extending the compositional limit of combustion-synthesized B₄C-TiB₂ composites by field activation. 475-480B

Combustion, Temperature effects

- Modeling of sequential reactions during micropyretic synthesis. 961-972A

Compacting

- Microstructure and tensile properties of compacted, mechanically alloyed, nanocrystalline Fe-Al. 3126-3134A

Composite materials, Synthesis

- Microstructure and properties of Al₂O₃-Al(Si) and Al₂O₃-Al(Si)-Si composites formed by in situ reaction of aluminum with aluminosilicate ceramics. 2122-2129A

Compression tests

- The relationship between microstructural and plastic instability in Al-4.0 wt.% Cu alloy. 2916-2922A
- Analysis of thermal residual stress in a thick-walled ring of Duralcan-base Al-SiC functionally graded material. 4145-4151A

Compressive strength

- Fracture and crushing strength of micrometer-size diamond abrasives used in microgrinding of optical glass. 1047-1053A

Compressive strength, Alloying effects

- Elevated temperature compressive properties of zirconium-modified NiAl. 2628-2641A
- Elevated temperature compressive properties of N-doped NiAl. 3170-3180A

Compressive strength, Microstructural effects

- NiTi and NiTi-TiC composites. II. Compressive mechanical properties. 183-191A

Compressive strength, Stress effects

- Prediction of fatigue crack formation in 304 stainless steel. 1267-1271A

Compressor blades, Nondestructive testing

- Determination of hydrogen in titanium alloys by cold neutron prompt gamma activation analysis. 3682-3687A

Computation

- A one-phase model of the mixing of Al-SiC composite melt. 1015-1023B

Computer simulation

- Materials and society—impacts and responsibilities. 337-350B
- Nucleation controlled solidification kinetics. 533-547A
- Viscosity of superalloy 718 by the oscillating vessel technique. 698-701B
- Mathematical modeling of tundish operation and flow control to reduce transition slabs. 745-756B
- Solid-state contributions to densification during liquid-phase sintering. 901-909B
- A one-phase model of the mixing of Al-SiC composite melt. 1015-1023B
- Computer simulation of reversible martensitic transformations. 1187-1201A
- Computer simulation of ledge migration under elastic interaction. 1489-1498A
- Orientation selective recrystallization of nonoriented electrical steels. 2347-2358A
- Simulation of the hot-tension test under cavitating conditions. 3112-3119A

Concentrates (ores)

- The mineralogical deportment of germanium in the Clarksville electrolytic zinc plant of Savage Zinc Inc. 567-576B

Concentration (composition)

- Intermixing model of continuous casting during a grade transition. 617-632B
- Splitting phenomena occurring in the martensitic transformation of Cr13 and CrMoV14 stainless steels in the absence of carbide precipitation. 1799-1805A
- Thermodynamic and kinetic study of diffusion paths in the system Cu-Fe-Ni. 2229-2238A
- Modeling of microsegregation in macrosegregation computations. 2314-2327A

Consolidation

- Dense CoAl-based alloys with improved ductility: solid-state synthesis and microstructure control. 2140-2150A

Contact angle, Temperature effects

- Variation of contact angles with temperature and time in the Al-Al₂O₃ system. 51-55B

Continuous annealing

- Modeling recovery and recrystallization kinetics in cold-rolled Ti-Nb stabilized interstitial-free steel. 3410-3423A

Continuous cast shapes, Crystal growth

- Analysis of shell thickness irregularity in continuously cast middle carbon steel slabs using mold thermocouple data. 1045-1056B

Continuous cast shapes, Diffusion

- Modeling of the peritectic reaction and macro-segregation in casting of low carbon steel. 999-1014B

Continuous casting

Effects of forced electromagnetic vibrations during the solidification of aluminum alloys. II. Solidification in the presence of colinear variable and stationary magnetic fields.

457-464B

Intermixing model of continuous casting during a grade transition.

617-632B

Flow and thermal behavior of the top surface flux/powder layers in continuous casting molds.

672-685B

Prediction of grain structures in various solidification processes.

695-705A

Cold model study of the surface profile in a continuous slab casting mold: effect of second phase.

695-697B

Mathematical modeling of tundish operation and flow control to reduce transition slabs.

745-756B

A water model study of the flow asymmetry inside a continuous slab casting mold.

757-764B

Modeling of the peritectic reaction and macro-segregation in casting of low carbon steel.

999-1014B

Analysis of shell thickness irregularity in continuously cast middle carbon steel slabs using mold thermocouple data.

1045-1056B

Convection

Some consequences of thermosolutal convection: the grain structure of castings.

569-581A

Time dependence of tip morphology during cellular/dendritic arrayed growth.

1111-1119A

Convection, Field effects

Convection during thermally unstable solidification of Pb-Sn in a magnetic field.

1095-1110A

Cooling rate

Solidification of particle-reinforced metal-matrix composites. Radioscopic visualization of isothermal solidification of eutectic Ga-In alloy.

663-671B

Prediction of dendrite arm spacing for low alloy steel casting processes.

686-689B

Modeling of the peritectic reaction and macro-segregation in casting of low carbon steel.

689-693B

Ferrite nucleation and growth during continuous cooling.

999-1014B

Austenite decomposition during continuous cooling of an HSLA-80 plate steel.

1544-1553A

The quench sensitivity of cast Al-7 wt.% Si-0.4 wt.% Mg alloy. Macrotransport-solidification kinetics modeling of equiaxed dendritic growth. II. Computation problems and validation on Inconel 718 superalloy casting.

1554-1568A

3983-3991A

4075-4083A

Cooling rate, Pressure effects

The squeeze casting of hypoeutectic binary Al-Cu.

4121-4132A

Copper, Alloying additive

Retardation of intermetallic phase formation in experimental superferitic stainless steels.

2436-2444A

The effect of metallic elements on the crystallization behavior of amorphous Fe-Si-B alloys.

3424-3430A

Copper, Binary systems

Critical evaluation and optimization of the thermodynamic properties of liquid tin solutions.

808-826B

Generalized enthalpy method for multicomponent phase change.

869-879B

Copper, Composite materials

Crep deformation of dispersion-strengthened copper.

1217-1227A

Thermal expansion of metals reinforced with ceramic particles and microcellular foams.

3700-3717A

Copper, Crystal growth

Aspects of dynamic recrystallization in shaped charge and explosively formed projectile devices.

1773-1778A

Copper, Diffusion

Anomalous diffusion of iron in liquid aluminum measured by the pulsed laser technique.

725-730A

Incipient chemical instabilities of nanophase Fe-Cu alloys prepared by mechanical alloying.

2934-2946A

Copper, Extraction

Kinetics of the flash converting of MK (chalcocite) concentrate. Kinetics of sulfation of chalcocite with steam and oxygen in the presence of ferric oxide.

163-175B

465-474B

Phase equilibria in the metal-sulfur-oxygen system and selective reduction of metal oxides and sulfides. I. The carbothermic reduction and calcination of complex mineral sulfides.

827-838B

Copper, Forming

Reply: Dynamic materials model. Basis and principles.

235-236A

Copper, Mechanical properties

The interrelationship between grain boundary sliding and cavitation during creep of polycrystalline copper.

901-907A

Increased ductility in high velocity electromagnetic ring expansion.

1837-1844A

Temperature dependence of the rate sensitivity and its effect on the activation energy for high-temperature flow.

3346-3348A

Plastic zones and fatigue-crack closure under plane-strain double slip.

3491-3502A

Copper, Oxidation

Oxidation-reduction equilibrium of $\text{Cu}^{2+}/\text{Cu}^+$ in binary alkaline sulfate melts.

385-392B

Copper, Powder technology

Preparation of fine copper powders from organic media by reaction with hydrogen under pressure. I. Experimental study.

577-584B

Preparation of fine copper powders from organic media by reaction with hydrogen under pressure. II. The kinetics of particle nucleation, growth, and dispersion.

585-594B

Milling dynamics. III. Integration of local and global modeling of mechanical alloying devices.

1999-2004A

Copper, Quaternary systems

Thermodynamic properties of complex oxides in the Sm-Ba-Cu-O system.

973-978B

Copper, Reactions (chemical)

Behavior of antimony (III) during copper electrowinning in chloride solutions.

157-162B

Transient liquid-phase bonding in the NiAl/Cu/Ni system—a microstructural investigation.

3621-3629A

Copper, Refining

Fundamental studies of copper anode passivation during electrorefining. I. Development of techniques.

393-398B

Fundamental studies of copper anode passivation during electrorefining. II. Surface morphology.

610-616B

The measurement of hydrogen activities in molten copper using an oxide protonic conductor.

929-935B

Influence of gold content on copper oxidation from silver-gold-copper alloys.

3187-3191A

Copper, Solubility

Solid-state contributions to densification during liquid-phase sintering.

901-909B

Copper, Ternary systems

Thermodynamic and kinetic study of diffusion paths in the system Cu-Fe-Ni.

2229-2238A

Copper base alloys

Thermoelastic martensite and shape memory effect in ductile Cu-Al-Mn alloys.

2187-2195A

Copper base alloys, Composite materials

Transient thermal analysis of solidification in a centrifugal casting for composite materials containing particle segregation.

277-285B

Permeability of microporous carbon preforms.

3669-3674A

Wear and friction behavior of metal impregnated microporous carbon composites.

3727-3738A

Copper base alloys, Corrosion

Discussion of "a fully plastic microcracking model for transgranular stress corrosion cracking in planar slip materials" and reply.

819-821A

Copper base alloys, Crystal growth

Microstructure of Cu-Co alloys solidified at various supercoolings.

4049-4059A

Copper base alloys, Diffusion

Average effective interdiffusion coefficients and the Matano plane composition.

2504-2509A

Incipient chemical instabilities of nanophase Fe-Cu alloys prepared by mechanical alloying.

2934-2946A

Copper base alloys, Forming

Reply: Dynamic materials model. Basis and principles.

235-236A

Copper base alloys, Mechanical properties

Predicting the orientation-dependent stress-induced transformation and detwinning response of shape memory alloy single crystals.

269-279A

The characteristics of cavitation in superplastic metals and ceramics.

873-878A

A model study of cavity growth in superplasticity using single premachined holes.

2532-2539A

Copper base alloys, Microstructure

Prediction of grain structures in various solidification processes.

695-705A

Copper base alloys, Phase transformations

A new characterization method of the microstructure using the macroscopic composition gradient in alloys.

945-949A

Thermoelastic martensite and shape memory effect in ductile Cu-Al-Mn alloys.

2187-2195A

Copper base alloys, Phases (state of matter)

Characterization of the formation of α_1 plates from the β_2 phase in a Cu-Zn-Au alloy.

719-724A

Formation of bainite in ferrous and nonferrous alloys through sympathetic nucleation and ledge growth mechanism.

1533-1543A

Copper compounds, Synthesis

Synthesis of nanocrystalline Ni_3Cu by sol-gel route.

4213-4216A

Corrosion environments

On the transition of fatigue crack growth from stage I to stage II in a corrosive environment. 471-476A

Studies on the influence of metallurgical variables on the stress corrosion behavior of AISI 304 stainless steel in sodium chloride solution using the fracture mechanics approach. 1313-1325A

Stress corrosion cracking of pressure vessel steels in high-temperature caustic aluminate solutions. 1327-1331A

Corrosion fatigue

The influence of aqueous environments on low ΔK and high ΔK fatigue crack propagation behavior in low carbon structural steels. 2678-2685A

Corrosion fatigue, Heating effects

Corrosion fatigue in nitrocarburized quenched and tempered steels. 1333-1346A

Corrosion potential, Alloying effects

Influence of microalloying on the corrosion resistance of steel in saturated calcium hydroxide. 1693-1699A

Corrosion rate

Studies on the corrosion and the behavior of inert anodes in aluminum electrolysis. 185-193B

Corrosion resistance

The improved microstructures and properties of 7075 alloys produced by a water-cooling centrifugal casting method. 1951-1962A

Corrosive wear of SiC whisker- and particulate-reinforced 6061 aluminum alloy composites. 2653-2662A

Effects of the alumina scale on the room-temperature tensile behavior of preoxidized MA 956. 3809-3816A

Corrosion resistance, Alloying effects

Influence of microalloying on the corrosion resistance of steel in saturated calcium hydroxide. 1693-1699A

Corrosion resistance, Heating effects

Influence of thermal aging on the intergranular corrosion resistance of types 304LN and 316LN stainless steels. 2881-2887A

Corrosion resistance, Microstructural effects

Retardation of intermetallic phase formation in experimental superferitic stainless steels. 2436-2444A

Corrosion resistance, Welding effects

Microstructural aspects of sulfide stress cracking in an API X-80 pipeline steel. 3601-3611A

Corrosion resistant steels

$M_{23}C_6$ carbide equilibria in the Fe-Cr-C system. 701-704B

Corrosive wear

Corrosive wear of SiC whisker- and particulate-reinforced 6061 aluminum alloy composites. 2653-2662A

Crack closure

Plastic zones and fatigue-crack closure under plane-strain double slip. 3491-3502A

Crack closure, Composition effects

Growth behavior of microstructurally short cracks in the 6061 aluminum alloy with and without 22 vol.% SiC whiskers. 2013-2021A

Crack initiation

An experimental and theoretical investigation of the rapid consolidation of continuously reinforced, metal-matrix composites. 1709-1720A

Deformation behavior of an Al-3.37 wt.% Li alloy. 2274-2284A

Copper-bearing high-strength low-alloy steels: the influence of microstructure on the initiation and growth of small fatigue cracks. 2540-2556A

Observation of short fatigue crack-growth process in SiC-fiber-reinforced Ti-15-3 alloy composite. 2843-2851A

Ballistic impact behavior of multilayered armor plates processed by hardfacing. 3335-3340A

Crack initiation, Coating effects

Isothermal fatigue of an aluminide-coated single-crystal superalloy. I. 353-361A

Crack initiation, Deformation effects

Analysis and prevention of vertical cracking phenomena during deep drawing of hot-rolled SG295 steel strips. 1241-1250A

Crack initiation, Heating effects

A strain-based fracture model for stress corrosion cracking of low-alloy steels. 291-304A

Effect of homogenization heat treatment on the microstructure and heat affected zone microfissuring in welded cast alloy 718. 785-790A

Crack initiation, Impurity effects

The effect of hydrogen on the fracture of alloy X-750. 101-110A

Crack initiation, Microstructural effects

Subcritical crack growth at bimaterial interfaces. II. Microstructural effects on fracture resistance of metal/ceramic interfaces. 213-219A

Creep deformation and crack growth behavior of a single-crystal nickel-base superalloy. 829-837A

Crack initiation, Stress effects

Subcritical crack growth at bimaterial interfaces. I. Flexural peel technique. 205-211A

Temperature and strain-rate effects on low-cycle fatigue behavior of alloy 800H. 255-267A

Stacking faults in SiC particles and their effect on the fracture behavior of a 15 vol.% SiC/6061-Al matrix composite. 459-485A

Detecting stable crack onset at ductile-brittle transition in steels. 469-471A

Reinforcement stresses during deformation of sphere- and particulate-reinforced aluminum-matrix composites. 486-490A

Discussion of "a fully plastic microcracking model for transgranular stress corrosion cracking in planar slip materials" and reply. 819-821A

Mechanisms of high-temperature fatigue failure in alloy 800H. 851-861A

Prediction of fatigue crack formation in 304 stainless steel. 1267-1271A

Crack initiation, Temperature effects

Heat-flow-based analysis of surface crack formation during the start-up of the direct chill casting process. I. Development of the inverse heat-transfer model. 119-127B

Heat-flow-based analysis of surface crack formation during the start-up of the direct chill casting process. II. Experimental study of an AA5182 rolling ingot. 129-137B

Isothermal fatigue of an aluminide-coated single-crystal superalloy. II. Effects of brittle precracking. 363-369A

Crack initiation, Welding effects

Cleavage initiation in the intercritically reheated coarse-grained heat affected zone. II. Failure criteria and statistical effects. 3019-3029A

Crack opening displacement

Effects of alkali-metal impurities on fracture toughness of 2090 Al-Li-Cu extrusions. 3530-3541A

Crack opening displacement, Welding effects

Cleavage initiation in the intercritically reheated coarse-grained heat affected zone. II. Failure criteria and statistical effects. 3019-3029A

Crack propagation

Copper-bearing high-strength low-alloy steels: the influence of microstructure on the initiation and growth of small fatigue cracks. 2540-2556A

Observation of short fatigue crack-growth process in SiC-fiber-reinforced Ti-15-3 alloy composite. 2843-2851A

The effects on fracture toughness of ductile-phase composition and morphology in Nb-Cr-Ti and Nb-Si in situ composites. 3007-3018A

Microstructure and tensile properties of compacted, mechanically alloyed, nanocrystalline Fe-Al. 3126-3134A

Plastic zones and fatigue-crack closure under plane-strain double slip. 3491-3502A

Effects of alkali-metal impurities on fracture toughness of 2090 Al-Li-Cu extrusions. 3530-3541A

The balance of mechanical and environmental properties of a multielement niobium-niobium silicide-based in situ composite. 3801-3808A

Conditioning monitoring by microstructural evaluation of cumulative fatigue damage. 3841-3851A

Crack propagation, Alloying effects

Effect of strontium modification on near-threshold fatigue crack growth in an Al-Si-Cu die cast alloy. 1293-1302A

Crack propagation, Composition effects

Effect of manganese dispersoid on the fatigue crack propagation of Al-Zn-Mg alloys. 490-493A

Growth behavior of microstructurally short cracks in the 6061 aluminum alloy with and without 22 vol.% SiC whiskers. 2013-2021A

Crack propagation, Deformation effects

Analysis and prevention of vertical cracking phenomena during deep drawing of hot-rolled SG295 steel strips. 1241-1250A

Crack propagation, Diffusion effects

Hydrogen-induced cleavage fracture of Fe₃Al-based intermetallics. 3949-3956A

Crack propagation, Environmental effects

On the transition of fatigue crack growth from stage I to stage II in a corrosive environment. 471-476A

Studies on the influence of metallurgical variables on the stress corrosion behavior of AISI 304 stainless steel in sodium chloride solution using the fracture mechanics approach. 1313-1325A

The influence of aqueous environments on low ΔK and high ΔK fatigue crack propagation behavior in low carbon structural steels. 2678-2685A

Microstructural aspects of sulfide stress cracking in an API X-80 pipeline steel. 3601-3611A

Crack propagation, Heating effects

A strain-based fracture model for stress corrosion cracking of low-alloy steels. 291-304A

Crack propagation, Impurity effects

The effect of hydrogen on the fracture of alloy X-750. 101-110A

Crack propagation, Microstructural effects

- The effects of microstructure, strength level, and crack propagation mode on stress corrosion cracking behavior of 4135 steel. 281-290A
- Creep deformation and crack growth behavior of a single-crystal nickel-base superalloy. 829-837A
- Bridge toughening enhancement in double-notched MoSi_2/Nb model composites. 909-921A
- Crystallographic preferred orientation induced by cyclic rolling contact loading. 3445-3465A
- Fracture and fatigue-crack growth behavior in ductile-phase toughened molybdenum disilicide: effects of niobium wire vs. particulate reinforcements. 3781-3792A

Crack propagation, Radiation effects

- The effect of high-energy electron-beam irradiation on microstructural modification of a high-speed steel roll. 3149-3161A

Crack propagation, Stress effects

- Subcritical crack growth at bimaterial interfaces. I. Flexural peel technique. 205-211A
- Subcritical crack growth at bimaterial interfaces. III. Shear-enhanced fatigue crack growth resistance at polymer/metal interface. 221-228A
- Temperature and strain-rate effects on low-cycle fatigue behavior of alloy 800H. 255-267A
- Stacking faults in SiC particles and their effect on the fracture behavior of a 15 vol.% SiC/6061-Al matrix composite. 459-465A
- Detecting stable crack onset at ductile-brittle transition in steels. 469-471A
- Reinforcement stresses during deformation of sphere- and particulate-reinforced aluminum-matrix composites. 486-490A
- Time-dependent, environmentally assisted crack growth in Nicalon-fiber-reinforced SiC composites at elevated temperatures. 839-849A
- Mechanisms of high-temperature fatigue failure in alloy 800H. 851-861A
- Evidence of fracture surface interference for cracks loaded in shear detected by phase-shifted speckle interferometry. 3853-3860A

Crack propagation, Temperature effects

- Heat-flow-based analysis of surface crack formation during the start-up of the direct chill casting process. I. Development of the inverse heat-transfer model. 119-127B
- Heat-flow-based analysis of surface crack formation during the start-up of the direct chill casting process. II. Experimental study of an AA5182 rolling ingot. 129-137B
- Isothermal fatigue of an aluminide-coated single-crystal superalloy. II. Effects of brittle precracking. 363-369A
- Temperature dependence of the intrinsic small fatigue crack growth behavior in nickel-base superalloys based on measurement of crack closure. 1021-1031A

Crack propagation, Welding effects

- Effect of postweld treatment on the fatigue crack growth rate of electron-beam-welded AISI 4130 steel. 3162-3169A

Cracking (fracturing)

- Multiple matrix cracking in a fiber-reinforced titanium matrix composite under high-cycle fatigue. 1899-1907A
- Influence of temperature transients on the hot workability of a two-phase gamma titanium aluminide alloy. 1933-1950A
- Solidification of an alloy 625 weld overlay. 3612-3620A
- Mathematical modeling of the extrusion of 6061/ $\text{Al}_2\text{O}_3/20\text{p}$ composite. 4095-4111A
- Modeling particle fracture during the extrusion of aluminum/alumina composites. 4113-4120A

Cracks

- Thermal expansion of metals reinforced with ceramic particles and microcellular foams. 3700-3717A

Creep (materials)

- Tensile ductility and fracture of superplastic aluminum-SiC composites under thermal cycling conditions. 2837-2842A
- Temperature dependence of the rate sensitivity and its effect on the activation energy for high-temperature flow. 3346-3348A

Creep (materials), Microstructural effects

- Creep deformation of dispersion-strengthened copper. 1217-1227A
- Preferential coarsening of γ' precipitates in Inconel 718 during creep. 3391-3398A

Creep (materials), Stress effects

- Time-dependent, environmentally assisted crack growth in Nicalon-fiber-reinforced SiC composites at elevated temperatures. 839-849A

Creep life

- Prediction of creep-rupture life of unidirectional titanium matrix composites subjected to transverse loading. 3074-3080A

Creep life, Microstructural effects

- Creep deformation and crack growth behavior of a single-crystal nickel-base superalloy. 829-837A
- The normalized Coffin-Manson plot in terms of a new damage function based on grain boundary cavitation under creep-fatigue condition. 1273-1281A

Creep lifetime prediction of oxide-dispersion-strengthened nickel-base superalloys: a micromechanically based approach.

3861-3870A

An evaluation of the creep properties of two Al-Si alloys produced by rapid solidification processing.

3871-3879A

Creep life, Stress effects

Effect of carbide precipitation on the creep behavior of alloy 800HT in the temperature range 700-900°C.

747-756A

Effect of multiaxial stresses on creep damage of 316 stainless steel weldments.

891-900A

Creep rate

The balance of mechanical and environmental properties of a multielement niobium-niobium silicide-based in situ composite.

3801-3808A

Creep rate, Microstructural effects

Effect of creep strain on microstructural stability and creep resistance of a TiAl/Ti₃Al lamellar alloy.

127-134A

Creep deformation and crack growth behavior of a single-crystal nickel-base superalloy.

829-837A

Effect of iron on ductility and cavitation in the superplastic An-22% Al eutectoid.

863-872A

On the influence of grain morphology on creep deformation and damage mechanisms in directionally solidified and oxide dispersion strengthened superalloys.

879-890A

Creep lifetime prediction of oxide-dispersion-strengthened nickel-base superalloys: a micromechanically based approach.

3861-3870A

An evaluation of the creep properties of two Al-Si alloys produced by rapid solidification processing.

3871-3879A

Creep rate, Stress effects

Effect of a solid solution on the steady-state creep behavior of an aluminum matrix composite.

305-316A

Effect of multiaxial stresses on creep damage of 316 stainless steel weldments.

891-900A

Creep deformation and damage in a continuous fiber-reinforced Ti-6Al-4V composite.

4193-4204A

Creep rupture strength

Prediction of creep-rupture life of unidirectional titanium matrix composites subjected to transverse loading.

3074-3080A

The balance of mechanical and environmental properties of a multielement niobium-niobium silicide-based in situ composite.

3801-3808A

Creep rupture strength, Microstructural effects

On the influence of grain morphology on creep deformation and damage mechanisms in directionally solidified and oxide dispersion strengthened superalloys.

879-890A

Creep lifetime prediction of oxide-dispersion-strengthened nickel-base superalloys: a micromechanically based approach.

3861-3870A

An evaluation of the creep properties of two Al-Si alloys produced by rapid solidification processing.

3871-3879A

Creep strength, Alloying effects

Elevated temperature compressive properties of N-doped NiAl.

3170-3180A

Creep strength, High temperature effects

High-temperature measurements of lattice parameters and internal stresses of a creep-deformed monocrystalline nickel-base superalloy.

1003-1014A

High-temperature deformation properties of NiAl single crystals.

1229-1240A

Creep strength, Microstructural effects

Effect of creep strain on microstructural stability and creep resistance of a TiAl/Ti₃Al lamellar alloy.

127-134A

Phase stability and atom probe field ion microscopy of type 308 CRE stainless steel weld metal.

763-774A

The inter-relationship between grain boundary sliding and cavitation during creep of polycrystalline copper.

901-907A

Tensile properties of mechanically alloyed/milled ODS-Ni-based alloys.

1371-1377A

Creep strength, Stress effects

Effect of a solid solution on the steady-state creep behavior of an aluminum matrix composite.

305-316A

Rafting in superalloys.

513-530A

Effect of carbide precipitation on the creep behavior of alloy 800HT in the temperature range 700-900°C.

747-756A

Effect of multiaxial stresses on creep damage of 316 stainless steel weldments.

891-900A

Creep strength, Temperature effects

Enhanced ductility in coarse-grained Al-Mg alloys.

343-352A

Observations of secondary carbide precipitation and its relation to high-temperature flow and fracture in HT-9 stainless steel.

467-469A

Creep tests

An evaluation of the creep properties of two Al-Si alloys produced by rapid solidification processing.

3871-3879A

Creep deformation and damage in a continuous fiber-reinforced Ti-6Al-4V composite.

4193-4204A

- Cryolite**
Electrical conductivity of molten cryolite based mixtures obtained with a tube type cell made of pyrolytic boron nitride. 255-261B
- Cryolite, Reactions (chemical)**
Liquidus temperatures for primary crystallization of cryolite in molten salt systems of interest for aluminum electrolysis. The transported entropy of Na⁺ in solid state cryolite. 739-744B
788-793B
- Crystal defects**
High-resolution electron microscopy analysis of structural defects in a (2/1, 5/3)-type approximant of a decagonal quasicrystal of an Al-Pd-Mn alloy. 2911-2915A
- Crystal growth**
Time dependence of tip morphology during cellular/dendritic arrayed growth. 1111-1119A
Crystal shapes and phase equilibria: a common mathematical basis. 1431-1440A
The Rayleigh instability and the origin of rows of droplets in the monotectic microstructure of zinc-bismuth alloys. 2053-2057A
Modeling of ferrite growth in nodular cast iron. 2209-2220A
- Crystal growth, Composition effects**
Effects of shear flow and anisotropic kinetics on the morphological stability of a binary alloy. 687-694A
- Crystal growth, Field effects**
Convection during thermally unstable solidification of Pb-Sn in a magnetic field. 1095-1110A
- Crystal structure**
Interdiffusion kinetics in oxide powder mixture using high temperature x-ray diffraction technique. 318-322B
The inter-relationship between grain boundary sliding and cavitation during creep of polycrystalline copper. 901-907A
Crystal shapes and phase equilibria: a common mathematical basis. 1431-1440A
Crystallography of grain boundary α precipitates in a β titanium alloy. 1630-1641A
Microstructure and phase identification in type 304 stainless steel-zirconium alloys. 2151-2159A
Thermoelastic martensite and shape memory effect in ductile Cu-Al-Mn alloys. 2187-2195A
Lattice misfits in four binary Ni-base γ/γ' alloys at ambient and elevated temperatures. 2888-2896A
- Crystal structure, Alloying effects**
Mechanical alloying of Nb-Al powders. 41-48A
Identification of precipitate phases in a mechanically alloyed rapidly solidified Al-Fe-Ce alloy. 1033-1041A
- Crystal structure, Coating effects**
Microstructural analysis and oxidation behavior of laser-processed Fe-Cr-Al-Y alloy coatings. 381-390A
- Crystal structure, Deformation effects**
Effects of alloy modification and thermomechanical processing on recrystallization of Al-Mg-Mn alloys. 2947-2957A
- Crystal structure, Heating effects**
Characterization of the formation of α_1 plates from the β_2 phase in a Cu-Zn-Au alloy. 719-724A
Neutron diffraction study of austempered ductile iron. 923-928A
- Crystal structure, Stress effects**
On the effect of stress on nucleation and growth of precipitates in an Al-Cu-Mg-Ag alloy. 3431-3444A
- Crystal structure, Temperature effects**
Eutectoid decomposition in Ag-Ga. 1676-1682A
- Crystallization**
Liquidus temperatures for primary crystallization of cryolite in molten salt systems of interest for aluminum electrolysis. 739-744B
Crystallization of amorphous phase in sputter-deposited Ti-Al alloy thin films. 2047-2050A
- Crystallization, Alloying effects**
The effect of metallic elements on the crystallization behavior of amorphous Fe-Si-B alloys. 3424-3430A
- Crystallization, Temperature effects**
Crystallization of amorphous alloys. 549-555A
- Crystals**
An optical method for determining the surface orientation of crystals. 2057-2061A
- Current density**
Physical modeling studies of electrolyte flow due to gas evolution and some aspects of bubble behavior in advanced Hall cells. III. Predicting the performance of advanced Hall cells. Effect of baking temperature and anode current density on anode carbon consumption. 177-183B
Structural characterization of martensitic iron-carbon alloy films electrodeposited from an iron(II) sulfate solution. 483-486A
- Cutting tool materials, Synthesis**
Synthesis of full-density nanocrystalline tungsten carbide by reduction of tungstic oxide at room temperature. 4210-4213A
- Cutting tools, Materials selection**
Synthesis of full-density nanocrystalline tungsten carbide by reduction of tungstic oxide at room temperature. 4210-4213A
- Cyanidation**
Electrochemical behavior of the dissolution of gold-silver alloys in cyanide solutions. 355-361B
- Cyclic loads**
Crystallographic preferred orientation induced by cyclic rolling contact loading. 3445-3465A
Fracture and fatigue-crack growth behavior in ductile-phase toughened molybdenum disilicide: effects of niobium wire vs. particulate reinforcements. 3781-3792A
- Damage**
Conditioning monitoring by microstructural evaluation of cumulative fatigue damage. 3841-3851A
- Damage, Stress effects**
Creep deformation and damage in a continuous fiber-reinforced Ti-6Al-4V composite. 4193-4204A
- Damage tolerance**
Conditioning monitoring by microstructural evaluation of cumulative fatigue damage. 3841-3851A
- Damage tolerance, Stress effects**
Effect of thermal cycling on the mechanical properties of 350 grade maraging steel. 757-761A
Effect of multiaxial stresses on creep damage of 316 stainless steel weldments. 891-900A
- Damping capacity**
Analysis of damping in particle-reinforced superplastic zinc composites. 2565-2573A
- Damping capacity, Composition effects**
The effect of volume percent and morphology of phases on the damping behavior of epoxy-aluminum composites. 2366-2373A
- Decomposition reactions**
Hydride formation and decomposition in electrolytically charged metastable austenitic stainless steels. 29-40A
A high-resolution transmission electron microscopy study of the precipitation process in a dilute Ti-N alloy. 2966-2977A
- Deep drawing**
Analysis and prevention of vertical cracking phenomena during deep drawing of hot-rolled SG295 steel strips. 1241-1250A
- Deformation**
Nanoscale brass/steel multilayer composites produced by cold rolling. 2383-2385A
Simulation of the hot-tension test under cavitating conditions. 3112-3119A
Hot deformation mechanisms of a solution-treated Al-Li-Cu-Mg-Zr alloy. 3478-3490A
Mathematical modeling of the extrusion of 6061/Al₂O₃/20p composite. 4095-4111A
Creep deformation and damage in a continuous fiber-reinforced Ti-6Al-4V composite. 4193-4204A
- Deformation, High temperature effects**
High-temperature deformation properties of NIAI single crystals. 1229-1240A
- Deformation, Temperature effects**
Elevated temperature deformation behavior of a dispersion-strengthened Al-Fe, V, Si alloy. 3913-3923A
An analysis of the flow stress of a two-phase alloy system, Ti-6Al-4V. 3957-3962A
- Deformation mechanisms**
Effect of phase composition and hydrogen level on the deformation behavior of titanium-hydrogen alloys. 1869-1876A
Characterization of superplastic deformation behavior of a fine grain 5083 Al alloy sheet. 1889-1898A
Deformation behavior of an Al-3.37 wt.% Li alloy. 2274-2284A
Hot deformation mechanisms of a solution-treated Al-Li-Cu-Mg-Zr alloy. 3478-3490A
Creep deformation and damage in a continuous fiber-reinforced Ti-6Al-4V composite. 4193-4204A
- Deformation resistance**
Prediction of creep-rupture life of unidirectional titanium matrix composites subjected to transverse loading. 3074-3080A
- Deformation resistance, Microstructural effects**
Van der Waals approximation for potassium bubbles in tungsten. 987-992B
- Deformation resistance, Temperature effects**
Influence of temperature transients on the hot workability of a two-phase gamma titanium aluminide alloy. 1933-1950A
- Dendritic structure**
Communication: Mechanical deformation of dendrites by fluid flow. 229-232A
Microstructure of bonding zones in laser-clad nickel-alloy-based composite coatings reinforced with various ceramic powders. 391-400A

- Interface attachment kinetics in alloy solidification. 671-686A
- Prediction of dendrite arm spacing for low alloy steel casting processes. 689-693B
- High-speed imaging and analysis of the solidification of undercooled nickel melts. 863-868B
- Generalized enthalpy method for multicomponent phase change. 869-879B
- On the influence of grain morphology on creep deformation and damage mechanisms in directionally solidified and oxide dispersion strengthened superalloys. 879-890A
- Time dependence of tip morphology during cellular/dendritic arrayed growth. 1111-1119A
- The Rayleigh instability and the origin of rows of droplets in the monotectic microstructure of zinc-bismuth alloys. 2053-2057A
- Effect of grain refinement on the fluidity of two commercial Al-Si foundry alloys. 2305-2313A
- Orientation dependence of primary dendrite spacing. 2727-2739A
- Equiaxed dendritic solidification with convection. I. Multiscale/multiphase modeling. 2754-2764A
- Equiaxed dendritic solidification with convection. II. Numerical simulations for an Al-4 wt.% Cu alloy. 2765-2783A
- Equiaxed dendritic solidification with convection. III. Comparisons with $\text{NH}_4\text{Cl-H}_2\text{O}$ experiments. 2784-2795A
- Microstructure of Cu-Co alloys solidified at various supercoolings. 4049-4059A
- Macrotransport-solidification kinetics modeling of equiaxed dendritic growth. I. Model development and discussion. 4061-4074A
- Macrotransport-solidification kinetics modeling of equiaxed dendritic growth. II. Computation problems and validation on Inconel 718 superalloy casting. 4075-4083A
- Modeling of primary and secondary dendrites in a Cu-6 wt.% tin alloy. 4085-4093A
- Dendritic structure, Alloying effects**
- The effect of iron and manganese on the recrystallization behavior of hot-rolled and solution-heat-treated aluminum alloy 6013. 19-27A
- The breakdown of single-crystal solidification in high refractory nickel-base alloys. 1081-1094A
- Dendritic structure, Cooling effects**
- Scaling of intragranular dendritic microstructure in ingot solidification. 101-113B
- Porosity formation in Al-9 wt.% Si-3 wt.% Cu alloy systems: metallographic observations. 415-429A
- The effect of bulk flow concentration on diffusion coupling between dendrites. 477-480A
- Solidification of binary hypoeutectic alloy matrix composite castings. 595-609A
- Numerical modeling of cellular/dendritic array growth: spacing and structure predictions. 611-623A
- Prediction of grain structures in various solidification processes. 695-705A
- Macrosegregation during dendritic arrayed growth of hypoeutectic Pb-Sn alloys: influence of primary arm spacing and mushy zone length. 1353-1362A
- Dendritic structure, Deformation effects**
- Precipitation behavior in a medium carbon, Ti-V-N microalloyed steel. 1149-1165A
- Dendritic structure, Field effects**
- Convection during thermally unstable solidification of Pb-Sn in a magnetic field. 1095-1110A
- Dendritic structure, Heating effects**
- Effect of superheat on the solidification structures of AISI 310S austenitic stainless steel. 287-296B
- Mechanical properties and 95°C aging characteristics of zircon reinforced Zn-4Al-3Cu alloy. 809-818A
- Dendritic structure, Stress effects**
- Creep deformation and crack growth behavior of a single-crystal nickel-base superalloy. 829-837A
- Dendritic structure, Temperature effects**
- Overview of geometric effects on coarsening of mushy zones. 557-567A
- Some consequences of thermosolutal convection: the grain structure of castings. 569-581A
- Morphological instabilities of lamellar eutectics. 635-656A
- The phase field method: simulation of alloy dendritic solidification during recalcification. 657-669A
- Densification**
- Theoretical modeling of densification during activated solid-state sintering. 441-450A
- Solid-state contributions to densification during liquid-phase sintering. 901-909B
- Pressure-assisted reactive synthesis of titanium aluminides from dense 50Al-50Ti elemental powder blends. 2130-2139A
- Dense CoAl-based alloys with improved ductility: solid-state synthesis and microstructure control. 2140-2150A
- Densification, Pressure effects**
- Synthesis of RuAl by reactive powder processing. 3688-3699A
- Density**
- The effect of Mo addition on the liquid-phase sintering of W heavy alloy. 3120-3125A
- Microstructure and tensile properties of compacted, mechanically alloyed, nanocrystalline Fe-Al. 3126-3134A
- Density, Alloying effects**
- Solid-state contributions to densification during liquid-phase sintering. 901-909B
- Deoxidizing**
- Activities in $\text{MnO-SiO}_2\text{-Al}_2\text{O}_3$ slags and deoxidation equilibria of manganese and silicon. 263-270B
- Use of solid-electrolyte galvanic cells to determine the activity of CaO in the CaO-ZrO₂ system and the standard Gibbs free energies of formation of CaZrO₃ from CaO and ZrO₂. 658-662B
- Thermodynamic properties of oxygen in yttrium-oxygen solid solutions. 839-845B
- The measurement of hydrogen activities in molten copper using an oxide protonic conductor. 929-935B
- Thermodynamics of calcium and oxygen in molten titanium and titanium-aluminum alloy. 967-972B
- Dephosphorizing**
- Thermodynamics of phosphorus in molten silicon. 937-941B
- Deposition**
- Formation of aluminum-silicon alloys from feldspars—determination of silicon, light, and heavy elements in silumin by scanning electron microscopy. 604-609B
- Desorption**
- Physical chemistry of the powder metallurgy of beryllium: chemical characterization of the powder in relation to its granularity. 371-379A
- Desorption, Temperature effects**
- Applicability of Butler's equation in interpreting the thermodynamic behavior of surfaces and adsorption in Fe-S-O melts. 241-253B
- Desulfurizing**
- Thermodynamics of sulfur in the BaO-MnO-SiO₂ flux system. Use of solid-electrolyte galvanic cells to determine the activity of CaO in the CaO-ZrO₂ system and the standard Gibbs free energies of formation of CaZrO₃ from CaO and ZrO₂. 658-662B
- Diamond pyramid hardness**
- Plastic zone and pileup around large indentations. 3793-3800A
- Diamond pyramid hardness, Alloying effects**
- Effect of magnesium on the aging behavior of Al-Zn-Mg-Cu/Al₂O₃ metal matrix composites. 2005-2012A
- Diamond pyramid hardness, Composition effects**
- Structural characterization of martensitic iron-carbon alloy films electrodeposited from an iron(II) sulfate solution. 483-486A
- Diamond pyramid hardness, Microstructural effects**
- Mechanical behavior of the in situ composite alloys in the Al-Ni-Ti system near the L₁₂ phase field. 71-79A
- Precipitation in lead-calcium alloys containing tin. 1668-1675A
- The effects on fracture toughness of ductile-phase composition and morphology in Nb-Cr-Ti and Nb-Si in situ composites. 3007-3018A
- Diamond pyramid hardness, Radiation effects**
- The effect of high-energy electron-beam irradiation on microstructural modification of a high-speed steel roll. 3149-3161A
- Diamonds, Coatings**
- Quenching C60 fullerene into diamond in the Fe-C alloy system by laser treatment. 2293-2296A
- Die casting**
- The design of feed systems for thin-walled zinc high-pressure die castings. 115-118B
- Die steels, Mechanical properties**
- The wear behavior between hardfacing materials. 3639-3648A
- Differential equations**
- Mathematical modeling of tundish operation and flow control to reduce transition slabs. 745-756B
- Differential thermal analysis**
- A study of the thermal decomposition of BaCO₃. 409-416B
- Thermally assisted and mechanically driven solid-state reactions for formation of amorphous Al₃₃Ta₆₇ alloy powders. 3267-3278A
- Diffusion**
- Probing the initial stage of synthesis of Al₂O₃/Al composites by directed oxidation of Al-Mg alloys. 43-50B
- Interdiffusion kinetics in oxide powder mixture using high temperature x-ray diffraction technique. 318-322B
- Theoretical modeling of densification during activated solid-state sintering. 441-450A
- Microstructure of Al₂O₃ fiber-reinforced superalloy (Inconel 718) composites. 451-458A
- Intermixing model of continuous casting during a grade transition. 617-632B
- The characteristics of cavitation in superplastic metals and ceramics. 873-878A

- Ostwald ripening in ternary alloys. 937-943A
Creep deformation of dispersion-strengthened copper. 1217-1227A
The mechanism of formation of a fine duplex microstructure in Ti-48Al-2Mn-2Nb alloys. 1655-1667A
Internal friction in hydrogen-charged CrNi and CrNiMn austenitic stainless steels. 1815-1821A
Control of iron nitride layers growth kinetics in the binary Fe-N system. 1823-1835A
Dense CoAl-based alloys with improved ductility: solid-state synthesis and microstructure control. 2140-2150A
Modeling of ferrite growth in nodular cast iron. 2209-2220A
Thermodynamic and kinetic study of diffusion paths in the system Cu-Fe-Ni. 2229-2238A
Modeling of microsegregation in macrosegregation computations. 2314-2327A
Infrared transient-liquid-phase joining of SCS-6/ β 21S titanium matrix composite. 4011-4018A
- Diffusion, Alloying effects**
Effects of nickel on the sintering behavior of Fe-Ni compacts made from composite and elemental powders. 203-211B
Electron microscope study of Al-Fe-Si intermetallics in 6201 aluminum alloy. 929-936A
- Diffusion, Cooling effects**
Porosity formation in Al-9 wt.% Si-3 wt.% Cu alloy systems: metallographic observations. 415-429A
The effect of bulk flow concentration on diffusion coupling between dendrites. 477-480A
Bainite in the light of rapid continuous cooling information. 1499-1510A
Ferrite nucleation and growth during continuous cooling. 1544-1553A
- Diffusion, Deformation effects**
Analysis on the amplitude of serrated flow associated with the Portevin-LeChatelier effect of substitutional fcc alloys. 1683-1686A
- Diffusion, Heating effects**
Characterization of the formation of α_1 plates from the β_3 phase in a Cu-Zn-Au alloy. 719-724A
Anomalous diffusion of iron in liquid aluminum measured by the pulsed laser technique. 725-730A
Heterogeneous nucleation of δ on dislocations in a dilute aluminum-lithium alloy. 1595-1605A
Transition between internal and external nitridation of Ni-Ti alloys. 1606-1617A
- Diffusion, High temperature effects**
Phase relations of a silicide/silica reaction couple at 2273K. 271-276B
- Diffusion, Pressure effects**
Pressure dependence of anomalous diffusion of zirconium in β -titanium. 1807-1814A
- Diffusion, Radiation effects**
Transmission electron microscopy study on the cross-sectional microstructure of an ion-nitriding layer. 1347-1352A
- Diffusion, Stress effects**
A study on coherency strain and precipitate morphology via a discrete atom method. 1449-1459A
Computer simulation of ledge migration under elastic interaction. 1489-1498A
- Diffusion rate, Microstructural effects**
Influence of interstitials on the mechanical properties of metallic materials. 3524-3529A
- Diffusion welding**
Microstructural development in NiAl/Ni-Si-B/Ni transient liquid phase bonds. 1925-1931A
- Diffusivity**
Average effective interdiffusion coefficients and the Matano plane composition. 2504-2509A
- Diffusivity, Heating effects**
Anomalous diffusion of iron in liquid aluminum measured by the pulsed laser technique. 725-730A
- Direct chill casting**
Heat-flow-based analysis of surface crack formation during the start-up of the direct chill casting process. I. Development of the inverse heat-transfer model. 119-127B
Heat-flow-based analysis of surface crack formation during the start-up of the direct chill casting process. II. Experimental study of an AA5182 rolling ingot. 129-137B
Modeling of ingot distortions during direct chill casting of aluminum alloys. 3214-3225A
- Directional solidification**
Hydrogen effects on directional solidification of tellurium-doped cast irons. 496-498A
Effects of flow on morphological stability during directional solidification. 583-593A
Solidification of binary hypoeutectic alloy matrix composite castings. 595-609A
Effects of shear flow and anisotropic kinetics on the morphological stability of a binary alloy. 687-694A
- Prediction of grain structures in various solidification processes. 695-705A
Real time x-ray transmission microscopy of solidifying Al-In alloys. 801-808A
Time dependence of tip morphology during cellular/dendritic arrayed growth. 1111-1119A
Macrosegregation during dendritic arrayed growth of hypoeutectic Pb-Sn alloys: influence of primary arm spacing and mushy zone length. 1353-1362A
Directional solidification of white cast iron. 2328-2337A
Transitions between type A flake, type D flake, and coral graphite eutectic structures in cast irons. 2740-2753A
- Directional solidification, Field effects**
Convection during thermally unstable solidification of Pb-Sn in a magnetic field. 1095-1110A
- Directionally solidified eutectics, Mechanical properties**
The fracture toughness of niobium-based, in situ composites. 2518-2531A
The effects on fracture toughness of ductile-phase composition and morphology in Nb-Cr-Ti and Nb-Si in situ composites. 3007-3018A
Loading rate and test temperature effects on fracture of in situ niobium silicide-niobium composites. 3292-3306A
The balance of mechanical and environmental properties of a multielement niobium-niobium silicide-based in situ composite. 3801-3808A
- Dislocation density**
Creep deformation of dispersion-strengthened copper. 1217-1227A
Tensile properties of mechanically alloyed/milled ODS-Ni-based alloys. 1371-1377A
The control of grain size and distribution of particles in a (6061 alloy)_m/(Al₂O₃)_p composite by solutionizing treatment. 2023-2034A
- Dislocation density, Composition effects**
Electron microscopic study of Cr₂N formation in thermally aged 316LN austenitic stainless steels. 1175-1186A
- Dislocation density, Deformation effects**
Effect of creep strain on microstructural stability and creep resistance of a TiAl/Ti₃Al lamellar alloy. 127-134A
The x-ray diffraction study of deformation in the composite matrix of Al-Mg-Zn and SiC. 503-505A
- Dislocation density, High temperature effects**
High-temperature deformation properties of NiAl single crystals. 1229-1240A
- Dislocation density, Radiation effects**
A model describing neutron irradiation-induced segregation to grain boundaries in dilute alloys. 3381-3390A
- Dislocation mobility**
Deformation behavior of an Al-3.37 wt.% Li alloy. 2274-2284A
- Dislocation mobility, Temperature effects**
Rafting in superalloys. 513-530A
- Dislocation pinning, Stress effects**
Elevated temperature deformation behavior of a dispersion-strengthened Al-Fe, V, Si alloy. 3913-3923A
- Dislocations**
NITi and NITi-TiC composites. II. Compressive mechanical properties. 183-191A
A high resolution transmission electron microscopy study of interfaces between the γ , β_2 , and α_2 phases in a Ti-Al-Mo alloy. 1618-1629A
Crystallography of grain boundary α precipitates in a β titanium alloy. 1630-1641A
Recrystallization in oxide-dispersion strengthened mechanically alloyed sheet steel. 1963-1978A
High-resolution transmission electron microscopy investigation of the face-centered cubic/hexagonal close-packed martensite transformation in Co-31.8 wt.% Ni alloy. I. Plate interfaces and growth ledges. 3362-3370A
- Dislocations, Deformation effects**
Analysis on the amplitude of serrated flow associated with the Portevin-LeChatelier effect of substitutional fcc alloys. 1683-1686A
- Dislocations, Stress effects**
Stacking faults in SiC particles and their effect on the fracture behavior of a 15 vol.% SiC/6061-Al matrix composite. 459-465A
Molecular dynamics simulation of martensitic transformations in NiAl. 1476-1488A
Computer simulation of ledge migration under elastic interaction. 1489-1498A
- Dislocations, Temperature effects**
A new characterization method of the microstructure using the macroscopic composition gradient in alloys. 945-949A
- Dispersion hardening**
Creep lifetime prediction of oxide-dispersion-strengthened nickel-base superalloys: a micromechanically based approach. 3861-3870A
Elevated temperature deformation behavior of a dispersion-strengthened Al-Fe, V, Si alloy. 3913-3923A

Dispersion hardening alloys, Crystal growth		
Recrystallization in oxide-dispersion strengthened mechanically alloyed sheet steel.	1963-1978A	
Dispersion hardening alloys, Diffusion		
Hydrogen trapping and permeation in nickel thoria.	2495-2503A	
Dispersion hardening alloys, Mechanical properties		
Creep lifetime prediction of oxide-dispersion-strengthened nickel-base superalloys: a micromechanically based approach.	3861-3870A	
Elevated temperature deformation behavior of a dispersion-strengthened Al-Fe, V, Si alloy.	3913-3923A	
Dispersions, High temperature effects		
Creep lifetime prediction of oxide-dispersion-strengthened nickel-base superalloys: a micromechanically based approach.	3861-3870A	
Dissimilar materials, Bonding		
Flow and fracture of bimaterial systems based on aluminum alloys.	3937-3947A	
Dissimilar metals, Welding		
Forming of tailor-welded blanks.	2605-2616A	
Dissipation, Deformation effects		
Communication: Discussion of "Modeling of dynamic materials behavior. A critical evaluation of the dissipator power cocontent approach".	232-235A	
Dissolution		
Interdiffusion kinetics in oxide powder mixture using high temperature x-ray diffraction technique.	318-322B	
Electrochemical behavior of the dissolution of gold-silver alloys in cyanide solutions.	355-361B	
Microstructure of bonding zones in laser-clad nickel-alloy-based composite coatings reinforced with various ceramic powders.	391-400A	
Interface characterization of ceramic fiber-reinforced titanium alloy composites manufactured by infrared processing.	1379-1394A	
Splitting phenomena occurring in the martensitic transformation of Cr13 and CrMoV14 stainless steels in the absence of carbide precipitation.	1799-1805A	
Dissolution, Alloying effects		
Solubility of carbon in CaO-Al ₂ O ₃ melts.	57-64B	
Effects of oxygen, selenium, and tellurium on the rate of nitrogen dissolution in molten iron.	846-851B	
Dissolution, Coating effects		
Microstructural analysis and oxidation behavior of laser-processed Fe-Cr-Al-Y alloy coatings.	381-390A	
Dissolution, Heating effects		
Microstructural aspects of the dissolution and melting of Al ₂ Cu phase in Al-Si alloys during solution heat treatment.	1785-1798A	
Distortion		
Modeling of ingot distortions during direct chill casting of aluminum alloys.	3214-3225A	
Domain walls		
Temperature dependent deformation of polydomain phases in an In-22.5 at.% Ti shape memory alloy.	1687-1692A	
Dual phase steels, Mechanical properties		
Theoretical calculation of the stress-strain behavior of dual-phase metals with randomly oriented spheroidal inclusions.	2359-2365A	
Ductile brittle transition		
Nonequilibrium grain-boundary segregation and ductile-brittle-ductile transition in Fe-Mn-Ni-Ti age-hardening alloy.	3059-3065A	
Ductile brittle transition, Corrosion effects		
Shear ligament phenomena in Fe ₃ Al intermetallics and micro-mechanics of shear ligament toughening.	3817-3825A	
Ductile brittle transition, Welding effects		
Microstructures relevant to brittle fracture initiation at the heat-affected zone of weldment of a low carbon steel.	2574-2582A	
Cleavage initiation in the intercritically reheated coarse-grained heat affected zone. II. Failure criteria and statistical effects.	3019-3029A	
Ductile fracture		
Microstructure and properties of Al ₂ O ₃ -Al(Si) and Al ₂ O ₃ -Al(Si)-Si composites formed by in situ reaction of aluminum with aluminosilicate ceramics.	2122-2129A	
The influence of stress triaxiality on the damage mechanisms in an equiaxed α/β Ti-6Al-4V alloy.	3043-3058A	
Simulation of the hot-tension test under cavitating conditions.	3112-3119A	
Ductile fracture, Microstructural effects		
The cracking mechanism of silicon particles in an A357 aluminum alloy.	3558-3568A	
Ductile fracture, Stress effects		
Discussion of "a fully plastic microcracking model for transgranular stress corrosion cracking in planar slip materials" and reply.	819-821A	
Ductility		
Thermal stability of SiC-SCS-6 fiber-reinforced IMI834 alloys.	1403-1405A	
The improved microstructures and properties of 7075 alloys produced by a water-cooling centrifugal casting method.	1951-1962A	
Thermoelastic martensite and shape memory effect in ductile Cu-Al-Mn alloys.	2187-2195A	
Investigation of the reaction zone between TiAl and molybdenum.	2285-2292A	
The fracture toughness of niobium-based, in situ composites.	2518-2531A	
Tensile ductility and fracture of superplastic aluminum-SiC composites under thermal cycling conditions.	2837-2842A	
Simulation of the hot-tension test under cavitating conditions.	3112-3119A	
Fracture and fatigue-crack growth behavior in ductile-phase toughened molybdenum disilicide: effects of niobium wire vs. particulate reinforcements.	3781-3792A	
Flow and fracture of bimaterial systems based on aluminum alloys.	3937-3947A	
Mathematical modeling of the extrusion of 6061/Al ₂ O ₃ /20p composite.	4095-4111A	
Ductility, Alloying effects		
Elevated temperature compressive properties of zirconium-modified NiAl.	2628-2641A	
Tension characteristics of notched specimens for Al-Li-Cu-Zr alloys sheets with various cerium contents.	3089-3094A	
Elevated temperature compressive properties of N-doped NiAl.	3170-3180A	
Ductility, Coating effects		
Isothermal fatigue of an aluminide-coated single-crystal superalloy. I.	353-361A	
Ductility, Composition effects		
Structural characterization of martensitic iron-carbon alloy films electrodeposited from an iron(II) sulfate solution.	483-486A	
Carbide diagrams and precipitation of alloying elements during aging of low-alloy steels.	498-502A	
Mechanical properties of Ru-Ni-Al alloys.	1395-1400A	
High-temperature behavior of precious metal base composites.	2642-2652A	
Ductility, Cooling effects		
Rapid solidification processing of a Mg-Li-Si-Ag alloy.	1363-1370A	
The quench sensitivity of cast Al-7 wt.% Si-0.4 wt.% Mg alloy.	3983-3991A	
Ductility, Corrosion effects		
Shear ligament phenomena in Fe ₃ Al intermetallics and micro-mechanics of shear ligament toughening.	3817-3825A	
Ductility, Deformation effects		
Micronecking and fracture in cavitated superplastic materials.	1043-1046A	
Increased ductility in high velocity electromagnetic ring expansion.	1837-1844A	
Effect of thermomechanical treatments on the room-temperature mechanical behavior of iron aluminide Fe ₃ Al.	2985-2993A	
Ductility, Heating effects		
Influence of long term annealing on tensile properties and fracture of near- α titanium alloy Ti-6Al-2.75Sn-4Zr-0.4Mo-0.45Si.	1700-1708A	
Ductility, Impurity effects		
The effect of hydrogen on the fracture of alloy X-750.	101-110A	
Ductility, Microstructural effects		
Mechanical behavior of the in situ composite alloys in the Al-Ni-Ti system near the L ₁₂ phase field.	71-79A	
Pearlite in ultrahigh carbon steels: heat treatments and mechanical properties.	111-118A	
Communication: Mechanical deformation of dendrites by fluid flow.	229-232A	
Mechanical behavior and properties of mechanically alloyed aluminum alloys.	737-745A	
Effect of iron on ductility and cavitation in the superplastic An-22% Al eutectoid.	863-872A	
Bridge toughening enhancement in double-notched MoSi ₂ /Nb model composites.	909-921A	
The embrittlement and de-embrittlement of grain boundaries in an Fe-Mn-Ni alloy due to grain boundary segregation of manganese.	1015-1020A	
On microsuperplasticity in AA7475 domes.	1400-1403A	
Dense CoAl-based alloys with improved ductility: solid-state synthesis and microstructure control.	2140-2150A	
Deformation behavior of an Al-3.37 wt.% Li alloy.	2274-2284A	
Microstructure and mechanical behavior of Cr-Cr ₂ Hf in situ intermetallic composites.	2583-2592A	
Reinforcement shape effects on the fracture behavior and ductility of particulate-reinforced 6061-Al matrix composites.	3739-3746A	
Microstructure and fracture of SiC-particulate-reinforced cast A356 aluminum alloy composites.	3893-3901A	
Ductility, Stress effects		
Detecting stable crack onset at ductile-brittle transition in steels.	469-471A	
Effect of thermal cycling on the mechanical properties of 350 grade maraging steel.	757-761A	
Ductility, Temperature effects		
Enhanced ductility in coarse-grained Al-Mg alloys.	343-352A	

Ductility, Welding effects

Effect of postweld treatment on the fatigue crack growth rate of electron-beam-welded AISI 4130 steel.

3162-3169A

Duplex stainless steels

Microstructure and tensile behavior of nitrogen-alloyed, dual-phase stainless steels.
Structural stability of super duplex stainless weld metals and its dependence on tungsten and copper.

1845-1859A

2196-2208A

Duplex stainless steels, Machining

Active wear and failure mechanisms of titanium nitride-coated high speed steel and titanium nitride-coated cemented carbide tools when machining powder metallurgically made stainless steels.

2796-2808A

Duplex stainless steels, Microstructure

Microstructure and tensile behavior of nitrogen-alloyed, dual-phase stainless steels.

1845-1859A

Duplex stainless steels, Welding

Structural stability of super duplex stainless weld metals and its dependence on tungsten and copper.

2196-2208A

Dynamics

Dynamic Behavior of Materials. II.

Milling dynamics. II. Dynamics of a SPM mill and a one-dimensional mill.

1991-1997A

Milling dynamics. III. Integration of local and global modeling of mechanical alloying devices.

1999-2004A

Dysprosium, Binary systems

Standard enthalpies of formation of dysprosium alloys, Dy+Me (Me=Ni, Ru, Rh, Pd, Ir, and Pt), by high-temperature direct synthesis calorimetry.

417-422B

Economics

Eco-techno-economic synthesis of process routes for the production of zinc using combinatorial optimization.

1031-1044B

Edge dislocations, Heating effects

Heterogeneous nucleation of δ on dislocations in a dilute aluminum-lithium alloy.

1595-1605A

Elastic anisotropy

The plastic anisotropy of an Al-Li-Cu-Zr alloy extrusion in unidirectional deformation.

3503-3512A

Elastic constants

A comprehensive dynamical study of nucleation and growth in a one-dimensional shear martensitic transition.

1203-1216A

Elastic constants, Stress effects

Computer simulation of reversible martensitic transformations. A study on coherency strain and precipitate morphology via a discrete atom method.

1187-1201A

1449-1459A

Elasticity, Deformation effects

Communication: Discussion of "Modeling of dynamic materials behavior. A critical evaluation of the dissipator power cocontent approach".

232-235A

Elasticity, Stress effects

Effect of uniaxial stress on coarsening of precipitate clusters.

1460-1475A

Electric fields

Effects of forced electromagnetic vibrations during the solidification of aluminum alloys. I. Solidification in the presence of crossed alternating electric fields and stationary magnetic fields.

445-455B

Electric potential

Chemical potentials of components of the system $\text{CaO}+\text{P}_2\text{O}_5+\text{Fe}_2\text{O}_3$ at 1673K.
Controversy on the free energy of formation of CaO —additional evidence in support of thermochemical data.

595-603B

647-651B

Electrical steels, Rolling

Orientation selective recrystallization of nonoriented electrical steels.

2347-2358A

Electrochemistry

Effect of baking temperature and anode current density on anode carbon consumption.
Electrochemical behavior of the dissolution of gold-silver alloys in cyanide solutions.

177-183B

355-361B

Chemical potentials of oxygen for mixtures of $\text{CaO(s)}+\text{Ca}_2\text{P}_2\text{O}_7\text{(s)}+(\text{CaO}+\text{P}_2\text{O}_5+\text{Fe}_2\text{O}_3)$ melts and $\text{Ca}_2\text{P}_2\text{O}_7\text{(s)}+\text{Ca}_3\text{P}_2\text{O}_8\text{(s)}+\text{CaO}+\text{P}_2\text{O}_5+\text{Fe}_2\text{O}_3$ melts.

375-378B

Fundamental studies of copper anode passivation during electrorefining. I. Development of techniques.

393-398B

Electrodeposition

Structural characterization of martensitic iron-carbon alloy films electrodeposited from an iron(II) sulfate solution.

483-486A

Electrodeposition, Impurity effects

Behavior of antimony(III) during copper electroplating in chloride solutions.

157-162B

Electrodes, Materials selection

Reference electrode of simple galvanic cells for developing sodium sensors for use in molten aluminum.

794-800B

Electrolysis

Studies on the corrosion and the behavior of inert anodes in aluminum electrolysis.
Liquidus temperatures for primary crystallization of cryolite in molten salt systems of interest for aluminum electrolysis.
The transported entropy of Na^+ in solid state cryolite.
Reference electrode of simple galvanic cells for developing sodium sensors for use in molten aluminum.

185-193B

739-744B

788-793B

794-800B

Electrolysis, Temperature effects

Electrical conductivity of molten cryolite based mixtures obtained with a tube type cell made of pyrolytic boron nitride.

255-261B

Electrolytic cells

Use of solid-electrolyte galvanic cells to determine the activity of CaO in the CaO-ZrO_2 system and the standard Gibbs free energies of formation of CaZrO_3 from CaO and ZrO_2 .
Preparation of pure silicon by electrowinning in a bytownite-cryolite melt.

658-662B

895-900B

Electrolytic cells, Development

Application of centrifugal fields in fused salt electrowinning with a view to reducing electrolytic energy consumption.

889-894B

Electromagnetic fields

Increased ductility in high velocity electromagnetic ring expansion.

1837-1844A

Electromagnetic testing

Alloy phase analysis from measurements of bulk magnetic properties.

2958-2965A

Electron beam welding

Effect of homogenization heat treatment on the microstructure and heat affected zone microfissuring in welded cast alloy 718.
Effect of postweld treatment on the fatigue crack growth rate of electron-beam-welded AISI 4130 steel.

785-790A

3162-3169A

Electron diffraction

Characterization of titanium thin films prepared by bias assisted magnetron sputtering.

1057-1060B

Electron energy loss spectroscopy

Incipient chemical instabilities of nanophase Fe-Cu alloys prepared by mechanical alloying.

2934-2946A

Electron microscopy

High-resolution electron microscopy analysis of structural defects in a (2/1, 5/3)-type approximant of a decagonal quasicrystal of an Al-Pd-Mn alloy.

2911-2915A

Electronic structure, Composition effects

Electron microscopic study of Cr_2N formation in thermally aged 316LN austenitic stainless steels.

1175-1186A

Electronic structure, Radiation effects

Sputter-induced pits on {100} nickel surfaces.

981-993A

Electroplating

Characterization of titanium thin films prepared by bias assisted magnetron sputtering.

1057-1060B

Electrorefining

Fundamental studies of copper anode passivation during electrorefining. I. Development of techniques.
Fundamental studies of copper anode passivation during electrorefining. II. Surface morphology.
Influence of gold content on copper oxidation from silver-gold-copper alloys.

393-398B

610-616B

3187-3191A

Electrowinning

Application of centrifugal fields in fused salt electrowinning with a view to reducing electrolytic energy consumption.
Preparation of pure silicon by electrowinning in a bytownite-cryolite melt.

889-894B

895-900B

Electrowinning, Impurity effects

Behavior of antimony(III) during copper electroplating in chloride solutions.

157-162B

Elongation

Thermal stability of SiC-SCS-6 fiber-reinforced IMI834 alloys.
Characterization and mechanical properties of ultrahigh boron steels produced by powder metallurgy.
Characterization of superplastic deformation behavior of a fine grain 5083 Al alloy sheet.
Simulation of the hot-tension test under cavitating conditions.
Notch fracture in γ -titanium aluminides.

1403-1405A

1861-1867A

1889-1898A

3112-3119A

3903-3912A

Elongation, Composition effects

A study of the influence of mischmetal additions to Al-7Si-0.3Mg (LM 25/356) alloy.

1283-1292A

Elongation, Deformation effects

Analysis and prevention of vertical cracking phenomena during deep drawing of hot-rolled SG295 steel strips.

1241-1250A

Elongation, Diffusion effects		
Hydrogen-induced cleavage fracture of Fe ₃ Al-based intermetallics.	3949-3956A	
Elongation, Impurity effects		
The effect of hydrogen on the fracture of alloy X-750.	101-110A	
Elongation, Microstructural effects		
Effect of iron on ductility and cavitation in the superplastic Al-22% Al eutectoid.	863-872A	
The embrittlement and de-embrittlement of grain boundaries in an Fe-Mn-Ni alloy due to grain boundary segregation of manganese.	1015-1020A	
Tensile properties of mechanically alloyed/milled ODS-Ni-based alloys.	1371-1377A	
Effect of bainite transformation and retained austenite on mechanical properties of austempered spheroidal graphite cast steel.	1585-1594A	
Fracture characteristics, microstructure, and tissue reaction of Ti-5Al-2.5Fe for orthopedic surgery.	3925-3935A	
Elongation, Stress effects		
Effect of thermal cycling on the mechanical properties of 350 grade maraging steel.	757-761A	
Elongation, Temperature effects		
Enhanced ductility in coarse-grained Al-Mg alloys.	343-352A	
Embrittlement, Microstructural effects		
The embrittlement and de-embrittlement of grain boundaries in an Fe-Mn-Ni alloy due to grain boundary segregation of manganese.	1015-1020A	
End uses		
Materials and society: impacts and responsibilities.	1413-1426A	
Energy conservation		
Application of centrifugal fields in fused salt electrowinning with a view to reducing electrolytic energy consumption.	889-894B	
Energy consumption		
The transported entropy of Na ⁺ in solid state cryolite.	788-793B	
Energy consumption, Field effects		
Application of centrifugal fields in fused salt electrowinning with a view to reducing electrolytic energy consumption.	889-894B	
Engine components		
Phase relations of a silicide/silica reaction couple at 2273K.	271-276B	
Materials and society—impacts and responsibilities.	337-350B	
Engine components, Materials selection		
Wear behavior of aluminum-based metal matrix composites reinforced with a preform of aluminosilicate fiber.	2385-2389A	
Prediction of creep-rupture life of unidirectional titanium matrix composites subjected to transverse loading.	3074-3080A	
Engines, Materials selection		
Prediction of creep-rupture life of unidirectional titanium matrix composites subjected to transverse loading.	3074-3080A	
Enthalpy		
Critical evaluation and optimization of the thermodynamic properties of liquid tin solutions.	808-826B	
Generalized enthalpy method for multicomponent phase change.	869-879B	
Thermodynamic properties of complex oxides in the Sm-Ba-Cu-O system.	973-978B	
Internal friction in hydrogen-charged CrNi and CrNiMn austenitic stainless steels.	1815-1821A	
Modeling of microsegregation in macrosegregation computations.	2314-2327A	
An analysis of the flow stress of a two-phase alloy system, Ti-6Al-4V.	3957-3962A	
Enthalpy, Composition effects		
Thermodynamic activities and partial enthalpies of mixing in the solid solution of Fe in Ni ₃ Al.	3569-3575A	
Entropy		
The transported entropy of Na ⁺ in solid state cryolite.	788-793B	
Entropy, Composition effects		
Thermodynamic activities and partial enthalpies of mixing in the solid solution of Fe in Ni ₃ Al.	3569-3575A	
Epoxy resins, Composite materials		
Subcritical crack growth at bimaterial interfaces. I. Flexural peel technique.	205-211A	
Subcritical crack growth at bimaterial interfaces. III. Shear-enhanced fatigue crack growth resistance at polymer/metal interfaces.	221-228A	
The effect of volume percent and morphology of phases on the damping behavior of epoxy-aluminum composites.	2366-2373A	
Equiaxed structure		
Characterization of superplastic deformation behavior of a fine grain 5083 Al alloy sheet.	1889-1898A	
The improved microstructures and properties of 7075 alloys produced by a water-cooling centrifugal casting method.	1951-1962A	
Lamellar growth of eutectic equiaxed grains.	4205-4210A	
Equilibrium		
Critical evaluation and optimization of the thermodynamic properties of liquid tin solutions.	808-826B	
Phase equilibria in the metal-sulfur-oxygen system and selective reduction of metal oxides and sulfides. I. The carbothermic reduction and calculation of complex mineral sulfides.	827-838B	
Thermodynamics of calcium and oxygen in molten titanium and titanium-aluminum alloy.	967-972B	
Inverse melting in binary systems: morphology and microscopy of catatetic alloys.	979-986B	
An isothermal section at 550°C in the Al-rich corner of the Al-Fe-Mn-Si system.	3357-3361A	
Eutectic reactions		
Generalized enthalpy method for multicomponent phase change.	869-879B	
Eutectics		
Radioscopic visualization of isothermal solidification of eutectic Ga-In alloy.	686-689B	
Microstructural aspects of the dissolution and melting of Al ₂ Cu phase in Al-Si alloys during solution heat treatment.	1785-1798A	
Directional solidification of white cast iron.	2328-2337A	
Retrograde solubility in semiconductors.	2704-2707A	
Transitions between type A flake, type D flake, and coral graphite eutectic structures in cast irons.	2740-2753A	
Eutectics, Mechanical properties		
High-temperature behavior of precious metal base composites.	2642-2652A	
Eutectics, Structural hardening		
Lamellar growth of eutectic equiaxed grains.	4205-4210A	
Eutectoid decomposition, Temperature effects		
Eutectoid decomposition in Ag-Ga.	1676-1682A	
Eutectoids		
Discussion of "Effects of tensile stress on microstructural change of eutectoid Zn-Al alloy" and authors' reply.	3330-3335A	
Evaporation, Cooling effects		
Vacuum evaporation of KCl-NaCl salts. II. Vaporization-rate model and experimental results.	433-443B	
Expansion		
Increased ductility in high velocity electromagnetic ring expansion.	1837-1844A	
Explosive cladding		
Wear-resistant coatings produced by shock-wave compaction of powders.	2297-2304A	
Explosive compacting		
Mechanistic processes influencing shock chemistry in powder mixtures of the Ti-Si, Ti-Al, and Ti-B systems.	1761-1771A	
Extrusion ingots, Mechanical properties		
The plastic anisotropy of an Al-Li-Cu-Zr alloy extrusion in unidirectional deformation.	3503-3512A	
Extrusions, Heat treatment		
A process model for on-line quenching of aluminum extrusions.	501-508B	
Extrusions, Mechanical properties		
Effects of alkali-metal impurities on fracture toughness of 2090 Al-Li-Cu extrusions.	3530-3541A	
Failure		
Failure characteristics of 6061/Al ₂ O ₃ /15 _p and 2014/Al ₂ O ₃ /15 _p composites as a function of loading rate.	3095-3107A	
High-temperature deformation and failure of an orthorhombic titanium aluminide sheet material.	3675-3681A	
Faraday effect		
Effect of baking temperature and anode current density on anode carbon consumption.	177-183B	
Fast nuclear reactors, Materials selection		
Influence of thermal aging on the intergranular corrosion resistance of types 304LN and 316LN stainless steels.	2881-2887A	
Fatigue (materials)		
The effects on fracture toughness of ductile-phase composition and morphology in Nb-Cr-Ti and Nb-Si in situ composites.	3007-3018A	
Crystallographic preferred orientation induced by cyclic rolling contact loading.	3445-3465A	
Plastic zones and fatigue-crack closure under plane-strain double slip.	3491-3502A	
Fatigue (materials), Environmental effects		
On the transition of fatigue crack growth from stage I to stage II in a corrosive environment.	471-476A	
Fatigue (materials), Stress effects		
Evidence of fracture surface interference for cracks loaded in shear detected by phase-shifted speckle interferometry.	3853-3860A	
Fatigue failure		
Observation of short fatigue crack-growth process in SiC-fiber-reinforced Ti-15-3 alloy composite.	2843-2851A	
Conditioning monitoring by microstructural evaluation of cumulative fatigue damage.	3841-3851A	

Fatigue life		
High-temperature low-cycle fatigue of a gamma titanium aluminide alloy Ti-48Al-2Nb-2Cr.	2239-2251A	
Copper-bearing high-strength low-alloy steels: the influence of microstructure on the initiation and growth of small fatigue cracks.	2540-2556A	
Conditioning monitoring by microstructural evaluation of cumulative fatigue damage.	3841-3851A	
Fatigue life, Coating effects		
Isothermal fatigue of an aluminide-coated single-crystal superalloy. I.	353-361A	
Fatigue life, Environmental effects		
The influence of aqueous environments on low ΔK and high ΔK fatigue crack propagation behavior in low carbon structural steels.	2678-2685A	
Fatigue life, Heating effects		
Corrosion fatigue in nitrocarburized quenched and tempered steels.	1333-1348A	
Fatigue life, Microstructural effects		
The normalized Coffin-Manson plot in terms of a new damage function based on grain boundary cavitation under creep-fatigue condition.	1273-1281A	
Fatigue life, Stress effects		
Mechanisms of high-temperature fatigue failure in alloy 800H.	851-861A	
Prediction of fatigue crack formation in 304 stainless steel.	1267-1271A	
Fatigue life, Temperature effects		
Isothermal fatigue of an aluminide-coated single-crystal superalloy. II. Effects of brittle precracking.	363-369A	
Fatigue limit, Heating effects		
High cycle fatigue behavior of gas-carburized medium carbon Cr-Mo steel.	2557-2564A	
Fatigue strength		
Copper-bearing high-strength low-alloy steels: the influence of microstructure on the initiation and growth of small fatigue cracks.	2540-2556A	
Observation of short fatigue crack-growth process in SiC-fiber-reinforced Ti-15-3 alloy composite.	2843-2851A	
Fatigue strength, Alloying effects		
Effect of strontium modification on near-threshold fatigue crack growth in an Al-Si-Cu die cast alloy.	1293-1302A	
Fatigue strength, Composition effects		
Effect of manganese dispersoid on the fatigue crack propagation of Al-Zn-Mg alloys.	490-493A	
Fatigue strength, Heating effects		
High cycle fatigue behavior of gas-carburized medium carbon Cr-Mo steel.	2557-2564A	
Fatigue strength, Microstructural effects		
Fracture characteristics, microstructure, and tissue reaction of Ti-5Al-2.5Fe for orthopedic surgery.	3925-3935A	
Fatigue strength, Stress effects		
Subcritical crack growth at bimaterial interfaces. III. Shear-enhanced fatigue crack growth resistance at polymer/metal interface.	221-228A	
Temperature dependence of the intrinsic small fatigue crack growth behavior in nickel-base superalloys based on measurement of crack closure.	1021-1031A	
Prediction of fatigue crack formation in 304 stainless steel.	1267-1271A	
Fatigue strength, Welding effects		
Effect of postweld treatment on the fatigue crack growth rate of electron-beam-welded AISI 4130 steel.	3162-3169A	
Fatigue tests		
Effect of postweld treatment on the fatigue crack growth rate of electron-beam-welded AISI 4130 steel.	3162-3169A	
FCC metals, Metallography		
An optical method for determining the surface orientation of crystals.	2057-2061A	
Feeders, Design		
The design of feed systems for thin-walled zinc high-pressure die castings.	115-118B	
Ferrite		
The effects of microstructure, strength level, and crack propagation mode on stress corrosion cracking behavior of 4135 steel.	281-290A	
Effect of holding time in the (α - γ) temperature range on toughness of specially austempered ductile iron.	1979-1989A	
Microstructure and phase identification in type 304 stainless steel-zirconium alloys.	2151-2159A	
Modeling of ferrite growth in nodular cast iron.	2209-2220A	
Ferrite, Cooling effects		
The role of grain corners in nucleation.	480-483A	
Ferrite nucleation and growth during continuous cooling.	1544-1553A	
Austenite decomposition during continuous cooling of an HSLA-80 plate steel.	1554-1568A	
Copper precipitation during continuous cooling and isothermal aging of A710 type steels.	1569-1584A	
Ferrite, Heating effects		
Neutron diffraction study of austempered ductile iron.	923-928A	
Bainitic microstructures formed by split isothermal transformation in an Fe-C-Si-Mn-Mo steel.	1141-1147A	
Ferrite, Temperature effects		
Phase stability and atom probe field ion microscopy of type 308 CRE stainless steel weld metal.	763-774A	
The formation mechanism(s), morphology, and crystallography of ferrite sideplates.	1517-1532A	
Ferritic stainless steels, Corrosion		
Retardation of intermetallic phase formation in experimental superferritic stainless steels.	2436-2444A	
Ferritic stainless steels, Mechanical properties		
Effects of nitrogen implantation on low cycle fatigue behavior of ferritic Fe-24Cr-4Al stainless alloy.	2663-2672A	
Ferritic stainless steels, Rolling		
Experimental investigation of the transformation texture in hot-rolled ferritic stainless steel using single orientation determination.	49-57A	
Ferromanganese		
Reaction equilibria in the production of manganese ferroalloys.	5-17B	
Ferrous alloys		
Recrystallization in oxide-dispersion strengthened mechanically alloyed sheet steel.	1963-1978A	
Ferrous alloys, Atomic properties		
Thermodynamics and long-range order of nitrogen in γ -Fe ₃ N ₄ .	1055-1061A	
Effects of low-temperature aging on the microstructure and soft magnetic properties of rapidly quenched Fe-Si-B alloys.	2454-2460A	
Ferrous alloys, Coatings		
Microstructural analysis and oxidation behavior of laser-processed Fe-Cr-Al-Y alloy coatings.	381-390A	
Ferrous alloys, Composite materials		
Kinetics of cyclic oxidation and cracking and finite element analysis of MA956 and sapphire/MA956 composite system.	3279-3291A	
Ferrous alloys, Corrosion		
Internal sulfide precipitation in low Cr-Fe alloys.	3192-3202A	
Ferrous alloys, Crystal growth		
Recrystallization in oxide-dispersion strengthened mechanically alloyed sheet steel.	1963-1978A	
The effect of metallic elements on the crystallization behavior of amorphous Fe-Si-B alloys.	3424-3430A	
Ferrous alloys, Diffusion		
Average effective interdiffusion coefficients and the Matano plane composition.	2504-2509A	
Incipient chemical instabilities of nanophase Fe-Cu alloys prepared by mechanical alloying.	2934-2946A	
Ferrous alloys, Heat treatment		
Mössbauer spectroscopy study of the aging and tempering of high nitrogen quenched Fe-N alloys: kinetics of formation of Fe ₁₆ N ₂ nitride by interstitial ordering in martensite.	2160-2177A	
Ferrous alloys, Magnetic properties		
Development of a magnetoelastic resonant sensor using iron-rich, nonzero magnetostrictive amorphous alloys.	3203-3213A	
Ferrous alloys, Mechanical properties		
Structural characterization of martensitic iron-carbon alloy films electrodeposited from an iron(II) sulfate solution.	483-486A	
Effect of carbide precipitation on the creep behavior of alloy 800HT in the temperature range 700-900°C.	747-756A	
Mechanisms of high-temperature fatigue failure in alloy 800H.	851-861A	
The embrittlement and de-embrittlement of grain boundaries in an Fe-Mn-Ni alloy due to grain boundary segregation of manganese.	1015-1020A	
Effect of thermomechanical treatments on the room-temperature mechanical behavior of iron aluminide Fe ₃ Al.	2985-2993A	
Nonequilibrium grain-boundary segregation and ductile-brittle transition in Fe-Mn-Ni-Ti age-hardening alloy.	3059-3065A	
Effects of the alumina scale on the room-temperature tensile behavior of preoxidized MA 956.	3809-3816A	
Ferrous alloys, Microstructure		
The role of grain corners in nucleation.	480-483A	
Crystallization of amorphous alloys.	549-555A	
Ferrous alloys, Phase transformations		
A study on morphology and plate mean dimensions in Fe-Ni and Fe-Ni-Cr alloys.	973-980A	
Ferrous alloys, Phases (state of matter)		
Nucleation controlled solidification kinetics.	533-547A	

An evaluation of the Fe-N phase diagram considering long-range order of nitrogen atoms in γ -Fe ₄ N _{1-x} and ϵ -Fe ₂ N _{1-x} . The formation mechanism(s), morphology, and crystallography of ferrite sideplates.	1063-1071A	Filaments, Mechanical properties	
Formation of bainite in ferrous and nonferrous alloys through sympathetic nucleation and ledge-wise growth mechanism.	1517-1532A	Van der Waals approximation for potassium bubbles in tungsten.	987-992B
Ferrous alloys, Powder technology	1533-1543A	Finite element method	
Effects of nickel on the sintering behavior of Fe-Ni compacts made from composite and elemental powders.	203-211B	Thermomechanics of the cooling stage in casting processes: three-dimensional finite element analysis and experimental validation.	81-99B
Characterization and mechanical properties of ultrahigh boron steels produced by powder metallurgy.	1861-1867A	Heat-flow-based analysis of surface crack formation during the start-up of the direct chill casting process. II. Experimental study of an AA5182 rolling ingot.	129-137B
Microstructure and tensile properties of compacted, mechanically alloyed, nanocrystalline Fe-Al.	3126-3134A	Subcritical crack growth at bimaterial interfaces. I. Flexural peel technique.	205-211A
Ferrous alloys, Solubility		A process model for on-line quenching of aluminum extrusions.	501-508B
Solubility of carbon in CaO-Al ₂ O ₃ melts.	57-64B	Flow and thermal behavior of the top surface flux/powder layers in continuous casting molds.	672-685B
Ferrous alloys, Steel making		Prediction of grain structures in various solidification processes.	695-705A
Influence of phosphorus addition on the surface tension of liquid iron and segregation of phosphorus on the surface of Fe-P alloy.	71-79B	Effect of multiaxial stresses on creep damage of 316 stainless steel weldments.	891-900A
Ferrous alloys, Welding		Modeling of ingot distortions during direct chill casting of aluminum alloys.	3214-3225A
Microstructural features of friction welded MA 956 superalloy material.	4019-4029A	Thermal residual stresses in functionally graded and layered 6061 Al/SiC materials.	3241-3249A
Fiber composites, Casting		Kinetics of cyclic oxidation and cracking and finite element analysis of MA956 and sapphire/MA956 composite system.	3279-3291A
Solidification of binary hypoeutectic alloy matrix composite castings.	595-609A	Plastic zones and fatigue-crack closure under plane-strain double slip.	3491-3502A
Infiltration of fibrous preform by molten aluminum in a centrifugal force field.	4163-4169A	Thermal expansion of metals reinforced with ceramic particles and microcellular foams.	3700-3717A
Fiber composites, Fabrication		Notch fracture in γ -titanium aluminides.	3903-3912A
Liquid state infrared processing of SCS-6/Ti-6Al-4V composites.	527-532B	Flow and fracture of bimaterial systems based on aluminum alloys.	3937-3947A
An experimental and theoretical investigation of the rapid consolidation of continuously reinforced, metal-matrix composites.	1709-1720A	Measurement of friction under sheet forming conditions.	3971-3981A
Fiber composites, Joining		Mathematical modeling of the extrusion of 6061/Al ₂ O ₃ /20p composite.	4095-4111A
Infrared transient-liquid-phase joining of SCS-6/ β 21S titanium matrix composite.	4011-4018A	Flash smelting	
Fiber composites, Mechanical properties		Kinetics of the flash converting of MK (chalcoite) concentrate.	163-175B
Effective elastic moduli of fiber-matrix interfaces in high-temperature composites.	165-182A	Experimental study of splash generation in a flash smelting furnace.	633-646B
Time-dependent, environmentally assisted crack growth in Nicalon-fiber-reinforced SiC composites at elevated temperatures.	839-849A	Fluid dynamics	
Bridge toughening enhancement in double-notched MoSi ₂ /Nb model composites.	909-921A	A water model study of the flow asymmetry inside a continuous slab casting mold.	757-764B
The Bauschinger effect in a SiC/Al composite.	995-1001A	Model study of bubble and liquid-flow characteristics in a bottom blown bath under reduced pressure.	765-772B
Thermal stability of SiC-SCS-6 fiber-reinforced IMI834 alloys.	1403-1405A	A one-phase model of the mixing of Al-SiC composite melt.	1015-1023B
Multiple matrix cracking in a fiber-reinforced titanium matrix composite under high-cycle fatigue.	1899-1907A	Fluid flow	
Interface effects on the micromechanical response of a transversely loaded single fiber SCS-6/Ti-6Al-4V composite.	2035-2043A	Flow and thermal behavior of the top surface flux/powder layers in continuous casting molds.	672-685B
The effect of volume percent and morphology of phases on the damping behavior of epoxy-aluminum composites.	2366-2373A	Cold model study of the surface profile in a continuous slab casting mold: effect of second phase.	695-697B
Wear behavior of aluminum-based metal matrix composites reinforced with a preform of aluminosilicate fiber.	2385-2389A	A water model study of the flow asymmetry inside a continuous slab casting mold.	757-764B
Observation of short fatigue crack-growth process in SiC-fiber-reinforced Ti-15-3 alloy composite.	2843-2851A	Model study of bubble and liquid-flow characteristics in a bottom blown bath under reduced pressure.	765-772B
Prediction of creep-rupture life of unidirectional titanium matrix composites subjected to transverse loading.	3074-3080A	Fluidized bed reduction	
Fracture and fatigue-crack growth behavior in ductile-phase toughened molybdenum disilicide: effects of niobium wire vs. particulate reinforcements.	3781-3792A	Preoxidation and hydrogen reduction of ilmenite in a fluidized bed reactor.	731-738B
Creep deformation and damage in a continuous fiber-reinforced Ti-6Al-4V composite.	4193-4204A	Flux core wire welding	
Fiber composites, Oxidation		Correlation of microstructure and fracture toughness in high-chromium white iron hardfacing alloys.	3881-3891A
Kinetics of cyclic oxidation and cracking and finite element analysis of MA956 and sapphire/MA956 composite system.	3279-3291A	Fluxes	
Fiber composites, Phases (state of matter)		Controversy on the free energy of formation of CaO—additional evidence in support of thermochemical data.	647-651B
Microstructure of Al ₂ O ₃ fiber-reinforced superalloy (Inconel 718) composites.	451-458A	Fluxes, Physical properties	
Fiber composites, Reactions (chemical)		Thermodynamics of sulfur in the BaO-MnO-SiO ₂ flux system.	652-657B
Interface characterization of ceramic fiber-reinforced titanium alloy composites manufactured by infrared processing.	1379-1394A	Foams, Composite materials	
Investigation of the reaction zone between TiAl and molybdenum.	2285-2292A	Thermal expansion of metals reinforced with ceramic particles and microcellular foams.	3700-3717A
Structure of phases in the δ -Al ₂ O ₃ fiber studied by convergent beam electron diffraction.	3318-3329A	Forging	
Fiber composites, Structural hardening		An experimental and theoretical investigation of the rapid consolidation of continuously reinforced, metal-matrix composites.	1709-1720A
Effect of magnesium on the aging behavior of Al-Zn-Mg-Cu/Al ₂ O ₃ metal matrix composites.	2005-2012A	Formability	
Fiber composites, Synthesis		Analysis and prevention of vertical cracking phenomena during deep drawing of hot-rolled SG295 steel strips.	1241-1250A
Extending the compositional limit of combustion-synthesized B ₄ C-TiB ₂ composites by field activation.	475-480B	Increased ductility in high velocity electromagnetic ring expansion.	1837-1844A
Fibers, Phases (state of matter)		High-temperature deformation processing of Ti-24Al-20Nb.	2593-2604A
Structure of phases in the δ -Al ₂ O ₃ fiber studied by convergent beam electron diffraction.	3318-3329A	Forming of tailor-welded blanks.	2605-2616A
		Measurement of friction under sheet forming conditions.	3971-3981A
		Formability, Microstructural effects	
		Microstructural evolution and superplastic deformation behavior of fine grain 5083Al.	3827-3839A

Fourier analysis

Analysis of shell thickness irregularity in continuously cast middle carbon steel slabs using mold thermocouple data.
Quantitative characterization of the surface topography of rolled sheets by laser scanning microscopy and Fourier transformation.

1045-1056B

Fractography

Loading rate and test temperature effects on fracture of in situ niobium silicide-niobium composites.
Effect of alloying additions on fracture behavior of molybdenum-containing secondary hardening steels.
Shear ligament phenomena in Fe₃Al intermetallics and micro-mechanics of shear ligament toughening.
Correlation of microstructure and fracture toughness in high-chromium white iron hardfacing alloys.
Microstructure and fracture of SiC-particulate-reinforced cast A356 aluminum alloy composites.
Notch fracture in γ -titanium aluminides.
Flow and fracture of bimaterial systems based on aluminum alloys.
Hydrogen-induced cleavage fracture of Fe₃Al-based intermetallics.

2338-2346A

3292-3306A

3343-3346A

3817-3825A

3881-3891A

3893-3901A

3903-3912A

3937-3947A

3949-3956A

Fracture mechanics

Subcritical crack growth at bimaterial interfaces. I. Flexural peel technique.
High Temperature Fracture Mechanisms in Advanced Materials. 825-1136, 8 1/2 in. x 11 in., Illustrated.
Studies on the influence of metallurgical variables on the stress corrosion behavior of AISI 304 stainless steel in sodium chloride solution using the fracture mechanics approach.
Cleavage initiation in the intercritically reheated coarse-grained heat affected zone. II. Failure criteria and statistical effects.
Loading rate and test temperature effects on fracture of in situ niobium silicide-niobium composites.
Effect of alloying additions on fracture behavior of molybdenum-containing secondary hardening steels.
Evidence of fracture surface interference for cracks loaded in shear detected by phase-shifted speckle interferometry.
Correlation of microstructure and fracture toughness in high-chromium white iron hardfacing alloys.

205-211A

825-1136, 8 1/2 in. x 11 in., Illustrated

1313-1325A

3019-3029A

3292-3306A

3343-3346A

3853-3860A

3881-3891A

Fracture strength

Failure characteristics of 6061/Al₂O₃/15_p and 2014/Al₂O₃/15_p composites as a function of loading rate.
Loading rate and test temperature effects on fracture of in situ niobium silicide-niobium composites.

3095-3107A

3292-3306A

Fracture strength, Composition effects

A study of the influence of mischmetal additions to Al-7Si-0.3Mg (LM 25/356) alloy.

1283-1292A

Fracture strength, Deformation effects

Effect of thermomechanical treatments on the room-temperature mechanical behavior of iron aluminide Fe₃Al.

2985-2993A

Fracture strength, Diffusion effects

Nonequilibrium grain-boundary segregation and ductile-brittle transition in Fe-Mn-Ni-Ti age-hardening alloy.

3059-3065A

Fracture strength, Microstructural effects

Mechanical behavior and properties of mechanically alloyed aluminum alloys.
Phase stability and atom probe field ion microscopy of type 308 CRE stainless steel weld metal.
The embrittlement and de-embrittlement of grain boundaries in an Fe-Mn-Ni alloy due to grain boundary segregation of manganese.
Creep deformation of dispersion-strengthened copper.

737-745A

763-774A

1015-1020A

1217-1227A

Fracture strength, Stress effects

Reinforcement stresses during deformation of sphere- and particulate-reinforced aluminum-matrix composites.

486-490A

Fracture strength, Temperature effects

Observations of secondary carbide precipitation and its relation to high-temperature flow and fracture in HT-9 stainless steel.

467-469A

Fracture toughness

Microstructure and properties of Al₂O₃-Al(Si) and Al₂O₃-Al(Si)-Si composites formed by in situ reaction of aluminum with aluminosilicate ceramics.
The fracture toughness of niobium-based, in situ composites.
Loading rate and test temperature effects on fracture of in situ niobium silicide-niobium composites.
The balance of mechanical and environmental properties of a multielement niobium-niobium silicide-based in situ composite.
Notch fracture in γ -titanium aluminides.

2122-2129A

2518-2531A

3292-3306A

3801-3808A

3903-3912A

Fracture toughness, Alloying effects

Effect of alloying additions on fracture behavior of molybdenum-containing secondary hardening steels.

3343-3346A

Fracture toughness, Composition effects

Effect of manganese dispersoid on the fatigue crack propagation of Al-Zn-Mg alloys.

490-493A

Fracture toughness, Corrosion effects

Shear ligament phenomena in Fe₃Al intermetallics and micro-mechanics of shear ligament toughening.

3817-3825A

Fracture toughness, Heating effects

Microstructural basis for the effect of chromium on the strength and toughness of AF1410-based high performance steels.

2510-2517A

Fracture toughness, Impurity effects

Microsegregation of oxygen in Zr-2.5Nb alloy materials.
Effects of alkali-metal impurities on fracture toughness of 2090 Al-Li-Cu extrusions.

431-440A

3530-3541A

Fracture toughness, Microstructural effects

Subcritical crack growth at bimaterial interfaces. II. Microstructural effects on fracture resistance of metal/ceramic interfaces.
A comparison of fracture behavior of low alloy steel with different sizes of carbide particles.
Microstructure and mechanical behavior of Cr-Cr₂Hf in situ intermetallic composites.
The effects on fracture toughness of ductile-phase composition and morphology in Nb-Cr-Ti and Nb-Si in situ composites.
Fracture and fatigue-crack growth behavior in ductile-phase toughened molybdenum disilicide: effects of niobium wire vs. particulate reinforcements.
Correlation of microstructure and fracture toughness in high-chromium white iron hardfacing alloys.
Microstructure and fracture of SiC-particulate-reinforced cast A356 aluminum alloy composites.
Fracture characteristics, microstructure, and tissue reaction of Ti-5Al-2.5Fe for orthopedic surgery.

213-219A

1909-1917A

2583-2592A

3007-3018A

3781-3792A

3881-3891A

3893-3901A

3925-3935A

Fracture toughness, Radiation effects

The effect of high-energy electron-beam irradiation on microstructural modification of a high-speed steel roll.

3149-3161A

Fracture toughness, Stress effects

Detecting stable crack onset at ductile-brittle transition in steels.

469-471A

Fracture toughness, Welding effects

Microstructures relevant to brittle fracture initiation at the heat-affected zone of weldment of a low carbon steel.

2574-2582A

Fracturing

High-temperature low-cycle fatigue of a gamma titanium aluminide alloy Ti-46Al-2Nb-2Cr.
The influence of stress triaxiality on the damage mechanisms in an equiaxed α/β Ti-6Al-4V alloy.
Microstructure and tensile properties of compacted, mechanically alloyed, nanocrystalline Fe-Al.

2239-2251A

3043-3058A

3126-3134A

Fracturing, Microstructural effects

Reinforcement shape effects on the fracture behavior and ductility of particulate-reinforced 6061-Al matrix composites.

3739-3746A

Free energy

Controversy on the free energy of formation of CaO—additional evidence in support of thermochemical data.
Use of solid-electrolyte galvanic cells to determine the activity of CaO in the CaO-ZrO₂ system and the standard Gibbs free energies of formation of CaZrO₃ from CaO and ZrO₂.
Discussion of "Representation of mixed reactive gases on free energy (Ellingham-Richardson) diagrams" and reply.
Critical evaluation and optimization of the thermodynamic properties of liquid tin solutions.
Phase equilibria in the metal-sulfur-oxygen system and selective reduction of metal oxides and sulfides. I. The carbothermic reduction and calcination of complex mineral sulfides.
Thermodynamics of phosphorus in molten silicon.
A thermodynamic evaluation of the Ti-Mo-C system.
Thermodynamics of calcium and oxygen in molten titanium and titanium-aluminum alloy.
Thermodynamic properties of complex oxides in the Sm-Ba-Cu-O system.
Gibbs energies of formation of chromium carbides.
Formation of structural intermetallics by reactive metal penetration of titanium and nickel oxides and aluminates.

647-651B

658-662B

693-694B

808-826B

827-838B

937-941B

955-966B

967-972B

973-978B

1919-1924A

2100-2104A

Free energy, Temperature effects

Representation of mixed reactive gases on free energy (Ellingham-Richardson) diagrams.

65-69B

Freezing

An adaptive mesh refinement scheme for solidification problems.

707-717A

Friability

Friability and crushing strength of micrometer-size diamond abrasives used in microgrinding of optical glass.

1047-1053A

Friction

Measurement of friction under sheet forming conditions.

3971-3981A

Friction welding

Microstructural features of friction welded MA 956 superalloy material.

4019-4029A

Frictional wear

- High-temperature wear and deformation processes in metal matrix composites. 3135-3148A
- Ni₃Al intermetallic particles as wear-resistant reinforcement for Al-base composites processed by powder metallurgy. 3259-3266A
- Characterization of the wear response of a modified zinc-based alloy vis-à-vis a conventional zinc-based alloy and a bearing bronze at a high sliding speed. 3513-3523A
- The wear behavior between hardfacing materials. 3639-3648A
- Wear and friction behavior of metal impregnated microporous carbon composites. 3727-3738A

Functionally gradient materials, Mechanical properties

- Thermal residual stresses in functionally graded and layered 6061 Al/SiC materials. 3241-3249A
- Analysis of thermal residual stress in a thick-walled ring of Duralcan-base Al-SiC functionally graded material. 4145-4151A

Functionally gradient materials, Structural hardening

- Theoretical analysis of the particle gradient distribution in centrifugal field during solidification. 1025-1029B

Fused salt electrolysis

- Application of centrifugal fields in fused salt electrowinning with a view to reducing electrolytic energy consumption. 889-894B

Gadolinium, Binary systems

- Inverse melting in binary systems: morphology and microscopy of catatectic alloys. 979-986B

Gallium base alloys, Melting

- Radioscopic visualization of isothermal solidification of eutectic Ga-In alloy. 686-689B

Galvanized steels

- Modeling iron enrichment in hot-dip galvanneal coatings on interstitial-free steels. 1132-1134A

Galvanized steels, Surface properties

- Measurement of friction under sheet forming conditions. 3971-3981A

Galvanizing

- Discussion of "The effect of steel chemistry on the formation of Fe-Zn intermetallic compounds of galvanneal-coated steel sheets" and authors' reply. 146-148B
- Kinetics of phase evolution of Zn-Fe intermetallics. 2904-2910A

Gas metal arc welding

- Dilution in single pass arc welds. 481-489B
- Solidification of an alloy 625 weld overlay. 3612-3620A

Gas phases

- Reaction equilibria in the production of manganese ferroalloys. 5-17B

Gas phases, Cooling effects

- Vacuum evaporation of KCl-NaCl salts. I. Vaporization-rate model and experimental results. 433-443B

Gas phases, Temperature effects

- A study of the thermal decomposition of BaCO₃. 409-416B

Gas pipelines, Corrosion

- Initiation of stress corrosion cracking for pipeline steels in a carbonate-bicarbonate solution. 2686-2691A

Gas tungsten arc welding

- Analysis of heat affected zone phase transformations using in situ spatially resolved x-ray diffraction with synchrotron radiation. 775-783A

Gas turbine engines, Materials selection

- Microstructural stability on aging of an α - β titanium alloy: Ti-6Al-1.6Zr-3.3Mo-0.30Si. 1167-1173A
- The fracture toughness of niobium-based, in situ composites. 2518-2531A

Gases

- Experimental study of splash generation in a flash smelting furnace. 633-646B
- Discussion of "Representation of mixed reactive gases on free energy (Ellingham-Richardson) diagrams" and reply. 693-694B
- A unified representation of the two-phase plume characteristics in gas-stirred ladle systems. 704-708B

Germanium, Binary systems

- Effects of shear flow and anisotropic kinetics on the morphological stability of a binary alloy. 687-694A

Germanium, Extraction

- The mineralogical deportment of germanium in the Clarksville electrolytic zinc plant of Savage Zinc Inc. 567-576B

Glow discharges

- Simultaneous plasma treatment for carburizing and carbonitriding using hollow cathode discharge. 401-405A

Gold, Binary systems

- Inverse melting in binary systems: morphology and microscopy of catatectic alloys. 979-986B

Gold, Extraction

- Electrochemical behavior of the dissolution of gold-silver alloys in cyanide solutions. 355-361B

Gold, Recovering

- Influence of gold content on copper oxidation from silver-gold-copper alloys. 3187-3191A

Gold, Ternary systems

- Thermodynamic investigations of the ternary Au-Sn-Zn system. 921-927B

Grain boundaries

- Modeling texture change during the static recrystallization of interstitial free steels. 155-164A
- The effects of microstructure, strength level, and crack propagation mode on stress corrosion cracking behavior of 4135 steel. 281-290A
- Structure, chemistry, and stress corrosion cracking of grain boundaries in alloys 600 and 690. 327-341A
- Theoretical modeling of densification during activated solid-state sintering. 441-450A
- Effect of iron on ductility and cavitation in the superplastic An-22% Al eutectoid. 863-872A
- The embrittlement and de-embrittlement of grain boundaries in an Fe-Mn-Ni alloy due to grain boundary segregation of manganese. 1015-1020A
- Crystallography of grain boundary α precipitates in a β titanium alloy. 1630-1641A
- An investigation by interactive electron backscatter pattern analysis of processing and superplasticity in an aluminum-magnesium alloy. 2252-2262A
- Orientation selective recrystallization of nonoriented electrical steels. 2347-2358A

Grain boundaries, Diffusion

- Analysis of mean square penetration depth in grain boundary diffusion. 3473-3477A

Grain boundaries, Heating effects

- Evolution of microstructures in the nickel modified titanium tri-aluminides near the L₁₂ phase field. 5-17A
- Surface morphology and compound layer pores of plasma nitrocarburized low carbon steel. 135-143A
- Effect of homogenization heat treatment on the microstructure and heat affected zone microfissuring in welded cast alloy 718. 785-790A
- Characterization of constitutional liquid film migration in nickel-base alloy 718. 2692-2703A

Grain boundaries, Radiation effects

- A model describing neutron irradiation-induced segregation to grain boundaries in dilute alloys. 3381-3390A

Grain boundaries, Stress effects

- Temperature and strain-rate effects on low-cycle fatigue behavior of alloy 800H. 255-267A

Grain boundaries, Temperature effects

- The formation mechanism(s), morphology, and crystallography of ferrite sideplates. 1517-1532A

Grain boundary migration

- Characterization of constitutional liquid film migration in nickel-base alloy 718. 2692-2703A

Grain boundary sliding

- The inter-relationship between grain boundary sliding and cavitation during creep of polycrystalline copper. 901-907A

Grain growth

- Microstructure of Al₂O₃ fiber-reinforced superalloy (Inconel 718) composites. 451-458A
- High-speed imaging and analysis of the solidification of undercooled nickel melts. 863-868B
- Generalized enthalpy method for multicomponent phase change. 869-879B
- The normalized Coffin-Manson plot in terms of a new damage function based on grain boundary cavitation under creep-fatigue condition. 1273-1281A
- Characterization of superplastic deformation behavior of a fine grain 5083 Al alloy sheet. 1889-1898A
- Austenite grain growth kinetics in Al-killed plain carbon steels. 3399-3409A
- Lamellar growth of eutectic equiaxed grains. 4205-4210A

Grain growth, Alloying effects

- Effects of nickel on the sintering behavior of Fe-Ni compacts made from composite and elemental powders. 203-211B

Grain growth, Coating effects

- Microstructural analysis and oxidation behavior of laser-processed Fe-Cr-Al-Y alloy coatings. 381-390A

Grain growth, Cooling effects

- Prediction of grain structures in various solidification processes. 695-705A

Grain growth, Deformation effects

- Microstructural evolution and superplastic deformation behavior of fine grain 5083Al. 3827-3839A

Grain growth, Heating effects

- Effect of primary grain size on the secondary recrystallization of mechanically alloyed oxide dispersion strengthened nickel-based superalloy. 493-496A
- The control of grain size and distribution of particles in a (6061 alloy)_m(Al₂O₃)_p composite by solutionizing treatment. 2023-2034A

Grain orientation

- An investigation by interactive electron backscatter pattern analysis of processing and superplasticity in an aluminum-magnesium alloy. 2252-2262A

Grain refinement

- The improved microstructures and properties of 7075 alloys produced by a water-cooling centrifugal casting method. 1951-1962A
- Effect of grain refinement on the fluidity of two commercial Al-Si foundry alloys. 2305-2313A

Grain refinement, Impurity effects

- Influence of chromium and impurities on the grain refining behavior of aluminum. 791-800A

Grain size

- The effects of microstructure, strength level, and crack propagation mode on stress corrosion cracking behavior of 4135 steel. 281-290A
- Theoretical modeling of densification during activated solid-state sintering. 441-450A
- Microstructure of Al₂O₃ fiber-reinforced superalloy (Inconel 718) composites. 451-458A
- Mechanical behavior and properties of mechanically alloyed aluminum alloys. 737-745A
- Effect of iron on ductility and cavitation in the superplastic Al-22% Al eutectoid. 863-872A
- Creep deformation of dispersion-strengthened copper. 1217-1227A
- The improved microstructures and properties of 7075 alloys produced by a water-cooling centrifugal casting method. 1951-1962A
- Effect of grain refinement on the fluidity of two commercial Al-Si foundry alloys. 2305-2313A
- Microstructure and tensile properties of compacted, mechanically alloyed, nanocrystalline Fe-Al. 3126-3134A
- Influence of titanium and carbon contents on the hydrogen trapping of microalloyed steels. 3773-3780A
- Microstructure of Cu-Co alloys solidified at various supercoolings. 4049-4059A
- Modeling recrystallization kinetics, grain sizes, and textures during multipass hot rolling. 4133-4144A

Grain size, Alloying effects

- Solid-state contributions to densification during liquid-phase sintering. 901-909B

Grain size, Cooling effects

- Ferrite nucleation and growth during continuous cooling. 1544-1553A
- Austenite decomposition during continuous cooling of an HSLA-80 plate steel. 1554-1568A
- Macrotransport-solidification kinetics modeling of equiaxed dendritic growth. II. Computation problems and validation on Inconel 718 superalloy casting. 4075-4083A

Grain size, Deformation effects

- Flow stress and microstructural evolution during hot working of alloy 22Cr-13Ni-5Mn-0.3N austenitic stainless steel. 1251-1266A
- Analysis on the amplitude of serrated flow associated with the Portevin-LeChatelier effect of substitutional fcc alloys. 1683-1686A
- Effects of alloy modification and thermomechanical processing on recrystallization of Al-Mg-Mn alloys. 2947-2957A
- Microstructural evolution and superplastic deformation behavior of fine grain 5083Al. 3827-3839A

Grain size, Field effects

- Characterization of titanium thin films prepared by bias assisted magnetron sputtering. 1057-1060B

Grain size, Heating effects

- Effect of primary grain size on the secondary recrystallization of mechanically alloyed oxide dispersion strengthened nickel-based superalloy. 493-496A
- Analysis of heat affected zone phase transformations using in situ spatially resolved x-ray diffraction with synchrotron radiation. 775-783A
- The control of grain size and distribution of particles in a (6061 alloy)_m(Al₂O₃)_p composite by solutionizing treatment. 2023-2034A
- An analysis of static recrystallization during continuous, rapid heat treatment. 2051-2053A

Grain size, Impurity effects

- Microsegregation of oxygen in Zr-2.5Nb alloy materials. 431-440A
- Influence of chromium and impurities on the grain refining behavior of aluminum. 791-800A

Grain size, Vibration effects

- Effects of forced electromagnetic vibrations during the solidification of aluminum alloys. II. Solidification in the presence of colinear variable and stationary magnetic fields. 457-464B

Grain size, Welding effects

- Microstructural features of friction welded MA 956 superalloy material. 4019-4029A
- Nonuniform distribution of carbonitride particles and its effect on prior austenite grain size in the simulated coarse-grained heat-affected zone of thermomechanical control-processed steels. 4031-4038A

Grain structure

- Mechanical behavior of the in situ composite alloys in the Al-Ni-Ti system near the L₁₂ phase field. 71-79A
- Subcritical crack growth at bimaterial interfaces. II. Microstructural effects on fracture resistance of metal/ceramic interfaces. 213-219A
- Structure, chemistry, and stress corrosion cracking of grain boundaries in alloys 600 and 690. 327-341A
- A study of typical yields of metals. 731-736A
- On the influence of grain morphology on creep deformation and damage mechanisms in directionally solidified and oxide dispersion strengthened superalloys. 879-890A
- The normalized Coffin-Manson plot in terms of a new damage function based on grain boundary cavitation under creep-fatigue condition. 1273-1281A
- On microsuperplasticity in AA7475 domes. 1400-1403A
- The mechanism of formation of a fine duplex microstructure in Ti-48Al-2Mn-2Nb alloys. 1655-1667A
- Modeling recrystallization kinetics, grain sizes, and textures during multipass hot rolling. 4133-4144A

Grain structure, Alloying effects

- The effect of iron and manganese on the recrystallization behavior of hot-rolled and solution-heat-treated aluminum alloy 6013. 19-27A
- The influence of niobium supersaturation in austenite on the static recrystallization behavior of low carbon microalloyed steels. 951-980A
- The breakdown of single-crystal solidification in high refractory nickel-base alloys. 1081-1094A
- Elevated temperature compressive properties of N-doped NIAL. 3170-3180A

Grain structure, Coating effects

- Microstructural analysis and oxidation behavior of laser-processed Fe-Cr-Al-Y alloy coatings. 381-390A

Grain structure, Cooling effects

- The role of grain corners in nucleation. 480-483A
- Prediction of grain structures in various solidification processes. 695-705A
- The squeeze casting of hypoeutectic binary Al-Cu. 4121-4132A

Grain structure, Deformation effects

- Experimental investigation of the transformation texture in hot-rolled ferritic stainless steel using single orientation determination. 49-57A
- Precipitation behavior in a medium carbon, Ti-V-N microalloyed steel. 1149-1165A
- Flow stress and microstructural evolution during hot working of alloy 22Cr-13Ni-5Mn-0.3N austenitic stainless steel. 1251-1266A
- Aspects of dynamic recrystallization in shaped charge and explosively formed projectile devices. 1773-1778A

Grain structure, Field effects

- Effects of forced electromagnetic vibrations during the solidification of aluminum alloys. I. Solidification in the presence of crossed alternating electric fields and stationary magnetic fields. 445-455B

Grain structure, Heating effects

- Effect of superheat on the solidification structures of AISI 310S austenitic stainless steel. 287-296B

Grain structure, Impurity effects

- Microsegregation of oxygen in Zr-2.5Nb alloy materials. 431-440A

Grain structure, Stress effects

- Effect of carbide precipitation on the creep behavior of alloy 800HT in the temperature range 700-900°C. 747-756A
- Creep deformation and crack growth behavior of a single-crystal nickel-base superalloy. 829-837A
- Effect of multiaxial stresses on creep damage of 316 stainless steel weldments. 891-900A

Grain structure, Temperature effects

- Crystallization of amorphous alloys. 549-555A
- Some consequences of thermosolutal convection: the grain structure of castings. 569-581A

Graphite, Composite materials

- Transient thermal analysis of solidification in a centrifugal casting for composite materials containing particle segregation. 277-285B

Graphitic structure, Cooling effects

- Transitions between type A flake, type D flake, and coral graphite eutectic structures in cast irons. 2740-2753A

- Graphitic structure, Heating effects**
Effect of bainite transformation and retained austenite on mechanical properties of austempered spheroidal graphite cast steel. 1585-1594A
- Gravitation**
On the reaction between Fe-Ti and Fe-C liquids under micro-gravity. 407-414A
- Gray Iron, Casting**
Hydrogen effects on directional solidification of tellurium-doped cast irons. 496-498A
- Grinding**
Friability and crushing strength of micrometer-size diamond abrasives used in microgrinding of optical glass. 1047-1053A
- Grinding mills**
Milling dynamics. II. Dynamics of a SPEX mill and a one-dimensional mill. 1991-1997A
Milling dynamics. III. Integration of local and global modeling of mechanical alloying devices. 1999-2004A
- Growth rate**
Orientation dependence of primary dendrite spacing. 2727-2739A
Abnormal growth of faceted (WC) grains in a (Co) liquid matrix. 2809-2819A
 M_2C precipitates in isothermal tempering of high Co-Ni secondary hardening steel. 3466-3472A
Modeling of primary and secondary dendrites in a Cu-6 wt.% tin alloy. 4085-4093A
- Guinier Preston zone**
Low quench sensitivity of superplastic 8090 Al-Li thin sheets. Alloy phase analysis from measurements of bulk magnetic properties. 2923-2933A
2958-2965A
- Guinier Preston zone, Alloying effects**
Effect of magnesium on the aging behavior of Al-Zn-Mg-Cu/ Al_2O_3 metal matrix composites. 2005-2012A
- Hafnium, Binary systems**
Thermochemistry of the Ni-Hf system—intermetallic phases. 3576-3590A
- Hall effect**
Physical modeling studies of electrolyte flow due to gas evolution and some aspects of bubble behavior in advanced Hall cells. III. Predicting the performance of advanced Hall cells. 19-27B
- Hall Heroult process**
Physical modeling studies of electrolyte flow due to gas evolution and some aspects of bubble behavior in advanced Hall cells. III. Predicting the performance of advanced Hall cells. Effect of baking temperature and anode current density on anode carbon consumption. 177-183B
Studies on the corrosion and the behavior of inert anodes in aluminum electrolysis. 185-193B
- Hard surfacing**
Correlation of microstructure and fracture toughness in high-chromium white iron hardfacing alloys. 3881-3891A
- Hardening, Composition effects**
Mechanical properties of Ru-Ni-Al alloys. 1395-1400A
- Hardness**
Microstructure and properties of Al_2O_3 -Al(Si) and Al_2O_3 -Al(Si)-Si composites formed by in situ reaction of aluminum with aluminosilicate ceramics. 2122-2129A
Investigation of the reaction zone between TiAl and molybdenum. 2285-2292A
Microstructure and tensile properties of compacted, mechanically alloyed, nanocrystalline Fe-Al. 3126-3134A
Analysis of the stress-strain curves of a modified 9Cr-1Mo steel by the Voce equation. 3340-3343A
- Hardness, Alloying effects**
Effect of alloying additions on fracture behavior of molybdenum-containing secondary hardening steels. 3343-3346A
- Hardness, Composition effects**
Mechanical properties of Ru-Ni-Al alloys. 1395-1400A
- Hardness, Heating effects**
Low quench sensitivity of superplastic 8090 Al-Li thin sheets. M_2C precipitates in isothermal tempering of high Co-Ni secondary hardening steel. 2923-2933A
3466-3472A
- Hardness, Microstructural effects**
The cracking mechanism of silicon particles in an A357 aluminum alloy. 3558-3568A
An evaluation of the creep properties of two Al-Si alloys produced by rapid solidification processing. 3871-3879A
Correlation of microstructure and fracture toughness in high-chromium white iron hardfacing alloys. 3881-3891A
Influence of matrix structure on the abrasion wear resistance and toughness of a hot isostatic pressed white iron matrix composites. 4183-4191A
- Heat affected zone**
Analysis of heat affected zone phase transformations using in situ spatially resolved x-ray diffraction with synchrotron radiation. 775-783A
Effect of homogenization heat treatment on the microstructure and heat affected zone microfissuring in welded cast alloy 718. 785-790A
Effect of multiaxial stresses on creep damage of 316 stainless steel weldments. 891-900A
- Heat affected zone, Mechanical properties**
Microstructures relevant to brittle fracture initiation at the heat-affected zone of weldment of a low carbon steel. 2574-2582A
Cleavage initiation in the intercritically reheated coarse-grained heat affected zone. II. Failure criteria and statistical effects. 3019-3029A
- Heat affected zone, Microstructure**
Nonuniform distribution of carbonitride particles and its effect on prior austenite grain size in the simulated coarse-grained heat-affected zone of thermomechanical control-processed steels. 4031-4038A
- Heat of crystallization**
Thermally assisted and mechanically driven solid-state reactions for formation of amorphous $Al_{33}Ta_{67}$ alloy powders. 3267-3278A
- Heat of formation**
Standard enthalpies of formation of dysprosium alloys, Dy+Me (Me=Ni, Ru, Rh, Pd, Ir, and Pt), by high-temperature direct synthesis calorimetry. 417-422B
Controversy on the free energy of formation of CaO—additional evidence in support of thermochemical data. 647-651B
Use of solid-electrolyte galvanic cells to determine the activity of CaO in the CaO-ZrO₂ system and the standard Gibbs free energies of formation of CaZrO₃ from CaO and ZrO₂. 658-662B
Gibbs energies of formation of chromium carbides. 1919-1924A
Formation of structural intermetallics by reactive metal penetration of titanium and nickel oxides and aluminates. 2100-2104A
- Heat of reaction**
Formation of structural intermetallics by reactive metal penetration of titanium and nickel oxides and aluminates. 2100-2104A
- Heat resistant steels**
 $M_{23}C_6$ carbide equilibria in the Fe-Cr-C system. 701-704B
- Heat transfer**
Thermomechanics of the cooling stage in casting processes: three-dimensional finite element analysis and experimental validation. 81-99B
Heat transfer and pressure drop considerations in the design of Siros melt lances. 221-230B
Solidification of particle-reinforced metal-matrix composites. 663-671B
Flow and thermal behavior of the top surface flux/powder layers in continuous casting molds. 672-685B
Generalized enthalpy method for multicomponent phase change. 869-879B
- Heat transfer, Cooling effects**
Vacuum evaporation of KCl-NaCl salts. II. Vaporization-rate model and experimental results. 433-443B
- Heat transfer, Temperature effects**
Heat-flow-based analysis of surface crack formation during the start-up of the direct chill casting process. I. Development of the inverse heat-transfer model. 119-127B
- Heat transmission, Temperature effects**
Heat-flow-based analysis of surface crack formation during the start-up of the direct chill casting process. I. Development of the inverse heat-transfer model. 119-127B
Heat-flow-based analysis of surface crack formation during the start-up of the direct chill casting process. II. Experimental study of an AA5182 rolling ingot. 129-137B
- Heterogeneous structure, Cooling effects**
The role of grain corners in nucleation. 480-483A
- Heterogeneous structure, Heating effects**
Microstructural stability on aging of an α - β titanium alloy: Ti-6Al-1.6Zr-3.3Mo-0.30Si. 1167-1173A
Heterogeneous nucleation of δ on dislocations in a dilute aluminum-lithium alloy. 1595-1605A
- Heterogeneous structure, Temperature effects**
Nucleation controlled solidification kinetics. 533-547A
Morphological instabilities of lamellar eutectics. 635-656A
- High alloy steels, Mechanical properties**
Microstructural basis for the effect of chromium on the strength and toughness of AF1410-based high performance steels. 2510-2517A
- High alloy steels, Microstructure**
 M_2C precipitates in isothermal tempering of high Co-Ni secondary hardening steel. 3466-3472A
- High carbon steels, Crystal growth**
Austenite grain growth kinetics in Al-killed plain carbon steels. 3399-3409A

- High carbon steels, Mechanical properties**
Pearlite in ultrahigh carbon steels: heat treatments and mechanical properties. 111-118A
- High cycle fatigue**
Multiple matrix cracking in a fiber-reinforced titanium matrix composite under high-cycle fatigue. 1899-1907A
- High speed steel tools, Mechanical properties**
Active wear and failure mechanisms of titanium nitride-coated high speed steel and titanium nitride-coated cemented carbide tools when machining powder metallurgically made stainless steels. 2796-2808A
- High speed tool steels, Irradiation**
The effect of high-energy electron-beam irradiation on microstructural modification of a high-speed steel roll. 3149-3161A
- High strength low alloy steels, Cladding**
Ballistic impact behavior of multilayered armor plates processed by hardfacing. 3335-3340A
- High strength low alloy steels, Corrosion**
Initiation of stress corrosion cracking for pipeline steels in a carbonate-bicarbonate solution.
Microstructural aspects of sulfide stress cracking in an API X-80 pipeline steel. 2686-2691A
3601-3611A
- High strength low alloy steels, Mechanical properties**
Copper-bearing high-strength low-alloy steels: the influence of microstructure on the initiation and growth of small fatigue cracks. 2540-2556A
Hydrogen-induced cleavage fracture of Fe₃Al-based intermetallics. 3949-3956A
- High strength low alloy steels, Phases (state of matter)**
Austenite decomposition during continuous cooling of an HSLA-80 plate steel. 1554-1568A
Copper precipitation during continuous cooling and isothermal aging of A710 type steels. 1569-1584A
- High strength low alloy steels, Welding**
Dilution in single pass arc welds.
Microstructures relevant to brittle fracture initiation at the heat-affected zone of weldment of a low carbon steel. 2574-2582A
Forming of tailor-welded blanks. 2605-2616A
Cleavage initiation in the intercritically reheated coarse-grained heat affected zone. II. Failure criteria and statistical effects. 3019-3029A
Nonuniform distribution of carbonitride particles and its effect on prior austenite grain size in the simulated coarse-grained heat-affected zone of thermomechanical control-processed steels. 4031-4038A
- High strength low alloy steels mech p**
The influence of aqueous environments on low ΔK and high ΔK fatigue crack propagation behavior in low carbon structural steels. 2678-2685A
- High strength steels, Cladding**
The wear behavior between hardfacing materials. 3639-3648A
- High strength steels, Mechanical properties**
Microstructural basis for the effect of chromium on the strength and toughness of AF1410-based high performance steels. 2510-2517A
- High strength steels, Microstructure**
M₂C precipitates in isothermal tempering of high Co-Ni secondary hardening steel. 3466-3472A
- High strength steels, Surface properties**
Measurement of friction under sheet forming conditions. 3971-3981A
- High temperature**
A study of solid-aqueous equilibria by the speciation approach in the hydronium alunite-sulfuric acid-water system at high temperatures. 555-566B
A unified representation of the two-phase plume characteristics in gas-stirred ladle systems. 704-708B
On the stable Mg-Zn-Y quasicrystals. 1779-1784A
Characterization and mechanical properties of ultrahigh boron steels produced by powder metallurgy. 1861-1867A
High-temperature low-cycle fatigue of a gamma titanium aluminide alloy Ti-46Al-2Nb-2Cr. 2239-2251A
- High temperature effects**
High Temperature Fracture Mechanisms in Advanced Materials. 825-1136, 8 1/2 in. x 11 in., IllustratedA
- Holes**
The measurement of hydrogen activities in molten copper using an oxide protonic conductor. 929-935B
- Homogeneity**
Microstructure and tensile behavior of nitrogen-alloyed, dual-phase stainless steels. 1845-1859A
On the role of magnesium and silicon in the formation of alumina from aluminum alloys by means of DIMOX processing. 2094-2099A
- Homogeneous structure**
Microstructure of Al₂O₃ fiber-reinforced superalloy (Inconel 718) composites. 451-458A
- Tensile properties of mechanically alloyed/milled ODS-Ni-based alloys. 1371-1377A
- Homogeneous structure, Cooling effects**
Solidification of binary hypoeutectic alloy matrix composite castings. 595-609A
- Homogeneous structure, Field effects**
Effects of forced electromagnetic vibrations during the solidification of aluminum alloys. I. Solidification in the presence of crossed alternating electric fields and stationary magnetic fields. 445-455B
- Homogenizing**
Evolution of microstructures in the nickel modified titanium tri-aluminides near the L₁₂ phase field.
The effect of thermal cycle on the microstructural development of a powder metallurgy superalloy braze material.
Effect of homogenization heat treatment on the microstructure and heat affected zone microfissuring in welded cast alloy 718. 5-17A
145-153A
785-790A
- Hot bonding**
Transient liquid-phase bonding in the NiAl/Cu/Ni system—a microstructural investigation. 3621-3629A
- Hot dip galvanizing**
The production of nickel-zinc alloys by powder injection.
Modeling iron enrichment in hot-dip galvanized coatings on interstitial-free steels. 780-787B
1132-1134A
- Hot extrusion**
Microsegregation of oxygen in Zr-2.5Nb alloy materials. 431-440A
- Hot forming**
Communication: Discussion of "Modeling of dynamic materials behavior. A critical evaluation of the dissipator power content approach". 232-235A
Reply: Dynamic materials model. Basis and principles. 235-236A
Micronecking and fracture in cavitated superplastic materials. 1043-1046A
- Hot isostatic pressing**
Characterization and mechanical properties of ultrahigh boron steels produced by powder metallurgy. 1861-1867A
Synthesis of RuAl by reactive powder processing. 3688-3699A
Influence of reinforcement volume fraction and size on the microstructure and abrasion wear resistance of hot isostatically pressed white iron matrix composites. 4171-4181A
Influence of matrix structure on the abrasion wear resistance and toughness of a hot isostatically pressed white iron matrix composites. 4183-4191A
- Hot pressing**
Microstructure and properties of Al₂O₃-Al(Si) and Al₂O₃-Al(Si)-Si composites formed by in situ reaction of aluminum with aluminosilicate ceramics. 2122-2129A
Microstructural development of a gas-atomized and hot-pressed super-O₂ alloy. 2221-2228A
The use of microstructural gradients in hot gas-pressure forming of Zn-Al sheet. 3250-3258A
- Hot pressing, Pressure effects**
Pressure-assisted reactive synthesis of titanium aluminides from dense 50Al-50Ti elemental powder blends. 2130-2139A
- Hot rolling**
Experimental investigation of the transformation texture in hot-rolled ferritic stainless steel using single orientation determination. 49-57A
Austenite grain growth kinetics in Al-killed plain carbon steels. 3399-3409A
Modeling recrystallization kinetics, grain sizes, and textures during multipass hot rolling. 4133-4144A
- Hot strip mills**
Austenite grain growth kinetics in Al-killed plain carbon steels. 3399-3409A
- Hot workability, Temperature effects**
Influence of temperature transients on the hot workability of a two-phase gamma titanium aluminide alloy. 1933-1950A
- Hot working**
Flow stress and microstructural evolution during hot working of alloy 22Cr-13Ni-5Mn-0.3N austenitic stainless steel. 1251-1266A
- Hydrides**
Hydride formation and decomposition in electrolytically charged metastable austenitic stainless steels. 29-40A
- Hydrodynamics**
Characteristics of eccentric bubble plumes in liquids. 231-239B
- Hydrogen, Alloying additive**
Effect of strain rate and temperature on the flow stress of β -phase titanium-hydrogen alloys. 1303-1312A
Effect of phase composition and hydrogen level on the deformation behavior of titanium-hydrogen alloys. 1869-1876A
Dynamic strain aging and hydrogen-induced softening in alpha titanium. 1877-1887A
Elastic moduli of titanium-hydrogen alloys in the temperature range 20°C to 1100°C. 3963-3970A

Hydrogen, Binary systems

Critical evaluation and optimization of the thermodynamic properties of liquid tin solutions.

808-826B

Hydrogen, Chemical analysis

Determination of hydrogen in titanium alloys by cold neutron prompt gamma activation analysis.

3682-3687A

Hydrogen, Diffusion

Internal friction in hydrogen-charged CrNi and CrNiMn austenitic stainless steels.

1815-1821A

Hydrogen trapping and permeation in nickel thoria.

2495-2503A

Influence of titanium and carbon contents on the hydrogen trapping of microalloyed steels.

3773-3780A

Hydrogen-induced cleavage fracture of Fe₃Al-based intermetallics.

3949-3956A

Hydrogen, Dopants

Hydride formation and decomposition in electrolytically charged metastable austenitic stainless steels.

29-40A

Hydrogen, Environment

Hydrogen effects on directional solidification of tellurium-doped cast irons.

496-498A

Hydrogen, Impurities

The effect of hydrogen on the fracture of alloy X-750.

101-110A

Physical chemistry of the powder metallurgy of beryllium: chemical characterization of the powder in relation to its granularity.

371-379A

Hydrogen, Reactions (chemical)

The measurement of hydrogen activities in molten copper using an oxide protonic conductor.

929-935B

Hydrogen embrittlement

The influence of aqueous environments on low ΔK and high ΔK fatigue crack propagation behavior in low carbon structural steels.

2678-2685A

Initiation of stress corrosion cracking for pipeline steels in a carbonate-bicarbonate solution.

2686-2691A

Determination of hydrogen in titanium alloys by cold neutron prompt gamma activation analysis.

3682-3687A

Shear ligament phenomena in Fe₃Al intermetallics and micro-mechanics of shear ligament toughening.

3817-3825A

Hydrogen-induced cleavage fracture of Fe₃Al-based intermetallics.

3949-3956A

Hydrogen embrittlement, Composition effects

Influence of titanium and carbon contents on the hydrogen trapping of microalloyed steels.

3773-3780A

Hydrogen embrittlement, Deformation effects

Effect of thermomechanical treatments on the room-temperature mechanical behavior of iron aluminide Fe₃Al.

2985-2993A

Hydrogen embrittlement, Environmental effects

Studies on the influence of metallurgical variables on the stress corrosion behavior of AlSi 304 stainless steel in sodium chloride solution using the fracture mechanics approach.

1313-1325A

Hydrogen embrittlement, Heating effects

A strain-based fracture model for stress corrosion cracking of low-alloy steels.

291-304A

Hydrogen embrittlement, Impurity effects

The effect of hydrogen on the fracture of alloy X-750.

101-110A

Hydrogen reduction

Preparation of fine copper powders from organic media by reaction with hydrogen under pressure. I. Experimental study.

577-584B

Preparation of fine copper powders from organic media by reaction with hydrogen under pressure. II. The kinetics of particle nucleation, growth, and dispersion.

585-594B

Discussion of "Representation of mixed reactive gases on free energy (Ellingham-Richardson) diagrams" and reply.

693-694B

Preoxidation and hydrogen reduction of ilmenite in a fluidized bed reactor.

731-738B

Hydrogen storage

Hydrogen trapping and permeation in nickel thoria.

2495-2503A

Hydrogen sulfide, Environment

Microstructural aspects of sulfide stress cracking in an API X-80 pipeline steel.

3601-3611A

Hydrogenation

Hydride formation and decomposition in electrolytically charged metastable austenitic stainless steels.

29-40A

Hydrometallurgy

Zinc reduction of MoO₃ in a self propagating high temperature synthesis process.

315-318B

A study of solid-aqueous equilibria by the speciation approach in the hydronium alunite-sulfuric acid-water system at high temperatures.

555-568B

The mineralogical deportment of germanium in the Clarksville electrolytic zinc plant of Savage Zinc Inc.

567-576B

Hypereutectic structures

Correlation of microstructure and fracture toughness in high-chromium white iron hardfacing alloys.

3881-3891A

Hysteresis

Internal friction in hydrogen-charged CrNi and CrNiMn austenitic stainless steels.

1815-1821A

Multiple matrix cracking in a fiber-reinforced titanium matrix composite under high-cycle fatigue.

1899-1907A

High-temperature low-cycle fatigue of a gamma titanium aluminide alloy Ti-46Al-2Nb-2Cr.

2239-2251A

Ilmenite, Reduction (chemical)

Preoxidation and hydrogen reduction of ilmenite in a fluidized bed reactor.

731-738B

Impact strength

Failure characteristics of 6061/Al₂O₃/15_p and 2014/Al₂O₃/15_p composites as a function of loading rate.

3095-3107A

Ballistic impact behavior of multilayered armor plates processed by hardfacing.

3335-3340A

Impact strength, Alloying effects

Effect of alloying additions on fracture behavior of molybdenum-containing secondary hardening steels.

3343-3346A

Impact strength, Heating effects

Microstructural basis for the effect of chromium on the strength and toughness of AF1410-based high performance steels.

2510-2517A

Impact strength, Microstructural effects

Effect of bainite transformation and retained austenite on mechanical properties of austempered spheroidal graphite cast steel.

1585-1594A

Influence of matrix structure on the abrasion wear resistance and toughness of a hot isostatic pressed white iron matrix composites.

4183-4191A

Impact strength, Stress effects

Effect of thermal cycling on the mechanical properties of 350 grade maraging steel.

757-761A

Impact tests

Cleavage initiation in the intercritically reheated coarse-grained heat affected zone. II. Failure criteria and statistical effects.

3019-3029A

Failure characteristics of 6061/Al₂O₃/15_p and 2014/Al₂O₃/15_p composites as a function of loading rate.

3095-3107A

Impurities, Chemical analysis

Physical chemistry of the powder metallurgy of beryllium: chemical characterization of the powder in relation to its granularity.

371-379A

Inclusions

Activities in MnO-SiO₂-Al₂O₃ slags and deoxidation equilibria of manganese and silicon.

263-270B

The improved microstructures and properties of 7075 alloys produced by a water-cooling centrifugal casting method.

1951-1962A

Theoretical calculation of the stress-strain behavior of dual-phase metals with randomly oriented spheroidal inclusions.

2359-2365A

Indentation

Plastic zone and pileup around large indentations.

3793-3800A

Indium base alloys, Mechanical properties

Temperature dependent deformation of polydomain phases in an In-22.5 at.% Ti shape memory alloy.

1687-1692A

Industrial wastes

Materials and society—impacts and responsibilities.

337-350B

The use of blast furnace slag and derived materials in the vitrification of electric arc furnace dust.

379-384B

Industrial wastes, Reactions (chemical)

Preparation of glass-forming materials from granulated blast furnace slag.

801-807B

Industrial wastes, Recovering

A kinetic study of the reaction of zinc oxide with iron powder.

363-374B

Infiltration

Microstructure and properties of Al₂O₃-Al(Si) and Al₂O₃-Al(Si)-Si composites formed by in situ reaction of aluminum with aluminosilicate ceramics.

2122-2129A

Permeability of microporous carbon preforms.

3669-3674A

Infiltration of fibrous preform by molten aluminum in a centrifugal force field.

4163-4169A

Infrared brazing

Infrared transient-liquid-phase joining of SCS-6/β21S titanium matrix composite.

4011-4018A

Infrared heating

Liquid state infrared processing of SCS-6/Ti-6Al-4V composites.

527-532B

Infrared radiation

Liquid state infrared processing of SCS-6/Ti-6Al-4V composites.

527-532B

Ingots		
Heat-flow-based analysis of surface crack formation during the start-up of the direct chill casting process. II. Experimental study of an AA5182 rolling ingot.	129-137B	
Ingots, Dimensional analysis		
Modeling of ingot distortions during direct chill casting of aluminum alloys.	3214-3225A	
Ingots, Microstructure		
The effect of iron and manganese on the recrystallization behavior of hot-rolled and solution-heat-treated aluminum alloy 6013.	19-27A	
Scaling of intragranular dendritic microstructure in ingot solidification.	101-113B	
Effect of superheat on the solidification structures of AISI 310S austenitic stainless steel.	287-296B	
Effects of forced electromagnetic vibrations during the solidification of aluminum alloys. I. Solidification in the presence of crossed alternating electric fields and stationary magnetic fields.	445-455B	
Ingots, Phases (state of matter)		
Electron microscope study of Al-Fe-Si intermetallics in 6201 aluminum alloy.	929-936A	
Injection		
Experimental study of splash generation in a flash smelting furnace.	633-646B	
A unified representation of the two-phase plume characteristics in gas-stirred ladle systems.	704-708B	
The separation of the solids from the carrier gas during submerged powder injection.	773-779B	
The production of nickel-zinc alloys by powder injection.	780-787B	
Injection molding		
Comparative study of pore structure evolution during solvent and thermal debinding of powder injection molded parts.	245-253A	
A statistical analysis of the effect of a mixture component on the rheology of alumina feedstocks.	399-408B	
Interface reactions		
Interface characterization of ceramic fiber-reinforced titanium alloy composites manufactured by infrared processing.	1379-1394A	
Investigation of the reaction zone between TiAl and molybdenum.	2285-2292A	
Structure of phases in the δ -Al ₂ O ₃ fiber studied by convergent beam electron diffraction.	3318-3329A	
Interface reactions, High temperature effects		
Phase relations of a silicide/silica reaction couple at 2273K.	271-276B	
Interface reactions, Pressure effects		
Mechanistic processes influencing shock chemistry in powder mixtures of the Ti-Si, Ti-Al, and Ti-B systems.	1761-1771A	
Interfaces		
Interface effects on the micromechanical response of a transversely loaded single fiber SCS-6/Ti-6Al-4V composite.	2035-2043A	
Interferometry		
Evidence of fracture surface interference for cracks loaded in shear detected by phase-shifted speckle interferometry.	3853-3860A	
Intergranular corrosion, Heating effects		
Influence of thermal aging on the intergranular corrosion resistance of types 304LN and 316LN stainless steels.	2881-2887A	
Intergranular corrosion, Microstructural effects		
Structure, chemistry, and stress corrosion cracking of grain boundaries in alloys 600 and 690.	327-341A	
Intergranular fracture, Diffusion effects		
Nonequilibrium grain-boundary segregation and ductile-brittle transition in Fe-Mn-Ni-Ti age-hardening alloy.	3059-3065A	
Intergranular fracture, Heating effects		
A strain-based fracture model for stress corrosion cracking of low-alloy steels.	291-304A	
Intergranular fracture, Microstructural effects		
Intergranular fracture in some precipitation-hardened aluminum alloys at low temperatures.	3081-3088A	
Intergranular structure, High temperature effects		
Creep lifetime prediction of oxide-dispersion-strengthened nickel-base superalloys: a micromechanically based approach.	3861-3870A	
Interlayers		
Microstructural development in NiAl/Ni-Si-B/Ni transient liquid phase bonds.	1925-1931A	
Intermetallic phases		
Mechanical behavior of the in situ composite alloys in the Al-Ni-Ti system near the L ₁₂ phase field.	71-79A	
Discussion of "The effect of steel chemistry on the formation of Fe-Zn intermetallic compounds of galvanneal-coated steel sheets" and authors' reply.	146-148B	
Physical chemistry of the powder metallurgy of beryllium: chemical characterization of the powder in relation to its granularity.	371-379A	
Microstructure of Al ₂ O ₃ fiber-reinforced superalloy (Inconel 718) composites.	451-458A	
Interface attachment kinetics in alloy solidification.	671-686A	
Interface characterization of ceramic fiber-reinforced titanium alloy composites manufactured by infrared processing.	1379-1394A	
Mechanical properties of Ru-Ni-Al alloys.	1395-1400A	
A high resolution transmission electron microscopy study of interfaces between the γ , B ₂ , and α_2 phases in a Ti-Al-Mo alloy.	1618-1629A	
Microstructure and phase identification in type 304 stainless steel-zirconium alloys.	2151-2159A	
Structural stability of super duplex stainless weld metals and its dependence on tungsten and copper.	2196-2208A	
Microstructural development of a gas-atomized and hot-pressed super- α_2 alloy.	2221-2228A	
Investigation of the reaction zone between TiAl and molybdenum.	2285-2292A	
Retardation of intermetallic phase formation in experimental superferitic stainless steels.	2436-2444A	
Thermodynamic activities and phase boundaries for the alloys of the Ni ₃ Al-Ni ₃ Ti pseudobinary section in the Ni-Al-Ti system.	2673-2677A	
Lattice misfits in four binary Ni-base γ/γ' alloys at ambient and elevated temperatures.	2888-2896A	
A thermodynamic evaluation of the nickel-silicon system.	2897-2903A	
Kinetics of phase evolution of Zn-Fe intermetallics.	2904-2910A	
Low quench sensitivity of superplastic 8090 Al-Li thin sheets.	2923-2933A	
Thermodynamic activities and partial enthalpies of mixing in the solid solution of Fe in Ni ₃ Al.	3569-3575A	
Thermochemistry of the Ni-Hf system—intermetallic phases.	3576-3590A	
The balance of mechanical and environmental properties of a multielement niobium-niobium silicide-based in situ composite.	3801-3808A	
Martensitic transformations in NiMnAl β phase alloys.	4153-4162A	
Intermetallic phases, Alloying effects		
Mechanical alloying of Nb-Al powders.	41-48A	
Electron microscope study of Al-Fe-Si intermetallics in 6201 aluminum alloy.	929-936A	
Identification of precipitate phases in a mechanically alloyed rapidly solidified Al-Fe-Ce alloy.	1033-1041A	
Intermetallic phases, Cooling effects		
Porosity formation in Al-9 wt.% Si-3 wt.% Cu alloy systems: metallographic observations.	415-429A	
Rapid solidification processing of a Mg-Li-Si-Ag alloy.	1363-1370A	
Intermetallic phases, Deformation effects		
The relationship between microstructural and plastic instability in Al-4.0 wt.% Cu alloy.	2916-2922A	
Preferential coarsening of γ' precipitates in Inconel 718 during creep.	3391-3398A	
Intermetallic phases, Heating effects		
Evolution of microstructures in the nickel modified titanium tri-aluminides near the L ₁₂ phase field.	5-17A	
Effect of homogenization heat treatment on the microstructure and heat affected zone microfissuring in welded cast alloy 718.	785-790A	
Phase transformations in Nb-Al-Ti alloys.	1642-1654A	
Microstructural aspects of the dissolution and melting of Al ₂ Cu phase in Al-Si alloys during solution heat treatment.	1785-1798A	
Intermetallic phases, High temperature effects		
Standard enthalpies of formation of dysprosium alloys, Dy+Me (Me=Ni, Ru, Rh, Pd, Ir, and Pt), by high-temperature direct synthesis calorimetry.	417-422B	
Intermetallic phases, Radiation effects		
Improved oxidation resistance of group VB refractory metals by Al ³⁺ ion implantation.	491-500B	
Intermetallic phases, Stress effects		
On the effect of stress on nucleation and growth of precipitates in an Al-Cu-Mg-Ag alloy.	3431-3444A	
Intermetallic phases, Temperature effects		
Nucleation controlled solidification kinetics.	533-547A	
Intermetallics		
Thermodynamic activities and phase boundaries for the alloys of the Ni ₃ Al-Ni ₃ Ti pseudobinary section in the Ni-Al-Ti system.	2673-2677A	
Intermetallics, Alloying elements		
Notch fracture in γ -titanium aluminides.	3903-3912A	
Intermetallics, Bonding		
Microstructural development in NiAl/Ni-Si-B/Ni transient liquid phase bonds.	1925-1931A	
Intermetallics, Coating		
The deposition of aluminide and silicide castings on γ -TiAl using the halide-activated pack cementation method.	3761-3772A	

Intermetallics, Coatings		
Isothermal fatigue of an aluminide-coated single-crystal superalloy. I.	353-361A	
Isothermal fatigue of an aluminide-coated single-crystal superalloy. II. Effects of brittle precracking.	363-369A	
Intermetallics, Composite materials		
Effective elastic moduli of fiber-matrix interphases in high-temperature composites.	165-182A	
Bridge toughening enhancement in double-notched MoSi ₂ /Nb model composites.	909-921A	
Formation of structural intermetallics by reactive metal penetration of titanium and nickel oxides and aluminates.	2100-2104A	
Investigation of the reaction zone between TiAl and molybdenum.	2285-2292A	
NiTi and NiTi-TiC composites. IV. Neutron diffraction study of twinning and shape-memory recovery.	2820-2836A	
Ni ₃ Al intermetallic particles as wear-resistant reinforcement for Al-base composites processed by powder metallurgy.	3259-3266A	
Fracture and fatigue-crack growth behavior in ductile-phase toughened molybdenum disilicide: effects of niobium wire vs. particulate reinforcements.	3781-3792A	
The balance of mechanical and environmental properties of a multielement niobium-niobium silicide-based in situ composite.	3801-3808A	
Intermetallics, Crystal growth		
Crystallization of amorphous phase in sputter-deposited Ti-Al alloy thin films.	2047-2050A	
Intermetallics, Joining		
Transient liquid-phase bonding in the NiAl/Cu/Ni system—a microstructural investigation.	3621-3629A	
Intermetallics, Mechanical properties		
Non-Schmid effects on the behavior of polycrystals, with applications to Ni ₃ Al.	81-99A	
Effect of creep strain on microstructural stability and creep resistance of a TiAl/Ti ₃ Al lamellar alloy.	127-134A	
Rafting in superalloys.	513-530A	
High-temperature deformation properties of NiAl single crystals.	1229-1240A	
Influence of temperature transients on the hot workability of a two-phase gamma titanium aluminide alloy.	1933-1950A	
High-temperature low-cycle fatigue of a gamma titanium aluminide alloy Ti-46Al-2Nb-2Cr.	2239-2251A	
High-temperature deformation processing of Ti-24Al-20Nb.	2583-2604A	
Elevated temperature compressive properties of zirconium-modified NiAl.	2628-2641A	
High-temperature behavior of precious metal base composites.	2642-2652A	
Effect of thermomechanical treatments on the room-temperature mechanical behavior of iron aluminide Fe ₃ Al.	2985-2993A	
The effects on fracture toughness of ductile-phase composition and morphology in Nb-Cr-Ti and Nb-Si in situ composites.	3007-3018A	
Elevated temperature compressive properties of N-doped NiAl.	3170-3180A	
High-temperature deformation and failure of an orthorhombic titanium aluminide sheet material.	3675-3681A	
Shear ligament phenomena in Fe ₃ Al intermetallics and micro-mechanics of shear ligament toughening.	3817-3825A	
Hydrogen-induced cleavage fracture of Fe ₃ Al-based intermetallics.	3949-3956A	
Intermetallics, Oxidation		
Phase relations of a silicide/silica reaction couple at 2273K.	271-276B	
High-temperature oxidation of Ti ₃ Al-based titanium aluminides in oxygen.	3993-4002A	
Effect of nitrogen on the oxidation behavior of Ti ₃ Al-based intermetallic alloys.	4003-4010A	
Intermetallics, Phase transformations		
Molecular dynamics simulation of martensitic transformations in NiAl.	1476-1488A	
Effect of alloying elements on martensitic transformation in the binary NiAl(β) phase alloys.	2445-2453A	
The effect of substrate constraint on the martensitic transformation of Ni-Ti thin films.	2858-2860A	
Intermetallics, Phases (state of matter)		
Stable and metastable ordered phases in microcrystalline alloys Ni (Fe, Mn, Ti).	2045-2046A	
Intermetallics, Powder technology		
Mechanistic processes influencing shock chemistry in powder mixtures of the Ti-Si, Ti-Al, and Ti-B systems.	1761-1771A	
Pressure-assisted reactive synthesis of titanium aluminides from dense 50Al-50Ti elemental powder blends.	2130-2139A	
Dense CoAl-based alloys with improved ductility: solid-state synthesis and microstructure control.	2140-2150A	
Kinetics of phase evolution of Zn-Fe intermetallics.	2904-2910A	
Synthesis of RuAl by reactive powder processing.	3688-3699A	
Intermetallics, Reactions (chemical)		
Modeling of sequential reactions during microprecipitation synthesis.	961-972A	
Thermodynamics of calcium and oxygen in molten titanium and titanium-aluminum alloy.	967-972B	
Intermetallics, Structural hardening		
Manifestations of dynamic strain aging in soft-oriented NiAl single crystals.	3542-3557A	
Intermetallics, Synthesis		
Synthesis of nanocrystalline Ni ₃ Cu by sol-gel route.	4213-4216A	
Intermetallics, Thermal properties		
Thermodynamic activities and partial enthalpies of mixing in the solid solution of Fe in Ni ₃ Al.	3569-3575A	
Internal friction		
Internal friction in hydrogen-charged CrNi and CrNiMn austenitic stainless steels.	1815-1821A	
Interstitial impurities		
The role of coincident site lattice boundaries during selective growth in interstitial-free steels.	2178-2186A	
Influence of interstitials on the mechanical properties of metallic materials.	3524-3529A	
Interstitial solutions		
Annealing and aging of interstitial C in α-Fe, as measured by internal friction.	2461-2469A	
Intragranular structure, Cooling effects		
Scaling of intragranular dendritic microstructure in ingot solidification.	101-113B	
Investment casting		
Prediction of grain structures in various solidification processes.	695-705A	
Viscosity of superalloy 718 by the oscillating vessel technique.	698-701B	
Ion implantation		
Improved oxidation resistance of group VB refractory metals by Al ⁺ ion implantation.	491-500B	
Effects of nitrogen implantation on low cycle fatigue behavior of ferritic Fe-24Cr-4Al stainless alloy.	2663-2672A	
The growth and structure of thin oxide films on cerium ion-implanted nickel.	3649-3661A	
Ion nitriding		
Transmission electron microscopy study on the cross-sectional microstructure of an ion-nitriding layer.	1347-1352A	
Effects of nitrogen implantation on low cycle fatigue behavior of ferritic Fe-24Cr-4Al stainless alloy.	2663-2672A	
Iridium, Binary systems		
Standard enthalpies of formation of dysprosium alloys, Dy+Me (Me=Ni, Ru, Rh, Pd, Ir, and Pt), by high-temperature direct synthesis calorimetry.	417-422B	
Iron, Alloying elements		
The effect of iron and manganese on the recrystallization behavior of hot-rolled and solution-heat-treated aluminum alloy 6013.	19-27A	
Iron, Binary systems		
Critical evaluation and optimization of the thermodynamic properties of liquid tin solutions.	808-826B	
Generalized enthalpy method for multicomponent phase change.	869-879B	
Control of iron nitride layers growth kinetics in the binary Fe-N system.	1823-1835A	
Iron, Chemical analysis		
Formation of aluminum-silicon alloys from feldspars—determination of silicon, light, and heavy elements in silumin by scanning electron microscopy.	604-609B	
Iron, Diffusion		
Anomalous diffusion of iron in liquid aluminum measured by the pulsed laser technique.	725-730A	
Iron, Extraction		
Phase equilibria in the metal-sulfur-oxygen system and selective reduction of metal oxides and sulfides. I. The carbothermic reduction and calcination of complex mineral sulfides.	827-838B	
Iron, Impurities		
Influence of chromium and impurities on the grain refining behavior of aluminum.	791-800A	
Iron, Irradiation		
Theoretical treatment of nitriding and nitrocarburizing of iron.	1073-1080A	
A model describing neutron irradiation-induced segregation to grain boundaries in dilute alloys.	3381-3390A	
Iron, Phase transformations		
Bainite in the light of rapid continuous cooling information.	1499-1510A	
Iron, Quaternary systems		
An experimental study and thermodynamic calculations of phase equilibria in the Fe-Mo-C-N system.	2869-2880A	
An isothermal section at 550°C in the Al-rich corner of the Al-Fe-Mn-Si system.	3357-3361A	
Iron, Solubility		
Effects of oxygen, selenium, and tellurium on the rate of nitrogen dissolution in molten iron.	846-851B	

Iron, Ternary systems

- Applicability of Butler's equation in interpreting the thermodynamic behavior of surfaces and adsorption in Fe-S-O melts. 241-253B
 $M_{23}C_6$ carbide equilibria in the Fe-Cr-C system. 701-704B
 Thermodynamic and kinetic study of diffusion paths in the system Cu-Fe-Ni. 2229-2238A
 Experimental study of the phase equilibria in the Fe-Mn-Al system. 2429-2435A
 Internal sulfide precipitation in low Cr-Fe alloys. 3192-3202A
 Solidification of undercooled Fe-Cr-Ni alloys. II. Microstructural evolution. 3226-3240A
 Thermodynamic activities and partial enthalpies of mixing in the solid solution of Fe in Ni_3Al . 3569-3575A

Iron and steel making

- Modeling and experimental study of gaseous oxidation of liquid iron alloys. 852-862B

Iron compounds, Mechanical properties

- Effect of thermomechanical treatments on the room-temperature mechanical behavior of iron aluminide Fe_3Al . 2985-2993A
 Shear ligament phenomena in Fe_3Al intermetallics and micro-mechanics of shear ligament toughening. 3817-3825A
 Hydrogen-induced cleavage fracture of Fe_3Al -based intermetallics. 3949-3956A

Iron compounds, Powder technology

- Kinetics of phase evolution of Zn-Fe intermetallics. 2904-2910A

Iron oxides, Metallography

- Real-time observations of the oxidation of mild steel at high temperature by neutron diffraction. 993-997B

Iron oxides, Ternary systems

- Chemical potentials of components of the system $CaO-P_2O_5-Fe_2O_3$ at 1673K. 595-603B

Ironmaking

- A multiphase fluid mechanics approach to gas holdup in bath smelting processes. 195-201B
 A study of the thermal decomposition of $BaCO_3$. 409-416B
 Alternative technologies in iron and steelmaking. 541-553B
 Reduction of FeO in smelting slags by solid carbon: experimental results. 717-730B
 Preparation of glass-forming materials from granulated blast furnace slag. 801-807B

Isothermal annealing

- Modeling recovery and recrystallization kinetics in cold-rolled Ti-Nb stabilized interstitial-free steel. 3410-3423A

Isothermal treatment

- The control of grain size and distribution of particles in a $(6061\text{ alloy})_m/(Al_2O_3)_p$ composite by solutionizing treatment. 2023-2034A
 An analysis of static recrystallization during continuous, rapid heat treatment. 2051-2053A
 M_2C precipitates in isothermal tempering of high Co-Ni secondary hardening steel. 3466-3472A

Joints, Microstructure

- Transient liquid-phase bonding in the NiAl/Cu/Ni system—a microstructural investigation. 3621-3629A

Killed steels, Steel making

- Activities in $MnO-SiO_2-Al_2O_3$ slags and deoxidation equilibria of manganese and silicon. 263-270B

Kinetics

- Recrystallization in oxide-dispersion strengthened mechanically alloyed sheet steel. 1963-1978A
 An analysis of static recrystallization during continuous, rapid heat treatment. 2051-2053A
 Thermodynamic and kinetic study of diffusion paths in the system Cu-Fe-Ni. 2229-2238A
 Modeling recrystallization kinetics, grain sizes, and textures during multipass hot rolling. 4133-4144A

Ladle metallurgy

- Characteristics of eccentric bubble plumes in liquids. 231-239B
 A unified representation of the two-phase plume characteristics in gas-stirred ladle systems. 704-708B
 Activities in $CaO-SiO_2-Al_2O_3$ slags and deoxidation equilibria of silicon and aluminum. 943-953B

Lamellar structure

- Microstructure and phase relations in a powder-processed Ti-22Al-12Nb alloy. 1121-1126A
 A high resolution transmission electron microscopy study of interfaces between the γ , B2, and α_2 phases in a Ti-Al-Mo alloy. 1618-1629A
 High-temperature low-cycle fatigue of a gamma titanium aluminide alloy Ti-46Al-2Nb-2Cr. 2239-2251A
 Directional solidification of white cast iron. 2328-2337A

Lamellar structure, Deformation effects

- Effect of creep strain on microstructural stability and creep resistance of a TiAl/Ti₃Al lamellar alloy. 127-134A

Lamellar structure, Heating effects

- The use of microstructural gradients in hot gas-pressure forming of Zn-Al sheet. 3250-3258A
 Discussion of "Effects of tensile stress on microstructural change of eutectoid Zn-Al alloy" and authors' reply. 3330-3335A

Lamellar structure, Temperature effects

- Morphological instabilities of lamellar eutectics. 635-656A
 Eutectoid decomposition in Ag-Ga. 1676-1682A

Laminates, Mechanical properties

- Subcritical crack growth at bimaterial interfaces. I. Flexural peel technique. 205-211A
 Subcritical crack growth at bimaterial interfaces. III. Shear-enhanced fatigue crack growth resistance at polymer/metal interface. 221-228A
 Bridge toughening enhancement in double-notched $MoSi_2/Nb$ model composites. 909-921A

Laminates, Reactions (chemical)

- Investigation of the reaction zone between TiAl and molybdenum. 2285-2292A

Laminates, Rolling

- Nanoscale brass/steel multilayer composites produced by cold rolling. 2383-2385A

Lances

- Heat transfer and pressure drop considerations in the design of Sirosmeit lances. 221-230B

Lanthanum, Binary systems

- Inverse melting in binary systems: morphology and microscopy of catatectic alloys. 979-986B

Laser beam heating

- Quenching C60 fullerene into diamond in the Fe-C alloy system by laser treatment. 2293-2296A

Laser beam melting

- Prediction of grain structures in various solidification processes. 695-705A
 Anomalous diffusion of iron in liquid aluminum measured by the pulsed laser technique. 725-730A
 Investigation of the temperature field developed by a spinning beam in laser processing. 4039-4047A

Laser beam welding

- Prediction of grain structures in various solidification processes. 695-705A
 Forming of tailor-welded blanks. 2605-2616A

Laser processing

- Quantitative characterization of the surface topography of rolled sheets by laser scanning microscopy and Fourier transformation. 2338-2346A

Latent heat

- Modeling of ingot distortions during direct chill casting of aluminum alloys. 3214-3225A

Lattice parameters

- Dense CoAl-based alloys with improved ductility: solid-state synthesis and microstructure control. 2140-2150A
 Microstructural development of a gas-atomized and hot-pressed super- α_2 alloy. 2221-2228A
 Lattice misfits in four binary Ni-base γ/γ' alloys at ambient and elevated temperatures. 2888-2896A

Lattice parameters, Alloying effects

- Identification of precipitate phases in a mechanically alloyed rapidly solidified Al-Fe-Ce alloy. 1033-1041A

Lattice parameters, Composition effects

- An evaluation of the Fe-N phase diagram considering long-range order of nitrogen atoms in $\gamma-Fe_4N_{1-x}$ and $\epsilon-Fe_2N_{1-x}$. 1063-1071A

Lattice parameters, Deformation effects

- The x-ray diffraction study of deformation in the composite matrix of Al-Mg-Zn and SiC. 503-505A

Lattice parameters, Heating effects

- Microstructural stability on aging of an $\alpha+\beta$ titanium alloy: Ti-6Al-1.6Zr-3.3Mo-0.30Si. 1167-1173A

Lattice parameters, High temperature effects

- High-temperature measurements of lattice parameters and internal stresses of a creep-deformed monocrystalline nickel-base superalloy. 1003-1014A

Lattice parameters, Stress effects

- Predicting the orientation-dependent stress-induced transformation and detwinning response of shape memory alloy single crystals. 269-279A

Lattice parameters, Temperature effects

- Rafting in superalloys. 513-530A

Lattice vacancies

- The characteristics of cavitation in superplastic metals and ceramics. 873-878A
 Creep deformation of dispersion-strengthened copper. 1217-1227A

Lattice vacancies, Deformation effects

- Analysis on the amplitude of serrated flow associated with the Portevin-LeChatelier effect of substitutional fcc alloys. 1683-1686A

Lattice vacancies, Radiation effects

- Theory of nucleation with cluster loss and injection: application to plastic deformation and irradiation. 1441-1448A

Laves phase

- Microstructure of Al_2O_3 fiber-reinforced superalloy (Inconel 718) composites. 451-458A
Microstructure and phase identification in type 304 stainless steel-zirconium alloys. 2151-2159A

Laves phase, Heating effects

- Effect of homogenization heat treatment on the microstructure and heat affected zone microfissuring in welded cast alloy 718. 785-790A

Leaching

- The mineralogical deportment of germanium in the Clarksville electrolytic zinc plant of Savage Zinc Inc. 567-576B

Lead base alloys, Casting

- Macrosegregation during dendritic arrayed growth of hypoeutectic Pb-Sn alloys: influence of primary arm spacing and mushy zone length. 1353-1362A

Lead base alloys, Crystal growth

- Convection during thermally unstable solidification of Pb-Sn in a magnetic field. 1095-1110A
Ostwald ripening of solid-liquid Pb-Sn dispersions. 2470-2478A

Lead base alloys, Phase transformations

- Banded solidification microstructures. 625-634A
Precipitation in lead-calcium alloys containing tin. 1668-1675A

Lime, Physical properties

- Controversy on the free energy of formation of CaO—additional evidence in support of thermochemical data. 647-651B

Lime, Reactions (chemical)

- Use of solid-electrolyte galvanic cells to determine the activity of CaO in the CaO-ZrO₂ system and the standard Gibbs free energies of formation of CaZrO₃ from CaO and ZrO₂. 658-662B
Activities in CaO-SiO₂-Al₂O₃ slags and deoxidation equilibria of silicon and aluminum. 943-953B
Thermodynamics of calcium and oxygen in molten titanium and titanium-aluminum alloy. 967-972B

Lime, Ternary systems

- Chemical potentials of components of the system CaO-P₂O₅-Fe₂O₃ at 1673K. 595-603B

Liquid metals, Physical properties

- Prediction of liquid metal viscosities using an adjustable hard sphere radial distribution curve. 29-34B

Liquid metals, Sorption

- Effects of oxygen, selenium, and tellurium on the rate of nitrogen dissolution in molten iron. 846-851B

Liquid metals, Surface properties

- Studies of interface deformations in single- and multi-layered liquid baths due to an impinging gas jet. 911-920B

Liquid phase sintering

- Solid-state contributions to densification during liquid-phase sintering. 901-909B
Abnormal growth of faceted (WC) grains in a (Co) liquid matrix. 2809-2819A

Liquid phase sintering, Alloying effects

- The effect of Mo addition on the liquid-phase sintering of W heavy alloy. 3120-3125A

Liquid phases

- Dynamic behavior of a liquid/liquid interface at an oscillating wall. 305-314B
Effects of flow on morphological stability during directional solidification. 583-593A
Interface attachment kinetics in alloy solidification. 671-686A
An adaptive mesh refinement scheme for solidification problems. 707-717A
Real time x-ray transmission microscopy of solidifying Al-In alloys. 801-808A
Microstructural development in NiAl/Ni-Si-B/Ni transient liquid phase bonds. 1925-1931A
The Rayleigh instability and the origin of rows of droplets in the monotectic microstructure of zinc-bismuth alloys. 2053-2057A
Transient liquid-phase bonding in the NiAl/Cu/Ni system—a microstructural investigation. 3621-3629A

Liquid phases, Cooling effects

- Vacuum evaporation of KCl-NaCl salts. II. Vaporization-rate model and experimental results. 433-443B

Liquid phases, Field effects

- On the reaction between Fe-Ti and Fe-C liquids under microgravity. 407-414A

Liquid phases, Pressure effects

- Vacuum evaporation of KCl-NaCl salts. I. Thermodynamic modeling of vapor pressures of solid and liquid solutions. 141-146B

Liquid phases, Temperature effects

- A study of the thermal decomposition of BaCO₃. 409-416B
Overview of geometric effects on coarsening of mushy zones. 557-567A
The phase field method: simulation of alloy dendritic solidification during recalcification. 657-669A

Liquidus

- Liquidus temperatures for primary crystallization of cryolite in molten salt systems of interest for aluminum electrolysis. 739-744B

Lithium, Alloying elements

- Low quench sensitivity of superplastic 8090 Al-Li thin sheets. 2923-2933A
Tension characteristics of notched specimens for Al-Li-Cu-Zr alloys sheets with various cerium contents. 3089-3094A

Lithium, Binary systems

- Thermodynamic studies and the phase diagram of the Li-Mg system. 2419-2428A

Loads (forces)

- Time-dependent, environmentally assisted crack growth in Nicalon-fiber-reinforced SiC composites at elevated temperatures. 839-849A
Mechanisms of high-temperature fatigue failure in alloy 800H. 851-861A
Mathematical modeling of the extrusion of 6061/Al₂O₃/20p composite. 4095-4111A

Long range order

- Interface attachment kinetics in alloy solidification. 671-686A
Stable and metastable ordered phases in microcrystalline alloys Ni (Fe, Mn, Ti). 2045-2046A

Long range order, Alloying effects

- Thermodynamics and long-range order of nitrogen in γ -Fe₄N₁. 1055-1061A

Long range order, Composition effects

- An evaluation of the Fe-N phase diagram considering long-range order of nitrogen atoms in γ -Fe₄N_{1-x} and ϵ -Fe₂N_{1-x}. 1063-1071A

Low alloy steels, Casting

- Prediction of dendrite arm spacing for low alloy steel casting processes. 689-693B

Low alloy steels, Coating

- Wear-resistant coatings produced by shock-wave compaction of powders. 2297-2304A

Low alloy steels, Corrosion

- Influence of titanium and carbon contents on the hydrogen trapping of microalloyed steels. 3773-3780A

Low alloy steels, Heat treatment

- Modeling recovery and recrystallization kinetics in cold-rolled Ti-Nb stabilized interstitial-free steel. 3410-3423A

Low alloy steels, Mechanical properties

- A comparison of fracture behavior of low alloy steel with different sizes of carbide particles. 1909-1917A

Low alloy steels, Phase transformations

- The driving force for martensitic transformations in low alloy steels. 1127-1132A

Low carbon steels, Casting

- Prediction of dendrite arm spacing for low alloy steel casting processes. 689-693B
Modeling of the peritectic reaction and macro-segregation in casting of low carbon steel. 999-1014B

Low carbon steels, Coating

- Correlation of microstructure and fracture toughness in high-chromium white iron hardfacing alloys. 3881-3891A

Low carbon steels, Composite materials

- Nanoscale brass/steel multilayer composites produced by cold rolling. 2383-2385A

Low carbon steels, Crystal growth

- An analysis of static recrystallization during continuous, rapid heat treatment. 2051-2053A
Austenite grain growth kinetics in Al-killed plain carbon steels. 3399-3409A

Low carbon steels, Heat treatment

- Surface morphology and compound layer pores of plasma nitrocarburized low carbon steel. 135-143A
Transmission electron microscopy study on the cross-sectional microstructure of an ion-nitriding layer. 1347-1352A

Low carbon steels, Mechanical properties

- Plastic anisotropy of sheets with continuously varying anisotropic parameters and flow stress. 317-326A
The influence of aqueous environments on low ΔK and high ΔK fatigue crack propagation behavior in low carbon structural steels. 2678-2685A

- Low carbon steels, Metal working**
The influence of niobium supersaturation in austenite on the static recrystallization behavior of low carbon microalloyed steels. 951-960A
- Low carbon steels, Microstructure**
Modeling texture change during the static recrystallization of interstitial free steels. 155-164A
The role of coincident site lattice boundaries during selective growth in interstitial-free steels. 2178-2186A
- Low carbon steels, Oxidation**
Real-time observations of the oxidation of mild steel at high temperature by neutron diffraction. 993-997B
- Low cycle fatigue**
High-temperature low-cycle fatigue of a gamma titanium aluminide alloy Ti-48Al-2Nb-2Cr. 2239-2251A
- Low cycle fatigue, Coating effects**
Isothermal fatigue of an aluminide-coated single-crystal superalloy. I. 353-361A
- Low cycle fatigue, Composition effects**
Effect of manganese dispersoid on the fatigue crack propagation of Al-Zn-Mg alloys. 490-493A
- Low cycle fatigue, Microstructural effects**
The normalized Coffin-Manson plot in terms of a new damage function based on grain boundary cavitation under creep-fatigue condition. 1273-1281A
- Low cycle fatigue, Radiation effects**
Effects of nitrogen implantation on low cycle fatigue behavior of ferritic Fe-24Cr-4Al stainless alloy. 2663-2672A
- Low cycle fatigue, Stress effects**
Temperature and strain-rate effects on low-cycle fatigue behavior of alloy 800H. 255-267A
Mechanisms of high-temperature fatigue failure in alloy 800H. 851-861A
- Magnesium, Alloying additive**
Effect of magnesium on the aging behavior of Al-Zn-Mg-Cu/Al₂O₃ metal matrix composites. 2005-2012A
- Magnesium, Binary systems**
Critical evaluation and optimization of the thermodynamic properties of liquid tin solutions. 808-826B
Thermodynamic studies and the phase diagram of the Li-Mg system. 2419-2428A
- Magnesium, Chemical analysis**
Formation of aluminum-silicon alloys from feldspars—determination of silicon, light, and heavy elements in silumin by scanning electron microscopy. 604-609B
- Magnesium, Forming**
Reply: Dynamic materials model. Basis and principles. 235-236A
- Magnesium base alloys, Forming**
Reply: Dynamic materials model. Basis and principles. 235-236A
- Magnesium base alloys, Mechanical properties**
Rapid solidification processing of a Mg-Li-Si-Ag alloy. 1363-1370A
- Magnesium base alloys, Microstructure**
On the stable Mg-Zn-Y quasicrystals. 1779-1784A
- Magnetic fields**
Effects of forced electromagnetic vibrations during the solidification of aluminum alloys. I. Solidification in the presence of crossed alternating electric fields and stationary magnetic fields. 445-455B
Effects of forced electromagnetic vibrations during the solidification of aluminum alloys. II. Solidification in the presence of collinear variable and stationary magnetic fields. 457-464B
Convection during thermally unstable solidification of Pb-Sn in a magnetic field. 1095-1110A
- Magnetic measurements**
Alloy phase analysis from measurements of bulk magnetic properties. 2958-2965A
- Magnetic permeability**
Alloy phase analysis from measurements of bulk magnetic properties. 2958-2965A
- Magnetic permeability, Heating effects**
Effects of low-temperature aging on the microstructure and soft magnetic properties of rapidly quenched Fe-Si-B alloys. 2454-2460A
- Magnetic testing**
Alloy phase analysis from measurements of bulk magnetic properties. 2958-2965A
- Magnetization**
Development of a magnetoelastic resonant sensor using iron-rich, nonzero magnetostrictive amorphous alloys. 3203-3213A
- Magnetoelastic effect**
Development of a magnetoelastic resonant sensor using iron-rich, nonzero magnetostrictive amorphous alloys. 3203-3213A
- Magnetostriction**
Development of a magnetoelastic resonant sensor using iron-rich, nonzero magnetostrictive amorphous alloys. 3203-3213A
- Manganese, Alloying additive**
Effects of alloy modification and thermomechanical processing on recrystallization of Al-Mg-Mn alloys. 2947-2957A
- Manganese, Alloying elements**
The effect of iron and manganese on the recrystallization behavior of hot-rolled and solution-heat-treated aluminum alloy 6013. 19-27A
- Manganese, Binary systems**
Inverse melting in binary systems: morphology and microscopy of catatectic alloys. 970-986B
- Manganese, Composite materials**
Effect of manganese dispersoid on the fatigue crack propagation of Al-Zn-Mg alloys. 490-493A
- Manganese, Phases (state of matter)**
Stable and metastable ordered phases in microcrystalline alloys Ni (Fe, Mn, Ti). 2045-2048A
- Manganese, Quaternary systems**
An isothermal section at 550°C in the Al-rich corner of the Al-Fe-Mn-Si system. 3357-3361A
- Manganese, Ternary systems**
Experimental study of the phase equilibria in the Fe-Mn-Al system. 2429-2435A
Martensitic transformations in NiMnAl β phase alloys. 4153-4162A
- Manganese base alloys, Phases (state of matter)**
Nucleation controlled solidification kinetics. 533-547A
- Manganese base alloys, Refining**
Thermodynamics of sulfur in the BaO-MnO-SiO₂ flux system. 652-657B
- Maraging steels, Mechanical properties**
Effect of thermal cycling on the mechanical properties of 350 grade maraging steel. 757-761A
- Martensite**
The effects of microstructure, strength level, and crack propagation mode on stress corrosion cracking behavior of 4135 steel. 281-290A
Microstructure and tensile behavior of nitrogen-alloyed, dual-phase stainless steels. 1845-1859A
Microstructural development in NiAl/Ni-Si-B/Ni transient liquid phase bonds. 1925-1931A
Mössbauer spectroscopy study of the aging and tempering of high nitrogen quenched Fe-N alloys: kinetics of formation of Fe₁₆N₂ nitride by interstitial ordering in martensite. 2160-2177A
- Martensite, Alloying effects**
A study on morphology and plate mean dimensions in Fe-Ni and Fe-Ni-Cr alloys. 973-980A
- Martensite, Composition effects**
Structural characterization of martensitic iron-carbon alloy films electrodeposited from an iron(II) sulfate solution. 483-486A
- Martensite, Cooling effects**
Bainite in the light of rapid continuous cooling information. 1499-1510A
Austenite decomposition during continuous cooling of an HSLA-80 plate steel. 1554-1568A
- Martensite, Deformation effects**
Experimental investigation of the transformation texture in hot-rolled ferritic stainless steel using single orientation determination. 49-57A
- Martensite, Heating effects**
Microstructural stability on aging of an α - β titanium alloy: Ti-6Al-1.6Zr-3.3Mo-0.30Si. 1167-1173A
- Martensite, High temperature effects**
Carbide diagrams and precipitation of alloying elements during aging of low-alloy steels. 498-502A
- Martensite, Temperature effects**
The driving force for martensitic transformations in low alloy steels. 1127-1132A
- Martensitic stainless steels, Mechanical properties**
Observations of secondary carbide precipitation and its relation to high-temperature flow and fracture in HT-9 stainless steel. 467-469A
- Martensitic stainless steels, Phase transformations**
Splitting phenomena occurring in the martensitic transformation of Cr13 and CrMoV14 stainless steels in the absence of carbide precipitation. 1799-1805A
- Martensitic transformations**
NiTi and NiTi-TiC composites. II. Compressive mechanical properties. 183-191A
A comprehensive dynamical study of nucleation and growth in a one-dimensional shear martensitic transition. 1203-1216A
Temperature dependent deformation of polydomain phases in an In-22.5 at.% Ti shape memory alloy. 1687-1692A

- Splitting phenomena occurring in the martensitic transformation of Cr13 and CrMoV14 stainless steels in the absence of carbide precipitation. 1799-1805A
- Thermoelastic martensite and shape memory effect in ductile Cu-Al-Mn alloys. 2187-2195A
- NI-Ti and NI-Ti-C composites. IV. Neutron diffraction study of twinning and shape-memory recovery. 2820-2836A
- The effect of substrate constraint on the martensitic transformation of Ni-Ti thin films. 2858-2860A
- Influence of training time and temperature on shape memory effect in Cu-Zn-Al alloys. 3108-3111A
- High-resolution transmission electron microscopy investigation of the face-centered cubic/hexagonal close-packed martensite transformation in Co-31.8 wt.% Ni alloy. I. Plate interfaces and growth ledges. 3362-3370A
- High-resolution transmission electron microscopy investigation of the face-centered cubic/hexagonal close-packed martensite transformation in Co-31.8 wt.% Ni alloy. II. Plate intersections, extended defects, and nucleation mechanisms. 3371-3380A
- Martensitic transformations in NiMnAl β phase alloys. 4153-4162A
- Martensitic transformations, Alloying effects**
- A study on morphology and plate mean dimensions in Fe-Ni and Fe-Ni-Cr alloys. 973-980A
- Effect of alloying elements on martensitic transformation in the binary NiAl(β) phase alloys. 2445-2453A
- Martensitic transformations, Cooling effects**
- NI-Ti and NI-Ti-C composites. III. Shape-memory recovery. Bainite in the light of rapid continuous cooling information. 193-203A
- 1499-1510A
- Martensitic transformations, Heating effects**
- Effect of aging on shape memory behavior of Ti-51.3 at.% Ni thin films. 3753-3759A
- Influence of reinforcement volume fraction and size on the microstructure and abrasion wear resistance of hot isostatically pressed white iron matrix composites. 4171-4181A
- Influence of matrix structure on the abrasion wear resistance and toughness of a hot isostatically pressed white iron matrix composites. 4183-4191A
- Martensitic transformations, Stress effects**
- Predicting the orientation-dependent stress-induced transformation and detwinning response of shape memory alloy single crystals. 269-279A
- Computer simulation of reversible martensitic transformations. Molecular dynamics simulation of martensitic transformations in NiAl. 1187-1201A
- Effect of stress state on the stress-induced martensitic transformation in polycrystalline Ni-Ti alloy. 1476-1488A
- 3066-3073A
- Martensitic transformations, Temperature effects**
- The driving force for martensitic transformations in low alloy steels. 1127-1132A
- Mass transfer**
- Control of iron nitride layers growth kinetics in the binary Fe-N system. 1823-1835A
- Mathematical analysis**
- Van der Waals approximation for potassium bubbles in tungsten. 987-992B
- Analysis of the stress-strain curves of a modified 9Cr-1Mo steel by the Voce equation. 3340-3343A
- Temperature dependence of the rate sensitivity and its effect on the activation energy for high-temperature flow. 3346-3348A
- An analysis of the flow stress of a two-phase alloy system, Ti-6Al-4V. 3957-3962A
- Mathematical models**
- Physical modeling studies of electrolyte flow due to gas evolution and some aspects of bubble behavior in advanced Hall cells. III. Predicting the performance of advanced Hall cells. Hydride formation and decomposition in electrolytically charged metastable austenitic stainless steels. 19-27B
- Prediction of liquid metal viscosities using an adjustable hard sphere radial distribution curve. 29-40A
- Solubility of carbon in CaO-Al₂O₃ melts. 29-34B
- Representation of mixed reactive gases on free energy (Ellingham-Richardson) diagrams. 57-64B
- Thermomechanics of the cooling stage in casting processes: three-dimensional finite element analysis and experimental validation. 65-69B
- Scaling of intragranular dendritic microstructure in ingot solidification. 81-99B
- Vacuum evaporation of KCl-NaCl salts. I. Thermodynamic modeling of vapor pressures of solid and liquid solutions. 101-113B
- Modeling texture change during the static recrystallization of interstitial free steels. 141-146B
- Effective elastic moduli of fiber-matrix interphases in high-temperature composites. 155-164A
- A multiphase fluid mechanics approach to gas holdup in bath smelting processes. 165-182A
- Dispersed phase holdup in liquid-liquid emulsions generated by high strength bottom gas injection. 185-201B
- 213-219B
- Heat transfer and pressure drop considerations in the design of Sirosmelt lances. 221-230B
- Communication: Mechanical deformation of dendrites by fluid flow. 229-232A
- Communication: Discussion of "Modeling of dynamic materials behavior. A critical evaluation of the dissipator power cocontent approach". 232-235A
- Applicability of Butler's equation in interpreting the thermodynamic behavior of surfaces and adsorption in Fe-S-O melts. 241-253B
- A strain-based fracture model for stress corrosion cracking of low-alloy steels. 291-304A
- An extended two-dimensional mathematical model of vertical ring furnaces. 297-304B
- Dynamic behavior of a liquid/liquid interface at an oscillating wall. 305-314B
- Interdiffusion kinetics in oxide powder mixture using high temperature x-ray diffraction technique. 318-322B
- Thermal decomposition of silicon carbides: discussion of "the effect of an electric field on self sustaining combustion synthesis, I and II", and author's reply. 322-325B
- Discussion of "derivation and consistency of the partial functions of the ternary system involving interaction coefficients" and author's reply. 325-327B
- Vacuum evaporation of KCl-NaCl salts. II. Vaporization-rate model and experimental results. 433-443B
- Theoretical modeling of densification during activated solid-state sintering. 441-450A
- The effect of bulk flow concentration on diffusion coupling between dendrites. 477-480A
- Dilution in single pass arc welds. 481-489B
- A process model for on-line quenching of aluminum extrusions. The x-ray diffraction study of deformation in the composite matrix of Al-Mg-Zn and SiC. 501-508B
- 503-505A
- Transient thermal model of the continuous single-wheel thin-strip casting process. 509-525B
- Rafting in superalloys. 513-530A
- Some consequences of thermosolutal convection: the grain structure of castings. 569-581A
- Numerical modeling of cellular/dendritic array growth: spacing and structure predictions. 611-623A
- Intermixing model of continuous casting during a grade transition. 617-632B
- Banded solidification microstructures. 625-634A
- The phase field method: simulation of alloy dendritic solidification during recalcification. 657-669A
- Effects of shear flow and anisotropic kinetics on the morphological stability of a binary alloy. 687-694A
- Prediction of dendrite arm spacing for low alloy steel casting processes. 689-693B
- An adaptive mesh refinement scheme for solidification problems. 707-717A
- A study of typical yields of metals. 731-736A
- Mathematical modeling of tundish operation and flow control to reduce transition slabs. 745-756B
- A water model study of the flow asymmetry inside a continuous slab casting mold. 757-764B
- Model study of bubble and liquid-flow characteristics in a bottom blown bath under reduced pressure. 765-772B
- The production of nickel-zinc alloys by powder injection. 780-787B
- Modeling and experimental study of gaseous oxidation of liquid iron alloys. 852-862B
- Generalized enthalpy method for multicomponent phase change. 869-879B
- Solid-state contributions to densification during liquid-phase sintering. 901-909B
- Bridge toughening enhancement in double-notched MoSi₂/Nb model composites. 909-921A
- Studies of interface deformations in single- and multi-layered liquid baths due to an impinging gas jet. 911-920B
- Ostwald ripening in ternary alloys. 937-943A
- A thermodynamic evaluation of the Ti-Mo-C system. 955-966B
- Modeling of the peritectic reaction and macro-segregation in casting of low carbon steel. 999-1014B
- A one-phase model of the mixing of Al-SiC composite melt. 1015-1023B
- Theoretical analysis of the particle gradient distribution in centrifugal field during solidification. 1025-1029B
- Thermodynamics and long-range order of nitrogen in γ -Fe₄N_{1-x}. 1055-1061A
- Theoretical treatment of nitriding and nitrocarburizing of iron. 1073-1080A
- Modeling iron enrichment in hot-dip galvanneal coatings on interstitial-free steels. 1132-1134A
- Computer simulation of reversible martensitic transformations. 1187-1201A
- A comprehensive dynamical study of nucleation and growth in a one-dimensional shear martensitic transition. 1203-1216A
- The normalized Coffin-Manson plot in terms of a new damage function based on grain boundary cavitation under creep-fatigue condition. 1273-1281A
- Theory of nucleation with cluster loss and injection: application to plastic deformation and irradiation. 1441-1448A
- Effect of uniaxial stress on coarsening of precipitate clusters. 1480-1475A
- Characterization of a massive transformation by microstructural analysis. 1511-1516A

- Heterogeneous nucleation of δ on dislocations in a dilute aluminum-lithium alloy. 2904-2910A
- Analysis on the amplitude of serrated flow associated with the Portevin-LeChatelier effect of substitutional fcc alloys. 2934-2946A
- Control of iron nitride layers growth kinetics in the binary Fe-N system. 3126-3134A
- Modeling of microsegregation in macrosegregation computations. 3267-3278A
- Theoretical calculation of the stress-strain behavior of dual-phase metals with randomly oriented spheroidal inclusions. 3718-3726A
- Average effective interdiffusion coefficients and the Matano plane composition. 1045-1056B
- A model for macrosegregation and its application to Al-Cu castings. 2293-2296A
- Determination of the solidification curves of commercial aluminum alloys. 1149-1165A
- Equiaxed dendritic solidification with convection. I. Multiscale/multiphase modeling. 477-480A
- Equiaxed dendritic solidification with convection. II. Numerical simulations for an Al-4 wt.% Cu alloy. 509-524A
- Equiaxed dendritic solidification with convection. III. Comparisons with $\text{NH}_4\text{Cl-H}_2\text{O}$ experiments. 1785-1798A
- A thermodynamic evaluation of the nickel-silicon system. 2314-2327A
- Constitutive behavior of tantalum and tantalum-tungsten alloys. 433-443B
- Control of superplastic deformation rate during uniaxial tensile tests. 773-779B
- Prediction of creep-rupture life of unidirectional titanium matrix composites subjected to transverse loading. 794-800B
- Tension characteristics of notched specimens for Al-Li-Cu-Zr alloys sheets with various cerium contents. 852-862B
- Simulation of the hot-tension test under cavitating conditions. 577-584B
- Modeling of ingot distortions during direct chill casting of aluminum alloys. 585-594B
- A model describing neutron irradiation-induced segregation to grain boundaries in dilute alloys. 2454-2460A
- Analysis of mean square penetration depth in grain boundary diffusion. 2047-2050A
- The plastic anisotropy of an Al-Li-Cu-Zr alloy extrusion in unidirectional deformation. 3424-3430A
- A model for coupled growth of reaction layers in reactive brazing of ZrO_2 -toughened Al_2O_3 . 3203-3213A
- Plastic zone and pileup around large indentations. 3267-3278A
- Shear ligament phenomena in Fe_3Al intermetallics and micro-mechanics of shear ligament toughening. 3357-3361A
- Evidence of fracture surface interference for cracks loaded in shear detected by phase-shifted speckle interferometry. 4049-4059A
- Creep lifetime prediction of oxide-dispersion-strengthened nickel-base superalloys: a micromechanically based approach. 1033-1041A
- Elevated temperature deformation behavior of a dispersion-strengthened Al-Fe, V, Si alloy. 1371-1377A
- Flow and fracture of bimaterial systems based on aluminum alloys. 1963-1978A
- Measurement of friction under sheet forming conditions. 1991-1997A
- High-temperature oxidation of Ti_3Al -based titanium aluminides in oxygen. 1999-2004A
- Infrared transient-liquid-phase joining of SCS-6/ β 21S titanium matrix composite. 41-48A
- Nonuniform distribution of carbonitride particles and its effect on prior austenite grain size in the simulated coarse-grained heat-affected zone of thermomechanical control-processed steels. 493-496A
- Macrotransport-solidification kinetics modeling of equiaxed dendritic growth. I. Model development and discussion. 1033-1041A
- Macrotransport-solidification kinetics modeling of equiaxed dendritic growth. II. Computation problems and validation on Inconel 718 superalloy casting. 1371-1377A
- Modeling of primary and secondary dendrites in a Cu-6 wt.% tin alloy. 1963-1978A
- Mathematical modeling of the extrusion of 6061/ Al_2O_3 /20p composite. 1991-1997A
- Modeling particle fracture during the extrusion of aluminum/alumina composites. 1999-2004A
- Modeling recrystallization kinetics, grain sizes, and textures during multipass hot rolling. 41-48A
- Lamellar growth of eutectic equiaxed grains. 493-496A
- Mechanical alloying**
- Mechanical alloying of Nb-Al powders. 41-48A
- Effect of primary grain size on the secondary recrystallization of mechanically alloyed oxide dispersion strengthened nickel-based superalloy. 493-496A
- Identification of precipitate phases in a mechanically alloyed rapidly solidified Al-Fe-Ce alloy. 1033-1041A
- Tensile properties of mechanically alloyed/milled ODS-Ni-based alloys. 1371-1377A
- Recrystallization in oxide-dispersion strengthened mechanically alloyed sheet steel. 1963-1978A
- Milling dynamics. II. Dynamics of a SPEX mill and a one-dimensional mill. 1991-1997A
- Milling dynamics. III. Integration of local and global modeling of mechanical alloying devices. 1999-2004A
- Kinetics of phase evolution of Zn-Fe intermetallics. 2904-2910A
- Incipient chemical instabilities of nanophase Fe-Cu alloys prepared by mechanical alloying. 2934-2946A
- Microstructure and tensile properties of compacted, mechanically alloyed, nanocrystalline Fe-Al. 3126-3134A
- Thermally assisted and mechanically driven solid-state reactions for formation of amorphous $\text{Al}_{33}\text{Ta}_{67}$ alloy powders. 3267-3278A
- Microstructural changes in a mechanically alloyed Al-6.2Zn-2.5Mg-1.7Cu alloy (7010) with and without particulate SiC reinforcement. 3718-3726A
- Medium carbon steels, Casting**
- Analysis of shell thickness irregularity in continuously cast middle carbon steel slabs using mold thermocouple data. 1045-1056B
- Medium carbon steels, Heat treatment**
- Quenching C80 fullerene into diamond in the Fe-C alloy system by laser treatment. 2293-2296A
- Medium carbon steels, Phase transformations**
- Precipitation behavior in a medium carbon, Ti-V-N microalloyed steel. 1149-1165A
- Melting**
- The effect of bulk flow concentration on diffusion coupling between dendrites. 477-480A
- Analysis and Modeling of Solidification. 509-524A
- Microstructural aspects of the dissolution and melting of Al_2Cu phase in Al-Si alloys during solution heat treatment. 1785-1798A
- Modeling of microsegregation in macrosegregation computations. 2314-2327A
- Melting points**
- Vacuum evaporation of KCl-NaCl salts. II. Vaporization-rate model and experimental results. 433-443B
- Melts**
- The separation of the solids from the carrier gas during submerged powder injection. 773-779B
- Melts, Chemical analysis**
- Reference electrode of simple galvanic cells for developing sodium sensors for use in molten aluminum. 794-800B
- Melts, Oxidation**
- Modeling and experimental study of gaseous oxidation of liquid iron alloys. 852-862B
- Metal powders, Synthesis**
- Preparation of fine copper powders from organic media by reaction with hydrogen under pressure. I. Experimental study. 577-584B
- Preparation of fine copper powders from organic media by reaction with hydrogen under pressure. II. The kinetics of particle nucleation, growth, and dispersion. 585-594B
- Metallic glasses, Atomic properties**
- Effects of low-temperature aging on the microstructure and soft magnetic properties of rapidly quenched Fe-Si-B alloys. 2454-2460A
- Metallic glasses, Crystal growth**
- Crystallization of amorphous phase in sputter-deposited Ti-Al alloy thin films. 2047-2050A
- The effect of metallic elements on the crystallization behavior of amorphous Fe-Si-B alloys. 3424-3430A
- Metallic glasses, Magnetic properties**
- Development of a magnetoelastic resonant sensor using iron-rich, nonzero magnetostrictive amorphous alloys. 3203-3213A
- Metallic glasses, Powder technology**
- Thermally assisted and mechanically driven solid-state reactions for formation of amorphous $\text{Al}_{33}\text{Ta}_{67}$ alloy powders. 3267-3278A
- Metallizing**
- Characterization of titanium thin films prepared by bias assisted magnetron sputtering. 1057-1060B
- Metastable phases**
- Interface attachment kinetics in alloy solidification. 671-686A
- Stable and metastable ordered phases in microcrystalline alloys Ni (Fe, Mn, Ti). 2045-2046A
- Microstructural development of a gas-atomized and hot-pressed super- α_2 alloy. 2221-2228A
- Kinetics of phase evolution of Zn-Fe intermetallics. 2904-2910A
- High-resolution electron microscopy analysis of structural defects in a (2/1, 5/3)-type approximant of a decagonal quasicrystal of an Al-Pd-Mn alloy. 2911-2915A
- Solidification of undercooled Fe-Cr-Ni alloys. II. Microstructural evolution. 3226-3240A
- An isothermal section at 550°C in the Al-rich corner of the Al-Fe-Mn-Si system. 3357-3361A
- Microstructure of Cu-Co alloys solidified at various supercoolings. 4049-4059A
- Metastable phases, Alloying effects**
- Identification of precipitate phases in a mechanically alloyed rapidly solidified Al-Fe-Ce alloy. 1033-1041A

Metastable phases, Composition effects		
Hydride formation and decomposition in electrolytically charged metastable austenitic stainless steels.	29-40A	
Metastable phases, Temperature effects		
Nucleation controlled solidification kinetics.	533-547A	
Eutectoid decomposition in Ag-Ga.	1676-1682A	
Microalloying		
Influence of microalloying on the corrosion resistance of steel in saturated calcium hydroxide.	1693-1699A	
Microhardness		
The control of grain size and distribution of particles in a (6061 alloy) _m /(Al ₂ O ₃) _p composite by solutionizing treatment.	2023-2034A	
Microhardness, Coating effects		
Microstructural analysis and oxidation behavior of laser-processed Fe-Cr-Al-Y alloy coatings.	381-390A	
Microhardness, Cooling effects		
Rapid solidification processing of a Mg-Li-Si-Ag alloy.	1363-1370A	
Microhardness, Heating effects		
Mechanical properties and 95°C aging characteristics of zircon reinforced Zn-4Al-3Cu alloy.	809-818A	
Influence of long term annealing on tensile properties and fracture of near- α titanium alloy Ti-6Al-2.75Sn-4Zr-0.4Mo-0.45Si.	1700-1708A	
Microhardness, Microstructural effects		
Mechanical behavior of the in situ composite alloys in the Al-Ni-Ti system near the L ₁₂ phase field.	71-79A	
Precipitation in lead-calcium alloys containing tin.	1668-1675A	
Microhardness, Welding effects		
Cleavage initiation in the intercritically reheated coarse-grained heat affected zone. II. Failure criteria and statistical effects.	3019-3029A	
Effect of postweld treatment on the fatigue crack growth rate of electron-beam-welded AISI 4130 steel.	3162-3169A	
Microporosity		
Permeability of microporous carbon preforms.	3669-3674A	
Microscopy		
Quantitative characterization of the surface topography of rolled sheets by laser scanning microscopy and Fourier transformation.	2338-2346A	
Microstructure		
The effect of thermal cycle on the microstructural development of a powder metallurgy superalloy braze material.	145-153A	
Comparative study of pore structure evolution during solvent and thermal debinding of powder injection molded parts.	245-253A	
Characterization and mechanical properties of ultrahigh boron steels produced by powder metallurgy.	1861-1867A	
On the role of magnesium and silicon in the formation of alumina from aluminum alloys by means of DIMOX processing.	2094-2099A	
Microstructure and properties of Al ₂ O ₃ -Al(Si) and Al ₂ O ₃ -Al(Si)-Si composites formed by in situ reaction of aluminum with aluminosilicate ceramics.	2122-2129A	
Microstructure, Heating effects		
Evolution of microstructures in the nickel modified titanium tri-aluminides near the L ₁₂ phase field.	5-17A	
Microstructure, High temperature effects		
Phase relations of a silicide/silica reaction couple at 2273K.	271-276B	
Mischmetal, Alloying additive		
A study of the influence of mischmetal additions to Al-7Si-0.3Mg (LM 25/356) alloy.	1283-1292A	
Miscibility		
Retrograde solubility in semiconductors.	2704-2707A	
Mixing		
Intermixing model of continuous casting during a grade transition.	617-632B	
Modulus of elasticity		
Communication: On the in situ formation of TiC and Ti ₂ C reinforcements in combustion-assisted synthesis of titanium matrix composites.	237-240A	
Thermal stability of SiC-SCS-6 fiber-reinforced IMI834 alloys.	1403-1405A	
Microstructure and properties of Al ₂ O ₃ -Al(Si) and Al ₂ O ₃ -Al(Si)-Si composites formed by in situ reaction of aluminum with aluminosilicate ceramics.	2122-2129A	
The effects on fracture toughness of ductile-phase composition and morphology in Nb-Cr-Ti and Nb-Si in situ composites.	3007-3018A	
The balance of mechanical and environmental properties of a multielement niobium-niobium silicide-based in situ composite.	3801-3808A	
Modulus of elasticity, Alloying effects		
Tension characteristics of notched specimens for Al-Li-Cu-Zr alloys sheets with various cerium contents.	3089-3094A	
Elastic moduli of titanium-hydrogen alloys in the temperature range 20°C to 1100°C.	3963-3970A	
Modulus of elasticity, High temperature effects		
Effective elastic moduli of fiber-matrix interphases in high-temperature composites.	165-182A	
Modulus of elasticity, Microstructural effects		
NiTi and NiTi-TiC composites. II. Compressive mechanical properties.	183-191A	
Effect of bainite transformation and retained austenite on mechanical properties of austempered spheroidal graphite cast steel.	1585-1594A	
Temperature dependent deformation of polydomain phases in an In-22.5 at.% Ti shape memory alloy.	1687-1692A	
Modulus of elasticity, Stress effects		
Subcritical crack growth at bimaterial interfaces. I. Flexural peel technique.	205-211A	
Temperature dependence of the intrinsic small fatigue crack growth behavior in nickel-base superalloys based on measurement of crack closure.	1021-1031A	
Modulus of elasticity, Temperature effects		
Observations of secondary carbide precipitation and its relation to high-temperature flow and fracture in HT-9 stainless steel.	467-469A	
Modulus of rupture in bending, Stress effects		
Subcritical crack growth at bimaterial interfaces. I. Flexural peel technique.	205-211A	
Subcritical crack growth at bimaterial interfaces. III. Shear-enhanced fatigue crack growth resistance at polymer/metal interface.	221-228A	
Molds		
A water model study of the flow asymmetry inside a continuous slab casting mold.	757-764B	
Molybdenum, Alloying additive		
The effect of Mo addition on the liquid-phase sintering of W heavy alloy.	3120-3125A	
Molybdenum, Binary systems		
Critical evaluation and optimization of the thermodynamic properties of liquid tin solutions.	808-826B	
Molybdenum, Composite materials		
Investigation of the reaction zone between TiAl and molybdenum.	2285-2292A	
Molybdenum, Extraction		
Zinc reduction of MoO ₃ in a self propagating high temperature synthesis process.	315-318B	
Molybdenum, Mechanical properties		
Plastic zone and pileup around large indentations.	3793-3800A	
Molybdenum, Quaternary systems		
An experimental study and thermodynamic calculations of phase equilibria in the Fe-Mo-C-N system.	2869-2880A	
Molybdenum, Ternary systems		
A thermodynamic evaluation of the Ti-Mo-C system.	955-966B	
Molybdenum compounds, Composite materials		
Bridge toughening enhancement in double-notched MoSi ₂ /Nb model composites.	909-921A	
Fracture and fatigue-crack growth behavior in ductile-phase toughened molybdenum disilicide: effects of niobium wire vs. particulate reinforcements.	3781-3792A	
Molybdenum compounds, Reactions (chemical)		
Modeling of sequential reactions during microprecipitation synthesis.	961-972A	
Molybdenum steels, Mechanical properties		
Effect of alloying additions on fracture behavior of molybdenum-containing secondary hardening steels.	3343-3346A	
Monitoring		
The measurement of hydrogen activities in molten copper using an oxide protonic conductor.	929-935B	
Moesbauer spectroscopy		
Incipient chemical instabilities of nanophase Fe-Cu alloys prepared by mechanical alloying.	2934-2946A	
Multilayers, Rolling		
Nanoscale brass/steel multilayer composites produced by cold rolling.	2383-2385A	
Nanomaterials, Microstructure		
Microstructure and tensile properties of compacted, mechanically alloyed, nanocrystalline Fe-Al.	3126-3134A	
Nanomaterials, Synthesis		
Synthesis of full-density nanocrystalline tungsten carbide by reduction of tungstic oxide at room temperature.	4210-4213A	
Synthesis of nanocrystalline Ni ₃ Cu by sol-gel route.	4213-4216A	
Near net shaping		
Optimization of cold and warm workability in 304 stainless steel using instability maps.	119-126A	
Liquid state infrared processing of SCS-6/Ti-6Al-4V composites.	527-532B	

- Phase transformations in condensed systems revisited: Industrial applications. 2397-2418A
- The plastic anisotropy of an Al-Li-Cu-Zr alloy extrusion in unidirectional deformation. 3503-3512A
- The squeeze casting of hypoeutectic binary Al-Cu. 4121-4132A
- Necking**
- Simulation of the hot-tension test under cavitating conditions. High-temperature deformation and failure of an orthorhombic titanium aluminide sheet material. 3112-3119A
- 3675-3681A
- Necking, Deformation effects**
- Micronecking and fracture in cavitated superplastic materials. 1043-1046A
- Necking, Microstructural effects**
- Bridge toughening enhancement in double-notched MoSi₂/Nb model composites. 909-921A
- Necking, Stress effects**
- Reinforcement stresses during deformation of sphere- and particulate-reinforced aluminum-matrix composites. 486-490A
- Neodymium, Binary systems**
- Inverse melting in binary systems: morphology and microscopy of catactetic alloys. 979-986B
- Neutron activation analysis**
- Determination of hydrogen in titanium alloys by cold neutron prompt gamma activation analysis. 3682-3687A
- Neutron diffraction**
- Neutron diffraction study of austempered ductile iron. Real-time observations of the oxidation of mild steel at high temperature by neutron diffraction. 923-928A
- 993-997B
- Neutron scattering**
- Incipient chemical instabilities of nanophase Fe-Cu alloys prepared by mechanical alloying. 2934-2946A
- New technology**
- Alternative technologies in iron and steelmaking. 541-553B
- Nickel, Alloying additive**
- Solid-state contributions to densification during liquid-phase sintering. 901-909B
- Nickel, Alloying elements**
- Effects of nickel on the sintering behavior of Fe-Ni compacts made from composite and elemental powders. 203-211B
- The production of nickel-zinc alloys by powder injection. 780-787B
- A study on morphology and plate mean dimensions in Fe-Ni and Fe-Ni-Cr alloys. 973-980A
- Nickel, Atomic properties**
- Sputter-induced pits on {100} nickel surfaces. 981-993A
- Nickel, Binary systems**
- Standard enthalpies of formation of dysprosium alloys, Dy+Me (Me=Ni, Ru, Rh, Pd, Ir, and Pt), by high-temperature direct synthesis calorimetry. 417-422B
- Critical evaluation and optimization of the thermodynamic properties of liquid tin solutions. 808-826B
- Generalized enthalpy method for multicomponent phase change. 869-879B
- A thermodynamic evaluation of the nickel-silicon system. 2897-2903A
- Thermochemistry of the Ni-Hf system—intermetallic phases. 3576-3590A
- Nickel, Bonding**
- Microstructural development in NiAl/Ni-Si-B/Ni transient liquid phase bonds. 1925-1931A
- Nickel, Crystal growth**
- High-speed imaging and analysis of the solidification of undercooled nickel melts. 863-868B
- Nickel, Diffusion**
- Hydrogen trapping and permeation in nickel thoria. 2495-2503A
- Nickel, Extraction**
- Bioleaching of lateritic nickel ore by ultrasound. 351-354B
- A study of solid-aqueous equilibria by the speciation approach in the hydronium alunite-sulfuric acid-water system at high temperatures. 555-566B
- Experimental study of splash generation in a flash smelting furnace. 633-646B
- Phase equilibria in the metal-sulfur-oxygen system and selective reduction of metal oxides and sulfides. I. The carbothermic reduction and calcination of complex mineral sulfides. 827-838B
- Nickel, Forming**
- Reply: Dynamic materials model. Basis and principles. 235-236A
- Nickel, Joining**
- Transient liquid-phase bonding in the NiAl/Cu/Ni system—a microstructural investigation. 3621-3629A
- Nickel, Metallurgy**
- An optical method for determining the surface orientation of crystals. 2057-2061A
- Nickel, Oxidation**
- The growth and structure of thin oxide films on cerium ion-implanted nickel. 3649-3661A
- Nickel, Ternary systems**
- Evolution of microstructures in the nickel modified titanium tri-aluminides near the L1₂ phase field. 5-17A
- Mechanical behavior of the in situ composite alloys in the Al-Ni-Ti system near the L1₂ phase field. 71-79A
- Mechanical properties of R'-Ni-Al alloys. 1395-1400A
- Thermodynamic and kinetic study of diffusion paths in the system Cu-Fe-Ni. 2229-2238A
- Thermodynamic activities and phase boundaries for the alloys of the Ni₃Al-Ni₃Ti pseudobinary section in the Ni-Al-Ti system. 2673-2677A
- Solidification of undercooled Fe-Cr-Ni alloys. II. Microstructural evolution. 3226-3240A
- Thermodynamic activities and partial enthalpies of mixing in the solid solution of Fe in Ni₃Al. 3569-3575A
- Martensitic transformations in NiMnAl β phase alloys. 4153-4162A
- Nickel base alloys**
- Recrystallization in oxide-dispersion strengthened mechanically alloyed sheet steel. 1963-1978A
- Nickel base alloys, Casting**
- Viscosity of superalloy 718 by the oscillating vessel technique. 698-701B
- Nickel base alloys, Claddings**
- Solidification of an alloy 625 weld overlay. 3612-3620A
- The wear behavior between hardfacing materials. 3639-3648A
- Nickel base alloys, Coating**
- Isothermal fatigue of an aluminide-coated single-crystal superalloy. I. 353-361A
- Isothermal fatigue of an aluminide-coated single-crystal superalloy. II. Effects of brittle precracking. 363-369A
- Nickel base alloys, Composite materials**
- Microstructure of bonding zones in laser-clad nickel-alloy-based composite coatings reinforced with various ceramic powders. 391-400A
- Microstructure of Al₂O₃ fiber-reinforced superalloy (Inconel 718) composites. 451-458A
- Effect of primary grain size on the secondary recrystallization of mechanically alloyed oxide dispersion strengthened nickel-based superalloy. 493-496A
- Tensile properties of mechanically alloyed/milled ODS-Ni-based alloys. 1371-1377A
- Nickel base alloys, Corrosion**
- Structure, chemistry, and stress corrosion cracking of grain boundaries in alloys 600 and 690. 327-341A
- Nickel base alloys, Crystal growth**
- Macrotransport-solidification kinetics modeling of equiaxed dendritic growth. I. Model development and discussion. 4061-4074A
- Macrotransport-solidification kinetics modeling of equiaxed dendritic growth. II. Computation problems and validation on Inconel 718 superalloy casting. 4075-4083A
- Nickel base alloys, Crystal lattices**
- Lattice misfits in four binary Ni-base γ/γ' alloys at ambient and elevated temperatures. 2888-2896A
- Nickel base alloys, Forming**
- Reply: Dynamic materials model. Basis and principles. 235-236A
- Nickel base alloys, Heat treatment**
- High-temperature nitridation of Ni-Cr alloys. 59-69A
- Effect of homogenization heat treatment on the microstructure and heat affected zone microfissuring in welded cast alloy 718. 785-790A
- Transition between internal and external nitridation of Ni-Ti alloys. 1606-1617A
- Nickel base alloys, Joining**
- Transient liquid-phase bonding in the NiAl/Cu/Ni system—a microstructural investigation. 3621-3629A
- Nickel base alloys, Mechanical properties**
- The effect of hydrogen on the fracture of alloy X-750. 101-110A
- Predicting the orientation-dependent stress-induced transformation and detwinning response of shape memory alloy single crystals. 269-279A
- Creep deformation and crack growth behavior of a single-crystal nickel-base superalloy. 829-837A
- On the influence of grain morphology on creep deformation and damage mechanisms in directionally solidified and oxide dispersion strengthened superalloys. 879-890A
- High-temperature measurements of lattice parameters and internal stresses of a creep-deformed monocrystalline nickel-base superalloy. 1003-1014A
- Temperature dependence of the intrinsic small fatigue crack growth behavior in nickel-base superalloys based on measurement of crack closure. 1021-1031A

- Nickel base alloys, Metal working**
Flow stress and microstructural evolution during hot working of alloy 22Cr-13Ni-5Mn-0.3N austenitic stainless steel. 1251-1266A
- Nickel base alloys, Microstructure**
Prediction of grain structures in various solidification processes. 695-705A
Characterization of constitutional liquid film migration in nickel-base alloy 718. 2692-2703A
- Nickel base alloys, Phase transformations**
Effect of alloying elements on martensitic transformation in the binary NiAl(β) phase alloys. 2445-2453A
The effect of substrate constraint on the martensitic transformation of Ni-Ti thin films. 2858-2860A
Effect of stress state on the stress-induced martensitic transformation in polycrystalline Ni-Ti alloy. 3066-3073A
Effect of aging on shape memory behavior of Ti-51.3 at.% Ni thin films. 3753-3759A
Martensitic transformations in NiMnAl β phase alloys. 4153-4162A
- Nickel base alloys, Phases (state of matter)**
Nucleation controlled solidification kinetics. 533-547A
The phase field method: simulation of alloy dendritic solidification during recalcification. 657-669A
The breakdown of single-crystal solidification in high refractory nickel-base alloys. 1081-1094A
- Nickel base alloys, Powder technology**
The effect of thermal cycle on the microstructural development of a powder metallurgy superalloy braze material. 145-153A
- Nickel base alloys, Structural hardening**
A study on coherency strain and precipitate morphology via a discrete atom method. 1449-1459A
Bauschinger effect in Haynes 230 alloy: influence of strain rate and temperature. 1739-1748A
Preferential coarsening of γ' precipitates in Inconel 718 during creep. 3391-3398A
Manifestations of dynamic strain aging in soft-oriented NiAl single crystals. 3542-3557A
Creep lifetime prediction of oxide-dispersion-strengthened nickel-base superalloys: a micromechanically based approach. 3861-3870A
- Nickel chromium molybdenum steels, Cladding**
Ballistic impact behavior of multilayered armor plates processed by hardfacing. 3335-3340A
- Nickel chromium molybdenum steels, Heat treatment**
The dependence of complex alloyed steel properties on quenching and tempering conditions. 2852-2858A
- Nickel chromium molybdenum steels, Mechanical properties**
On the transition of fatigue crack growth from stage I to stage II in a corrosive environment. 471-476A
High cycle fatigue behavior of gas-carburized medium carbon Cr-Mo steel. 2557-2564A
Effect of alloying additions on fracture behavior of molybdenum-containing secondary hardening steels. 3343-3346A
Conditioning monitoring by microstructural evaluation of cumulative fatigue damage. 3841-3851A
- Nickel chromium molybdenum steels, Phases (state of matter)**
Copper precipitation during continuous cooling and isothermal aging of A710 type steels. 1569-1584A
- Nickel compounds**
Martensitic transformations in NiMnAl β phase alloys. 4153-4162A
- Nickel compounds, Bonding**
Microstructural development in NiAl/Ni-Si-B/Ni transient liquid phase bonds. 1925-1931A
- Nickel compounds, Composite materials**
NiTi and NiTi-TiC composites. II. Compressive mechanical properties. 183-191A
NiTi and NiTi-TiC composites. III. Shape-memory recovery. 193-203A
Formation of structural intermetallics by reactive metal penetration of titanium and nickel oxides and aluminates. 2100-2104A
Ni₃Al intermetallic particles as wear-resistant reinforcement for Al-base composites processed by powder metallurgy. 3259-3266A
- Nickel compounds, Joining**
Transient liquid-phase bonding in the NiAl/Cu/Ni system—a microstructural investigation. 3621-3629A
- Nickel compounds, Mechanical properties**
Non-Schmid effects on the behavior of polycrystals, with applications to Ni₃Al. 81-99A
Ratting in superalloys. 513-530A
High-temperature deformation properties of NiAl single crystals. 1229-1240A
Elevated temperature compressive properties of zirconium-modified NiAl. 2628-2641A
Elevated temperature compressive properties of N-doped NiAl. 3170-3180A
- Nickel compounds, Phase transformations**
Molecular dynamics simulation of martensitic transformations in NiAl. 1476-1488A
Effect of alloying elements on martensitic transformation in the binary NiAl(β) phase alloys. 2445-2453A
NiTi and NiTi-TiC composites. IV. Neutron diffraction study of twinning and shape-memory recovery. 2820-2836A
The effect of substrate constraint on the martensitic transformation of Ni-Ti thin films. 2858-2860A
- Nickel compounds, Phases (state of matter)**
Stable and metastable ordered phases in microcrystalline alloys Ni (Fe, Mn, Ti). 2045-2046A
- Nickel compounds, Structural hardening**
Manifestations of dynamic strain aging in soft-oriented NiAl single crystals. 3542-3557A
- Nickel compounds, Synthesis**
Synthesis of nanocrystalline Ni₃Cu by sol-gel route. 4213-4216A
- Nickel compounds, Thermal properties**
Thermodynamic activities and partial enthalpies of mixing in the solid solution of Fe in Ni₃Al. 3569-3575A
- Nickel ores**
Bioleaching of lateritic nickel ore by ultrasound. 351-354B
- Niobium, Alloying additive**
The effect of metallic elements on the crystallization behavior of amorphous Fe-Si-B alloys. 3424-3430A
- Niobium, Alloying elements**
Mechanical alloying of Nb-Al powders. 41-48A
The influence of niobium supersaturation in austenite on the static recrystallization behavior of low carbon microalloyed steels. 951-960A
The effects on fracture toughness of ductile-phase composition and morphology in Nb-Cr-Ti and Nb-Si in situ composites. 3007-3018A
- Niobium, Binary systems**
Thermodynamic assessment of the Nb-N system. 3591-3600A
- Niobium, Composite materials**
Loading rate and test temperature effects on fracture of in situ niobium silicide-niobium composites. 3292-3306A
Fracture and fatigue-crack growth behavior in ductile-phase toughened molybdenum disilicide: effects of niobium wire vs. particulate reinforcements. 3781-3792A
- Niobium, Diffusion**
Analysis of mean square penetration depth in grain boundary diffusion. 3473-3477A
- Niobium, Dopants**
High-temperature oxidation of Ti₃Al-based titanium aluminides in oxygen. 3993-4002A
- Niobium, Heat treatment**
Improved oxidation resistance of group VB refractory metals by Al³⁺ ion implantation. 491-500B
- Niobium, Mechanical properties**
Influence of interstitials on the mechanical properties of metallic materials. 3524-3529A
- Niobium, Powder technology**
Milling dynamics. III. Integration of local and global modeling of mechanical alloying devices. 1999-2004A
- Niobium base alloys, Composite materials**
The fracture toughness of niobium-based, in situ composites. 2518-2531A
The effects on fracture toughness of ductile-phase composition and morphology in Nb-Cr-Ti and Nb-Si in situ composites. 3007-3018A
The balance of mechanical and environmental properties of a multielement niobium-niobium silicide-based in situ composite. 3801-3808A
- Niobium base alloys, Phases (state of matter)**
Phase transformations in Nb-Al-Ti alloys. 1642-1654A
- Niobium compounds, Composite materials**
Loading rate and test temperature effects on fracture of in situ niobium silicide-niobium composites. 3292-3306A
The balance of mechanical and environmental properties of a multielement niobium-niobium silicide-based in situ composite. 3801-3808A
- Nitrides**
Microstructure and tensile behavior of nitrogen-alloyed, dual-phase stainless steels. 1845-1859A
Mössbauer spectroscopy study of the aging and tempering of high nitrogen quenched Fe-N alloys: kinetics of formation of Fe₁₆N₂ nitride by interstitial ordering in martensite. 2160-2177A
- Nitriding**
High-temperature nitriding of Ni-Cr alloys. 59-69A
Theoretical treatment of nitriding and nitrocarburizing of iron. 1073-1080A
Transition between internal and external nitriding of Ni-Ti alloys. 1606-1617A

- Control of iron nitride layers growth kinetics in the binary Fe-N system. 1823-1835A
- Nitrogen, Alloying additive**
Elevated temperature compressive properties of N-doped NiAl. 3170-3180A
- Nitrogen, Alloying elements**
Thermodynamics and long-range order of nitrogen in γ -Fe₄N_{1-x}. 1055-1061A
An evaluation of the Fe-N phase diagram considering long-range order of nitrogen atoms in γ -Fe₄N_{1-x} and ϵ -Fe₂N_{1-x}. 1063-1071A
Electron microscopic study of Cr₂N formation in thermally aged 316LN austenitic stainless steels. 1175-1186A
- Nitrogen, Binary systems**
Control of iron nitride layers growth kinetics in the binary Fe-N system. 1823-1835A
Thermodynamic assessment of the Nb-N system. 3591-3600A
- Nitrogen, Environment**
Effect of nitrogen on the oxidation behavior of Ti₃Al-based intermetallic alloys. 4003-4010A
- Nitrogen, Impurities**
Physical chemistry of the powder metallurgy of beryllium: chemical characterization of the powder in relation to its granularity. 371-379A
- Nitrogen, Quaternary systems**
An experimental study and thermodynamic calculations of phase equilibria in the Fe-Mo-C-N system. 2869-2880A
- Nitrogen, Reactions (chemical)**
Modeling and experimental study of gaseous oxidation of liquid iron alloys. 852-862B
- Nitrogen, Solubility**
Effects of oxygen, selenium, and tellurium on the rate of nitrogen dissolution in molten iron. 846-851B
- Nodular iron**
Modeling of ferrite growth in nodular cast iron. 2209-2220A
- Nodular iron, Crystal growth**
Modeling of ferrite growth in nodular cast iron. 2209-2220A
- Nodular iron, Mechanical properties**
Effect of holding time in the (α + γ) temperature range on toughness of specially austempered ductile iron. 1979-1989A
- Nodular iron, Microstructure**
Neutron diffraction study of austempered ductile iron. 923-928A
- Nonferrous metals, Extraction**
The separation of the solids from the carrier gas during submerged powder injection. 773-779B
- Notch sensitivity**
A comparison of fracture behavior of low alloy steel with different sizes of carbide particles. 1909-1917A
- Notch strength**
Notch fracture in γ -titanium aluminides. 3903-3912A
- Notch strength, Alloying effects**
Tension characteristics of notched specimens for Al-Li-Cu-Zr alloys sheets with various cerium contents. 3089-3094A
- Notch strength, Welding effects**
Cleavage initiation in the intercritically reheated coarse-grained heat affected zone. II. Failure criteria and statistical effects. 3019-3029A
- Nuclear fusion reactors, Irradiation**
Theory of nucleation with cluster loss and injection: application to plastic deformation and irradiation. 1441-1448A
- Nuclear power generation**
Gibbs energies of formation of chromium carbides. 1919-1924A
- Nuclear reactor components, Corrosion**
Structure, chemistry, and stress corrosion cracking of grain boundaries in alloys 600 and 690. 327-341A
Influence of thermal aging on the intergranular corrosion resistance of types 304LN and 316LN stainless steels. 2881-2887A
- Nuclear reactor components, Extrusion**
Microsegregation of oxygen in Zr-2.5Nb alloy materials. 431-440A
- Nucleation**
Atomistic Mechanisms of Nucleation and Growth in Solids. Modeling texture change during the static recrystallization of interstitial free steels. 155-164A
Preparation of fine copper powders from organic media by reaction with hydrogen under pressure. II. The kinetics of particle nucleation, growth, and dispersion. 585-594B
High-speed imaging and analysis of the solidification of undercooled nickel melts. 863-868B
Creep deformation of dispersion-strengthened copper. 1217-1227A
Characterization of a massive transformation by microstructural analysis. 1511-1516A
Formation of bainite in ferrous and nonferrous alloys through sympathetic nucleation and ledge growth mechanism. 1533-1543A
- Crystallography of grain boundary α precipitates in a β titanium alloy. 1630-1641A
The mechanism of formation of a fine duplex microstructure in Ti-48Al-2Mn-2Nb alloys. 1655-1667A
On the role of magnesium and silicon in the formation of alumina from aluminum alloys by means of DIMOX processing. 2094-2099A
The role of coincident site lattice boundaries during selective growth in interstitial-free steels. 2178-2186A
Modeling recrystallization kinetics, grain sizes, and textures during multipass hot rolling. 4133-4144A
- Nucleation, Cooling effects**
The role of grain corners in nucleation. 480-483A
Prediction of grain structures in various solidification processes. 695-705A
- Nucleation, Heating effects**
Effect of superheat on the solidification structures of AISI 310S austenitic stainless steel. 287-296B
Effect of primary grain size on the secondary recrystallization of mechanically alloyed oxide dispersion strengthened nickel-based superalloy. 493-496A
Characterization of the formation of α_1 plates from the β_2 phase in a Cu-Zn-Au alloy. 719-724A
Heterogeneous nucleation of δ on dislocations in a dilute aluminum-lithium alloy. 1595-1605A
- Nucleation, Radiation effects**
Theory of nucleation with cluster loss and injection: application to plastic deformation and irradiation. 1441-1448A
- Nucleation, Stress effects**
On the effect of stress on nucleation and growth of precipitates in an Al-Cu-Mg-Ag alloy. 3431-3444A
- Nucleation, Temperature effects**
Rafting in superalloys. 513-530A
Nucleation controlled solidification kinetics. 533-547A
Banded solidification microstructures. 625-634A
Morphological instabilities of lamellar eutectics. 635-656A
The formation mechanism(s), morphology, and crystallography of ferrite sideplates. 1517-1532A
- Numerical analysis**
Interface effects on the micromechanical response of a transversely loaded single fiber SCS-6/Ti-6Al-4V composite. 2035-2043A
A model for macrosegregation and its application to Al-Cu castings. 2708-2721A
Equiaxed dendritic solidification with convection. II. Numerical simulations for an Al-4 wt.% Cu alloy. 2765-2783A
Equiaxed dendritic solidification with convection. III. Comparisons with NH₄Cl-H₂O experiments. 2784-2795A
Modeling of ingot distortions during direct chill casting of aluminum alloys. 3214-3225A
Evidence of fracture surface interference for cracks loaded in shear detected by phase-shifted speckle interferometry. 3853-3860A
Modeling of primary and secondary dendrites in a Cu-6 wt.% tin alloy. 4085-4093A
- Oils, Environment**
Hydrogen-induced cleavage fracture of Fe₃Al-based intermetallics. 3949-3956A
- Optical microscopy**
Inverse melting in binary systems: morphology and microscopy of catatctic alloys. 979-986B
An optical method for determining the surface orientation of crystals. 2057-2061A
Thermally assisted and mechanically driven solid-state reactions for formation of amorphous Al₃₃Ta₆₇ alloy powders. 3267-3278A
Infrared transient-liquid-phase joining of SCS-6/ β 21S titanium matrix composite. 4011-4018A
Microstructural features of friction welded MA 956 superalloy material. 4019-4029A
Creep deformation and damage in a continuous fiber-reinforced Ti-6Al-4V composite. 4193-4204A
- Order disorder**
Mössbauer spectroscopy study of the aging and tempering of high nitrogen quenched Fe-N alloys: kinetics of formation of Fe₁₆N₂ nitride by interstitial ordering in martensite. 2160-2177A
Thermoelastic martensite and shape memory effect in ductile Cu-Al-Mn alloys. 2187-2195A
Microstructural development of a gas-atomized and hot-pressed super- α_2 alloy. 2221-2228A
A thermodynamic evaluation of the nickel-silicon system. 2897-2903A
- Order disorder, Heating effects**
Characterization of the formation of α_1 plates from the β_2 phase in a Cu-Zn-Au alloy. 719-724A
- Order disorder, Temperature effects**
Rafting in superalloys. 513-530A
- Organic compounds**
Preparation of fine copper powders from organic media by reaction with hydrogen under pressure. I. Experimental study. 577-584B

- Preparation of fine copper powders from organic media by reaction with hydrogen under pressure. II. The kinetics of particle nucleation, growth, and dispersion. 585-594B
- Orientation**
An optical method for determining the surface orientation of crystals. 2057-2061A
- Oscillations**
Viscosity of superalloy 718 by the oscillating vessel technique. 698-701B
- Ostwald ripening**
Ostwald ripening in ternary alloys. 937-943A
Ostwald ripening of solid-liquid Pb-Sn dispersions. 2470-2478A
Precipitation behaviors in Al-Cu-Mg and 2024 aluminum alloys. 2479-2494A
Preferential coarsening of γ' precipitates in Inconel 718 during creep. 3391-3398A
 $M_{23}C_6$ precipitates in isothermal tempering of high Co-Ni secondary hardening steel. 3466-3472A
- Oxidation**
Probing the initial stage of synthesis of Al_2O_3/Al composites by directed oxidation of Al-Mg alloys. 43-50B
Representation of mixed reactive gases on free energy (Ellingham-Richardson) diagrams. 65-69B
Reoxidation of aluminum in Fe-Al-M (M=C, Mn, and Ti) melts with $CaO-Al_2O_3-FeO$ (3 mass%) slags. 423-431B
On the stable Mg-Zn-Y quasicrystals. 1779-1784A
The balance of mechanical and environmental properties of a multielement niobium-niobium silicide-based in situ composite. 3801-3808A
Effects of the alumina scale on the room-temperature tensile behavior of preoxidized MA 956. 3809-3816A
- Oxidation, Alloying effects**
Influence of microalloying on the corrosion resistance of steel in saturated calcium hydroxide. 1693-1699A
- Oxidation, Composition effects**
On the role of magnesium and silicon in the formation of alumina from aluminum alloys by means of DIMOX processing. 2094-2099A
- Oxidation, Environmental effects**
Oxidation-reduction equilibrium of Cu^{2+}/Cu^+ in binary alkaline sulfate melts. 385-392B
- Oxidation, High temperature effects**
Phase relations of a silicide/silica reaction couple at 2273K. 271-276B
- Oxidation rate**
Probing the initial stage of synthesis of Al_2O_3/Al composites by directed oxidation of Al-Mg alloys. 43-50B
- Oxidation rate, High temperature effects**
Kinetics of cyclic oxidation and cracking and finite element analysis of MA956 and sapphire/MA956 composite system. 3279-3291A
- Oxidation rate, Radiation effects**
The growth and structure of thin oxide films on cerium ion-implanted nickel. 3649-3661A
- Oxidation resistance**
The balance of mechanical and environmental properties of a multielement niobium-niobium silicide-based in situ composite. 3801-3808A
Effects of the alumina scale on the room-temperature tensile behavior of preoxidized MA 956. 3809-3816A
- Oxidation resistance, Alloying effects**
High-temperature oxidation of Ti_3Al -based titanium aluminides in oxygen. 3993-4002A
- Oxidation resistance, Coating effects**
Microstructural analysis and oxidation behavior of laser-processed Fe-Cr-Al-Y alloy coatings. 381-390A
- Oxidation resistance, Environmental effects**
Effect of nitrogen on the oxidation behavior of Ti_3Al -based intermetallic alloys. 4003-4010A
- Oxidation resistance, Radiation effects**
Improved oxidation resistance of group VB refractory metals by Al^+ ion implantation. 491-500B
- Oxides, Composite materials**
Effect of primary grain size on the secondary recrystallization of mechanically alloyed oxide dispersion strengthened nickel-based superalloy. 493-496A
Tensile properties of mechanically alloyed/milled ODS-Ni-based alloys. 1371-1377A
- Oxides, Reactions (chemical)**
Thermodynamic properties of complex oxides in the Sm-Ba-Cu-O system. 973-978B
- Oxides, Reduction (chemical)**
Discussion of "Representation of mixed reactive gases on free energy (Ellingham-Richardson) diagrams" and reply. 693-694B
- Oxidizing atmospheres**
Oxidation-reduction equilibrium of Cu^{2+}/Cu^+ in binary alkaline sulfate melts. 385-392B
- Oxygen, Alloying additive**
Effects of oxygen, selenium, and tellurium on the rate of nitrogen dissolution in molten iron. 846-851B
- Oxygen, Binary systems**
Critical evaluation and optimization of the thermodynamic properties of liquid tin solutions. 808-826B
- Oxygen, Impurities**
Physical chemistry of the powder metallurgy of beryllium: chemical characterization of the powder in relation to its granularity. 371-379A
Microsegregation of oxygen in Zr-2.5Nb alloy materials. 431-440A
Thermodynamic properties of oxygen in yttrium-oxygen solid solutions. 839-845B
- Oxygen, Quaternary systems**
Thermodynamic properties of complex oxides in the Sm-Ba-Cu-O system. 973-978B
- Oxygen, Ternary systems**
Applicability of Butler's equation in interpreting the thermodynamic behavior of surfaces and adsorption in Fe-S-O melts. 241-253B
- Pack cementation**
The deposition of aluminide and silicide castings on γ -TiAl using the halide-activated pack cementation method. 3761-3772A
- Pack silicizing**
The deposition of aluminide and silicide castings on γ -TiAl using the halide-activated pack cementation method. 3761-3772A
- Palladium, Binary systems**
Standard enthalpies of formation of dysprosium alloys, Dy+Me (Me=Ni, Ru, Rh, Pd, Ir, and Pt), by high-temperature direct synthesis calorimetry. 417-422B
- Partial pressure**
Thermodynamics of sulfur in the BaO-MnO-SiO₂ flux system. 652-657B
- Particle shape**
Preparation of fine copper powders from organic media by reaction with hydrogen under pressure. I. Experimental study. 577-584B
Preparation of fine copper powders from organic media by reaction with hydrogen under pressure. II. The kinetics of particle nucleation, growth, and dispersion. 585-594B
Reinforcement shape effects on the fracture behavior and ductility of particulate-reinforced 6061-Al matrix composites. 3739-3746A
- Particle size**
A one-phase model of the mixing of Al-SiC composite melt. 1015-1023B
A comparison of fracture behavior of low alloy steel with different sizes of carbide particles. 1909-1917A
The effect of volume percent and morphology of phases on the damping behavior of epoxy-aluminum composites. 2366-2373A
The effects on fracture toughness of ductile-phase composition and morphology in Nb-Cr-Ti and Nb-Si in situ composites. 3007-3018A
Microstructure and fracture of SiC-particulate-reinforced cast A356 aluminum alloy composites. 3893-3901A
Modeling of primary and secondary dendrites in a Cu-6 wt.% tin alloy. 4085-4093A
Synthesis of nanocrystalline Ni_3Cu by sol-gel route. 4213-4216A
- Particle size, High temperature effects**
Creep lifetime prediction of oxide-dispersion-strengthened nickel-base superalloys: a micromechanically based approach. 3861-3870A
- Particle size, Welding effects**
Microstructural features of friction welded MA 956 superalloy material. 4019-4029A
- Particle size distribution**
Preparation of fine copper powders from organic media by reaction with hydrogen under pressure. I. Experimental study. 577-584B
A one-phase model of the mixing of Al-SiC composite melt. 1015-1023B
Theoretical analysis of the particle gradient distribution in centrifugal field during solidification. 1025-1029B
Microstructure and fracture of SiC-particulate-reinforced cast A356 aluminum alloy composites. 3893-3901A
Modeling of primary and secondary dendrites in a Cu-6 wt.% tin alloy. 4085-4093A
Modeling particle fracture during the extrusion of aluminum/alumina composites. 4113-4120A
Synthesis of nanocrystalline Ni_3Cu by sol-gel route. 4213-4216A
- Particle size distribution, Heating effects**
The control of grain size and distribution of particles in a (6061 alloy)_m(Al_2O_3)_p composite by solutionizing treatment. 2023-2034A
- Particle size distribution, Welding effects**
Microstructural features of friction welded MA 956 superalloy material. 4019-4029A
Nonuniform distribution of carbonitride particles and its effect on prior austenite grain size in the simulated coarse-grained heat-affected zone of thermomechanical control-processed steels. 4031-4038A

Particulate composites, Brazing

A model for coupled growth of reaction layers in reactive brazing of ZrO_2 -toughened Al_2O_3 .

3630-3638A

Particulate composites, Casting

Transient thermal analysis of solidification in a centrifugal casting for composite materials containing particle segregation. Solidification of particle-reinforced metal-matrix composites. A one-phase model of the mixing of Al-SiC composite melt.

277-285B
663-671B
1015-1023B**Particulate composites, Coatings**

Microstructure of bonding zones in laser-clad nickel-alloy-based composite coatings reinforced with various ceramic powders.

391-400A

Particulate composites, Extrusion

Mathematical modeling of the extrusion of 6061/ Al_2O_3 /20p composite. Modeling particle fracture during the extrusion of aluminum/alumina composites.

4095-4111A
4113-4120A**Particulate composites, Heat treatment**

The control of grain size and distribution of particles in a (6061 alloy)_m/(Al_2O_3)_p composite by solutionizing treatment.

2023-2034A

Particulate composites, Mechanical properties

NiTi and NiTi-TiC composites. II. Compressive mechanical properties. NiTi and NiTi-TiC composites. III. Shape-memory recovery. Subcritical crack growth at bimaterial interfaces. II. Microstructural effects on fracture resistance of metal/ceramic interfaces.

183-191A
193-203A
213-219A

Effect of a solid solution on the steady-state creep behavior of an aluminum matrix composite.

305-316A

Reinforcement stresses during deformation of sphere- and particulate-reinforced aluminum-matrix composites.

486-490A

Effect of manganese dispersoid on the fatigue crack propagation of Al-Zn-Mg alloys.

490-493A

Mechanical properties and 95°C aging characteristics of zircon reinforced Zn-4Al-3Cu alloy.

809-818A

Creep deformation of dispersion-strengthened copper.

1217-1227A

Tensile properties of mechanically alloyed/milled ODS-Ni-based alloys.

1371-1377A

The effect of volume percent and morphology of phases on the damping behavior of epoxy-aluminum composites.

2366-2373A

Analysis of damping in particle-reinforced superplastic zinc composites.

2585-2573A

Corrosive wear of SiC whisker- and particulate-reinforced 6061 aluminum alloy composites.

2653-2662A

Tensile ductility and fracture of superplastic aluminum-SiC composites under thermal cycling conditions.

2837-2842A

Failure characteristics of 6061/ Al_2O_3 /15_p and 2014/ Al_2O_3 /15_p composites as a function of loading rate.

3095-3107A

High-temperature wear and deformation processes in metal matrix composites.

3135-3148A

Ni_3Al intermetallic particles as wear-resistant reinforcement for Al-base composites processed by powder metallurgy.

3259-3266A

Reinforcement shape effects on the fracture behavior and ductility of particulate-reinforced 6061-Al matrix composites.

3739-3746A

Microstructure and fracture of SiC-particulate-reinforced cast A356 aluminum alloy composites.

3893-3901A

Analysis of thermal residual stress in a thick-walled ring of Duran-base Al-SiC functionally graded material.

4145-4151A

Influence of reinforcement volume fraction and size on the microstructure and abrasion wear resistance of hot isostatic pressed white iron matrix composites.

4171-4181A

Influence of matrix structure on the abrasion wear resistance and toughness of a hot isostatic pressed white iron matrix composites.

4183-4191A

Particulate composites, Microstructure

Stacking faults in SiC particles and their effect on the fracture behavior of a 15 vol.% SiC/6061-Al matrix composite.

459-465A

Effect of primary grain size on the secondary recrystallization of mechanically alloyed oxide dispersion strengthened nickel-based superalloy.

493-496A

The x-ray diffraction study of deformation in the composite matrix of Al-Mg-Zn and SiC.

503-505A

Particulate composites, Physical properties

Thermal expansion of metals reinforced with ceramic particles and microcellular foams.

3700-3717A

Particulate composites, Powder technology

Microstructural changes in a mechanically alloyed Al-6.2Zn-2.5Mg-1.7Cu alloy (7010) with and without particulate SiC reinforcement.

3718-3726A

Particulate composites, Structural hardening

Theoretical analysis of the particle gradient distribution in centrifugal field during solidification.

1025-1029B

Particulate composites, Synthesis

Probing the initial stage of synthesis of Al_2O_3 /Al composites by directed oxidation of Al-Mg alloys.

43-50B

Communication: On the in situ formation of TiC and Ti_3C reinforcements in combustion-assisted synthesis of titanium matrix composites.

237-240A

On the role of magnesium and silicon in the formation of alumina from aluminum alloys by means of DIMOX processing.

2094-2099A

Formation of structural intermetallics by reactive metal penetration of titanium and nickel oxides and aluminates.

2100-2104A

Passivation

Fundamental studies of copper anode passivation during electrorefining. I. Development of techniques.

393-398B

Fundamental studies of copper anode passivation during electrorefining. II. Surface morphology.

610-616B

Pearlite

Effect of holding time in the (α - γ) temperature range on toughness of specially austempered ductile iron.

1979-1989A

Pearlite, Deformation effects

Analysis and prevention of vertical cracking phenomena during deep drawing of hot-rolled SG295 steel strips.

1241-1250A

Pearlite, Heating effects

Pearlite in ultrahigh carbon steels: heat treatments and mechanical properties.

111-118A

Pearlite, Temperature effects

Eutectoid decomposition in Ag-Ga.

1676-1682A

Peel strength, Stress effects

Subcritical crack growth at bimaterial interfaces. I. Flexural peel technique.

205-211A

Subcritical crack growth at bimaterial interfaces. III. Shear-enhanced fatigue crack growth resistance at polymer/metal interface.

221-228A

Penetration

Analysis of mean square penetration depth in grain boundary diffusion.

3473-3477A

Influence of titanium and carbon contents on the hydrogen trapping of microalloyed steels.

3773-3780A

Peritectic reactions

Generalized enthalpy method for multicomponent phase change.

869-879B

Peritectic reactions, Alloying effects

Electron microscope study of Al-Fe-Si intermetallics in 6201 aluminum alloy.

929-936A

Peritectic reactions, Cooling effects

Modeling of the peritectic reaction and macro-segregation in casting of low carbon steel.

999-1014B

Permanent mold casting

Microstructure and fracture of SiC-particulate-reinforced cast A356 aluminum alloy composites.

3893-3901A

Permeability

Hydrogen trapping and permeation in nickel thoria.

2495-2503A

Permeability, Microstructural effects

Permeability of microporous carbon preforms.

3669-3674A

Petroleum pipelines, Corrosion

Microstructural aspects of sulfide stress cracking in an API X-80 pipeline steel.

3601-3611A

Phase boundary

Kinetics of sulfation of chalcopyrite with steam and oxygen in the presence of ferric oxide.

465-474B

Thermodynamic activities and partial enthalpies of mixing in the solid solution of Fe in Ni_3Al .

3569-3575A

Phase boundary, Composition effects

An evaluation of the Fe-N phase diagram considering long-range order of nitrogen atoms in γ - Fe_4N_{1-x} and ϵ - Fe_2N_{1-x} .

1063-1071A

Phase boundary, Cooling effects

Ferrite nucleation and growth during continuous cooling.

1544-1553A

Phase boundary, Heating effects

Analysis of heat affected zone phase transformations using in situ spatially resolved x-ray diffraction with synchrotron radiation.

775-783A

Phase boundary, Temperature effects

Overview of geometric effects on coarsening of mushy zones. A new characterization method of the microstructure using the macroscopic composition gradient in alloys.

557-567A

945-949A

Phase decomposition

Microstructural development of a gas-atomized and hot-pressed super- α_2 alloy.

2221-2228A

Phase transformations in condensed systems revisited: industrial applications.

2397-2418A

A thermodynamic evaluation of the nickel-silicon system. Alloy phase analysis from measurements of bulk magnetic properties.

2897-2903A

A high-resolution transmission electron microscopy study of the precipitation process in a dilute Ti-N alloy.

2958-2965A

2966-2977A

- Phase decomposition, Alloying effects**
Electron microscope study of Al-Fe-Si intermetallics in 6201 aluminum alloy. 929-936A
Retardation of intermetallic phase formation in experimental superferitic stainless steels. 2436-2444A
- Phase decomposition, Cooling effects**
Ferrite nucleation and growth during continuous cooling. Austenite decomposition during continuous cooling of an HSLA-80 plate steel. 1544-1553A
1554-1568A
- Phase decomposition, Heating effects**
Phase transformations in Nb-Al-Ti alloys. 1642-1654A
- Phase decomposition, Radiation effects**
The effect of high-energy electron-beam irradiation on microstructural modification of a high-speed steel roll. 3149-3161A
- Phase decomposition, Temperature effects**
A study of the thermal decomposition of BaCO_3 . 409-416B
- Phase diagrams**
Liquidus temperatures for primary crystallization of cryolite in molten salt systems of interest for aluminum electrolysis. Critical evaluation and optimization of the thermodynamic properties of liquid tin solutions. Generalized enthalpy method for multicomponent phase change. A thermodynamic evaluation of the Ti-Mo-C system. Inverse melting in binary systems: morphology and microscopy of catalectic alloys. Thermodynamic studies and the phase diagram of the Li-Mg system. Experimental study of the phase equilibria in the Fe-Mn-Al system. An experimental study and thermodynamic calculations of phase equilibria in the Fe-Mo-C-N system. A thermodynamic evaluation of the nickel-silicon system. An isothermal section at 550°C in the Al-rich corner of the Al-Fe-Mn-Si system. Thermochemistry of the Ni-Hf system—intermetallic phases. Thermodynamic assessment of the Nb-N system. Synthesis of RuAl by reactive powder processing. The deposition of aluminide and silicide castings on γ -TiAl using the halide-activated pack cementation method. Martensitic transformations in NiMnAl β phase alloys. 739-744B
808-826B
869-879B
955-966B
979-986B
2419-2428A
2429-2435A
2869-2880A
2897-2903A
3357-3361A
3576-3590A
3591-3600A
3688-3699A
3761-3772A
4153-4162A
- Phase stability**
Thermal decomposition of silicon carbides: discussion of "the effect of an electric field on self sustaining combustion synthesis, I and II", and author's reply. Effects of flow on morphological stability during directional solidification. A thermodynamic evaluation of the Ti-Mo-C system. A high resolution transmission electron microscopy study of interfaces between the γ , B2, and α_2 phases in a Ti-Al-Mo alloy. On the stable Mg-Zn-Y quasicrystals. Microstructural aspects of the dissolution and melting of Al_2Cu phase in Al-Si alloys during solution heat treatment. Stable and metastable ordered phases in microcrystalline alloys Ni (Fe, Mn, Ti). Thermoelastic martensite and shape memory effect in ductile Cu-Al-Mn alloys. Structural stability of super duplex stainless steel weld metals and its dependence on tungsten and copper. Alloy phase analysis from measurements of bulk magnetic properties. An isothermal section at 550°C in the Al-rich corner of the Al-Fe-Mn-Si system. 322-325B
583-593A
955-966B
1618-1629A
1779-1784A
1785-1798A
2045-2046A
2187-2195A
2196-2208A
2958-2965A
3357-3361A
- Phase stability, Alloying effects**
Mechanical alloying of Nb-Al powders. Effect of alloying elements on martensitic transformation in the binary NiAl(β) phase alloys. 41-48A
2445-2453A
- Phase stability, Environmental effects**
Oxidation-reduction equilibrium of $\text{Cu}^{2+}/\text{Cu}^+$ in binary alkaline sulfate melts. 385-392B
- Phase stability, Heating effects**
Evolution of microstructures in the nickel modified titanium-titanium aluminides near the L_{12} phase field. 5-17A
- Phase stability, Temperature effects**
Phase stability and atom probe field ion microscopy of type 308 CRE stainless steel weld metal. 763-774A
- Phase transformations**
Dynamic behavior of a liquid/liquid interface at an oscillating wall. Thermal decomposition of silicon carbides: discussion of "the effect of an electric field on self sustaining combustion synthesis, I and II", and author's reply. Effects of flow on morphological stability during directional solidification. Thermodynamics of sulfur in the BaO-MnO-SiO_2 flux system. Interface attachment kinetics in alloy solidification. An adaptive mesh refinement scheme for solidification problems. Real time x-ray transmission microscopy of solidifying Al-Ni alloys. Generalized enthalpy method for multicomponent phase change. Ostwald ripening in ternary alloys. Crystal shapes and phase equilibria: a common mathematical basis. Characterization of a massive transformation by microstructural analysis. The mechanism of formation of a fine duplex microstructure in Ti-48Al-2Mn-2Nb alloys. Kinetics of phase evolution of Zn-Fe intermetallics. Solidification of undercooled Fe-Cr-Ni alloys. II. Microstructural evolution. 707-717A
801-808A
869-879B
937-943A
1431-1440A
1511-1516A
1655-1667A
2904-2910A
3226-3240A
- Phase transformations, Alloying effects**
Effects of nickel on the sintering behavior of Fe-Ni compacts made from composite and elemental powders. Electron microscope study of Al-Fe-Si intermetallics in 6201 aluminum alloy. The breakdown of single-crystal solidification in high refractory nickel-base alloys. Effect of strain rate and temperature on the flow stress of β -phase titanium-hydrogen alloys. Precipitation in lead-calcium alloys containing tin. 203-211B
929-936A
1081-1094A
1303-1312A
1668-1675A
- Phase transformations, Composition effects**
Hydride formation and decomposition in electrolytically charged metastable austenitic stainless steels. 29-40A
- Phase transformations, Cooling effects**
The role of grain corners in nucleation. Ferrite nucleation and growth during continuous cooling. Austenite decomposition during continuous cooling of an HSLA-80 plate steel. 480-483A
1544-1553A
1554-1568A
- Phase transformations, Deformation effects**
Experimental investigation of the transformation texture in hot-rolled ferritic stainless steel using single orientation determination. 49-57A
- Phase transformations, Field effects**
On the reaction between Fe-Ti and Fe-C liquids under microgravity. 407-414A
- Phase transformations, Heating effects**
Characterization of the formation of α_1 plates from the β_2 phase in a Cu-Zn-Au alloy. Analysis of heat affected zone phase transformations using in situ spatially resolved x-ray diffraction with synchrotron radiation. Bainitic microstructures formed by split isothermal transformation in an Fe-C-Si-Mn-Mo steel. Effect of bainite transformation and retained austenite on mechanical properties of austempered spheroidal graphite cast steel. Phase transformations in Nb-Al-Ti alloys. 719-724A
775-783A
1141-1147A
1585-1594A
1642-1654A
- Phase transformations, Stress effects**
Computer simulation of ledge migration under elastic interaction. 1489-1498A
- Phase transformations, Temperature effects**
A study of the thermal decomposition of BaCO_3 . Overview of geometric effects on coarsening of mushy zones. Banded solidification microstructures. Phase stability and atom probe field ion microscopy of type 308 CRE stainless steel weld metal. A new characterization method of the microstructure using the macroscopic composition gradient in alloys. The formation mechanism(s), morphology, and crystallography of ferrite sideplates. Eutectoid decomposition in Ag-Ga. 409-416B
557-567A
625-634A
763-774A
945-949A
1517-1532A
1676-1682A
- Phases (state of matter)**
The mineralogical deportment of germanium in the Clarksville electrolytic zinc plant of Savage Zinc Inc. Mg_2C_6 carbide equilibria in the Fe-Cr-C system. Microstructure and phase relations in a powder-processed Ti-22Al-12Nb alloy. Crystal shapes and phase equilibria: a common mathematical basis. Control of iron nitride layers growth kinetics in the binary Fe-N system. 567-576B
701-704B
1121-1126A
1431-1440A
1823-1835A
- Phases (state of matter), Composition effects**
An evaluation of the Fe-N phase diagram considering long-range order of nitrogen atoms in $\gamma\text{-Fe}_3\text{N}_{1-x}$ and $\epsilon\text{-Fe}_2\text{N}_{1-x}$. Electron microscopic study of Cr_2N formation in thermally aged 316LN austenitic stainless steels. 1063-1071A
1175-1186A
- Phases (state of matter), Deformation effects**
Reply: Dynamic materials model. Basis and principles. 235-236A

Phases (state of matter), Radiation effects Transmission electron microscopy study on the cross-sectional microstructure of an ion-nitriding layer.	1347-1352A	Plastic flow Aspects of dynamic recrystallization in shaped charge and explosively formed projectile devices. Control of superplastic deformation rate during uniaxial tensile tests. Flow and fracture of bimaterial systems based on aluminum alloys.	1773-1778A 3030-3042A 3937-3947A
Phosphorus, Alloying additive Influence of phosphorus addition on the surface tension of liquid iron and segregation of phosphorus on the surface of Fe-P alloy.	71-79B	Plastic flow, Temperature effects Influence of temperature transients on the hot workability of a two-phase gamma titanium aluminide alloy. Temperature dependence of the rate sensitivity and its effect on the activation energy for high-temperature flow.	1933-1950A 3346-3348A
Phosphorus, Binary systems Critical evaluation and optimization of the thermodynamic properties of liquid tin solutions.	808-826B	Plasticity High-temperature deformation processing of Ti-24Al-20Nb. Plastic zones and fatigue-crack closure under plane-strain double slip.	2593-2604A 3491-3502A
Phosphorus, Impurities Thermodynamics of phosphorus in molten silicon.	937-941B	Plasticity, Composition effects A statistical analysis of the effect of a mixture component on the rheology of alumina feedstocks.	399-408B
Phosphorus compounds, Ternary systems Chemical potentials of components of the system $\text{CaO}+\text{P}_2\text{O}_5+\text{Fe}_2\text{O}_3$ at 1673K.	595-603B	Plasticity, Environmental effects On the transition of fatigue crack growth from stage I to stage II in a corrosive environment.	471-476A
Photoelectron spectroscopy Physical chemistry of the powder metallurgy of beryllium: chemical characterization of the powder in relation to its granularity.	371-379A	Plasticity, Heating effects The plastic anisotropy of an Al-Li-Cu-Zr alloy extrusion in unidirectional deformation.	3503-3512A
Pistons, Materials selection Structure of phases in the $\delta\text{-Al}_2\text{O}_3$ fiber studied by convergent beam electron diffraction.	3318-3329A	Plasticity, Impurity effects The effect of hydrogen on the fracture of alloy X-750.	101-110A
Pitting (corrosion), Heating effects Corrosion fatigue in nitrocarburized quenched and tempered steels.	1333-1346A	Plasticity, Microstructural effects The use of microstructural gradients in hot gas-pressure forming of Zn-Al sheet.	3250-3258A
Pitting (corrosion), Microstructural effects Retardation of intermetallic phase formation in experimental superferitic stainless steels.	2436-2444A	Plate metal, Coating Correlation of microstructure and fracture toughness in high-chromium white iron hardfacing alloys.	3881-3891A
Plasma arc welding Dilution in single pass arc welds. The wear behavior between hardfacing materials.	481-489B 3639-3648A	Plate metal, Mechanical properties Conditioning monitoring by microstructural evaluation of cumulative fatigue damage.	3841-3851A
Plastic deformation Non-Schmid effects on the behavior of polycrystals, with applications to Ni_3Al . Communication: Discussion of "Modeling of dynamic materials behavior. A critical evaluation of the dissipator power cocontent approach". A study of typical yields of metals. High-temperature deformation processing of Ti-24Al-20Nb. The relationship between microstructural and plastic instability in Al-4.0 wt.% Cu alloy. Plastic zones and fatigue-crack closure under plane-strain double slip. The plastic anisotropy of an Al-Li-Cu-Zr alloy extrusion in unidirectional deformation. Influence of plastic deformation upon the half-width of engineering metallic materials in hard state. High-temperature deformation and failure of an orthorhombic titanium aluminide sheet material. Plastic zone and pileup around large indentations. Microstructural evolution and superplastic deformation behavior of fine grain 5083Al.	81-99A 232-235A 731-736A 2593-2604A 2916-2922A 3491-3502A 3503-3512A 3662-3668A 3675-3681A 3793-3800A 3827-3839A	Plate metal, Phase transformations A study on morphology and plate mean dimensions in Fe-Ni and Fe-Ni-Cr alloys. Plate metal, Phases (state of matter) Characterization of the formation of α_1 plates from the β_2 phase in a Cu-Zn-Al alloy. Austenite decomposition during continuous cooling of an HSLA-80 plate steel.	973-980A 719-724A 1554-1568A
Plastic deformation, Composition effects Mechanical properties of Ru-Ni-Al alloys.	1395-1400A	Platinum, Binary systems Standard enthalpies of formation of dysprosium alloys, Dy+Me (Me=Ni, Ru, Rh, Pd, Ir, and Pt), by high-temperature direct synthesis calorimetry.	417-422B
Plastic deformation, Diffusion effects Hydrogen-induced cleavage fracture of Fe_3Al -based intermetallics.	3949-3956A	Plutonium, Extraction Vacuum evaporation of KCl-NaCl salts. I. Thermodynamic modeling of vapor pressures of solid and liquid solutions.	141-146B
Plastic deformation, High temperature effects High-temperature measurements of lattice parameters and internal stresses of a creep-deformed monocrystalline nickel-base superalloy.	1003-1014A	Point defects, Radiation effects Sputter-induced pits on {100} nickel surfaces.	981-993A
Plastic deformation, Impurity effects The effect of hydrogen on the fracture of alloy X-750.	101-110A	Poissons ratio, Alloying effects Elastic moduli of titanium-hydrogen alloys in the temperature range 20°C to 1100°C.	3963-3970A
Plastic deformation, Microstructural effects NiTi and NiTi-TiC composites. II. Compressive mechanical properties.	183-191A	Pole figures Crystallographic preferred orientation induced by cyclic rolling contact loading.	3445-3465A
Plastic deformation, Radiation effects Theory of nucleation with cluster loss and injection: application to plastic deformation and irradiation.	1441-1448A	Pollution abatement Eco-techno-economic synthesis of process routes for the production of zinc using combinatorial optimization.	1031-1044B
Plastic deformation, Stress effects Plastic anisotropy of sheets with continuously varying anisotropic parameters and flow stress. Reinforcement stresses during deformation of sphere- and particulate-reinforced aluminum-matrix composites. Rafing in superalloys. Discussion of "a fully plastic microcracking model for transgranular stress corrosion cracking in planar slip materials" and reply.	317-326A 486-490A 513-530A 819-821A	Porosity Comparative study of pore structure evolution during solvent and thermal debinding of powder injection molded parts. Characterization and mechanical properties of ultrahigh boron steels produced by powder metallurgy. A model for macrosegregation and its application to Al-Cu castings. The effect of Mo addition on the liquid-phase sintering of W heavy alloy.	245-253A 1861-1867A 2708-2721A 3120-3125A
Plastic deformation, Temperature effects Manifestations of dynamic strain aging in soft-oriented NiAl single crystals.	3542-3557A	Porosity, Cooling effects Porosity formation in Al-9 wt.% Si-3 wt.% Cu alloy systems: metallographic observations.	415-429A
		Porous materials, Physical properties Permeability of microporous carbon preforms.	3669-3674A
		Potassium, Chemical analysis Formation of aluminum-silicon alloys from feldspars—determination of silicon, light, and heavy elements in silumin by scanning electron microscopy.	604-609B

- Potassium, Dopants**
Van der Waals approximation for potassium bubbles in tungsten. 987-992B
- Powder coating**
Kinetics of phase evolution of Zn-Fe intermetallics. 2904-2910A
- Powder coatings, Materials selection**
Kinetics of phase evolution of Zn-Fe intermetallics. 2904-2910A
- Powder compacts, Mechanical properties**
Microstructure and tensile properties of compacted, mechanically alloyed, nanocrystalline Fe-Al. 3126-3134A
- Powder metallurgy**
The effect of thermal cycle on the microstructural development of a powder metallurgy superalloy braze material. 145-153A
Physical chemistry of the powder metallurgy of beryllium: chemical characterization of the powder in relation to its granularity. 371-379A
- Powder metallurgy parts, Machining**
Active wear and failure mechanisms of titanium nitride-coated high speed steel and titanium nitride-coated cemented carbide tools when machining powder metallurgically made stainless steels. 2796-2808A
- Powder technology**
A statistical analysis of the effect of a mixture component on the rheology of alumina feedstocks. 399-408B
- Precious metal alloys, Mechanical properties**
High-temperature behavior of precious metal base composites. 2642-2652A
- Precipitates**
Structural stability of super duplex stainless weld metals and its dependence on tungsten and copper. 2196-2208A
Lattice misfits in four binary Ni-base γ/γ' alloys at ambient and elevated temperatures. 2888-2896A
The relationship between microstructural and plastic instability in Al-4.0 wt.% Cu alloy. 2916-2922A
A high-resolution transmission electron microscopy study of the precipitation process in a dilute Ti-N alloy. 2966-2977A
Internal sulfide precipitation in low Cr-Fe alloys. 3192-3202A
Influence of titanium and carbon contents on the hydrogen trapping of microalloyed steels. 3773-3780A
An evaluation of the creep properties of two Al-Si alloys produced by rapid solidification processing. 3871-3879A
Correlation of microstructure and fracture toughness in high-chromium white iron hardfacing alloys. 3881-3891A
- Precipitates, Crystal growth**
Ostwald ripening of solid-liquid Pb-Sn dispersions. 2470-2478A
Precipitation behaviors in Al-Cu-Mg and 2024 aluminum alloys. 2479-2494A
Preferential coarsening of γ' precipitates in Inconel 718 during creep. 3391-3398A
On the effect of stress on nucleation and growth of precipitates in an Al-Cu-Mg-Ag alloy. 3431-3444A
M₂C precipitates in isothermal tempering of high Co-Ni secondary hardening steel. 3466-3472A
- Precipitation**
Mechanical behavior of the in situ composite alloys in the Al-Ni-Ti system near the L₁₂ phase field. 71-79A
The effects of microstructure, strength level, and crack propagation mode on stress corrosion cracking behavior of 4135 steel. 281-290A
Structure, chemistry, and stress corrosion cracking of grain boundaries in alloys 600 and 690. 327-341A
Preparation of fine copper powders from organic media by reaction with hydrogen under pressure. I. Experimental study. 577-584B
Preparation of fine copper powders from organic media by reaction with hydrogen under pressure. II. The kinetics of particle nucleation, growth, and dispersion. 585-594B
Crystallography of grain boundary α precipitates in a β titanium alloy. 1630-1641A
Splitting phenomena occurring in the martensitic transformation of Cr13 and CrMoV14 stainless steels in the absence of carbide precipitation. 1799-1805A
Microstructural development in NIAI/Ni-Si-B/Ni transient liquid phase bonds. 1925-1931A
Modeling of microsegregation in macrosegregation computations. 2314-2327A
Internal sulfide precipitation in low Cr-Fe alloys. 3192-3202A
- Precipitation, Alloying effects**
The effect of iron and manganese on the recrystallization behavior of hot-rolled and solution-heat-treated aluminum alloy 6013. 19-27A
The influence of niobium supersaturation in austenite on the static recrystallization behavior of low carbon microalloyed steels. 951-960A
Identification of precipitate phases in a mechanically alloyed rapidly solidified Al-Fe-Ce alloy. 1033-1041A
Precipitation in lead-calcium alloys containing tin. 1668-1675A
- Precipitation, Composition effects**
Electron microscopic study of Cr₂N formation in thermally aged 316LN austenitic stainless steels. 1175-1186A
- Precipitation, Cooling effects**
Porosity formation in Al-9 wt.% Si-3 wt.% Cu alloy systems: metallographic observations. 415-429A
Copper precipitation during continuous cooling and isothermal aging of A710 type steels. 1569-1584A
- Precipitation, Deformation effects**
Reply: Dynamic materials model. Basis and principles. 235-236A
Precipitation behavior in a medium carbon, Ti-V-N microalloyed steel. 1149-1165A
- Precipitation, Field effects**
On the reaction between Fe-Ti and Fe-C liquids under microgravity. 407-414A
- Precipitation, Heating effects**
Evolution of microstructures in the nickel modified titanium tri-aluminides near the L₁₂ phase field. 5-17A
High-temperature nitridation of Ni-Cr alloys. 59-69A
Mechanical properties and 95°C aging characteristics of zircon reinforced Zn-4Al-3Cu alloy. 809-818A
Microstructural stability on aging of an α - β titanium alloy: Ti-6Al-1.6Zr-3.3Mo-0.30Si. 1167-1173A
Transition between internal and external nitridation of Ni-Ti alloys. 1606-1617A
Phase transformations in Nb-Al-Ti alloys. 1642-1654A
M₂C precipitates in isothermal tempering of high Co-Ni secondary hardening steel. 3466-3472A
- Precipitation, High temperature effects**
Phase relations of a silicide/silica reaction couple at 2273K. 271-276B
Carbide diagrams and precipitation of alloying elements during aging of low-alloy steels. 498-502A
- Precipitation, Radiation effects**
Transmission electron microscopy study on the cross-sectional microstructure of an ion-nitriding layer. 1347-1352A
- Precipitation, Stress effects**
Temperature and strain-rate effects on low-cycle fatigue behavior of alloy 800H. 255-267A
Effect of carbide precipitation on the creep behavior of alloy 800HT in the temperature range 700-900°C. 747-756A
A study on coherency strain and precipitate morphology via a discrete atom method. 1449-1459A
Effect of uniaxial stress on coarsening of precipitate clusters. 1460-1475A
On the effect of stress on nucleation and growth of precipitates in an Al-Cu-Mg-Ag alloy. 3431-3444A
- Precipitation, Temperature effects**
Phase stability and atom probe field ion microscopy of type 308 CRE stainless steel weld metal. 763-774A
A new characterization method of the microstructure using the macroscopic composition gradient in alloys. 945-949A
The formation mechanism(s), morphology, and crystallography of ferrite sideplates. 1517-1532A
- Precipitation hardening**
Bauschinger effect in Haynes 230 alloy: influence of strain rate and temperature. 1739-1748A
Phase transformations in condensed systems revisited: industrial applications. 2397-2418A
Precipitation behaviors in Al-Cu-Mg and 2024 aluminum alloys. 2479-2494A
Low quench sensitivity of superplastic 8090 Al-Li thin sheets. 2923-2933A
Alloy phase analysis from measurements of bulk magnetic properties. 2958-2965A
A high-resolution transmission electron microscopy study of the precipitation process in a dilute Ti-N alloy. 2966-2977A
On the effect of stress on nucleation and growth of precipitates in an Al-Cu-Mg-Ag alloy. 3431-3444A
Creep lifetime prediction of oxide-dispersion-strengthened nickel-base superalloys: a micromechanically based approach. 3861-3870A
- Precipitation hardening, Alloying effects**
Effect of magnesium on the aging behavior of Al-Zn-Mg-Cu/Al₂O₃ metal matrix composites. 2005-2012A
- Precipitation hardening, Stress effects**
A study on coherency strain and precipitate morphology via a discrete atom method. 1449-1459A
An evaluation of the creep properties of two Al-Si alloys produced by rapid solidification processing. 3871-3879A
- Precipitation hardening alloys, Mechanical properties**
Microstructure and mechanical behavior of Cr-Cr₂Hf in situ intermetallic composites. 2583-2592A
Intergranular fracture in some precipitation-hardened aluminum alloys at low temperatures. 3081-3088A
- Precipitation hardening steels, Mechanical properties**
Microstructural basis for the effect of chromium on the strength and toughness of AF1410-based high performance steels. 2510-2517A

- Precision forming**
Comparative study of pore structure evolution during solvent and thermal debinding of powder injection molded parts. 245-253A
- Preferred orientation, Stress effects**
Crystallographic preferred orientation induced by cyclic rolling contact loading. 3445-3465A
- Preforming**
Permeability of microporous carbon preforms. 3669-3674A
- Press forming**
Forming of tailor-welded blanks. 2605-2616A
- Pressure**
Pressure dependence of anomalous diffusion of zirconium in β -titanium. 1807-1814A
- Pressure castings, Microstructure**
The squeeze casting of hypoeutectic binary Al-Cu. 4121-4132A
- Pressure vessels, Corrosion**
Stress corrosion cracking of pressure vessel steels in high-temperature caustic aluminate solutions. 1327-1331A
- Pressure vessels, Extrusion**
Microsegregation of oxygen in Zr-2.5Nb alloy materials. 431-440A
- Pressure vessels, Irradiation**
Theory of nucleation with cluster loss and injection: application to plastic deformation and irradiation. 1441-1448A
- Pressure vessels, Materials selection**
Conditioning monitoring by microstructural evaluation of cumulative fatigue damage. 3841-3851A
- Pressure vessels, Metal working**
Analysis and prevention of vertical cracking phenomena during deep drawing of hot-rolled SG295 steel strips. 1241-1250A
- Probes, Development**
The measurement of hydrogen activities in molten copper using an oxide protonic conductor. 929-935B
- Process control**
The measurement of hydrogen activities in molten copper using an oxide protonic conductor. 929-935B
Eco-techno-economic synthesis of process routes for the production of zinc using combinatorial optimization. 1031-1044B
- Projectiles**
Aspects of dynamic recrystallization in shaped charge and explosively formed projectile devices. 1773-1778A
- Proof stress, Composition effects**
High-temperature behavior of precious metal base composites. 2642-2652A
- Proof stress, Microstructural effects**
Fracture characteristics, microstructure, and tissue reaction of Ti-5Al-2.5Fe for orthopedic surgery. 3925-3935A
- Prosthetics, Materials selection**
Fracture characteristics, microstructure, and tissue reaction of Ti-5Al-2.5Fe for orthopedic surgery. 3925-3935A
- Protective coatings, Heat treatment**
Quenching C60 fullerene into diamond in the Fe-C alloy system by laser treatment. 2293-2296A
- Protective coatings, Melting**
The production of nickel-zinc alloys by powder injection. 780-787B
- Purification**
Thermodynamics of phosphorus in molten silicon. 937-941B
- Pyrometallurgy**
Vacuum evaporation of KCl-NaCl salts. I. Thermodynamic modeling of vapor pressures of solid and liquid solutions. 141-146B
Electrical conductivity of molten cryolite based mixtures obtained with a tube type cell made of pyrolytic boron nitride. 255-261B
Zinc reduction of MoO_3 in a self propagating high temperature synthesis process. 315-318B
A kinetic study of the reaction of zinc oxide with iron powder. 363-374B
Chemical potentials of oxygen for mixtures of $\text{CaO(s)} + \text{Ca}_2\text{P}_2\text{O}_7\text{(s)} + (\text{CaO} + \text{P}_2\text{O}_5 + \text{Fe}_2\text{O}_3)$ melts and $\text{Ca}_2\text{P}_2\text{O}_7\text{(s)} + \text{Ca}_3\text{P}_2\text{O}_7\text{(s)} + \text{CaO} + \text{P}_2\text{O}_5 + \text{Fe}_2\text{O}_3$ melts. 375-378B
Oxidation-reduction equilibrium of $\text{Cu}^{2+}/\text{Cu}^+$ in binary alkaline sulfate melts. 385-392B
The separation of the solids from the carrier gas during submerged powder injection. 773-779B
- Qualitative analysis**
Determination of hydrogen in titanium alloys by cold neutron prompt gamma activation analysis. 3682-3687A
- Quantitative analysis**
Physical chemistry of the powder metallurgy of beryllium: chemical characterization of the powder in relation to its granularity. 371-379A
- Quasicrystalline structure**
On the stable Mg-Zn-Y quasicrystals. 1779-1784A
- High-resolution electron microscopy analysis of structural defects in a (2/1, 5/3)-type approximant of a decagonal quasicrystal of an Al-Pd-Mn alloy. 2911-2915A
- Quaternary systems, Phases (state of matter)**
Thermodynamic properties of complex oxides in the Sm-Ba-Cu-O system. 973-978B
An experimental study and thermodynamic calculations of phase equilibria in the Fe-Mo-C-N system. 2869-2880A
- Quenching (cooling)**
Quenching C60 fullerene into diamond in the Fe-C alloy system by laser treatment. 2293-2296A
High cycle fatigue behavior of gas-carburized medium carbon Cr-Mo steel. 2557-2564A
Low quench sensitivity of superplastic 8090 Al-Li thin sheets. 2923-2933A
The quench sensitivity of cast Al-7 wt.% Si-0.4 wt.% Mg alloy. 3983-3991A
- Quenching and tempering**
Corrosion fatigue in nitrocarburized quenched and tempered steels. 1333-1346A
The dependence of complex alloyed steel properties on quenching and tempering conditions. 2852-2858A
- Radiation damage**
Theory of nucleation with cluster loss and injection: application to plastic deformation and irradiation. 1441-1448A
- Radioactive waste**
Preparation of glass-forming materials from granulated blast furnace slag. 801-807B
Microstructure and phase identification in type 304 stainless steel-zirconium alloys. 2151-2159A
- Rapid solidification**
Interface attachment kinetics in alloy solidification. 671-686A
High-speed imaging and analysis of the solidification of under-cooled nickel melts. 863-868B
Identification of precipitate phases in a mechanically alloyed rapidly solidified Al-Fe-Ce alloy. 1033-1041A
Rapid solidification processing of a Mg-Li-Si-Ag alloy. 1363-1370A
Characterization and mechanical properties of ultrahigh boron steels produced by powder metallurgy. 1861-1867A
An evaluation of the creep properties of two Al-Si alloys produced by rapid solidification processing. 3871-3879A
Elevated temperature deformation behavior of a dispersion-strengthened Al-Fe, V, Si alloy. 3913-3923A
- Reaction kinetics**
Kinetics of sulfation of chalcocopyrite with steam and oxygen in the presence of ferric oxide. 465-474B
Preparation of fine copper powders from organic media by reaction with hydrogen under pressure. II. The kinetics of particle nucleation, growth, and dispersion. 585-594B
Reduction of FeO in smelting slags by solid carbon: experimental results. 717-730B
Formation of structural intermetallics by reactive metal penetration of titanium and nickel oxides and aluminates. 2100-2104A
Mössbauer spectroscopy study of the aging and tempering of high nitrogen quenched Fe-N alloys: kinetics of formation of Fe_{16}N_2 nitride by interstitial ordering in martensite. 2160-2177A
- Reaction kinetics, Composition effects**
On the role of magnesium and silicon in the formation of alumina from aluminum alloys by means of DIMOX processing. 2094-2099A
- Reactions (chemical)**
Symposium on In Situ Reactions for Synthesis of Composites, Ceramics, and Intermetallics. II. A study of solid-aqueous equilibria by the speciation approach in the hydronium alunite-sulfuric acid-water system at high temperatures. 555-566B
- Recovery, Alloying effects**
Modeling recovery and recrystallization kinetics in cold-rolled Ti-Nb stabilized interstitial-free steel. 3410-3423A
- Recrystallization**
Mechanical behavior of the in situ composite alloys in the Al-Ni-Ti system near the L_{12} phase field. 71-79A
Modeling texture change during the static recrystallization of interstitial free steels. 155-164A
Recrystallization in oxide-dispersion strengthened mechanically alloyed sheet steel. 1963-1978A
The role of coincident site lattice boundaries during selective growth in interstitial-free steels. 2178-2186A
Orientation selective recrystallization of nonoriented electrical steels. 2347-2358A
Effects of alloy modification and thermomechanical processing on recrystallization of Al-Mg-Mn alloys. 2947-2957A
Modeling recrystallization kinetics, grain sizes, and textures during multipass hot rolling. 4133-4144A
- Recrystallization, Alloying effects**
The effect of iron and manganese on the recrystallization behavior of hot-rolled and solution-heat-treated aluminum alloy 6013. 19-27A

- The influence of niobium supersaturation in austenite on the static recrystallization behavior of low carbon microalloyed steels. 951-960A
- Modeling recovery and recrystallization kinetics in cold-rolled Ti-Nb stabilized interstitial-free steel. 3410-3423A
- Recrystallization, Deformation effects**
- Experimental investigation of the transformation texture in hot-rolled ferritic stainless steel using single orientation determination. 49-57A
- Aspects of dynamic recrystallization in shaped charge and explosively formed projectile devices. 1773-1778A
- Recrystallization, Heating effects**
- Effect of primary grain size on the secondary recrystallization of mechanically alloyed oxide dispersion strengthened nickel-based superalloy. 493-496A
- An analysis of static recrystallization during continuous, rapid heat treatment. 2051-2053A
- Reduction (chemical), Environmental effects**
- Oxidation-reduction equilibrium of $\text{Cu}^{2+}/\text{Cu}^0$ in binary alkaline sulfate melts. 385-392B
- Relaxation**
- Internal friction in hydrogen-charged CrNi and CrNiMn austenitic stainless steels. 1815-1821A
- Residual stress**
- The Bauschinger effect in a SiC/Al composite. 995-1001A
- High-temperature measurements of lattice parameters and internal stresses of a creep-deformed monocrystalline nickel-base superalloy. 1003-1014A
- Recrystallization in oxide-dispersion strengthened mechanically alloyed sheet steel. 1963-1978A
- Thermal residual stresses in functionally graded and layered 6061 Al/SiC materials. 3241-3249A
- Residual stress, Cooling effects**
- Analysis of thermal residual stress in a thick-walled ring of Duralcan-base Al-SiC functionally graded material. 4145-4151A
- Residual stress, Corrosion effects**
- Effects of the alumina scale on the room-temperature tensile behavior of preoxidized MA 956. 3809-3816A
- Residual stress, Field effects**
- Characterization of titanium thin films prepared by bias assisted magnetron sputtering. 1057-1060B
- Residual stress, Microstructural effects**
- Influence of interstitials on the mechanical properties of metallic materials. 3524-3529A
- Residual stress, Welding effects**
- Effect of postweld treatment on the fatigue crack growth rate of electron-beam-welded AISI 4130 steel. 3162-3169A
- Residues**
- The mineralogical deportment of germanium in the Clarksville electrolytic zinc plant of Savage Zinc Inc. 567-576B
- Resistivity**
- Physical modeling studies of electrolyte flow due to gas evolution and some aspects of bubble behavior in advanced Hall cells. III. Predicting the performance of advanced Hall cells. 19-27B
- Resistivity, Composition effects**
- A study of the influence of mischmetal additions to Al-7Si-0.3Mg (LM 25/356) alloy. 1283-1292A
- Resistivity, Microstructural effects**
- Precipitation in lead-calcium alloys containing tin. 1668-1675A
- Resistivity, Temperature effects**
- Electrical conductivity of molten cryolite based mixtures obtained with a tube type cell made of pyrolytic boron nitride. 255-261B
- Retained austenite, Crystal lattices**
- Nonuniform distribution of carbonitride particles and its effect on prior austenite grain size in the simulated coarse-grained heat-affected zone of thermomechanical control-processed steels. 4031-4038A
- Retained austenite, Heating effects**
- Influence of reinforcement volume fraction and size on the microstructure and abrasion wear resistance of hot isostatically pressed white iron matrix composites. 4171-4181A
- Influence of matrix structure on the abrasion wear resistance and toughness of a hot isostatically pressed white iron matrix composites. 4183-4191A
- Rhenium, Alloying elements**
- The breakdown of single-crystal solidification in high refractory nickel-base alloys. 1081-1094A
- Rheological properties, Composition effects**
- A statistical analysis of the effect of a mixture component on the rheology of alumina feedstocks. 399-408B
- Rhodium, Binary systems**
- Standard enthalpies of formation of dysprosium alloys, Dy+Me (Me=Ni, Ru, Rh, Pd, Ir, and Pt), by high-temperature direct synthesis calorimetry. 417-422B
- Roasting**
- Kinetics of sulfation of chalcocopyrite with steam and oxygen in the presence of ferric oxide. 465-474B
- Rockwell hardness**
- Quenching C60 fullerene into diamond in the Fe-C alloy system by laser treatment. 2293-2296A
- Rockwell hardness, Alloying effects**
- Effect of magnesium on the aging behavior of Al-Zn-Mg-Cu/ Al_2O_3 metal matrix composites. 2005-2012A
- Rod milling**
- Thermally assisted and mechanically driven solid-state reactions for formation of amorphous $\text{Al}_{33}\text{Ta}_{67}$ alloy powders. 3267-3278A
- Rolling contact**
- Crystallographic preferred orientation induced by cyclic rolling contact loading. 3445-3465A
- Rolling texture**
- Modeling recrystallization kinetics, grain sizes, and textures during multipass hot rolling. 4133-4144A
- Rolls, Irradiation**
- The effect of high-energy electron-beam irradiation on microstructural modification of a high-speed steel roll. 3149-3161A
- Roughness**
- Quantitative characterization of the surface topography of rolled sheets by laser scanning microscopy and Fourier transformation. 2338-2346A
- Ruthenium, Binary systems**
- Standard enthalpies of formation of dysprosium alloys, Dy+Me (Me=Ni, Ru, Rh, Pd, Ir, and Pt), by high-temperature direct synthesis calorimetry. 417-422B
- Ruthenium, Ternary systems**
- Mechanical properties of Ru-Ni-Al alloys. 1395-1400A
- Ruthenium base alloys, Powder technology**
- Synthesis of RuAl by reactive powder processing. 3688-3699A
- Ruthenium compounds, Powder technology**
- Synthesis of RuAl by reactive powder processing. 3688-3699A
- Rutile, Reduction (chemical)**
- Preoxidation and hydrogen reduction of ilmenite in a fluidized bed reactor. 731-738B
- S N diagrams**
- Fracture characteristics, microstructure, and tissue reaction of Ti-5Al-2.5Fe for orthopedic surgery. 3925-3935A
- Sag**
- Van der Waals approximation for potassium bubbles in tungsten. 987-992B
- Salt water, Environment**
- Corrosive wear of SiC whisker- and particulate-reinforced 6061 aluminum alloy composites. 2653-2662A
- The influence of aqueous environments on low ΔK and high ΔK fatigue crack propagation behavior in low carbon structural steels. 2678-2685A
- Samarium, Binary systems**
- Inverse melting in binary systems: morphology and microscopy of catatectic alloys. 979-986B
- Samarium, Quaternary systems**
- Thermodynamic properties of complex oxides in the Sm-Ba-Cu-O system. 973-978B
- Sapphire, Composite materials**
- Kinetics of cyclic oxidation and cracking and finite element analysis of MA956 and sapphire/MA956 composite system. 3279-3291A
- Scale (corrosion)**
- A study of solid-aqueous equilibria by the speciation approach in the hydronium alunite-sulfuric acid-water system at high temperatures. 555-566B
- Kinetics of cyclic oxidation and cracking and finite element analysis of MA956 and sapphire/MA956 composite system. 3279-3291A
- Effects of the alumina scale on the room-temperature tensile behavior of preoxidized MA 956. 3809-3816A
- Scale (corrosion), Metallography**
- Real-time observations of the oxidation of mild steel at high temperature by neutron diffraction. 993-997B
- Scanning electron microscopy**
- Formation of aluminum-silicon alloys from feldspars—determination of silicon, light, and heavy elements in silumin by scanning electron microscopy. 604-609B
- Inverse melting in binary systems: morphology and microscopy of catatectic alloys. 979-986B

- Real-time observations of the oxidation of mild steel at high temperature by neutron diffraction.** 993-997B
- The formation mechanism(s), morphology, and crystallography of ferrite sideplates.** 1517-1532A
- The relationship between microstructural and plastic instability in Al-4.0 wt.% Cu alloy.** 2916-2922A
- Thermally assisted and mechanically driven solid-state reactions for formation of amorphous $Al_{53}Ta_{47}$ alloy powders.** 3267-3278A
- Discussion of "Effects of tensile stress on microstructural change of eutectoid Zn-Al alloy" and authors' reply.** 3330-3335A
- Shear ligament phenomena in Fe_3Al intermetallics and micro-mechanics of shear ligament toughening.** 3817-3825A
- Correlation of microstructure and fracture toughness in high-chromium white iron hardfacing alloys.** 3881-3891A
- Microstructure and fracture of SiC-particulate-reinforced cast A356 aluminum alloy composites.** 3893-3901A
- Notch fracture in γ -titanium aluminides.** 3903-3912A
- High-temperature oxidation of Ti_3Al -based titanium aluminides in oxygen.** 3993-4002A
- Effect of nitrogen on the oxidation behavior of Ti_3Al -based intermetallic alloys.** 4003-4010A
- Infrared transient-liquid-phase joining of SCS-6/ β 21S titanium matrix composite.** 4011-4018A
- Nonuniform distribution of carbonitride particles and its effect on prior austenite grain size in the simulated coarse-grained heat-affected zone of thermomechanical control-processed steels.** 4031-4038A
- Modeling of primary and secondary dendrites in a Cu-6 wt.% tin alloy.** 4085-4093A
- Creep deformation and damage in a continuous fiber-reinforced Ti-6Al-4V composite.** 4193-4204A
- Secondary hardening**
- Effect of alloying additions on fracture behavior of molybdenum-containing secondary hardening steels.** 3343-3346A
- M_2C precipitates in isothermal tempering of high Co-Ni secondary hardening steel.** 3468-3472A
- Segregations**
- Theoretical modeling of densification during activated solid-state sintering.** 441-450A
- The embrittlement and de-embrittlement of grain boundaries in an Fe-Mn-Ni alloy due to grain boundary segregation of manganese.** 1015-1020A
- Modeling of microsegregation in macrosegregation computations.** 2314-2327A
- A model for macrosegregation and its application to Al-Cu castings.** 2708-2721A
- Equiaxed dendritic solidification with convection. II. Numerical simulations for an Al-4 wt.% Cu alloy.** 2765-2783A
- Equiaxed dendritic solidification with convection. III. Comparisons with NH_4Cl-H_2O experiments.** 2784-2795A
- Incipient chemical instabilities of nanophase Fe-Cu alloys prepared by mechanical alloying.** 2934-2948A
- Nonequilibrium grain-boundary segregation and ductile-brittle-ductile transition in Fe-Mn-Ni-Ti age-hardening alloy.** 3059-3065A
- Macrotransport-solidification kinetics modeling of equiaxed dendritic growth. II. Computation problems and validation on Inconel 718 superalloy casting.** 4075-4083A
- Segregations, Alloying effects**
- Influence of phosphorus addition on the surface tension of liquid iron and segregation of phosphorus on the surface of Fe-P alloy.** 71-79B
- Segregations, Cooling effects**
- Transient thermal analysis of solidification in a centrifugal casting for composite materials containing particle segregation.** 277-285B
- Modeling of the peritectic reaction and macro-segregation in casting of low carbon steel.** 999-1014B
- Macrosegregation during dendritic arrayed growth of hypoeutectic Pb-Sn alloys: influence of primary arm spacing and mushy zone length.** 1353-1362A
- The squeeze casting of hypoeutectic binary Al-Cu.** 4121-4132A
- Segregations, Field effects**
- Convection during thermally unstable solidification of Pb-Sn in a magnetic field.** 1095-1110A
- Segregations, Heating effects**
- Effect of homogenization heat treatment on the microstructure and heat affected zone microfissuring in welded cast alloy 718.** 785-790A
- Neutron diffraction study of austempered ductile iron.** 923-928A
- Segregations, Impurity effects**
- Microsegregation of oxygen in Zr-2.5Nb alloy materials.** 431-440A
- Segregations, Radiation effects**
- A model describing neutron irradiation-induced segregation to grain boundaries in dilute alloys.** 3381-3390A
- Seizing, Composition effects**
- Characterization of the wear response of a modified zinc-based alloy vis-à-vis a conventional zinc-based alloy and a bearing bronze at a high sliding speed.** 3513-3523A
- Selenium, Alloying additive**
- Effects of oxygen, selenium, and tellurium on the rate of nitrogen dissolution in molten iron.** 846-851B
- Selenium, Binary systems**
- Critical evaluation and optimization of the thermodynamic properties of liquid tin solutions.** 808-826B
- Self-propagating synthesis**
- Synthesis of RuAl by reactive powder processing.** 3688-3699A
- Self-propagating synthesis, Pressure effects**
- Pressure-assisted reactive synthesis of titanium aluminides from dense 50Al-50Ti elemental powder blends.** 2130-2139A
- Semiconductors, Solubility**
- Retrograde solubility in semiconductors.** 2704-2707A
- Sensitizing**
- Influence of thermal aging on the intergranular corrosion resistance of types 304LN and 316LN stainless steels.** 2881-2887A
- Sensors**
- Reference electrode of simple galvanic cells for developing sodium sensors for use in molten aluminum.** 794-800B
- Sensors, Development**
- The measurement of hydrogen activities in molten copper using an oxide protonic conductor.** 929-935B
- Sensors, Materials selection**
- Development of a magnetoelastic resonant sensor using iron-rich, nonzero magnetostrictive amorphous alloys.** 3203-3213A
- Serrated yielding, Temperature effects**
- Manifestations of dynamic strain aging in soft-oriented NIAI single crystals.** 3542-3557A
- Service life, Composition effects**
- Carbide diagrams and precipitation of alloying elements during aging of low-alloy steels.** 498-502A
- Shaft furnaces**
- Modeling and experimental study of gaseous oxidation of liquid iron alloys.** 852-882B
- Shape, Pressure effects**
- Studies of interface deformations in single- and multi-layered liquid baths due to an impinging gas jet.** 911-920B
- Shape memory**
- The effect of substrate constraint on the martensitic transformation of Ni-Ti thin films.** 2858-2860A
- Shape memory, Cooling effects**
- NiTi and NiTi-TiC composites. III. Shape-memory recovery.** 193-203A
- Shape memory, Heating effects**
- Effect of aging on shape memory behavior of Ti-51.3 at.% Ni thin films.** 3753-3759A
- Shape memory, Microstructural effects**
- Temperature dependent deformation of polydomain phases in an In-22.5 at.% Ti shape memory alloy.** 1687-1692A
- Shape memory, Stress effects**
- Predicting the orientation-dependent stress-induced transformation and detwinning response of shape memory alloy single crystals.** 269-279A
- Shape memory, Temperature effects**
- Influence of training time and temperature on shape memory effect in Cu-Zn-Al alloys.** 3108-3111A
- Shape memory alloys, Heat treatment**
- Effect of aging on shape memory behavior of Ti-51.3 at.% Ni thin films.** 3753-3759A
- Shape memory alloys, Phase transformations**
- Predicting the orientation-dependent stress-induced transformation and detwinning response of shape memory alloy single crystals.** 269-279A
- Thermoelastic martensite and shape memory effect in ductile Cu-Al-Mn alloys.** 2187-2195A
- Effect of stress state on the stress-induced martensitic transformation in polycrystalline Ni-Ti alloy.** 3086-3073A
- Influence of training time and temperature on shape memory effect in Cu-Zn-Al alloys.** 3108-3111A
- Martensitic transformations in NiMnAl β phase alloys.** 4153-4162A
- Shear modulus**
- Communication: On the in situ formation of TiC and Ti_2C reinforcements in combustion-assisted synthesis of titanium matrix composites.** 237-240A
- Shear modulus, Alloying effects**
- Elastic moduli of titanium-hydrogen alloys in the temperature range 20°C to 1100°C.** 3963-3970A
- Shear properties**
- A comprehensive dynamical study of nucleation and growth in a one-dimensional shear martensitic transition.** 1203-1216A

- Shear properties, Composition effects**
Effects of shear flow and anisotropic kinetics on the morphological stability of a binary alloy. 687-694A
- Shear properties, Microstructural effects**
Bridge toughening enhancement in double-notched MoSi₂/Nb model composites. 909-921A
- Shear strength**
Interface effects on the micromechanical response of a transversely loaded single fiber SCS-6/Ti-6Al-4V composite. 2035-2043A
Wear-resistant coatings produced by shock-wave compaction of powders. 2297-2304A
- Shear stress**
Water model experiment on the liquid flow behavior in a bottom blown bath with top layer. 35-41B
Subcritical crack growth at bimaterial interfaces. I. Flexural peel technique. 205-211A
Interface effects on the micromechanical response of a transversely loaded single fiber SCS-6/Ti-6Al-4V composite. 2035-2043A
Evidence of fracture surface interference for cracks loaded in shear detected by phase-shifted speckle interferometry. 3853-3860A
- Shear stress, Temperature effects**
Manifestations of dynamic strain aging in soft-oriented NiAl single crystals. 3542-3557A
- Sheet metal, Heat treatment**
Low quench sensitivity of superplastic 8090 Al-Li thin sheets. 2923-2933A
- Sheet metal, Mechanical properties**
Plastic anisotropy of sheets with continuously varying anisotropic parameters and flow stress. 317-326A
Tension characteristics of notched specimens for Al-Li-Cu-Zr alloys sheets with various cerium contents. 3089-3094A
High-temperature deformation and failure of an orthorhombic titanium aluminide sheet material. 3675-3681A
- Sheet metal, Rolling**
Quantitative characterization of the surface topography of rolled sheets by laser scanning microscopy and Fourier transformation. 2338-2346A
- Sheet metal, Surface properties**
Measurement of friction under sheet forming conditions. 3971-3981A
- Sheet metal, Welding**
Forming of tailor-welded blanks. 2605-2616A
- Shielded metal arc welding**
Structural stability of super duplex stainless weld metals and its dependence on tungsten and copper. 2196-2208A
- Shock loading**
Mechanistic processes influencing shock chemistry in powder mixtures of the Ti-Si, Ti-Al, and Ti-B systems. 1761-1771A
- Shock waves**
Aspects of dynamic recrystallization in shaped charge and explosively formed projectile devices. 1773-1778A
- Short range order**
Stable and metastable ordered phases in microcrystalline alloys Ni (Fe, Mn, Ti). 2045-2046A
- Shot peening**
Influence of plastic deformation upon the half-width of engineering metallic materials in hard state. 3662-3668A
- Shrinkage, Cooling effects**
Thermomechanics of the cooling stage in casting processes: three-dimensional finite element analysis and experimental validation. 81-99B
- Shrinkage, Radiation effects**
Sputter-induced pits on {100} nickel surfaces. 981-993A
- Silicides, Coatings**
The deposition of aluminide and silicide castings on γ -TiAl using the halide-activated pack cementation method. 3761-3772A
- Silicides, Composite materials**
Bridge toughening enhancement in double-notched MoSi₂/Nb model composites. 909-921A
Loading rate and test temperature effects on fracture of in situ niobium silicide-niobium composites. 3292-3306A
Fracture and fatigue-crack growth behavior in ductile-phase toughened molybdenum disilicide: effects of niobium wire vs. particulate reinforcements. 3781-3792A
The balance of mechanical and environmental properties of a multielement niobium-niobium silicide-based in situ composite. 3801-3808A
- Silicides, Oxidation**
Phase relations of a silicide/silica reaction couple at 2273K. 271-276B
- Silicides, Powder technology**
Mechanistic processes influencing shock chemistry in powder mixtures of the Ti-Si, Ti-Al, and Ti-B systems. 1761-1771A
- Silicides, Reactions (chemical)**
Modeling of sequential reactions during micropolytropic synthesis. 961-972A
- Silicon, Alloying elements**
The effects on fracture toughness of ductile-phase composition and morphology in Nb-Cr-Ti and Nb-Si in situ composites. 3007-3018A
The cracking mechanism of silicon particles in an A357 aluminum alloy. 3558-3568A
- Silicon, Binary systems**
Thermal decomposition of silicon carbides: discussion of "the effect of an electric field on self sustaining combustion synthesis, I and II", and author's reply. 322-325B
Effects of shear flow and anisotropic kinetics on the morphological stability of a binary alloy. 687-694A
Critical evaluation and optimization of the thermodynamic properties of liquid tin solutions. 808-826B
Mechanistic processes influencing shock chemistry in powder mixtures of the Ti-Si, Ti-Al, and Ti-B systems. 1761-1771A
A thermodynamic evaluation of the nickel-silicon system. 2897-2903A
- Silicon, Chemical analysis**
Formation of aluminum-silicon alloys from feldspars—determination of silicon, light, and heavy elements in silumin by scanning electron microscopy. 604-609B
- Silicon, Extraction**
Preparation of pure silicon by electrowinning in a bytownite-cryolite melt. 895-900B
- Silicon, Impurities**
Influence of chromium and impurities on the grain refining behavior of aluminum. 791-800A
- Silicon, Quaternary systems**
An isothermal section at 550°C in the Al-rich corner of the Al-Fe-Mn-Si system. 3357-3361A
- Silicon, Refining**
Thermodynamics of phosphorus in molten silicon. 937-941B
- Silicon carbide, Coatings**
Investigation of the temperature field developed by a spinning beam in laser processing. 4039-4047A
- Silicon carbide, Composite materials**
Effective elastic moduli of fiber-matrix interphases in high-temperature composites. 165-182A
Transient thermal analysis of solidification in a centrifugal casting for composite materials containing particle segregation. 277-285B
Effect of a solid solution on the steady-state creep behavior of an aluminum matrix composite. 305-316A
Stacking faults in SiC particles and their effect on the fracture behavior of a 15 vol.% SiC/6061-Al matrix composite. 459-465A
The x-ray diffraction study of deformation in the composite matrix of Al-Mg-Zn and SiC. 503-505A
Liquid state infrared processing of SCS-6/Ti-6Al-4V composites. 527-532B
Solidification of particle-reinforced metal-matrix composites. 663-671B
The Bauschinger effect in a SiC/Al composite. 995-1001A
A one-phase model of the mixing of Al-SiC composite melt. 1015-1023B
Theoretical analysis of the particle gradient distribution in centrifugal field during solidification. 1025-1029B
Interface characterization of ceramic fiber-reinforced titanium alloy composites manufactured by infrared processing. 1379-1394A
Thermal stability of SiC-SCS-6 fiber-reinforced IMI834 alloys. 1403-1405A
An experimental and theoretical investigation of the rapid consolidation of continuously reinforced, metal-matrix composites. 1709-1720A
Multiple matrix cracking in a fiber-reinforced titanium matrix composite under high-cycle fatigue. 1899-1907A
Growth behavior of microstructurally short cracks in the 6061 aluminum alloy with and without 22 vol.% SiC whiskers. 2013-2021A
Interface effects on the micromechanical response of a transversely loaded single fiber SCS-6/Ti-6Al-4V composite. 2035-2043A
Corrosive wear of SiC whisker- and particulate-reinforced 6061 aluminum alloy composites. 2653-2662A
Tensile ductility and fracture of superplastic aluminum-SiC composites under thermal cycling conditions. 2837-2842A
Observation of short fatigue crack-growth process in SiC-fiber-reinforced Ti-15-3 alloy composite. 2843-2851A
Prediction of creep-rupture life of unidirectional titanium matrix composites subjected to transverse loading. 3074-3080A
Thermal residual stresses in functionally graded and layered 6061 Al/SiC materials. 3241-3249A
Thermal expansion of metals reinforced with ceramic particles and microcellular foams. 3700-3717A
Microstructural changes in a mechanically alloyed Al-6.2Zn-2.5Mg-1.7Cu alloy (7010) with and without particulate SiC reinforcement. 3718-3726A
Microstructure and fracture of SiC-particulate-reinforced cast A356 aluminum alloy composites. 3893-3901A
Infrared transient-liquid-phase joining of SCS-6/ β 21S titanium matrix composite. 4011-4018A
Analysis of thermal residual stress in a thick-walled ring of Duralcan-base Al-SiC functionally graded material. 4145-4151A

- Creep deformation and damage in a continuous fiber-reinforced Ti-6Al-4V composite.** 4193-4204A
- Silicon dioxide, Reactions (chemical)**
Activities in $\text{CaO-SiO}_2\text{-Al}_2\text{O}_3$ slags and deoxidation equilibria of silicon and aluminum. 943-953B
- Silver, Binary systems**
Generalized enthalpy method for multicomponent phase change. 869-879B
- Silver, Diffusion**
Analysis of mean square penetration depth in grain boundary diffusion. 3473-3477A
- Silver, Extraction**
Electrochemical behavior of the dissolution of gold-silver alloys in cyanide solutions. 355-361B
- Silver, Recovering**
Influence of gold content on copper oxidation from silver-gold-copper alloys. 3187-3191A
- Silver base alloys, Brazing**
A model for coupled growth of reaction layers in reactive brazing of ZrO_2 -toughened Al_2O_3 . 3630-3638A
- Silver base alloys, Phase transformations**
Characterization of a massive transformation by microstructural analysis. 1511-1516A
- Silver base alloys, Phases (state of matter)**
Eutectoid decomposition in Ag-Ga. 1676-1682A
- Simulation**
Cold model study of the surface profile in a continuous slab casting mold: effect of second phase. 695-697B
Eco-techno-economic synthesis of process routes for the production of zinc using combinatorial optimization. 1031-1044B
Thermal expansion of metals reinforced with ceramic particles and microcellular foams. 3700-3717A
Evidence of fracture surface interference for cracks loaded in shear detected by phase-shifted speckle interferometry. 3853-3860A
Measurement of friction under sheet forming conditions. 3971-3981A
- Sinterability, Alloying effects**
The effect of Mo addition on the liquid-phase sintering of W heavy alloy. 3120-3125A
- Sintered compacts, Physical properties**
The effect of Mo addition on the liquid-phase sintering of W heavy alloy. 3120-3125A
- Sintering (powder metallurgy)**
Effects of nickel on the sintering behavior of Fe-Ni compacts made from composite and elemental powders. 203-211B
Comparative study of pore structure evolution during solvent and thermal debinding of powder injection molded parts. 245-253A
Theoretical modeling of densification during activated solid-state sintering. 441-450A
Microstructure and phase relations in a powder-processed Ti-22Al-12Nb alloy. 1121-1126A
- Slab casting**
Flow and thermal behavior of the top surface flux/powder layers in continuous casting molds. 672-685B
Cold model study of the surface profile in a continuous slab casting mold: effect of second phase. 695-697B
Analysis of shell thickness irregularity in continuously cast middle carbon steel slabs using mold thermocouple data. 1045-1056B
- Slabs, Casting**
A water model study of the flow asymmetry inside a continuous slab casting mold. 757-764B
- Slag disposal**
Preparation of glass-forming materials from granulated blast furnace slag. 801-807B
- Slags**
A multiphase fluid mechanics approach to gas holdup in bath smelting processes. 195-201B
Activities in $\text{MnO-SiO}_2\text{-Al}_2\text{O}_3$ slags and deoxidation equilibria of manganese and silicon. 263-270B
Controversy on the free energy of formation of CaO —additional evidence in support of thermochemical data. 647-651B
Cold model study of the surface profile in a continuous slab casting mold: effect of second phase. 695-697B
- Slags, Reactions (chemical)**
Chemical potentials of components of the system $\text{CaO-P}_2\text{O}_5\text{-Fe}_2\text{O}_3$ at 1673K. 595-603B
Reduction of FeO in smelting slags by solid carbon: experimental results. 717-730B
Activities in $\text{CaO-SiO}_2\text{-Al}_2\text{O}_3$ slags and deoxidation equilibria of silicon and aluminum. 943-953B
- Slags, Solubility**
Solubility of carbon in $\text{CaO-Al}_2\text{O}_3$ melts. 57-64B
- Slags, Surface properties**
Studies of interface deformations in single- and multi-layered liquid baths due to an impinging gas jet. 911-920B
- Slaked lime, Environment**
Influence of microalloying on the corrosion resistance of steel in saturated calcium hydroxide. 1693-1699A
- Sliding friction**
High-temperature wear and deformation processes in metal matrix composites. 3135-3148A
 Ni_3Al intermetallic particles as wear-resistant reinforcement for Al-base composites processed by powder metallurgy. 3259-3266A
Characterization of the wear response of a modified zinc-based alloy vis-à-vis a conventional zinc-based alloy and a bearing bronze at a high sliding speed. 3513-3523A
The wear behavior between hardfacing materials. 3639-3648A
- Slip**
NiTi and NiTi-TiC composites. II. Compressive mechanical properties. 183-191A
Crystallography of grain boundary α precipitates in a β titanium alloy. 1630-1641A
Bauschinger effect in Haynes 230 alloy: influence of strain rate and temperature. 1739-1748A
- Slip, Composition effects**
Effect of manganese dispersoid on the fatigue crack propagation of Al-Zn-Mg alloys. 490-493A
- Slip, Environmental effects**
On the transition of fatigue crack growth from stage I to stage II in a corrosive environment. 471-476A
- Slip, Stress effects**
Discussion of "a fully plastic microcracking model for transgranular stress corrosion cracking in planar slip materials" and reply. 819-821A
- Slip planes**
Plastic zones and fatigue-crack closure under plane-strain double slip. 3491-3502A
- Smelting**
A multiphase fluid mechanics approach to gas holdup in bath smelting processes. 195-201B
Heat transfer and pressure drop considerations in the design of Sirosmeit lances. 221-230B
Influence of gold content on copper oxidation from silver-gold-copper alloys. 3187-3191A
- Snoek effect**
Influence of interstitials on the mechanical properties of metallic materials. 3524-3529A
- Sodium, Binary systems**
Critical evaluation and optimization of the thermodynamic properties of liquid tin solutions. 808-826B
- Sodium, Chemical analysis**
Formation of aluminum-silicon alloys from feldspars—determination of silicon, light, and heavy elements in silumin by scanning electron microscopy. 604-609B
Reference electrode of simple galvanic cells for developing sodium sensors for use in molten aluminum. 794-800B
- Sodium, Thermal properties**
The transported entropy of Na⁺ in solid state cryolite. 788-793B
- Sodium chloride, Environment**
Studies on the influence of metallurgical variables on the stress corrosion behavior of AISI 304 stainless steel in sodium chloride solution using the fracture mechanics approach. 1313-1325A
- Sol gel process**
Preparation of glass-forming materials from granulated blast furnace slag. 801-807B
Synthesis of nanocrystalline Ni_3Cu by sol-gel route. 4213-4216A
- Solar generators**
Thermodynamics of phosphorus in molten silicon. 937-941B
- Solid phases**
Interdiffusion kinetics in oxide powder mixture using high temperature x-ray diffraction technique. 318-322B
Effects of flow on morphological stability during directional solidification. 583-593A
Interface attachment kinetics in alloy solidification. 671-686A
An adaptive mesh refinement scheme for solidification problems. 707-717A
Real time x-ray transmission microscopy of solidifying Al-In alloys. 801-808A
Inverse melting in binary systems: morphology and microscopy of catatetic alloys. 979-986B
Characterization of a massive transformation by microstructural analysis. 1511-1516A
- Solid phases, Alloying effects**
Precipitation in lead-calcium alloys containing tin. 1668-1675A

- Solid phases, Heating effects**
High-temperature nitridation of Ni-Cr alloys 59-69A
Pearlite in ultrahigh carbon steels: heat treatments and mechanical properties. 111-118A
- Solid phases, Pressure effects**
Vacuum evaporation of KCl-NaCl salts. I. Thermodynamic modeling of vapor pressures of solid and liquid solutions. 141-146B
- Solid phases, Temperature effects**
A study of the thermal decomposition of BaCO₃. 409-416B
Overview of geometric effects on coarsening of mushy zones. The phase field method: simulation of alloy dendritic solidification during recalcification. 557-567A
657-669A
- Solid solubility**
The production of nickel-zinc alloys by powder injection. Solid-state contributions to densification during liquid-phase sintering. 780-787B
901-909B
Retrograde solubility in semiconductors. 2704-2707A
Thermodynamic activities and partial enthalpies of mixing in the solid solution of Fe in Ni₃Al. 3569-3575A
- Solid solubility, Alloying effects**
Mechanical alloying of Nb-Al powders. 41-48A
- Solid solubility, Composition effects**
Microstructural changes in a mechanically alloyed Al-6.22Zn-2.5Mg-1.7Cu alloy (7010) with and without particulate SiC reinforcement. 3718-3726A
- Solid solutions, Mechanical properties**
Influence of interstitials on the mechanical properties of metallic materials. 3524-3529A
- Solid state**
Dense CoAl-based alloys with improved ductility: solid-state synthesis and microstructure control. 2140-2150A
- Solidification**
Thermomechanics of the cooling stage in casting processes: three-dimensional finite element analysis and experimental validation. 81-99B
Scaling of intragranular dendritic microstructure in ingot solidification. 101-113B
Transient thermal analysis of solidification in a centrifugal casting for composite materials containing particle segregation. 277-285B
Effect of superheat on the solidification structures of AISI 310S austenitic stainless steel. 287-296B
Porosity formation in Al-9 wt.% Si-3 wt.% Cu alloy systems: metallographic observations. 415-429A
Effects of forced electromagnetic vibrations during the solidification of aluminum alloys. I. Solidification in the presence of crossed alternating electric fields and stationary magnetic fields. 445-455B
Microstructure of Al₂O₃ fiber-reinforced superalloy (Inconel 718) composites. 451-458A
Effects of forced electromagnetic vibrations during the solidification of aluminum alloys. II. Solidification in the presence of colinear variable and stationary magnetic fields. 457-464B
The effect of bulk flow concentration on diffusion coupling between dendrites. 477-480A
Analysis and Modeling of Solidification. 509-824A
Intermixing model of continuous casting during a grade transition. 617-632B
Solidification of particle-reinforced metal-matrix composites. 663-671B
Radioscopic visualization of isothermal solidification of eutectic Ga-In alloy. 686-689B
An adaptive mesh refinement scheme for solidification problems. 707-717A
Inverse melting in binary systems: morphology and microscopy of catatetic alloys. 979-986B
Modeling of the peritectic reaction and macro-segregation in casting of low carbon steel. 999-1014B
Theoretical analysis of the particle gradient distribution in centrifugal field during solidification. 1025-1029B
Analysis of shell thickness irregularity in continuously cast middle carbon steel slabs using mold thermocouple data. 1045-1056B
Modeling of ferrite growth in nodular cast iron. 2209-2220A
Modeling of microsegregation in macrosegregation computations. 2314-2327A
A model for macrosegregation and its application to Al-Cu castings. 2708-2721A
Determination of the solidification curves of commercial aluminum alloys. 2722-2726A
Orientation dependence of primary dendrite spacing. 2727-2739A
Equiaxed dendritic solidification with convection. I. Multiscale/multiphase modeling. 2754-2764A
Equiaxed dendritic solidification with convection. II. Numerical simulations for an Al-4 wt.% Cu alloy. 2765-2783A
Equiaxed dendritic solidification with convection. III. Comparisons with NH₄Cl-H₂O experiments. 2784-2795A
Solidification of an alloy 625 weld overlay. 3612-3620A
Macrotransport-solidification kinetics modeling of equiaxed dendritic growth. I. Model development and discussion. 4061-4074A
- Macrotransport-solidification kinetics modeling of equiaxed dendritic growth. II. Computation problems and validation on Inconel 718 superalloy casting. 4075-4083A
Modeling of primary and secondary dendrites in a Cu-6 wt.% tin alloy. 4085-4093A
- Solidification, Alloying effects**
The breakdown of single-crystal solidification in high refractory nickel-base alloys. 1081-1094A
- Solidification, Cooling effects**
Numerical modeling of cellular/dendritic array growth: spacing and structure predictions. 611-623A
- Solidification, Field effects**
On the reaction between Fe-Ti and Fe-C liquids under microgravity. 407-414A
- Solidification, Pressure effects**
The squeeze casting of hypoeutectic binary Al-Cu. 4121-4132A
- Solidification, Temperature effects**
Nucleation controlled solidification kinetics. 533-547A
Overview of geometric effects on coarsening of mushy zones. 557-567A
Banded solidification microstructures. 625-634A
The phase field method: simulation of alloy dendritic solidification during recalcification. 657-669A
- Solidification point**
Solidification of an alloy 625 weld overlay. 3612-3620A
- Solubility, Alloying effects**
Solubility of carbon in CaO-Al₂O₃ melts. 57-64B
Effects of oxygen, selenium, and tellurium on the rate of nitrogen dissolution in molten iron. 846-851B
- Solutes**
Modeling of microsegregation in macrosegregation computations. 2314-2327A
- Solution heat treatment**
Microstructural aspects of the dissolution and melting of Al₂Cu phase in Al-Si alloys during solution heat treatment. 1785-1798A
The control of grain size and distribution of particles in a (6061 alloy)_m/(Al₂O₃)_p composite by solutionizing treatment. 2023-2034A
Dense CoAl-based alloys with improved ductility: solid-state synthesis and microstructure control. 2140-2150A
Hot deformation mechanisms of a solution-treated Al-Li-Cu-Mg-Zr alloy. 3478-3490A
- Sour gas, Environment**
Microstructural aspects of sulfide stress cracking in an API X-80 pipeline steel. 3601-3611A
- Spalling**
Kinetics of cyclic oxidation and cracking and finite element analysis of MA956 and sapphire/MA956 composite system. 3279-3291A
Effects of the alumina scale on the room-temperature tensile behavior of preoxidized MA 956. 3809-3816A
- Specific heat**
Modeling of ingot distortions during direct chill casting of aluminum alloys. 3214-3225A
- Spheroidal structure, Deformation effects**
Effect of creep strain on microstructural stability and creep resistance of a TiAl/Ti₃Al lamellar alloy. 127-134A
- Spheroidal structure, Heating effects**
Pearlite in ultrahigh carbon steels: heat treatments and mechanical properties. 111-118A
Effect of bainite transformation and retained austenite on mechanical properties of austempered spheroidal graphite cast steel. 1585-1594A
- Spheroidizing**
Bainitic microstructures formed by split isothermal transformation in an Fe-C-Si-Mn-Mo steel. 1141-1147A
- Spinodal decomposition, Stress effects**
Molecular dynamics simulation of martensitic transformations in NiAl. 1476-1488A
- Splitting**
Splitting phenomena occurring in the martensitic transformation of Cr13 and CrMoV14 stainless steels in the absence of carbide precipitation. 1799-1805A
- Squeeze casting**
Microstructure and fracture of SiC-particulate-reinforced cast A356 aluminum alloy composites. 3893-3901A
The squeeze casting of hypoeutectic binary Al-Cu. 4121-4132A
- Stability**
The relationship between microstructural and plastic instability in Al-4.0 wt.% Cu alloy. 2916-2922A
- Stacking fault energy**
Reply: Dynamic materials model. Basis and principles. 235-236A

Stacking faults

The mechanism of formation of a fine duplex microstructure in Ti-48Al-2Mn-2Nb alloys.

1655-1667A

High-resolution transmission electron microscopy investigation of the face-centered cubic/hexagonal close-packed martensite transformation in Co-31.8 wt.% Ni alloy. II. Plate intersections, extended defects, and nucleation mechanisms.

3371-3380A

Stacking faults, Deformation effects

The x-ray diffraction study of deformation in the composite matrix of Al-Mg-Zn and SiC.

503-505A

Stacking faults, Radiation effects

Transmission electron microscopy study on the cross-sectional microstructure of an ion-nitriding layer.

1347-1352A

Stacking faults, Stress effects

Stacking faults in SiC particles and their effect on the fracture behavior of a 15 vol.% SiC/6061-Al matrix composite.

459-465A

Stainless steels, Casting

Intermixing model of continuous casting during a grade transition.

617-632B

Stainless steels, Forming

Reply: Dynamic materials model. Basis and principles.

235-236A

Stainless steels, Microstructure

Prediction of grain structures in various solidification processes.

695-705A

Statistical analysis

A statistical analysis of the effect of a mixture component on the rheology of alumina feedstocks.

399-408B

Steam turbines, Service life

Carbide diagrams and precipitation of alloying elements during aging of low-alloy steels.

498-502A

Steel making

Representation of mixed reactive gases on free energy (Ellingham-Richardson) diagrams.

65-69B

Dispersed phase holdup in liquid-liquid emulsions generated by high strength bottom gas injection.

213-219B

Characteristics of eccentric bubble plumes in liquids.

231-239B

The use of blast furnace slag and derived materials in the vitrification of electric arc furnace dust.

379-384B

A study of the thermal decomposition of BaCO₃.

409-416B

Reoxidation of aluminum in Fe-Al-M (M=C, Mn, and Ti) melts with CaO-Al₂O₃-FeO (3 mass%) slags.

423-431B

Transient thermal model of the continuous single-wheel thin-strip casting process.

509-525B

Alternative technologies in iron and steelmaking.

541-553B

Model study of bubble and liquid-flow characteristics in a bottom blown bath under reduced pressure.

765-772B

Activities in CaO-SiO₂-Al₂O₃ slags and deoxidation equilibria of silicon and aluminum.

943-953B

Steels, Casting

Transient thermal model of the continuous single-wheel thin-strip casting process.

509-525B

Flow and thermal behavior of the top surface flux/powder layers in continuous casting molds.

672-685B

Mathematical modeling of tundish operation and flow control to reduce transition slabs.

745-756B

Steels, Coating

Discussion of "The effect of steel chemistry on the formation of Fe-Zn intermetallic compounds of galvanneal-coated steel sheets" and authors' reply.

146-148B

Microstructure of bonding zones in laser-clad nickel-alloy-based composite coatings reinforced with various ceramic powders.

391-400A

The production of nickel-zinc alloys by powder injection.

780-787B

Kinetics of phase evolution of Zn-Fe intermetallics.

2904-2910A

Steels, Corrosion

Stress corrosion cracking of pressure vessel steels in high-temperature caustic aluminate solutions.

1327-1331A

Steels, Diffusion

Annealing and aging of interstitial C in α -Fe, as measured by internal friction.

2461-2469A

Steels, Heat treatment

Effect of bainite transformation and retained austenite on mechanical properties of austempered spheroidal graphite cast steel.

1585-1594A

Steels, Irradiation

Theory of nucleation with cluster loss and injection: application to plastic deformation and irradiation.

1441-1448A

Steels, Mechanical properties

Detecting stable crack onset at ductile-brittle transition in steels.

469-471A

Steels, Melting

Studies of interface deformations in single- and multi-layered liquid baths due to an impinging gas jet.

911-920B

Steels, Phase transformations

On the reaction between Fe-Ti and Fe-C liquids under microgravity.

407-414A

Bainitic microstructures formed by split isothermal transformation in an Fe-C-Si-Mn-Mo steel.

1141-1147A

Steels, Quality control

Effects of oxygen, selenium, and tellurium on the rate of nitrogen dissolution in molten iron.

846-851B

Steels, Refining

Thermodynamics of sulfur in the BaO-MnO-SiO₂ flux system. Use of solid-electrolyte galvanic cells to determine the activity of CaO in the CaO-ZrO₂ system and the standard Gibbs free energies of formation of CaZrO₃ from CaO and ZrO₂.

652-657B

Model study of bubble and liquid-flow characteristics in a bottom blown bath under reduced pressure.

658-662B

Steels, Steel making

Water model experiment on the liquid flow behavior in a bottom blown bath with top layer.

765-772B

Steels, Surface finishing

Influence of plastic deformation upon the half-width of engineering metallic materials in hard state.

35-41B

Steels, Surface finishing

Influence of plastic deformation upon the half-width of engineering metallic materials in hard state.

3662-3668A

Stiffness

Microstructure and properties of Al₂O₃-Al(Si) and Al₂O₃-Al(Si)-Si composites formed by in situ reaction of aluminum with aluminosilicate ceramics.

2122-2129A

The effect of volume percent and morphology of phases on the damping behavior of epoxy-aluminum composites.

2366-2373A

Stiffness, High temperature effects

Effective elastic moduli of fiber-matrix interphases in high-temperature composites.

165-182A

Stirring

A unified representation of the two-phase plume characteristics in gas-stirred ladle systems.

704-708B

Stoichiometry

Formation of structural intermetallics by reactive metal penetration of titanium and nickel oxides and aluminates.

2100-2104A

Dense CoAl-based alloys with improved ductility: solid-state synthesis and microstructure control.

2140-2150A

Strain

Effect of creep strain on microstructural stability and creep resistance of a TiAl/Ti₃Al lamellar alloy.

127-134A

Mechanisms of high-temperature fatigue failure in alloy 800H. The influence of niobium supersaturation in austenite on the static recrystallization behavior of low carbon microalloyed steels.

851-861A

The Bauschinger effect in a SiC/Al composite.

951-960A

Increased ductility in high velocity electromagnetic ring expansion.

995-1001A

The effects on fracture toughness of ductile-phase composition and morphology in Nb-Cr-Ti and Nb-Si in situ composites.

1837-1844A

Analysis of the stress-strain curves of a modified 9Cr-1Mo steel by the Voce equation.

3007-3018A

Analysis of the stress-strain curves of a modified 9Cr-1Mo steel by the Voce equation.

3340-3343A

Strain, Cooling effects

NiTi and NiTi-TiC composites. III. Shape-memory recovery.

193-203A

Strain, Environmental effects

On the transition of fatigue crack growth from stage I to stage II in a corrosive environment.

471-476A

Strain, Heating effects

Heterogeneous nucleation of δ on dislocations in a dilute aluminum-lithium alloy.

1595-1605A

Strain, Stress effects

Computer simulation of reversible martensitic transformations. A study on coherency strain and precipitate morphology via a discrete atom method.

1187-1201A

Effect of uniaxial stress on coarsening of precipitate clusters.

1449-1459A

Strain aging

Temperature and strain-rate effects on low-cycle fatigue behavior of alloy 800H.

1460-1475A

Dynamic strain aging and hydrogen-induced softening in alpha titanium.

255-267A

The relationship between microstructural and plastic instability in Al-4.0 wt.% Cu alloy.

1877-1887A

Strain aging, Microstructural effects

Influence of interstitials on the mechanical properties of metallic materials.

2916-2922A

Strain aging, Temperature effects

Manifestations of dynamic strain aging in soft-oriented NiAl single crystals.

3524-3529A

- Strain hardenability**
Constitutive behavior of tantalum and tantalum-tungsten alloys. 2994-3006A
- Strain hardening**
NiTi and NiTi-TiC composites. II. Compressive mechanical properties. 183-191A
Constitutive behavior of tantalum and tantalum-tungsten alloys. 2994-3006A
Influence of interstitials on the mechanical properties of metallic materials. 3524-3529A
- Strain hardening, Alloying effects**
Effect of phase composition and hydrogen level on the deformation behavior of titanium-hydrogen alloys. 1869-1876A
Dynamic strain aging and hydrogen-induced softening in alpha titanium. 1877-1887A
- Strain hardening, Deformation effects**
Non-Schmid effects on the behavior of polycrystals, with applications to Ni₃Al. 81-99A
The x-ray diffraction study of deformation in the composite matrix of Al-Mg-Zn and SiC. 503-505A
- Strain hardening, Microstructural effects**
Reinforcement shape effects on the fracture behavior and ductility of particulate-reinforced 6061-Al matrix composites. 3739-3748A
- Strain hardening, Temperature effects**
Enhanced ductility in coarse-grained Al-Mg alloys. 343-352A
Manifestations of dynamic strain aging in soft-oriented NiAl single crystals. 3542-3557A
- Strain rate**
Bauschinger effect in Haynes 230 alloy: influence of strain rate and temperature. 1739-1748A
Characterization and mechanical properties of ultrahigh boron steels produced by powder metallurgy. 1861-1867A
Deformation behavior of an Al-3.37 wt.% Li alloy. 2274-2284A
Constitutive behavior of tantalum and tantalum-tungsten alloys. 2994-3006A
Control of superplastic deformation rate during uniaxial tensile tests. 3030-3042A
Effect of stress state on the stress-induced martensitic transformation in polycrystalline Ni-Ti alloy. 3066-3073A
Failure characteristics of 6061/Al₂O₃/15_p and 2014/Al₂O₃/15_p composites as a function of loading rate. 3095-3107A
High-temperature deformation and failure of an orthorhombic titanium aluminide sheet material. 3675-3681A
Hydrogen-induced cleavage fracture of Fe₃Al-based intermetallics. 3949-3956A
An analysis of the flow stress of a two-phase alloy system, Ti-6Al-4V. 3957-3962A
Microstructural features of friction welded MA 956 superalloy material. 4019-4029A
Mathematical modeling of the extrusion of 6061/Al₂O₃/20p composite. 4095-4111A
- Strain rate, Alloying effects**
Effect of strain rate and temperature on the flow stress of β -phase titanium-hydrogen alloys. 1303-1312A
Dynamic strain aging and hydrogen-induced softening in alpha titanium. 1877-1887A
- Strain rate, Corrosion effects**
Effects of the alumina scale on the room-temperature tensile behavior of preoxidized MA 956. 3809-3816A
- Strain rate, Deformation effects**
Optimization of cold and warm workability in 304 stainless steel using instability maps. 119-126A
Flow stress and microstructural evolution during hot working of alloy 22Cr-13Ni-5Mn-0.3N austenitic stainless steel. 1251-1266A
Analysis on the amplitude of serrated flow associated with the Portevin-LeChatelier effect of substitutional fcc alloys. 1683-1686A
- Strain rate, High temperature effects**
High-temperature deformation properties of NiAl single crystals. 1229-1240A
- Strain rate, Impurity effects**
The effect of hydrogen on the fracture of alloy X-750. 101-110A
- Strain rate, Microstructural effects**
Effect of iron on ductility and cavitation in the superplastic An-22% Al eutectoid. 863-872A
The inter-relationship between grain boundary sliding and cavitation during creep of polycrystalline copper. 901-907A
Creep deformation of dispersion-strengthened copper. 1217-1227A
Influence of interstitials on the mechanical properties of metallic materials. 3524-3529A
- Strain rate, Temperature effects**
Temperature and strain-rate effects on low-cycle fatigue behavior of alloy 800H. 255-267A
Enhanced ductility in coarse-grained Al-Mg alloys. 343-352A
Temperature dependence of the rate sensitivity and its effect on the activation energy for high-temperature flow. 3346-3348A
- Manifestations of dynamic strain aging in soft-oriented NiAl single crystals. 3542-3557A
- Strain softening**
Dynamic strain aging and hydrogen-induced softening in alpha titanium. 1877-1887A
- Strain softening, Alloying effects**
Effect of phase composition and hydrogen level on the deformation behavior of titanium-hydrogen alloys. 1869-1876A
- Stress analysis**
Evidence of fracture surface interference for cracks loaded in shear detected by phase-shifted speckle interferometry. 3853-3860A
Creep lifetime prediction of oxide-dispersion-strengthened nickel-base superalloys: a micromechanically based approach. 3861-3870A
Elevated temperature deformation behavior of a dispersion-strengthened Al-Fe, V, Si alloy. 3913-3923A
Analysis of thermal residual stress in a thick-walled ring of Duralcan-base Al-SiC functionally graded material. 4145-4151A
- Stress concentration**
Interface effects on the micromechanical response of a transversely loaded single fiber SCS-6/Ti-6Al-4V composite. 2035-2043A
The effect of volume percent and morphology of phases on the damping behavior of epoxy-aluminum composites. 2366-2373A
Tension characteristics of notched specimens for Al-Li-Cu-Zr alloys sheets with various cerium contents. 3089-3094A
- Stress concentration, Stress effects**
Evidence of fracture surface interference for cracks loaded in shear detected by phase-shifted speckle interferometry. 3853-3860A
- Stress corrosion cracking**
Discussion of "a fully plastic microcracking model for transgranular stress corrosion cracking in planar slip materials" and reply. 819-821A
Initiation of stress corrosion cracking for pipeline steels in a carbonate-bicarbonate solution. 2686-2691A
- Stress corrosion cracking, Environmental effects**
Studies on the influence of metallurgical variables on the stress corrosion behavior of AISI 304 stainless steel in sodium chloride solution using the fracture mechanics approach. 1313-1325A
Stress corrosion cracking of pressure vessel steels in high-temperature caustic aluminate solutions. 1327-1331A
Microstructural aspects of sulfide stress cracking in an API X-80 pipeline steel. 3601-3611A
- Stress corrosion cracking, Heating effects**
A strain-based fracture model for stress corrosion cracking of low-alloy steels. 291-304A
Atmospheric stress corrosion cracking of a superplastic 7475 aluminum alloy. 2617-2627A
Influence of thermal aging on the intergranular corrosion resistance of types 304LN and 316LN stainless steels. 2881-2887A
- Stress corrosion cracking, Microstructural effects**
The effects of microstructure, strength level, and crack propagation mode on stress corrosion cracking behavior of 4135 steel. 281-290A
Structure, chemistry, and stress corrosion cracking of grain boundaries in alloys 600 and 690. 327-341A
- Stress cycle**
Temperature and strain-rate effects on low-cycle fatigue behavior of alloy 800H. 255-267A
Effect of thermal cycling on the mechanical properties of 350 grade maraging steel. 757-761A
- Stress intensity**
Effect of creep strain on microstructural stability and creep resistance of a TiAl/Ti₆Al lamellar alloy. 127-134A
Effect of a solid solution on the steady-state creep behavior of an aluminum matrix composite. 305-316A
Rafting in superalloys. 513-530A
Effect of carbide precipitation on the creep behavior of alloy 800HT in the temperature range 700-900°C. 747-756A
Creep deformation and crack growth behavior of a single-crystal nickel-base superalloy. 829-837A
Time-dependent, environmentally assisted crack growth in Nicalon-fiber-reinforced SiC composites at elevated temperatures. 839-849A
Temperature dependence of the intrinsic small fatigue crack growth behavior in nickel-base superalloys based on measurement of crack closure. 1021-1031A
Analysis on the amplitude of serrated flow associated with the Portevin-LeChatelier effect of substitutional fcc alloys. 1683-1686A
- Stress relaxation**
Influence of interstitials on the mechanical properties of metallic materials. 3524-3529A
- Stress strain curves**
Mechanical behavior of the in situ composite alloys in the Al-Ni-Ti system near the L₁₂ phase field. 71-79A

Optimization of cold and warm workability in 304 stainless steel using instability maps.	119-126A	Sulfides, Crystal growth Internal sulfide precipitation in low Cr-Fe alloys.	3192-3202A
NTI and NTI-TiC composites. II. Compressive mechanical properties.	183-191A	Sulfides, Reduction (chemical) Phase equilibria in the metal-sulfur-oxygen system and selective reduction of metal oxides and sulfides. I. The carbothermic reduction and calcination of complex mineral sulfides.	827-838B
Subcritical crack growth at bimaterial interfaces. III. Shear-enhanced fatigue crack growth resistance at polymer/metal interface.	221-228A	Sulfur, Binary systems Critical evaluation and optimization of the thermodynamic properties of liquid tin solutions.	808-826B
Temperature and strain-rate effects on low-cycle fatigue behavior of alloy 800H.	255-267A	Sulfur, Physical properties Thermodynamics of sulfur in the BaO-MnO-SiO ₂ flux system.	652-657B
Predicting the orientation-dependent stress-induced transformation and detwinning response of shape memory alloy single crystals.	269-279A	Sulfur, Ternary systems Applicability of Butler's equation in interpreting the thermodynamic behavior of surfaces and adsorption in Fe-S-O melts.	241-253B
Plastic anisotropy of sheets with continuously varying anisotropic parameters and flow stress.	317-326A	Internal sulfide precipitation in low Cr-Fe alloys.	3192-3202A
Reinforcement stresses during deformation of sphere- and particulate-reinforced aluminum-matrix composites.	486-490A	Sulfuric acid leaching A study of solid-aqueous equilibria by the speciation approach in the hydronium alunite-sulfuric acid-water system at high temperatures.	555-566B
The characteristics of cavitation in superplastic metals and ceramics.	873-878A	Sulfurization Internal sulfide precipitation in low Cr-Fe alloys.	3192-3202A
Characterization of superplastic deformation behavior of a fine grain 5083 Al alloy sheet.	1889-1898A	Superalloys Recrystallization in oxide-dispersion strengthened mechanically alloyed sheet steel.	1963-1978A
Influence of temperature transients on the hot workability of a two-phase gamma titanium aluminide alloy.	1933-1950A	Superalloys, Casting Viscosity of superalloy 718 by the oscillating vessel technique.	698-701B
Interface effects on the micromechanical response of a transversely loaded single fiber SCS-6/Ti-6Al-4V composite.	2035-2043A	Superalloys, Claddings Solidification of an alloy 625 weld overlay.	3612-3620A
High-temperature deformation processing of Ti-24Al-20Nb.	2593-2604A	The wear behavior between hardfacing materials.	3639-3648A
The relationship between microstructural and plastic instability in Al-4.0 wt.% Cu alloy.	2916-2922A	Superalloys, Coating Isothermal fatigue of an aluminide-coated single-crystal superalloy. I.	353-361A
Effect of thermomechanical treatments on the room-temperature mechanical behavior of iron aluminide Fe ₃ Al.	2985-2993A	Isothermal fatigue of an aluminide-coated single-crystal superalloy. II. Effects of brittle precracking.	363-369A
Constitutive behavior of tantalum and tantalum-tungsten alloys.	2994-3006A	Superalloys, Composite materials Microstructure of Al ₂ O ₃ fiber-reinforced superalloy (Inconel 718) composites.	451-458A
Control of superplastic deformation rate during uniaxial tensile tests.	3030-3042A	Effect of primary grain size on the secondary recrystallization of mechanically alloyed oxide dispersion strengthened nickel-based superalloy.	493-496A
Effect of stress state on the stress-induced martensitic transformation in polycrystalline Ni-Ti alloy.	3066-3073A	Kinetics of cyclic oxidation and cracking and finite element analysis of MA956 and sapphire/MA956 composite system.	3279-3291A
Simulation of the hot-tension test under cavitating conditions.	3112-3119A	Superalloys, Corrosion Structure, chemistry, and stress corrosion cracking of grain boundaries in alloys 600 and 690.	327-341A
Elevated temperature compressive properties of N-doped NIAI.	3170-3180A	Superalloys, Crystal growth Recrystallization in oxide-dispersion strengthened mechanically alloyed sheet steel.	1963-1978A
Thermal residual stresses in functionally graded and layered 6061 Al/SiC materials.	3241-3249A	Macrotransport-solidification kinetics modeling of equiaxed dendritic growth. I. Model development and discussion.	4061-4074A
The use of microstructural gradients in hot gas-pressure forming of Zn-Al sheet.	3250-3258A	Macrotransport-solidification kinetics modeling of equiaxed dendritic growth. II. Computation problems and validation on Inconel 718 superalloy casting.	4075-4083A
Analysis of the stress-strain curves of a modified 9Cr-1Mo steel by the Voce equation.	3340-3343A	Superalloys, Forming Reply: Dynamic materials model. Basis and principles.	235-236A
Hot deformation mechanisms of a solution-treated Al-Li-Cu-Mg-Zr alloy.	3478-3490A	Superalloys, Heat treatment Effect of homogenization heat treatment on the microstructure and heat affected zone microfissuring in welded cast alloy 718.	785-790A
Plastic zones and fatigue-crack closure under plane-strain double slip.	3491-3502A	Superalloys, Joining Transient liquid-phase bonding in the NIAI/Cu/Ni system—a microstructural investigation.	3621-3629A
Manifestations of dynamic strain aging in soft-oriented NIAI single crystals.	3542-3557A	Superalloys, Mechanical properties The effect of hydrogen on the fracture of alloy X-750.	101-110A
High-temperature deformation and failure of an orthorhombic titanium aluminide sheet material.	3675-3681A	Rattling in superalloys.	513-530A
Plastic zone and pileup around large indentations.	3793-3800A	Effect of carbide precipitation on the creep behavior of alloy 800HT in the temperature range 700-900°C.	747-756A
Effects of the alumina scale on the room-temperature tensile behavior of preoxidized MA 956.	3809-3816A	Creep deformation and crack growth behavior of a single-crystal nickel-base superalloy.	829-837A
Microstructural evolution and superplastic deformation behavior of fine grain 5083Al.	3827-3839A	Mechanisms of high-temperature fatigue failure in alloy 800H.	851-861A
Creep lifetime prediction of oxide-dispersion-strengthened nickel-base superalloys: a micromechanically based approach.	3861-3870A	On the influence of grain morphology on creep deformation and damage mechanisms in directionally solidified and oxide dispersion strengthened superalloys.	879-890A
Notch fracture in γ -titanium aluminides.	3903-3912A	High-temperature measurements of lattice parameters and internal stresses of a creep-deformed monocrystalline nickel-base superalloy.	1003-1014A
Creep deformation and damage in a continuous fiber-reinforced Ti-6Al-4V composite.	4193-4204A	Temperature dependence of the intrinsic small fatigue crack growth behavior in nickel-base superalloys based on measurement of crack closure.	1021-1031A
Stress strain curves, Alloying effects Elevated temperature compressive properties of zirconium-modified NIAI.	2628-2641A	Effects of the alumina scale on the room-temperature tensile behavior of preoxidized MA 956.	3809-3816A
Stress strain curves, Microstructural effects Theoretical calculation of the stress-strain behavior of dual-phase metals with randomly oriented spheroidal inclusions.	2359-2365A		
Stresses Multiple matrix cracking in a fiber-reinforced titanium matrix composite under high-cycle fatigue.	1899-1907A		
Strip casting Transient thermal model of the continuous single-wheel thin-strip casting process.	509-525B		
Strip steel, Metal working Analysis and prevention of vertical cracking phenomena during deep drawing of hot-rolled SG295 steel strips.	1241-1250A		
Strontium, Alloying elements Electron microscope study of Al-Fe-Si intermetallics in 6201 aluminum alloy.	929-936A		
Effect of strontium modification on near-threshold fatigue crack growth in an Al-Si-Cu die cast alloy.	1293-1302A		
Submerged arc welding Dilution in single pass arc welds.	481-489B		
Sulfation Kinetics of sulfation of chalcopyrite with steam and oxygen in the presence of ferric oxide.	465-474B		

Superalloys, Metal working		
Flow stress and microstructural evolution during hot working of alloy 22Cr-13Ni-5Mn-0.3N austenitic stainless steel.	1251-1266A	
Superalloys, Microstructure		
Prediction of grain structures in various solidification processes.	695-705A	
Characterization of constitutional liquid film migration in nickel-base alloy 718.	2692-2703A	
Superalloys, Phases (state of matter)		
The breakdown of single-crystal solidification in high refractory nickel-base alloys.	1081-1094A	
Superalloys, Powder technology		
The effect of thermal cycle on the microstructural development of a powder metallurgy superalloy braze material.	145-153A	
Superalloys, Structural hardening		
A study on coherency strain and precipitate morphology via a discrete atom method.	1449-1459A	
Bauschinger effect in Haynes 230 alloy: influence of strain rate and temperature.	1739-1748A	
Preferential coarsening of γ' precipitates in Inconel 718 during creep.	3391-3398A	
Creep lifetime prediction of oxide-dispersion-strengthened nickel-base superalloys: a micromechanically based approach.	3861-3870A	
Superalloys, Welding		
Microstructural features of friction welded MA 956 superalloy material.	4019-4029A	
Superconductors		
A thermodynamic evaluation of the Ti-Mo-C system.	955-966B	
Supercooling		
The role of grain comers in nucleation.	480-483A	
High-speed imaging and analysis of the solidification of undercooled nickel melts.	863-868B	
Solidification of undercooled Fe-Cr-Ni alloys. II. Microstructural evolution.	3226-3240A	
Microstructure of Cu-Co alloys solidified at various supercoolings.	4049-4059A	
Superlattices		
Stable and metastable ordered phases in microcrystalline alloys Ni (Fe, Mn, Ti).	2045-2046A	
Superplastic forming		
Effects of alloy modification and thermomechanical processing on recrystallization of Al-Mg-Mn alloys.	2947-2957A	
Microstructural evolution and superplastic deformation behavior of fine grain 5083Al.	3827-3839A	
Superplasticity		
Characterization of superplastic deformation behavior of a fine grain 5083 Al alloy sheet.	1889-1898A	
Pressure-assisted reactive synthesis of titanium aluminides from dense 50Al-50Ti elemental powder blends.	2130-2139A	
An investigation by interactive electron backscatter pattern analysis of processing and superplasticity in an aluminum-magnesium alloy.	2252-2262A	
A model study of cavity growth in superplasticity using single premachined holes.	2532-2539A	
Tensile ductility and fracture of superplastic aluminum-SiC composites under thermal cycling conditions.	2837-2842A	
Control of superplastic deformation rate during uniaxial tensile tests.	3030-3042A	
The behavior of internal markers in Ti-6Al-4V deformed in superplastic tension.	3747-3748A	
Superplasticity, Deformation effects		
Micronecking and fracture in cavitated superplastic materials.	1043-1046A	
Superplasticity, Heating effects		
Low quench sensitivity of superplastic 8090 Al-Li thin sheets.	2923-2933A	
Superplasticity, Mechanical properties		
The characteristics of cavitation in superplastic metals and ceramics.	873-878A	
Superplasticity, Microstructural effects		
Effect of iron on ductility and cavitation in the superplastic Al-22% Al eutectoid.	863-872A	
On microsuperplasticity in AA7475 domes.	1400-1403A	
Microstructural evolution and superplastic deformation behavior of fine grain 5083Al.	3827-3839A	
Superplasticity, Stress effects		
Predicting the orientation-dependent stress-induced transformation and detwinning response of shape memory alloy single crystals.	269-279A	
Supersaturation		
Incipient chemical instabilities of nanophase Fe-Cu alloys prepared by mechanical alloying.	2934-2946A	
Surface chemistry		
Studies on the corrosion and the behavior of inert anodes in aluminum electrolysis.		185-183B
Physical chemistry of the powder metallurgy of beryllium: chemical characterization of the powder in relation to its granularity.		371-379A
Fundamental studies of copper anode passivation during electrorefining. II. Surface morphology.		610-616B
Surface chemistry, Temperature effects		
Variation of contact angles with temperature and time in the Al-Al ₂ O ₃ system.		51-55B
Surface hardening		
Quenching C60 fullerene into diamond in the Fe-C alloy system by laser treatment.		2293-2296A
Surface hardness, Deformation effects		
Influence of plastic deformation upon the half-width of engineering metallic materials in hard state.		3662-3668A
Surface hardness, Radiation effects		
Simultaneous plasma treatment for carburizing and carbonitriding using hollow cathode discharge.		401-405A
Surface layer		
Flow and thermal behavior of the top surface flux/powder layers in continuous casting molds.		672-685B
Control of iron nitride layers growth kinetics in the binary Fe-N system.		1823-1835A
Surface structure		
Physical chemistry of the powder metallurgy of beryllium: chemical characterization of the powder in relation to its granularity.		371-379A
Bridge toughening enhancement in double-notched MoSi ₂ /Nb model composites.		909-921A
Interface characterization of ceramic fiber-reinforced titanium alloy composites manufactured by infrared processing.		1379-1394A
On microsuperplasticity in AA7475 domes.		1400-1403A
Formation of bainite in ferrous and nonferrous alloys through sympathetic nucleation and ledge growth mechanism.		1533-1543A
A high resolution transmission electron microscopy study of interfaces between the γ , B2, and α_2 phases in a Ti-Al-Mo alloy.		1618-1629A
Surface structure, Alloying effects		
Effects of nickel on the sintering behavior of Fe-Ni compacts made from composite and elemental powders.		203-211B
Surface structure, Deformation effects		
Quantitative characterization of the surface topography of rolled sheets by laser scanning microscopy and Fourier transformation.		2338-2346A
Surface structure, Environmental effects		
On the transition of fatigue crack growth from stage I to stage II in a corrosive environment.		471-476A
Surface structure, Heating effects		
Surface morphology and compound layer pores of plasma nitrocarburized low carbon steel.		135-143A
Transition between internal and external nitridation of Ni-Ti alloys.		1606-1617A
Surface structure, Temperature effects		
Overview of geometric effects on coarsening of mushy zones.		557-567A
Surface temperature		
Heat-flow-based analysis of surface crack formation during the start-up of the direct chill casting process. I. Development of the inverse heat-transfer model.		119-127B
Surface tension, Alloying effects		
Influence of phosphorus addition on the surface tension of liquid iron and segregation of phosphorus on the surface of Fe-P alloy.		71-79B
Surface tension, Pressure effects		
The influence of oxygen pressure and P ₂ O ₅ on the surface tension of liquid iron oxide at 1435°C.		139-141B
Surface tension, Temperature effects		
Applicability of Butler's equation in interpreting the thermodynamic behavior of surfaces and adsorption in Fe-S-O melts.		241-253B
Surgical implants, Materials selection		
Fracture characteristics, microstructure, and tissue reaction of Ti-5Al-2.5Fe for orthopedic surgery.		3925-3935A
Synthesis		
Symposium on In Situ Reactions for Synthesis of Composites, Ceramics, and Intermetallics. II.		
Modeling of sequential reactions during microalloyed synthesis.		961-972A
Formation of structural intermetallics by reactive metal penetration of titanium and nickel oxides and aluminates.		2100-2104A
Tantalum, Alloying elements		
The breakdown of single-crystal solidification in high refractory nickel-base alloys.		1081-1094A

- Tantalum, Crystal growth**
Aspects of dynamic recrystallization in shaped charge and explosively formed projectile devices. 1773-1778A
- Tantalum, Heat treatment**
Improved oxidation resistance of group VB refractory metals by Al³⁺ ion implantation. 491-500B
- Tantalum, Structural hardening**
Constitutive behavior of tantalum and tantalum-tungsten alloys. 2994-3006A
- Tantalum base alloys, Powder technology**
Thermally assisted and mechanically driven solid-state reactions for formation of amorphous Al₃₃Ta₆₇ alloy powders. 3267-3278A
- Tantalum base alloys, Structural hardening**
Constitutive behavior of tantalum and tantalum-tungsten alloys. 2994-3006A
- Tellurium, Alloying additive**
Effects of oxygen, selenium, and tellurium on the rate of nitrogen dissolution in molten iron. 846-851B
- Tellurium, Dopants**
Hydrogen effects on directional solidification of tellurium-doped cast irons. 496-498A
- Temperature**
Influence of temperature transients on the hot workability of a two-phase gamma titanium aluminide alloy. 1933-1950A
Mathematical modeling of the extrusion of 6061/Al₂O₃/20p composite. 4095-4111A
- Temperature distribution**
Flow and thermal behavior of the top surface flux/powder layers in continuous casting molds. 672-685B
- Tempering**
A strain-based fracture model for stress corrosion cracking of low-alloy steels. 291-304A
Mössbauer spectroscopy study of the aging and tempering of high nitrogen quenched Fe-N alloys: kinetics of formation of Fe₁₆N₂ nitride by interstitial ordering in martensite. 2160-2177A
Microstructural basis for the effect of chromium on the strength and toughness of AF1410-based high performance steels. 2510-2517A
Atmospheric stress corrosion cracking of a superplastic 7475 aluminum alloy. 2617-2627A
M₂C precipitates in isothermal tempering of high Co-Ni secondary hardening steel. 3466-3472A
- Tensile properties, Heating effects**
The dependence of complex alloyed steel properties on quenching and tempering conditions. 2852-2858A
- Tensile properties, Microstructural effects**
Microstructure and tensile behavior of nitrogen-alloyed, dual-phase stainless steels. 1845-1859A
A comparison of fracture behavior of low alloy steel with different sizes of carbide particles. 1909-1917A
- Tensile strength**
Thermal stability of SiC-SCS-6 fiber-reinforced IM1834 alloys. 1403-1405A
Characterization and mechanical properties of ultrahigh boron steels produced by powder metallurgy. 1861-1867A
Tensile ductility and fracture of superplastic aluminum-SiC composites under thermal cycling conditions. 2837-2842A
Microstructure and tensile properties of compacted, mechanically alloyed, nanocrystalline Fe-Al. 3126-3134A
Analysis of the stress-strain curves of a modified 9Cr-1Mo steel by the Voce equation. 3340-3343A
The balance of mechanical and environmental properties of a multielement niobium-niobium silicide-based in situ composite. 3801-3808A
- Tensile strength, Alloying effects**
Effect of strontium modification on near-threshold fatigue crack growth in an Al-Si-Cu die cast alloy. 1293-1302A
Tension characteristics of notched specimens for Al-Li-Cu-Zr alloys sheets with various cerium contents. 3089-3094A
- Tensile strength, Cooling effects**
The quench sensitivity of cast Al-7 wt.% Si-0.4 wt.% Mg alloy. 3983-3991A
- Tensile strength, Corrosion effects**
Effects of the alumina scale on the room-temperature tensile behavior of preoxidized MA 956. 3809-3816A
- Tensile strength, Heating effects**
Influence of long term annealing on tensile properties and fracture of near- α titanium alloy Ti-6Al-2.75Sn-4Zr-0.4Mo-0.45Si. 1700-1708A
Microstructural basis for the effect of chromium on the strength and toughness of AF1410-based high performance steels. 2510-2517A
Low quench sensitivity of superplastic 8090 Al-Li thin sheets. 2923-2933A
- Tensile strength, Impurity effects**
Microsegregation of oxygen in Zr-2.5Nb alloy materials. 431-440A
- Tensile strength, Microstructural effects**
Pearlite in ultrahigh carbon steels: heat treatments and mechanical properties. 111-118A
- The embrittlement and de-embrittlement of grain boundaries in an Fe-Mn-Ni alloy due to grain boundary segregation of manganese. 1015-1020A
- Tensile properties of mechanically alloyed/milled ODS-Ni-based alloys.** 1371-1377A
- Effect of bainite transformation and retained austenite on mechanical properties of austempered spheroidal graphite cast steel.** 1585-1594A
- Microstructural aspects of the dissolution and melting of Al₂Cu phase in Al-Si alloys during solution heat treatment.** 1785-1798A
- Fracture characteristics, microstructure, and tissue reaction of Ti-5Al-2.5Fe for orthopedic surgery.** 3925-3935A
- Tensile strength, Pressure effects**
Synthesis of RuAl by reactive powder processing. 3688-3699A
- Tensile strength, Stress effects**
Temperature and strain-rate effects on low-cycle fatigue behavior of alloy 800H. 255-267A
Rafting in superalloys. 513-530A
Effect of thermal cycling on the mechanical properties of 350 grade maraging steel. 757-761A
Effect of uniaxial stress on coarsening of precipitate clusters. 1460-1475A
- Tensile strength, Temperature effects**
Observations of secondary carbide precipitation and its relation to high-temperature flow and fracture in HT-9 stainless steel. 467-469A
- Tensile stress**
Subcritical crack growth at bimaterial interfaces. I. Flexural peel technique. 205-211A
Subcritical crack growth at bimaterial interfaces. III. Shear-enhanced fatigue crack growth resistance at polymer/metal interface. 221-228A
Mechanisms of high-temperature fatigue failure in alloy 800H. 851-861A
The Bauschinger effect in a SiC/Al composite. 995-1001A
- Tension tests**
Control of superplastic deformation rate during uniaxial tensile tests. 3030-3042A
Simulation of the hot-tension test under cavitating conditions. 3112-3119A
Effect of postweld treatment on the fatigue crack growth rate of electron-beam-welded AISI 4130 steel. 3162-3169A
The use of microstructural gradients in hot gas-pressure forming of Zn-Al sheet. 3250-3258A
An evaluation of the creep properties of two Al-Si alloys produced by rapid solidification processing. 3871-3879A
- Tension tests, Development**
Measurement of friction under sheet forming conditions. 3971-3981A
- Ternary systems**
Discussion of "derivation and consistency of the partial functions of the ternary system involving interaction coefficients" and author's reply. 325-327B
- Ternary systems, Diffusion**
Thermodynamic and kinetic study of diffusion paths in the system Cu-Fe-Ni. 2229-2238A
- Ternary systems, Mechanical properties**
Mechanical behavior of the in situ composite alloys in the Al-Ni-Ti system near the L₁₂ phase field. 71-79A
Mechanical properties of Ru-Ni-Al alloys. 1395-1400A
- Ternary systems, Phases (state of matter)**
Evolution of microstructures in the nickel modified titanium tri-aluminides near the L₁₂ phase field. 5-17A
M₂₃C₆ carbide equilibria in the Fe-Cr-C system. 701-704B
Critical evaluation and optimization of the thermodynamic properties of liquid tin solutions. 808-826B
Thermodynamic investigations of the ternary Au-Sn-Zn system. 921-927B
A thermodynamic evaluation of the Ti-Mo-C system. 955-966B
Experimental study of the phase equilibria in the Fe-Mn-Al system. 2429-2435A
Thermodynamic activities and phase boundaries for the alloys of the Ni₃Al-Ni₃Ti pseudobinary section in the Ni-Al-Ti system. 2673-2677A
Internal sulfide precipitation in low Cr-Fe alloys. 3192-3202A
Solidification of undercooled Fe-Cr-Ni alloys. II. Microstructural evolution. 3226-3240A
Thermodynamic activities and partial enthalpies of mixing in the solid solution of Fe in Ni₃Al. 3569-3575A
Martensitic transformations in NiMnAl β phase alloys. 4153-4162A
- Ternary systems, Reactions (chemical)**
Chemical potentials of components of the system CaO+P₂O₅+Fe₂O₃ at 1673K. 595-603B
- Ternary systems, Surface properties**
Applicability of Butler's equation in interpreting the thermodynamic behavior of surfaces and adsorption in Fe-S-O melts. 241-253B
- Texture**
Modeling texture change during the static recrystallization of interstitial free steels. 155-164A

- Recrystallization in oxide-dispersion strengthened mechanically alloyed sheet steel. 1963-1978A
- The role of coincident site lattice boundaries during selective growth in interstitial-free steels. 2178-2186A
- An investigation by interactive electron backscatter pattern analysis of processing and superplasticity in an aluminum-magnesium alloy. 2252-2262A
- Orientation selective recrystallization of nonoriented electrical steels. 2347-2358A
- Nanoscale brass/steel multilayer composites produced by cold rolling. 2383-2385A
- Texture, Deformation effects**
- Experimental investigation of the transformation texture in hot-rolled ferritic stainless steel using single orientation determination. 49-57A
- Non-Schmid effects on the behavior of polycrystals, with applications to Ni_3Al . 81-99A
- Aspects of dynamic recrystallization in shaped charge and explosively formed projectile devices. 1773-1778A
- Texture, Stress effects**
- Plastic anisotropy of sheets with continuously varying anisotropic parameters and flow stress. 317-326A
- Crystallographic preferred orientation induced by cyclic rolling contact loading. 3445-3465A
- Thermal conductivity**
- Solidification of particle-reinforced metal-matrix composites. Modeling of ingot distortions during direct chill casting of aluminum alloys. 663-671B
3214-3225A
- Thermal conductivity, Temperature effects**
- Heat-flow-based analysis of surface crack formation during the start-up of the direct chill casting process. II. Experimental study of an AA5182 rolling ingot. 129-137B
- Thermal cycling**
- The effect of thermal cycle on the microstructural development of a powder metallurgy superalloy braze material. 145-153A
- Thermal expansion**
- Microstructure and properties of $\text{Al}_2\text{O}_3\text{-Al}(\text{Si})$ and $\text{Al}_2\text{O}_3\text{-Al}(\text{Si})\text{-Si}$ composites formed by in situ reaction of aluminum with aluminosilicate ceramics. 2122-2129A
- The balance of mechanical and environmental properties of a multielement niobium-niobium silicide-based in situ composite. 3801-3808A
- Thermal expansion, Microstructural effects**
- Thermal expansion of metals reinforced with ceramic particles and microcellular foams. 3700-3717A
- Thermal fatigue, Temperature effects**
- Isothermal fatigue of an aluminide-coated single-crystal superalloy. II. Effects of brittle precracking. 363-369A
- Thermal stability**
- Thermal stability of SiC-SCS-6 fiber-reinforced IMI834 alloys. 1403-1405A
- Thermal stability, Cooling effects**
- Rapid solidification processing of a Mg-Li-Si-Ag alloy. 1363-1370A
- Thermal stresses**
- Effect of carbide precipitation on the creep behavior of alloy 800HT in the temperature range 700-900°C. 747-756A
- Effect of thermal cycling on the mechanical properties of 350 grade maraging steel. 757-761A
- Thermal residual stresses in functionally graded and layered 6061 Al/SiC materials. 3241-3249A
- Thermit brazing**
- A model for coupled growth of reaction layers in reactive brazing of ZrO_2 -toughened Al_2O_3 . 3630-3638A
- Thermochemistry**
- Thermochemistry of the Ni-Hf system—intermetallic phases. 3576-3590A
- Thermocouples**
- Analysis of shell thickness irregularity in continuously cast middle carbon steel slabs using mold thermocouple data. 1045-1056B
- Thermodynamics**
- Vacuum evaporation of KCl-NaCl salts. I. Thermodynamic modeling of vapor pressures of solid and liquid solutions. Applicability of Butler's equation in interpreting the thermodynamic behavior of surfaces and adsorption in Fe-S-O melts. Discussion of "derivation and consistency of the partial functions of the ternary system involving interaction coefficients" and author's reply. 325-327B
- Kinetics of sulfation of chalcopyrite with steam and oxygen in the presence of ferric oxide. 465-474B
- Overview of geometric effects on coarsening of mushy zones. Thermodynamics of sulfur in the BaO-MnO-SiO₂ flux system. Discussion of "Representation of mixed reactive gases on free energy (Elliingham-Richardson) diagrams" and reply. 557-567A
652-657B
- Thermodynamic investigations of the ternary Au-Sn-Zn system. 693-694B
- Thermodynamics of phosphorus in molten silicon. 921-927B
937-941B
- Activities in $\text{CaO-SiO}_2\text{-Al}_2\text{O}_3$ slags and deoxidation equilibria of silicon and aluminum. 943-953B
- A thermodynamic evaluation of the Ti-Mo-C system. 955-966B
- Thermodynamics of calcium and oxygen in molten titanium and titanium-aluminum alloy. 967-972B
- Thermodynamic properties of complex oxides in the Sm-Ba-Cu-O system. 973-978B
- Thermodynamics and long-range order of nitrogen in $\gamma\text{-Fe}_4\text{N}_x$. 1055-1061A
- Crystal shapes and phase equilibria: a common mathematical basis. 1431-1440A
- Thermodynamic and kinetic study of diffusion paths in the system Cu-Fe-Ni. 2229-2238A
- Thermodynamic studies and the phase diagram of the Li-Mg system. 2419-2428A
- Thermodynamic activities and phase boundaries for the alloys of the $\text{Ni}_3\text{Al-Ni}_3\text{Ti}$ pseudobinary section in the Ni-Al-Ti system. 2673-2677A
- An experimental study and thermodynamic calculations of phase equilibria in the Fe-Mo-C-N system. 2869-2880A
- A thermodynamic evaluation of the nickel-silicon system. 2897-2903A
- Kinetics of phase evolution of Zn-Fe intermetallics. 2904-2910A
- Incipient chemical instabilities of nanophase Fe-Cu alloys prepared by mechanical alloying. 2934-2946A
- An isothermal section at 550°C in the Al-rich corner of the Al-Fe-Mn-Si system. 3357-3361A
- Thermodynamic activities and partial enthalpies of mixing in the solid solution of Fe in Ni_3Al . 3569-3575A
- Thermochemistry of the Ni-Hf system—intermetallic phases. Thermodynamic assessment of the Nb-N system. 3576-3590A
3591-3600A
- Thermoelastic properties**
- Modeling of ingot distortions during direct chill casting of aluminum alloys. 3214-3225A
- Thermoelastic properties, Cooling effects**
- Thermomechanics of the cooling stage in casting processes: three-dimensional finite element analysis and experimental validation. 81-99B
- Thermoelastic properties, Temperature effects**
- Observations of secondary carbide precipitation and its relation to high-temperature flow and fracture in HT-9 stainless steel. 467-469A
- Thermogravimetric analysis**
- A study of the thermal decomposition of BaCO_3 . High-temperature oxidation of Ti_3Al -based titanium aluminides in oxygen. 409-416B
- Effect of nitrogen on the oxidation behavior of Ti_3Al -based intermetallic alloys. 3993-4002A
4003-4010A
- Thermomechanical treatment**
- The influence of niobium supersaturation in austenite on the static recrystallization behavior of low carbon microalloyed steels. 951-960A
- An investigation by interactive electron backscatter pattern analysis of processing and superplasticity in an aluminum-magnesium alloy. 2252-2262A
- Effects of alloy modification and thermomechanical processing on recrystallization of Al-Mg-Mn alloys. 2947-2957A
- Effect of thermomechanical treatments on the room-temperature mechanical behavior of iron aluminide Fe_3Al . 2985-2993A
- Nonuniform distribution of carbonitride particles and its effect on prior austenite grain size in the simulated coarse-grained heat-affected zone of thermomechanical control-processed steels. 4031-4038A
- Thickness**
- Analysis of shell thickness irregularity in continuously cast middle carbon steel slabs using mold thermocouple data. 1045-1056B
- Thin films**
- Crystallization of amorphous phase in sputter-deposited Ti-Al alloy thin films. 2047-2050A
- Thin films, Microstructure**
- Morphological instabilities of lamellar eutectics. Microstructural stability on aging of an $\alpha+\beta$ titanium alloy: Ti-6Al-1.6Zr-3.3Mo-0.30Si. 635-656A
1167-1173A
- Tin, Alloying elements**
- Precipitation in lead-calcium alloys containing tin. 1668-1675A
- Tin, Binary systems**
- Critical evaluation and optimization of the thermodynamic properties of liquid tin solutions. 808-826B
- Tin, Ternary systems**
- Thermodynamic investigations of the ternary Au-Sn-Zn system. 921-927B
- Tin base alloys, Phases (state of matter)**
- Overview of geometric effects on coarsening of mushy zones. 557-567A
- Titanium, Alloying additive**
- The effects on fracture toughness of ductile-phase composition and morphology in Nb-Cr-Ti and Nb-Si in situ composites. 3007-3018A

Titanium, Alloying elements

- Influence of microalloying on the corrosion resistance of steel in saturated calcium hydroxide.
Influence of titanium and carbon contents on the hydrogen trapping of microalloyed steels.

1693-1699A

3773-3780A

Titanium, Binary systems

- Critical evaluation and optimization of the thermodynamic properties of liquid tin solutions.
Mechanistic processes influencing shock chemistry in powder mixtures of the Ti-Si, Ti-Al, and Ti-B systems.

808-826B

1761-1771A

Titanium, Chemical analysis

- Formation of aluminum-silicon alloys from feldspars—determination of silicon, light, and heavy elements in silumin by scanning electron microscopy.

604-609B

Titanium, Coatings

- Characterization of titanium thin films prepared by bias assisted magnetron sputtering.

1057-1060B

Titanium, Composite materials

- Communication: On the in situ formation of TiC and Ti₂C reinforcements in combustion-assisted synthesis of titanium matrix composites.
Interface characterization of ceramic fiber-reinforced titanium alloy composites manufactured by infrared processing.

237-240A

1379-1394A

Titanium, Crystal growth

- An analysis of static recrystallization during continuous, rapid heat treatment.

2051-2053A

Titanium, Diffusion

- Pressure dependence of anomalous diffusion of zirconium in β -titanium.

1807-1814A

Titanium, Extraction

- Preoxidation and hydrogen reduction of ilmenite in a fluidized bed reactor.

731-738B

Titanium, Mechanical properties

- Temperature dependence of the rate sensitivity and its effect on the activation energy for high-temperature flow.
Plastic zone and pileup around large indentations.

3346-3348A

3793-3800A

Titanium, Phases (state of matter)

- Stable and metastable ordered phases in microcrystalline alloys Ni (Fe, Mn, Ti).

2045-2046A

Titanium, Reactions (chemical)

- Thermodynamics of calcium and oxygen in molten titanium and titanium-aluminum alloy.

967-972B

Titanium, Ternary systems

- Evolution of microstructures in the nickel modified titanium tri-aluminides near the L₁₂ phase field.
Mechanical behavior of the in situ composite alloys in the Al-Ni-Ti system near the L₁₂ phase field.
A thermodynamic evaluation of the Ti-Mo-C system.
Thermodynamic activities and phase boundaries for the alloys of the Ni₃Al-Ni₃Ti pseudobinary section in the Ni-Al-Ti system.

5-17A

71-79A

955-966B

2673-2677A

Titanium, Welding

- Analysis of heat affected zone phase transformations using in situ spatially resolved x-ray diffraction with synchrotron radiation.

775-783A

Titanium base alloys

- Effect of nitrogen on the oxidation behavior of Ti₃Al-based intermetallic alloys.

4003-4010A

Titanium base alloys, Chemical analysis

- Determination of hydrogen in titanium alloys by cold neutron prompt gamma activation analysis.

3682-3687A

Titanium base alloys, Composite materials

- Liquid state infrared processing of SCS-6/Ti-6Al-4V composites.
Thermal stability of SiC-SCS-6 fiber-reinforced IMI834 alloys.
An experimental and theoretical investigation of the rapid consolidation of continuously reinforced, metal-matrix composites.
Multiple matrix cracking in a fiber-reinforced titanium matrix composite under high-cycle fatigue.
Interface effects on the micromechanical response of a transversely loaded single fiber SCS-6/Ti-6Al-4V composite.
Observation of short fatigue crack-growth process in SiC-fiber-reinforced Ti-15-3 alloy composite.
Prediction of creep-rupture life of unidirectional titanium matrix composites subjected to transverse loading.
Infrared transient-liquid-phase joining of SCS-6/ β 21S titanium matrix composite.
Creep deformation and damage in a continuous fiber-reinforced Ti-6Al-4V composite.

527-532B

1403-1405A

1709-1720A

1899-1907A

2035-2043A

2843-2851A

3074-3080A

4011-4018A

4193-4204A

Titanium base alloys, Forming

- Reply: Dynamic materials model. Basis and principles.

235-236A

Titanium base alloys, Heat treatment

- Influence of long term annealing on tensile properties and fracture of near- α titanium alloy Ti-6Al-2.75Sn-4Zr-0.4Mo-0.45Si.

1700-1708A

Titanium base alloys, Mechanical properties

- Effect of strain rate and temperature on the flow stress of β -phase titanium-hydrogen alloys.
High-temperature deformation processing of Ti-24Al-20Nb.
The influence of stress triaxiality on the damage mechanisms in an equiaxed α/β Ti-6Al-4V alloy.
High-temperature deformation and failure of an orthorhombic titanium aluminide sheet material.
The behavior of internal markers in Ti-6Al-4V deformed in superplastic tension.
Plastic zone and pileup around large indentations.
Notch fracture in γ -titanium aluminides.
Fracture characteristics, microstructure, and tissue reaction of Ti-5Al-2.5Fe for orthopedic surgery.
An analysis of the flow stress of a two-phase alloy system, Ti-6Al-4V.
Elastic moduli of titanium-hydrogen alloys in the temperature range 20°C to 1100°C.

1303-1312A

2593-2604A

3043-3058A

3675-3681A

3747-3748A

3793-3800A

3903-3912A

3925-3935A

3957-3962A

3963-3970A

Titanium base alloys, Microstructure

- Microstructural stability on aging of an $\alpha+\beta$ titanium alloy: Ti-6Al-1.6Zr-3.3Mo-0.30Si.
Crystallography of grain boundary α precipitates in a β titanium alloy.
The mechanism of formation of a fine duplex microstructure in Ti-48Al-2Mn-2Nb alloys.
Microstructural development of a gas-atomized and hot-pressed super- α_2 alloy.

1167-1173A

1630-1641A

1655-1667A

2221-2228A

Titanium base alloys, Oxidation

- High-temperature oxidation of Ti₃Al-based titanium aluminides in oxygen.

3993-4002A

Titanium base alloys, Phase transformations

- A high-resolution transmission electron microscopy study of the precipitation process in a dilute Ti-N alloy.
Effect of stress state on the stress-induced martensitic transformation in polycrystalline Ni-Ti alloy.

2966-2977A

3066-3073A

Titanium base alloys, Powder technology

- Microstructure and phase relations in a powder-processed Ti-22Al-12Nb alloy.

1121-1126A

Titanium base alloys, Reactions (chemical)

- Thermodynamics of calcium and oxygen in molten titanium and titanium-aluminum alloy.

967-972B

Titanium base alloys, Structural hardening

- Effect of phase composition and hydrogen level on the deformation behavior of titanium-hydrogen alloys.
Dynamic strain aging and hydrogen-induced softening in alpha titanium.

1869-1876A

1877-1887A

Titanium base alloys, Surface finishing

- Investigation of the temperature field developed by a spinning beam in laser processing.

4039-4047A

Titanium carbide, Composite materials

- NiTi and NiTi-TiC composites. II. Compressive mechanical properties.
NiTi and NiTi-TiC composites. III. Shape-memory recovery.
Communication: On the in situ formation of TiC and Ti₂C reinforcements in combustion-assisted synthesis of titanium matrix composites.
Analysis of damping in particle-reinforced superplastic zinc composites.
NiTi and NiTi-TiC composites. IV. Neutron diffraction study of twinning and shape-memory recovery.
Influence of reinforcement volume fraction and size on the microstructure and abrasion wear resistance of hot isostatically pressed white iron matrix composites.
Influence of matrix structure on the abrasion wear resistance and toughness of a hot isostatically pressed white iron matrix composites.

183-191A

193-203A

237-240A

2565-2573A

2820-2836A

4171-4181A

4183-4191A

Titanium compounds, Alloying elements

- Notch fracture in γ -titanium aluminides.

3903-3912A

Titanium compounds, Coating

- The deposition of aluminide and silicide castings on γ -TiAl using the halide-activated pack cementation method.

3761-3772A

Titanium compounds, Composite materials

- NiTi and NiTi-TiC composites. II. Compressive mechanical properties.
NiTi and NiTi-TiC composites. III. Shape-memory recovery.
Formation of structural intermetallics by reactive metal penetration of titanium and nickel oxides and aluminates.
Investigation of the reaction zone between TiAl and molybdenum.

183-191A

193-203A

2100-2104A

2285-2292A

Titanium compounds, Crystal growth

- Crystallization of amorphous phase in sputter-deposited Ti-Al alloy thin films.

2047-2050A

Titanium compounds, Mechanical properties

- Effect of creep strain on microstructural stability and creep resistance of a TiAl/Ti₃Al lamellar alloy. 127-134A
- Influence of temperature transients on the hot workability of a two-phase gamma titanium aluminide alloy. 1933-1950A
- High-temperature low-cycle fatigue of a gamma titanium aluminide alloy Ti-46Al-2Nb-2Cr. 2239-2251A
- High-temperature deformation processing of Ti-24Al-20Nb. 2593-2604A
- High-temperature deformation and failure of an orthorhombic titanium aluminide sheet material. 3675-3681A

Titanium compounds, Oxidation

- High-temperature oxidation of Ti₃Al-based titanium aluminides in oxygen. 3993-4002A
- Effect of nitrogen on the oxidation behavior of Ti₃Al-based intermetallic alloys. 4003-4010A

Titanium compounds, Phase transformations

- NiTi and NiTi-TiC composites. IV. Neutron diffraction study of twinning and shape-memory recovery. 2820-2836A
- The effect of substrate constraint on the martensitic transformation of Ni-Ti thin films. 2858-2860A

Titanium compounds, Powder technology

- Mechanistic processes influencing shock chemistry in powder mixtures of the Ti-Si, Ti-Al, and Ti-B systems. 1761-1771A
- Pressure-assisted reactive synthesis of titanium aluminides from dense 50Al-50Ti elemental powder blends. 2130-2139A

Titanium compounds, Reactions (chemical)

- Thermodynamics of calcium and oxygen in molten titanium and titanium-aluminum alloy. 967-972B

Titanium nitride, Coatings

- Active wear and failure mechanisms of titanium nitride-coated high speed steel and titanium nitride-coated cemented carbide tools when machining powder metallurgically made stainless steels. 2796-2808A

Tool life, Coating effects

- Active wear and failure mechanisms of titanium nitride-coated high speed steel and titanium nitride-coated cemented carbide tools when machining powder metallurgically made stainless steels. 2796-2808A

Tool steels, Coating

- Wear-resistant coatings produced by shock-wave compaction of powders. 2297-2304A

Topography

- Quantitative characterization of the surface topography of rolled sheets by laser scanning microscopy and Fourier transformation. 2338-2346A

Toughness

- Failure characteristics of 6061/Al₂O₃/15_p and 2014/Al₂O₃/15_p composites as a function of loading rate. 3095-3107A

Toughness, Composition effects

- Mechanical properties of Ru-Ni-Al alloys. 1395-1400A

Toughness, Heating effects

- Effect of holding time in the ($\alpha+\gamma$) temperature range on toughness of specially austempered ductile iron. 1979-1989A

Toughness, Microstructural effects

- Mechanical behavior and properties of mechanically alloyed aluminum alloys. 737-745A

Toxicology

- The use of blast furnace slag and derived materials in the vitrification of electric arc furnace dust. 379-384B

Transgranular corrosion, Stress effects

- Discussion of "a fully plastic microcracking model for transgranular stress corrosion cracking in planar slip materials" and reply. 819-821A

Transgranular fracture

- Microstructure and tensile behavior of nitrogen-alloyed, dual-phase stainless steels. 1845-1859A
- The influence of stress triaxiality on the damage mechanisms in an equiaxed α/β Ti-6Al-4V alloy. 3043-3058A

Transgranular fracture, Heating effects

- A strain-based fracture model for stress corrosion cracking of low-alloy steels. 291-304A

Transition metals, Alloying additive

- Effect of alloying elements on martensitic transformation in the binary NiAl(B) phase alloys. 2445-2453A

Transmission electron microscopy

- Real time x-ray transmission microscopy of solidifying Al-In alloys. 801-808A
- Characterization of titanium thin films prepared by bias assisted magnetron sputtering. 1057-1060B
- Transmission electron microscopy study on the cross-sectional microstructure of an ion-nitriding layer. 1347-1352A
- The formation mechanism(s), morphology, and crystallography of ferrite sideplates. 1517-1532A

- The relationship between microstructural and plastic instability in Al-4.0 wt.% Cu alloy. 2916-2922A

A high-resolution transmission electron microscopy study of the precipitation process in a dilute Ti-N alloy.

- 2966-2977A

Thermally assisted and mechanically driven solid-state reactions for formation of amorphous Al₃₃Ta₆₇ alloy powders.

- 3267-3278A

- High-resolution transmission electron microscopy investigation of the face-centered cubic/hexagonal close-packed martensite transformation in Co-31.8 wt.% Ni alloy. I. Plate interfaces and growth ledges. 3362-3370A

- High-resolution transmission electron microscopy investigation of the face-centered cubic/hexagonal close-packed martensite transformation in Co-31.8 wt.% Ni alloy. II. Plate intersections, extended defects, and nucleation mechanisms. 3371-3380A

- Effect of aging on shape memory behavior of Ti-51.3 at.% Ni thin films. 3753-3759A

- Influence of titanium and carbon contents on the hydrogen trapping of microalloyed steels. 3773-3780A

- Creep lifetime prediction of oxide-dispersion-strengthened nickel-base superalloys: a micromechanically based approach. 3861-3870A

- Elevated temperature deformation behavior of a dispersion-strengthened Al-Fe, V, Si alloy. 3913-3923A

- Hydrogen-induced cleavage fracture of Fe₃Al-based intermetallics. 3949-3956A

- The quench sensitivity of cast Al-7 wt.% Si-0.4 wt.% Mg alloy. 3983-3991A

- Microstructural features of friction welded MA 956 superalloy material. 4019-4029A

- Nonuniform distribution of carbonitride particles and its effect on prior austenite grain size in the simulated coarse-grained heat-affected zone of thermomechanical control-processed steels. 4031-4038A

- Martensitic transformations in NiMnAl β phase alloys. 4153-4162A

Tribology

- Ni₃Al intermetallic particles as wear-resistant reinforcement for Al-base composites processed by powder metallurgy. 3259-3266A

Tribology, Radiation effects

- Simultaneous plasma treatment for carburizing and carbonitriding using hollow cathode discharge. 401-405A

Tundishes

- Intermixing model of continuous casting during a grade transition. 617-632B

- Mathematical modeling of tundish operation and flow control to reduce transition slabs. 745-756B

Tungsten, Alloying elements

- The breakdown of single-crystal solidification in high refractory nickel-base alloys. 1081-1094A

- Constitutive behavior of tantalum and tantalum-tungsten alloys. 2994-3006A

Tungsten, Powder technology

- Theoretical modeling of densification during activated solid-state sintering. 441-450A

Tungsten, Solubility

- Solid-state contributions to densification during liquid-phase sintering. 901-909B

Tungsten, Structural hardening

- Van der Waals approximation for potassium bubbles in tungsten. 987-992B

Tungsten base alloys, Powder technology

- Solid-state contributions to densification during liquid-phase sintering. 901-909B

- The effect of Mo addition on the liquid-phase sintering of W heavy alloy. 3120-3125A

Tungsten carbide, Synthesis

- Synthesis of full-density nanocrystalline tungsten carbide by reduction of tungstic oxide at room temperature. 4210-4213A

Turbine blades, Microstructure

- Prediction of grain structures in various solidification processes. 695-705A

Turbine blades, Service life

- Creep lifetime prediction of oxide-dispersion-strengthened nickel-base superalloys: a micromechanically based approach. 3861-3870A

Turbulence

- Experimental study of splash generation in a flash smelting furnace. 633-646B

- A unified representation of the two-phase plume characteristics in gas-stirred ladle systems. 704-708B

Twin roll casting

- Quantitative characterization of the surface topography of rolled sheets by laser scanning microscopy and Fourier transformation. 2338-2346A

Twinning NiTi and NiTi-TiC composites. II. Compressive mechanical properties. An optical method for determining the surface orientation of crystals.	183-191A 2057-2061A		Void, Stress effects The influence of stress triaxiality on the damage mechanisms in an equiaxed α/β Ti-6Al-4V alloy.	3043-3058A
Twinning, Cooling effects The role of grain corners in nucleation.	480-483A		Warm working Optimization of cold and warm workability in 304 stainless steel using instability maps.	119-126A
Twinning, Deformation effects The x-ray diffraction study of deformation in the composite matrix of Al-Mg-Zn and SiC.	503-505A		Waste disposal Oxidation-reduction equilibrium of $\text{Cu}^{2+}/\text{Cu}^+$ in binary alkaline sulfate melts. Vacuum evaporation of KCl-NaCl salts. II. Vaporization-rate model and experimental results. Preparation of glass-forming materials from granulated blast furnace slag. Microstructure and phase identification in type 304 stainless steel-zirconium alloys.	385-392B 433-443B 801-807B 2151-2159A
Twinning, Stress effects Predicting the orientation-dependent stress-induced transformation and detwinning response of shape memory alloy single crystals.	269-279A		Wastes Eco-techno-economic synthesis of process routes for the production of zinc using combinatorial optimization.	1031-1044B
Ultrasonic testing Elastic moduli of titanium-hydrogen alloys in the temperature range 20°C to 1100°C.	3963-3970A		Water A water model study of the flow asymmetry inside a continuous slab casting mold.	757-764B
Vacuum refining Thermodynamics of phosphorus in molten silicon.	937-941B		Water cooling The improved microstructures and properties of 7075 alloys produced by a water-cooling centrifugal casting method.	1951-1962A
Vanadium, Alloying additive The effect of metallic elements on the crystallization behavior of amorphous Fe-Si-B alloys.	3424-3430A		Water quenching A process model for on-line quenching of aluminum extrusions.	501-508B
Vanadium, Alloying elements Influence of microalloying on the corrosion resistance of steel in saturated calcium hydroxide.	1693-1699A		Wear particles Ni_3Al intermetallic particles as wear-resistant reinforcement for Al-base composites processed by powder metallurgy.	3259-3266A
Vanadium, Heat treatment Improved oxidation resistance of group VB refractory metals by Al^+ ion implantation.	491-500B		Wear rate High-temperature wear and deformation processes in metal matrix composites.	3135-3148A
Vapor pressure Vacuum evaporation of KCl-NaCl salts. I. Thermodynamic modeling of vapor pressures of solid and liquid solutions.	141-146B		Wear rate, Coating effects Active wear and failure mechanisms of titanium nitride-coated high speed steel and titanium nitride-coated cemented carbide tools when machining powder metallurgically made stainless steels.	2796-2808A
Vaporizing, Cooling effects Vacuum evaporation of KCl-NaCl salts. II. Vaporization-rate model and experimental results.	433-443B		Wear rate, Composition effects Characterization of the wear response of a modified zinc-based alloy vis-à-vis a conventional zinc-based alloy and a bearing bronze at a high sliding speed.	3513-3523A
Velocity Increased ductility in high velocity electromagnetic ring expansion.	1837-1844A		Wear resistance Corrosive wear of SiC whisker- and particulate-reinforced 6061 aluminum alloy composites. High-temperature wear and deformation processes in metal matrix composites. The wear behavior between hardfacing materials. Wear and friction behavior of metal impregnated microporous carbon composites.	2653-2662A 3135-3148A 3639-3648A 3727-3738A
Vertical shaft furnaces An extended two-dimensional mathematical model of vertical ring furnaces.	297-304B		Wear resistance, Coating effects Wear-resistant coatings produced by shock-wave compaction of powders.	2297-2304A
Video Experimental study of splash generation in a flash smelting furnace.	633-646B		Wear resistance, Composition effects Wear behavior of aluminum-based metal matrix composites reinforced with a preform of aluminosilicate fiber.	2385-2389A
Viscoplasticity, Cooling effects Thermomechanics of the cooling stage in casting processes: three-dimensional finite element analysis and experimental validation.	81-99B		Wear resistance, Heating effects Mechanical properties and 95°C aging characteristics of zircon reinforced Zn-4Al-3Cu alloy.	809-818A
Viscoplasticity, Deformation effects Non-Schmid effects on the behavior of polycrystals, with applications to Ni_3Al . Communication: Discussion of "Modeling of dynamic materials behavior. A critical evaluation of the dissipator power cocontent approach".	81-99A 232-235A		Wear resistance, Microstructural effects Correlation of microstructure and fracture toughness in high-chromium white iron hardfacing alloys. Influence of reinforcement volume fraction and size on the microstructure and abrasion wear resistance of hot isostatically pressed white iron matrix composites. Influence of matrix structure on the abrasion wear resistance and toughness of a hot isostatically pressed white iron matrix composites.	3881-3891A 4171-4181A 4183-4191A
Viscosity Water model experiment on the liquid flow behavior in a bottom blown bath with top layer. Viscosity of superalloy 718 by the oscillating vessel technique. Effect of grain refinement on the fluidity of two commercial Al-Si foundry alloys.	35-41B 698-701B 2305-2313A		Wear tests High-temperature wear and deformation processes in metal matrix composites.	3135-3148A
Viscosity, Composition effects A statistical analysis of the effect of a mixture component on the rheology of alumina feedstocks.	399-408B		Weld cladding Ballistic impact behavior of multilayered armor plates processed by hardfacing. Solidification of an alloy 625 weld overlay. The wear behavior between hardfacing materials.	3335-3340A 3612-3620A 3639-3648A
Viscosity, Temperature effects Prediction of liquid metal viscosities using an adjustable hard sphere radial distribution curve.	29-34B		Weld defects Solidification of an alloy 625 weld overlay.	3612-3620A
Vitrification Preparation of glass-forming materials from granulated blast furnace slag.	801-807B		Weld deposited coatings, Crystal growth Solidification of an alloy 625 weld overlay.	3612-3620A
Void ratio, Deformation effects Microstructural evolution and superplastic deformation behavior of fine grain 5083Al.	3827-3839A		Weld deposited coatings, Mechanical properties The wear behavior between hardfacing materials.	3639-3648A
Vooids The measurement of hydrogen activities in molten copper using an oxide protonic conductor. Thermal expansion of metals reinforced with ceramic particles and microcellular foams.	929-935B 3700-3717A			
Vooids, Radiation effects Sputter-induced pits on {100} nickel surfaces. Theory of nucleation with cluster loss and injection: application to plastic deformation and irradiation.	981-993A 1441-1448A			

Weld metal, Microstructure		
Structural stability of super duplex stainless weld metals and its dependence on tungsten and copper.	2196-2208A	
Welded joints, Heat treatment		
Effect of homogenization heat treatment on the microstructure and heat affected zone microfissuring in welded cast alloy 718.	785-790A	
Welded joints, Mechanical properties		
Effect of multiaxial stresses on creep damage of 316 stainless steel weldments.	891-900A	
Microstructures relevant to brittle fracture initiation at the heat-affected zone of weldment of a low carbon steel.	2574-2582A	
Forming of tailor-welded blanks.	2605-2616A	
Effect of postweld treatment on the fatigue crack growth rate of electron-beam-welded AISI 4130 steel.	3162-3169A	
Welded joints, Microstructure		
Microstructural features of friction welded MA 956 superalloy material.	4019-4029A	
Welded joints, Phase transformations		
Analysis of heat affected zone phase transformations using in situ spatially resolved x-ray diffraction with synchrotron radiation.	775-783A	
Welded joints, Phases (state of matter)		
Phase stability and atom probe field ion microscopy of type 308 CRE stainless steel weld metal.	763-774A	
Wetting, Temperature effects		
Variation of contact angles with temperature and time in the Al-Al ₂ O ₃ system.	51-55B	
Whisker composites, Mechanical properties		
Growth behavior of microstructurally short cracks in the 6061 aluminum alloy with and without 22 vol.% SiC whiskers.	2013-2021A	
Corrosive wear of SiC whisker- and particulate-reinforced 6061 aluminum alloy composites.	2653-2662A	
White iron, Casting		
Hydrogen effects on directional solidification of tellurium-doped cast irons.	496-498A	
White iron, Claddings		
Ballistic impact behavior of multilayered armor plates processed by hardfacing.	3335-3340A	
White iron, Coatings		
Correlation of microstructure and fracture toughness in high-chromium white iron hardfacing alloys.	3881-3891A	
White iron, Composite materials		
Influence of reinforcement volume fraction and size on the microstructure and abrasion wear resistance of hot isostatically pressed white iron matrix composites.	4171-4181A	
Influence of matrix structure on the abrasion wear resistance and toughness of a hot isostatically pressed white iron matrix composites.	4183-4191A	
White iron, Crystal growth		
Directional solidification of white cast iron.	2328-2337A	
Widmanstätten structure		
Dense CoAl-based alloys with improved ductility: solid-state synthesis and microstructure control.	2140-2150A	
Fracture characteristics, microstructure, and tissue reaction of Ti-5Al-2.5Fe for orthopedic surgery.	3925-3935A	
Workability		
High-temperature deformation and failure of an orthorhombic titanium aluminide sheet material.	3675-3681A	
X ray analysis		
Radioscopic visualization of isothermal solidification of eutectic Ga-In alloy.	686-689B	
X ray diffraction		
Interdiffusion kinetics in oxide powder mixture using high temperature x-ray diffraction technique.	318-322B	
Analysis of heat affected zone phase transformations using in situ spatially resolved x-ray diffraction with synchrotron radiation.	775-783A	
Characterization of titanium thin films prepared by bias assisted magnetron sputtering.	1057-1060B	
Lattice misfits in four binary Ni-base γ/γ' alloys at ambient and elevated temperatures.	2888-2896A	
Incipient chemical instabilities of nanophase Fe-Cu alloys prepared by mechanical alloying.	2934-2946A	
Thermally assisted and mechanically driven solid-state reactions for formation of amorphous Al ₃₃ Ta ₆₇ alloy powders.	3267-3278A	
Discussion of "Effects of tensile stress on microstructural change of eutectoid Zn-Al alloy" and authors' reply.	3330-3335A	
Effect of aging on shape memory behavior of Ti-51.3 at.% Ni thin films.	3753-3759A	
High-temperature oxidation of Ti ₃ Al-based titanium aluminides in oxygen.	3993-4002A	
Martensitic transformations in NiMnAl β phase alloys.	4153-4162A	
X ray microscopy		
Real time x-ray transmission microscopy of solidifying Al-In alloys.		801-808A
Yield		
Preparation of fine copper powders from organic media by reaction with hydrogen under pressure. I. Experimental study.		577-584B
Thermodynamics of phosphorus in molten silicon.		937-941B
Yield strength		
Communication: On the in situ formation of TiC and Ti ₂ C reinforcements in combustion-assisted synthesis of titanium matrix composites.		237-240A
A study of typical yields of metals.		731-736A
An experimental and theoretical investigation of the rapid consolidation of continuously reinforced, metal-matrix composites.		1709-1720A
Bauschinger effect in Haynes 230 alloy: influence of strain rate and temperature.		1739-1748A
Deformation behavior of an Al-3.37 wt.% Li alloy.		2274-2284A
The effects on fracture toughness of ductile-phase composition and morphology in Nb-Cr-Ti and Nb-Si in situ composites.		3007-3018A
Plastic zone and pileup around large indentations.		3793-3800A
Notch fracture in γ -titanium aluminides.		3903-3912A
Yield strength, Alloying effects		
Effect of strain rate and temperature on the flow stress of β -phase titanium-hydrogen alloys.		1303-1312A
Effect of phase composition and hydrogen level on the deformation behavior of titanium-hydrogen alloys.		1869-1876A
Dynamic strain aging and hydrogen-induced softening in alpha titanium.		1877-1887A
Yield strength, Composition effects		
Effect of manganese dispersoids on the fatigue crack propagation of Al-Zn-Mg alloys.		490-493A
Yield strength, Cooling effects		
The quench sensitivity of cast Al-7 wt.% Si-0.4 wt.% Mg alloy.		3983-3991A
Yield strength, Corrosion effects		
Effects of the alumina scale on the room-temperature tensile behavior of preoxidized MA 956.		3809-3816A
Yield strength, Deformation effects		
Non-Schmid effects on the behavior of polycrystals, with applications to Ni ₃ Al.		81-99A
Flow stress and microstructural evolution during hot working of alloy 22Cr-13Ni-5Mn-0.3N austenitic stainless steel.		1251-1266A
Constitutive behavior of tantalum and tantalum-tungsten alloys.		2994-3006A
Influence of plastic deformation upon the half-width of engineering metallic materials in hard state.		3662-3668A
Yield strength, Heating effects		
Influence of long term annealing on tensile properties and fracture of near- α titanium alloy Ti-6Al-2.75Sn-4Zr-0.4Mo-0.45Si.		1700-1708A
Low quench sensitivity of superplastic 8090 Al-Li thin sheets.		2923-2933A
Hot deformation mechanisms of a solution-treated Al-Li-Cu-Mg-Zr alloy.		3478-3490A
The plastic anisotropy of an Al-Li-Cu-Zr alloy extrusion in unidirectional deformation.		3503-3512A
Yield strength, Impurity effects		
The effect of hydrogen on the fracture of alloy X-750.		101-110A
Yield strength, Microstructural effects		
Pearlite in ultrahigh carbon steels: heat treatments and mechanical properties.		111-118A
NiTi and NiTi-TiC composites. II. Compressive mechanical properties.		183-191A
Subcritical crack growth at bimaterial interfaces. II. Microstructural effects on fracture resistance of metal/ceramic interfaces.		213-219A
Microstructural aspects of the dissolution and melting of Al ₂ Cu phase in Al-Si alloys during solution heat treatment.		1785-1798A
Theoretical calculation of the stress-strain behavior of dual-phase metals with randomly oriented spherulitic inclusions.		2359-2365A
The use of microstructural gradients in hot gas-pressure forming of Zn-Al sheet.		3250-3258A
Influence of interstitials on the mechanical properties of metallic materials.		3524-3529A
The cracking mechanism of silicon particles in an A357 aluminum alloy.		3558-3568A
Reinforcement shape effects on the fracture behavior and ductility of particulate-reinforced 6061-Al matrix composites.		3739-3746A
The behavior of internal markers in Ti-6Al-4V deformed in superplastic tension.		3747-3748A
Influence of titanium and carbon contents on the hydrogen trapping of microalloyed steels.		3773-3780A
Yield strength, Stress effects		
Plastic anisotropy of sheets with continuously varying anisotropic parameters and flow stress.		317-326A
Detecting stable crack onset at ductile-brittle transition in steels.		469-471A

Effect of thermal cycling on the mechanical properties of 350 grade maraging steel.	757-781A	
The Bauschinger effect in a SiC/Al composite.	995-1001A	
Yield strength, Temperature effects		
Observations of secondary carbide precipitation and its relation to high-temperature flow and fracture in HT-9 stainless steel.	467-469A	
High-temperature wear and deformation processes in metal matrix composites.	3135-3148A	
Manifestations of dynamic strain aging in soft-oriented NiAl single crystals.	3542-3557A	
An analysis of the flow stress of a two-phase alloy system, Ti-6Al-4V.	3957-3962A	
Yttrium, Refining		
Thermodynamic properties of oxygen in yttrium-oxygen solid solutions.	839-845B	
Zinc, Composite materials		
Analysis of damping in particle-reinforced superplastic zinc composites.	2565-2573A	
Zinc, Extraction		
The mineralogical deportment of germanium in the Clarksville electrolytic zinc plant of Savage Zinc Inc.	567-576B	
Application of centrifugal fields in fused salt electrowinning with a view to reducing electrolytic energy consumption.	889-894B	
Eco-techno-economic synthesis of process routes for the production of zinc using combinatorial optimization.	1031-1044B	
Zinc, Recovering		
A kinetic study of the reaction of zinc oxide with iron powder.	363-374B	
Zinc, Ternary systems		
Thermodynamic investigations of the ternary Au-Sn-Zn system.	921-927B	
Zinc base alloys, Casting		
The design of feed systems for thin-walled zinc high-pressure die castings.	115-118B	
Zinc base alloys, Composite materials		
Mechanical properties and 95°C aging characteristics of zircon reinforced Zn-4Al-3Cu alloy.	809-818A	
Zinc base alloys, Forming		
The use of microstructural gradients in hot gas-pressure forming of Zn-Al sheet.	3250-3258A	
Zinc base alloys, Mechanical properties		
Effect of iron on ductility and cavitation in the superplastic An-22% Al eutectoid.	863-872A	
Characterization of the wear response of a modified zinc-based alloy vis-à-vis a conventional zinc-based alloy and a bearing bronze at a high sliding speed.	3513-3523A	
Zinc base alloys, Melting		
The production of nickel-zinc alloys by powder injection.	780-787B	
Zinc base alloys, Microstructure		
The Rayleigh instability and the origin of rows of droplets in the monotectic microstructure of zinc-bismuth alloys.	2053-2057A	
Zinc base alloys, Phase transformations		
Discussion of "Effects of tensile stress on microstructural change of eutectoid Zn-Al alloy" and authors' reply.	3330-3335A	
Zinc base alloys, Powder technology		
Kinetics of phase evolution of Zn-Fe intermetallics.	2904-2910A	
Zinc compounds, Powder technology		
Kinetics of phase evolution of Zn-Fe intermetallics.	2904-2910A	
Zinc dust, Recovering		
A kinetic study of the reaction of zinc oxide with iron powder.	363-374B	
Zircon, Composite materials		
Mechanical properties and 95°C aging characteristics of zircon reinforced Zn-4Al-3Cu alloy.	809-818A	
Zirconium, Alloying additive		
Microstructure and phase identification in type 304 stainless steel-zirconium alloys.	2151-2159A	
Elevated temperature compressive properties of zirconium-modified NiAl.	2628-2641A	
Effects of alloy modification and thermomechanical processing on recrystallization of Al-Mg-Mn alloys.	2947-2957A	
The effect of metallic elements on the crystallization behavior of amorphous Fe-Si-B alloys.	3424-3430A	
Zirconium, Diffusion		
Pressure dependence of anomalous diffusion of zirconium in β -titanium.	1807-1814A	
Zirconium, Mechanical properties		
Influence of interstitials on the mechanical properties of metallic materials.	3524-3529A	
Zirconium base alloys, Extrusion		
Microsegregation of oxygen in Zr-2.5Nb alloy materials.	431-440A	
Zirconium base alloys, Forming		
Reply: Dynamic materials model. Basis and principles.	235-236A	
Zirconium base alloys, Phases (state of matter)		
Microstructure and phase identification in type 304 stainless steel-zirconium alloys.	2151-2159A	
Zirconium compounds, Composite materials		
A model for coupled growth of reaction layers in reactive brazing of ZrO ₂ -toughened Al ₂ O ₃ .	3630-3638A	
Zirconium compounds, Oxidation		
Phase relations of a silicide/silica reaction couple at 2273K.	271-276B	

